People's Democratic Republic of Algeria
Ministry of Higher Education and Scientific Research
Mohamed Larbi Ben M'hidi University, Oum el Bouaghi
Faculty of Sciences and Applied Sciences
Department of Electrical Engineering

Order N°: ....

THESIS

Presented to obtain the 3rd cycle doctorate degree on:

Electronics

Option: Materials

By

Mr. Boumediene SADOUN

Theme

STUDY OF THE OPTICAL PROPERTIES OF PHOTONIC CRYSTALS ON ENHANCING THE ABSORPTION IN PHOTOVOLTAIC CELLS

Presented on: 02/12/2021

The jury committee:

President	Kheireddine LAMAMRA, Prof	Oum El Bouaghi University
Reporter	Souheil MOUETSI, Prof	Oum El Bouaghi University
Examiner	Mohamed Redha LEBBAL, Prof	Constantine 1University
Examiner	Djamel KHEDROUCHE, Prof	M'sila University
Examiner	Djamil RECHEM, Prof	Oum El Bouaghi University
Examiner	Salima BENKARA, MCA	Oum El Bouaghi University

Academic year 2021-2022

Work carried out at the Electronics and New Technologies Laboratory (LENT),
Faculty of Sciences and Applied Sciences, Department of electrical engineering,
University Larbi ben M'hidi, Pole of Ain El Beida, Oum El Bouaghi, Algeria

République Algérienne Démocratique et Populaire
Ministère de l'Enseignement Supérieur et de la Recherche Scientifique
Université Mohamed Larbi Ben M'hidi, Oum el Bouaghi
Faculté des sciences et sciences appliquées
Département de Génie électrique

N° d'ordre .....

THÈSE

Présenté pour l'obtention du doctorat de 3éme cycle sur:

Electronique

Option: Matériaux

Par

Mr. Boumediene SADOUN

Thème

ETUDE DES PROPRIETES OPTIQUES DES CRISTAUX PHOTONIQUES POUR L'AMELIORATION DE L'ABSORPTION DES CELLULES PHOTOVOLTAIQUE

Soutenu le: 02/12/2021

Devant la commission de jury:

Président	Kheireddine LAMAMRA, Prof	Université d'Oum El Bouaghi
Rapporteur	Souheil MOUETSI, Prof	Université d'Oum El Bouaghi
Examinateur	Mohamed Redha LEBBAL, Prof	Université de Constantine 1
Examinateur	Djamel KHEDROUCHE, Prof	Université de M'sila
Examinateur	Djamil RECHEM, Prof	Université d'Oum El Bouaghi
Examinateur	Salima BENKARA, MCA	Université d'Oum El Bouaghi

Année universitaire 2021-2022

Travaux réalisés au Laboratoire d'Electronique et des Nouvelles Technologies (LENT),
Faculté des sciences et sciences appliquées, Département de génie électrique,
Université Larbi ben M'hidi, Pôle d'Ain El Beida, Oum El Bouaghi, Algérie.

Dedication

In loving memory of the people who could not be here today;

To my father Abdelouaheb for his wise words empowering me not to settle for anything less;

To my mother Saida for her guidance and strength that made me the person i am;

To my wife and to my beautiful future family;

To my siblings for their unwavering belief in me, for their support and love during the darkest of times;

To the best of friends, the best support group for all our years together, i would express my appreciation and gratitude towards the best of people to cross roads;

My gratefulness goes to all the teachers and administrators, who left an imprint in my life over the past four years;

My appreciation also goes to everyone who helped me throughout this work;

My heartfelt wishes for success to all my fellow graduates.

Boumediene

Acknowledgment

In the name of Allah, most gracious, most merciful;

Praise be to Allah, the sustainer of the worlds;

The first praise will be devoted to our lord, Allah the most compassionate, the most merciful;

My profound gratitude goes to my judicious supervisor Prof. Souheil MOUETSI who steered me to this field of studies that i came to appreciate a little more each passing day, whose words count for much of my motivation to work harder, his infinite and insightful guidance have been the compass guiding me to finish this work;

To the members of the jury:

Kheireddine LAAMAMRA, Professor at the University of Oum elbouaghi, for doing me the honor of participating in my thesis jury as President. I am sincerely grateful for all the relevant comments and for his interest in this work;

Mohamed Redha LEBBAL, Professor at the Constantine 1 university, for his interest in this work and for agreeing to be an examiner for this thesis;

Djamel KHEDROUCHE, professor at Mohamed Boudiaf Msila University, for having honored me with his presence as a member of the jury, I very respectfully thank him for having accepted to judge this work;

Djamil RECHAM, Professor at Oum elbouaghi University, for his interest in this modest work and for honoring me by agreeing to examine it by participating in the thesis jury;

Salima BENKARA, MCA at Oum elbouaghi University, for the interest he showed in my work and for the honor he did me by agreeing to examine it by participating in the thesis jury;

I would like to thank all the members of the electronics and new technology laboratory of the university of larbi ben m'hidi, as well as the signals and systems analysis laboratory of the university of m’sila;

My deep gratitude goes to all the professors and administrators of the sciences and applied sciences faculty at the university of Oum el bouaghi.

List of acronyms

α	Optical absorption coefficient
$\vec{k}$	Wave vector.
$\Delta\omega$	The width at mid-height of the resonance.
µc-Si	Microcrystalline silicon.
1DPC	One Dimensional Photonic Crystal.
2DPC	Two Dimensional Photonic Crystal.
3DPC	Three Dimensional Photonic Crystal.
a-Si	Amorphous Silicon.
a-Si:H	Hydrogenated Amorphous Silicon.
a-SiGe:H	Hydrogenated Amorphous Silicon germanium.
PBG	Photonic Band Gap.
c	Speed of light in the void.
C_B	Conduction Band.
CFC	Cubic Face Cantered.
E_C	Conduction band energy.
E_f	Fermi energy.
E_V	Valence band energy.
ff	Filling factor.
GaAs	Galium arsenide.
GUI	Graphical User Interface.
h	Blanck cte.
Isol(λ)	Solar irradiance.
J_m	Maximum current density.
K_B	Boltzmann cte.
L	Period.
n	Refractive index.
nc-Si	Nanocrystalline silicon.
N-I-P	Junction NIP.
PCs	Photonic Crystals.
PECVD	Plasma enhanced Chemical Vapor Deposition.
P-I-N	Junction PIN.
P_m	Maximum power.
PV	Photovoltaic.
Q	Quality factors.
q	Electron charge.
r	Radius of photonic crystal.
RCWA	Rigorous Coupled Waves Analysis.
SC	Solar Cell.
Si SCs	Silicon Solar Cell.
SiO_2	Dioxyde silicon.
SZC	Space Zone Charge.
TE	Electrical Transverse.
TM	Magnetically Transverse.
V_B	Valence Band.
Vm	The maximum voltage.
Voc	Open circuit voltage.
ZB	Brillouin area.
ε	Dielectric Permittivity.
λ	Wavelength.

τ:	The lifetime of the photon in the cavity.
ω	The resonance frequency of the cavity.
$\boldsymbol{\eta}$	PV conversion efficiency.
E(r)	Electric field.
H(r)	Magnetic field.
μ_0	Magnetic permitivity.
CFC	Cubic face centered.
IQI	Internal Quantum Efficiency.
EQE	External Quantum Efficiency.
TCO	Transparent conductive oxides.
R(λ)	Fraction of photons reflected at wavelength λ.
T(λ)	Fraction of photons transmitted at wavelength λ.
I_0	Incident intensity.
V_m	The voltage corresponding to the max power.
I_m	The current corresponding to the max power.
CIGS	Copper indium gallium selenide.
CdTe	Cadmium telluride.
TiO_2	Titanium dioxide.
ZnO:Al	Aluminium doped zinc oxide.
H_2	Hydrogen atom.
HWCVD	Hotwire chemical vapour deposition.
PWE	Plane wave expansion.
FDTD	Finite difference time Domain.
TM	Transfer matrix.
DM	Diffusion matrix.
PDEs	Partial differential equations.

List of figures

Figure I.1: Represents the PV cell.
Figure I.2: Principle of photovoltaic conversion.
Figure I.3: The absorption of a photon by a semiconductor; (a): before absorption the electron is in the ground state in the valence band, (b): after absorption the electron is transferred into the conduction band.
Figure I.4: P-N junction, creation of a space load zone.
Figure I.5: Spectral distribution of solar illuminance under AM1.5G conditions.
Figure I.6: (a) Incident spectral radiation from the sun for terrestrial applications (AM1.5G and AM1.5D) and space applications (AM_0); (b) Schockley-Queisser limit: maximum theoretical efficiency of a solar cell according to its band gap, with the best experimental efficiencies.
Figure I.7: NREL graph with temporal evolution of the best efficiency of conversion of research cells for different technologies.
Figure I.8: World map representing Direct Normal Irradiation (DNI) energy.
Figure I.9: A monochromatic light passing through an absorbent solution of concentration C contained in a tank of thickness L.
Figure I.10: Schematic diagrams of the operation of a SC with P-N junction.
Figure I.11: I(V) characteristic of a SC.
Figure I.12: Cumulative overall PV capacity by 2030.
Figure I.13: The PV Cell Generation.
Figure I.14: Organic PV cell of the third generation.
Figure I.15: Multi-junction PV cell of the ^{3rd} generation.
Figure I.16: Third generation concentration PV cell.
Figure I.17: Structure of a perovskite PV cell.
Figure I.18: The different structures of a perovskite cell.
Figure I.19: Principle of operation of a Grätzel cell.
Figure I.20: Grätzel Cell.
Figure I.21: Monocrystalline PV cell.
Figure I.22: Poly-crystalline PV cell.
Figure I.23: Amorphous photovoltaic cell.
Figure I.24: Simple structure of a CIGS-based cell.
Figure I.25: Structure of a PV cell at CdTe, The absorbent layer doped P rests under another doped semiconductor N (CdS), the two layers form a heterojunction.
Figure I.26: Structure of the classical cell.
Figure I.27: Superstrate structure of the solar cell in Glass, ZnO:Al, i-ZnO, CIGS in thin films.
Figure I.28: Tandem cell based on CuInSe2 and CuGaSe2.
Figure I.29: Structure of a Schottky cell (right) and representation of ITO energy levels/organic material/Al (left).
Figure I.30: Structure of a heterojunction cell (right) and representation of the energy levels of an ITO/donor/acceptor/Al contact (left).
Figure I.31: Structure of an interpenetrated grating cell (a) and (b) load transfer mechanism.
Figure I.32: Schematic representation of the structure of a BSF bifacial SC.
Figure I.33: Typical structure of a SC based on CdTe active layer.
Figure I.34: Schematic representation of the atomic structure of crystalline silicon (at left) and amorphous silicon (right).
Figure I.35: Schematic diagram showing the particular microstructure of μc-Si:H.
Figure I.36: Absorption coefficient α crystalline silicon (c-Si), amorphous silicon hydrogenated (a-Si:H) and hydrogenated microcrystalline silicon (μc-Si:H), measured by Photo thermal deviation spectroscopy (PDS).
Figure I.37: (Left) Bar graph of a P-N junction representing the case of a SC based on c-Si, (Right) bar chart of a P-I-N diode corresponding to the case of SC based on a-Si:H and μc-Si:H.
Figure I.38: Equivalent circuit for a P-I-N diode.

Figure I.39: Schematic representation of SC in P-I-N configuration (left) and N-I-P (right). The silver grid of the N-I-P cell, normally deposited on the contact before TCO, is not represented.
Figure. II.1: Schematic representations of PCs where the refractive index varies periodically according to one, two or three dimensions.
Figure. II.2: Shows scanning electron microscopy (SEM) images of different artificial PCs.
Figure. II.3: Scanning electron microscope (SEM) images of different types of PCs: (a) Bragg's grating; (b) planar PC and (c) three dimensional PC.
Figure. II.4: Natural PCs: (a) peacock feather, the box on the right is a scanning electron microscope (SEM) image of the cut of a green barb, the two dimensional PC structure is composed of melanin pillars bound by keratin as well as air holes; (b) morphic butterfly (c) bracelet mounted with an almost periodic natural opal of silica.
Figure. II.5: Schematic representation of an absorbent layer of a two dimensional PC in a dielectric plane guide.
Figure. II.6: The periods of a one dimensional PC.
Figure. II.7: (a) Defect; (b) and (c) Substitution defects.
Figure. II.8: Transmission spectrum of a hexagonal crystal of dielectric rods with or without defect.
Figure. II.9: Example of a W_1 guide to hexagonal PC of air holes on a silicon substrate on insulator.
Figure. II.10: One-dimensional structure.
Figure. II.11: Schematic representation of the interference of the waves reflected by each Dioptre.
Figure. II.12: Photonic band structures for Bragg gratings of step a with: (a) permittivity layers ε=13 and 12 and (b) permittivity ε=13 and 1.
Figure. II.13: Schematic representation of the shift of the central frequency as a function of the location of the electric field in the grating; (a) the electric field at its maximum amplitude in areas of high permittivity; (b) the electric field has its maximum amplitude in areas of low permittivity.
Figure. II.14: (a) Dispersion relationship of a homogeneous medium, folding is due to artificial periodization, (b) opening of a band gap when $\varepsilon_{1,}\varepsilon_{2;}$ (c) the band gap is all the wider the greater the index contrast.
Figure. II.15: Two-dimensional structures: (a) connected, (b) disconnected.
Figure. II.16: The Brillouin zones of the reciprocal grating of a square structure.
Figure. II.17: Representation of a two dimensional structure; (a) a square grating; (b) a triangular grating.
Figure. II.18: Graphite structure.
Figure. II.19: Boron nitride.
Figure. II.20: Diagram band of a square mesh structure of cylindrical studs in the air.
Figure. II.21: Representation of the triangular grating in real space, in reciprocal space, and representation of the first Brillouin zone with the irreducible Brillouin zone formed by the triangle ΓMK.
Figure. II.22: (a) 2D bar graph of the triangular grating for a fill factor of 0.3; (b): map of band gaps according to the standard radius r/a.
Figure. II.23: Two types of one dimensional crystals: (a) with spheres; (b) with stems.
Figure. II.24: Examples of three dimensional PC; (a) MEB image of a wood pile structure made by UV lithography in silicon; (b) 3-dimensional diamond periodic structure made of PMMA by X-lithography at the IEF.
Figure. II.25: Example of three dimensional PC, Yablonovite.
Figure. II.26: Different types of PC cavities.
Figure. II.27: Spectral signatures of hexagonal cavities obtained by photoluminescence.
Figure. II.28: Example of a square cavity in a square photonic crystal with a mesh parameter 600nm.
Figure. II.29: Example of a triangular cavity in a triangular PC with grating parameters 600nm.
Figure. II.30: Example of a rectangular cavity in a triangular PC with a 560nm mesh parameter.

Figure. II.31: Representative diagram of the phenomenon of light scattering by microstructures in front of a SC.
Figure. II.32: Design of one dimensional PC with different profile: (a) rectangular; (b) triangular; and (c) circular.
Figure III.1: Schematic presentation of a holographic installation.
Figure III.2: Solving Maxwell's equations.
Figure III.3: The RSoft CAD window, showing the menu bar at the top, the toolbars at the top and left and the status line at the bottom.
Figure III.4: The start window.
Figure III.5: Illustration of a layout window where components are added to the circuit. The simulation area and the launch field are also displayed.
Figure III.6: The symbol table editor.
Figure III.7: a) A fibre component as it appears in the XZ plane after the drawing, and b) Multi-pane view clearly showing the fibre component. Multi-pane view is not available for 2D structures.
Figure III.8: The Component Properties dialog box for the fibre component.
Figure III.9: The Index profile calculation dialog box.
Figure III.10: The Simulation tool option as indicated in the Global Parameters dialog box.
Figure III.11: The DiffractMOD Simulation Parameters window where the basic digital simulation parameters are entered.
Figure III.12: The section of the DiffractMOD Simulation Settings dialog box where the primary direction is chosen.
Figure III.13: The principal direction is defined as being transverse to the periodicity and to the principal direction in which the incident light travels.
Figure III.14: The part of the plane Wave Launch Options dialog box where the k-Vector (input angle) options are set.
Figure III.15: The two angle conventions supported by DiffractMOD: a) The RSoft relative angle convention and b) the standard spherical angle convention.
Figure III.16: The part of the Plane Wave Launch Options dialog box where the E-vector (polarization) options are set.
Figure III.17: The plane of plane wave polarization for three dimensional DiffractMOD simulations: a) the plane of polarization (PS) is normal to the wave vector k, and b) the plane of polarization with the represented s and p components of the field E.
Figure III.18: The SC Utility dialog box.
Figure III.19: The simulation window of the SC utility with the default J-V output. The shaded rectangle represents the fill factor, the point on the curve where V=0 is the short-circuit current Jsc, the point on the curve with a current of 0 is the open-circuit voltage Voc, and the point on the curve that defines the shaded rectangle is the optimal bias point.
Figure III.20: The utility simulation window showing a) the quantum efficiency results, and b) the spectral results showing the incident, sampled and absorbed spectra.
Figure VI.1: (a) Unpatterned layer SC structure on a glass substrate, (b) one dimensional PC.
Figure VI.2: (a) Thin film SC structure made by unpatterned layer on a glass substrate; (b) The patterned layer with 1DPC.
Figure VI.3: The variation of the absorption power of a:Si-H and Si, on (a) Thin layer patterned Spectral structure of the 1DPC, (b) thin layer un-patterned spectral structure.
Figure VI.4: Variation of lattice parameter (L=400nm, L=500 nm and L=600nm) on the absorption power of a:Si-H (a) and Si (b) with a thickness of layer 100nm.
Figure VI.5: (a) Unpatterned and (b) 1DPC lattice structures, made by a-Si:H and a-SiGe:H respectively.
Figure VI.6: Optical absorption of (a) a-Si:H thin film made by unpatterned and 1DPC, (b) a-SiGe:H thin film made by unpatterned and 1DPC lattice structures.
Figure VI.7: Geometrical grating of (a) half circle, (b) triangle gratings made by a-Si:H and a-SiGe:H.
Figure VI.8: Dimensions of the simple proposed gratings of (a) half circle and (b) isometric triangle.

Figure VI.9: Optical absorption of the half circle and triangle gratings made by (a) a-Si:H and (b) a-SiGe:H.

Figure VI.10: (a) the EQE graphs, (b) the J-V curves and (c) smooth spectral distribution of the studied AM1.5 solar spectrum with different grating structures studied made by a-Si:H of thin film SCs.

Figure VI.11: (a) The EQE graphs, (b) the J-V curves and (c) the smoothened spectral distribution, studied by different grating structures studied, made by a-SiGe:H thin film.

Figure VI.12: Incidence angle effect on absorbent layer of different gratings made by (a) a-Si:H and (b) a-SiGe:H.

Figure VI.13: (a) planar, (b) 1DPC and (c) trapezoidal grating structures made by GaAs, respectively.

Figure VI.14: Represent the contour map of (a) planar, (b) 1DPC and (c) trapezoidal grating structures made by GaAs, respectively.

Figure VI.15: Absorption energy of GaAs thin film made by planar, 1DPC and trapezoidal grating structures.

Figure VI.16: Trapezoidal parametric effect of (a) heights and (b) widths variations made by GaAs.

Figure VI.17: Optical absorption of trapezoidal grating with different and mixed (a) heights and (b) widths, made by GaAs.

Figure VI.18: (a) the J-V SC characteristics, (b) the external quantum efficiency and (c) smooth spectral distribution of the studied AM1.5 solar spectrum, with simple grating of planar, 1DPC and trapezoidal structures studied, made by GaAs of thin absorber layer of a solar cell.

Figure VI.19: (a) the J-V SC characteristics, (b) the external quantum efficiency and (c) the smoothened spectral distribution for the considered AM1.5 solar spectrum, studied by parametric effect of mixed and simple precision heights of trapezoidal grating structure made by GaAs of thin film SCs.

Figure VI.20: (a) the J-V SC characteristics, (b) the external quantum efficiency and (c) the smoothened spectral distribution, studied by parametric effect of mixed and simple precision widths of trapezoidal grating structure made by GaAs of thin film SCs.

List of tables

Table I.1: The difference between the two types of silicon in the first generation.
Table I.2: Data form the three generations of SCs.
Table VI.1: Physical properties of the Si and a-Si:H.
Table VI.2: The physical parameters of a-Si:H and a-SiGe:H thin films.
Table VI.3: The used parameters of a-Si:H well as a-SiGe:H for thin film PV cells with PCs used in the linear regime.
Table VI.4: The simulation results of a-Si:H thin film SC energy conversion efficiency.
Table VI.5: The energy conversion efficiency simulation results of a-SiGe:H thin film solar cell.
Table VI.6: The most physical parameters of GaAs**.**
Table VI.7: The used parameters of GaAs thin film PV cell with PCs used in the linear regime.
Table VI.8: The energy conversion efficiency of GaAs thin film PV cells with different structures.

Table of contents

General Introduction……..…(1)
Chapter I: Concepts on Photovoltaic
I.1. Introduction……..…(6)
I.2. Photovoltaic cells…….(6)
I.2.1. Energy and wavelength of photons……...…(7)
I.2.2. The conversion principle……..……(8)
I.2.3. Photovoltaic energy……(9)
I.2.4. Absorption in the optical state……..……(11)
I.3. The operation of a solar cell……..……(13)
I.3.1. Characteristic under illumination and parameters of the solar cell……..……(14)
I.4. History....……..……(16)
I.5. Generations of photovoltaic cells…….....……(17)
I.5.1. First generation……...……...…(17)
I.5.2. Second generation……..……(18)
I.5.3. Third generation……..…...…(19)
I.6. Solar cell design and architecture……..……(23)
I.6.1. Silicon solar cell……...……(23)
I.6.2. Thin film solar cells……...…(25)
I.6.3. The classical substrate structure…….....….(26)
I.6.4. The superstrat structure…….....….(27)
I.6.5. Tandem cells…….....….(28)
I.6.6. Organic photovoltaic cells…….....…….(29)
I.6.7. Bifacial cells…….....….(30)
I.6.8. Cells of CdTe tape structure…….....…..(30)
I.7. The art state …….....…….....….....…..(31)
I.7.1. Material properties and silicon deposition……...…….……(31)
I.7.2. Principle of operation of Solar cells…….....…(33)
I.7.3. Equivalent circuit for a P-I-N diode…….....…(34)
I.7.4. Solar cells in P-I-N and N-I-P configurations……...……...…….(35)
I.7.5. Doping of silicon nanoparticles…….....……(36)
I.7.6. Fundamental and technological losses limiting performance…….....(36)
I.8. Conclusion……...…….....……(37)
Chapter II: Concepts and generalities on photonic crystals
II.1 Introduction…….....……(43)
II.2 Definition…….....……(43)
II.3 History…….....……(45)
II.4 Natural photonic crystals…….....…..……(45)
II.5 Planar photonic crystals…….....…..……(46)
II.5.1 Illumining modes…….....…..……(47)
II.5.2 Localized modes…….....…..……(47)
II.5.3 Guide modes…….....……(47)
II.5.4 Resonant modes…….....……(47)
II.6 Geometric and physical characteristic of photonic crystals…….....……...…(47)
II.6.1 Index contrast…….....…(47)
II.6.2 Periods…….....……(47)
II.6.3 The filling factor…….....…...…(48)
II.7 Defects…….....…...…(48)
II.7.1 Defect strategies in photonic crystals…….....…...…(48)
II.8 Properties of photonic crystals…….....……(50)
II.8.1 The "electron-photon" analogy…….....……..……(50)
II.9 Types of photonic crystals…….....……(52)
II.9.1 One dimensional photonic crystal (Bragg mirror) …….....…….....……...…(52)
II.9.2 Two dimensional photonic crystal…….....…..…(54)
II.9.3 Three dimensional photonic crystal…….....…(59)

II.10 Photonic crystal cavity……(61)
II.11 The art state ……(63)
II.11.1 Random texturing substrates……(64)
II.11.2 Diffraction gratings……(65)
II.11.3 Waveguide improvement based on dispersion in photonic crystals……(66)
II.11.5 Coupling light to super-collimating photonic crystals……(66)
II.11.6 Absorbent photonic crystals……(68)
II.12 Conclusion……(68)
Chapter III: Simulation tools and numerical modelling
III.1. Introduction……(76)
III.2. Modeling of the propagation of light in periodic areas……(76)
III.3. The most used simulation methods and means……(77)
III.3.1. The plane wave expansion method (PWE)……(77)
III.3.2. The finite difference time domain method (FDTD)……(77)
III.3.3. The rigorous coupled wave analysis method (RCWA)……(78)
III.4. The state of the art……(82)
III.5. Simulation software……(83)
III.5.1. Foreword of RSoft CAD……(83)
III.5.2. Numerical simulation steps with RSoft CAD……(83)
III.5.3. Associated simulation modules……(87)
III.6. Conclusion……(95)
Chapter VI: Results and discussions
VI.1 Introduction……(100)
VI.2 Adopted strategy for the nanophotonic structures development……(101)
VI.3 Process for manufacturing ultra-fine nanostructured silicon solar cells……(101)
VI.4 Increase absorption in absorbing layers……(101)
VI.5 Association of an optimal photonic crystal in a photovoltaic system……(101)
VI.6 Optoelectronic properties and design of an absorbing photonic crystals……(101)
VI.6.1 Optoelectronic properties……(101)
VI.6.2 Integration and conception of a photonic crystal in an absorbent thin film photovoltaic system……(102)
VI.6.3 Results and discussions……(103)
VI. 6.4 The importance of optimizing geometric parameters for optical trapping……(104)
VI. 6.5 Analysis of the results……(105)
VI. 6.5.1 The absorption with the patterned and the unpatterned thin layers……(105)
VI. 6.5.2 The lattices parameters variation……(106)
VI.7 Morphological effect of the photonic crystals structures……(108)
VI.7.1 Analysis of the results……(109)
VI.7.1.1 Optical Properties……(110)
VI.7.1.2 Optimal morphological design……(112)
VI.7.1.3 Electronic properties……(114)
VI.7.1.4The incidence angle (θi) effect……(119)
VI.8 Effects of the mixture ultra-precision gratings in photonic crystals……(120)
VI.8.1 Analysis of the results……(122)
VI.8.2 Optical properties……(123)
VI.8.3 Optical absorption in simple lattices……(125)
VI.8.4 Parametric effect……(126)
VI.8.5 Solar cell J-V characteristics……(128)
VI.9. Conclusion……(132)
General conclusion……(137)
Annex: scientific production……(139)
Abstracts in English, French and Arabic……(141)

General Introduction

General introduction

Human evolution has always been closely linked to his ability to control and harness the energy sources that surround him. In the beginning, they could only rely on his own bodily energy to survive, to carry out daily tasks or to move around. Then, with the mastery of fire, new perspectives opened up to him. Very early on, man knew how to use wind energy to move around, aboard sailboats for example, or geothermal energy to have hot springs. Much later, with technological advancements and his growing understanding of the world around him, man has been able to convert solar energy into electrical energy through the conversation of the photovoltaic (PV) effect. In this context, PV technology is presented as a non-polluting solution to the problem of electric energy production [1]. Driven by a favorable economic and social context, research in the field of PV cells has intensified for more than two decades, with the common theme of the desire to create a mature and competitive technology.

In this context, the optimization of the materials and technological processes used has long been in the foreground. With the development of thin film solar cells, an important step has been taken in reducing costs by reducing the thickness of the active layer [2].

Actually, PV conversion contributes very little to global energy production because of the cost per kWh of around 10 to 20 times higher than that of fossil fuels. As well, photovoltaic technology is at the crossroads of profound changes. Most of its industry currently relies on so-called first generation cells, the base material of which is a silicon wafer, mono-crystalline or multicrystalline. This poses a double problem: the availability of the material and the preponderance of the cost of the latter in the price of the cells.

The challenge is therefore to use second-generation cells which, in recent years, have been the subject of intensive research throughout the world: the technology of polycrystalline thin-film cells. The latter is called upon to play a considerable role in reducing the cost of manufacturing cells.

However, the low absorption of light, especially for wavelengths located near the gap of the absorbent material, was quickly identified as the main limitation of these cells. Particular attention has therefore been paid to these optical losses, which are even more critical when considering ultrathin layers whose thicknesses are on the order of micrometers or even less. To deal with this problem, geometrical optic texturizations for cells based on silicon wafers have proved to be unsuitable because of dimensions much greater than the thickness of a thin film. The original idea developed by Yablonovitch [3], was to use the Photonic Band Gap (PBG), to inhibit spontaneous emission by annihilating the density of states of photons. The approach of designing them from organic compounds is promising, due to the advantages associated with this technology such as: ease of design, diversity of components, and lower cost compared to silicon-based devices. In order to improve the photovoltaic performance of solar cells, several works have been undertaken. Thus, a wide variety of organic materials (small molecules, conjugated polymers, dyes) or organic/inorganic mixtures promoting charge creation, transport and collection, have been tested as components of such cells. Further investigations have been made consisting of the development of new cell architectures [4].

Optimizing the performance of thin film silicon SCs linked to cost reduction remains a key issue for industrial production. In order to achieve high efficiencies, thin film silicon solar cells must exhibit strong light absorption. This results in an increase in the PV current. Finding new structures or optical devices to trap light in solar cells is a real challenge for researchers. The authors of [5] proposed to use metal nanoparticles to increase light absorption in solar cells to thin films of silicon.

This last point constitutes the objective of light trapping methods which aim to extend this condition to the entire useful spectrum. The notion of "*light trapping*" appeared in the early 1970s to improve light absorption and the performance of silicon photodetectors, particularly in the near infrared [6]. In order to address this problem, it has been proposed to completely etch this layer to form a photonic crystals and to optimize its parameters (period L and filling factor *ff*) in order to increase the local density of photonic states at long wavelengths [7]. In the case of [8], they sought to take advantage of the particular and adjustable optical properties of photonic crystals, which are structures characterized by a periodic index of refraction in one, two or three directions of space. More precisely, they proposed to etch the active layer to form a photonic crystals in order to control the residence time of photon beams, and thus to increase the absorption over a wide spectral range with a large angular acceptance. Because of this, more advanced photonic engineering concepts have been developed by introducing nanostructures to improve light collection, but also to ensure efficient trapping of photons beam in the active layer for wavelengths where the absorption is normally low.

The objective of this work lies in the study of thin film SC based on silicon (Si), hydrogenated amorphous silicon (a-Si:H), hydrogenated amorphous silicon germanium (a-SiGe:H) to study the geometrical effect to enhance the optical absorption, as well as the effect of the morphological structure to improve the optoelectronic properties of the absorbent layer SC with a thickness of up to 100nm. On the other hand, the optical absorption with the JV SC characteristics were studied by the parametric effect (heights/widths), where the ultra-precise values of a cell with a trapezoidal grating were mixed using gallium arsenide (GaAs) semiconductor materials.

To achieve this goal, our thesis has been structured into four complementary chapters:

- **Chapter I:** In this chapter, we will introduce the general operation of a thin film PV cell, the history of PV energy, the associated technological sectors and the operating principle of a SC. In addition, we will describe the conditions for depositing and preparing nanostructures. To mention the adequate trapping of light in thin film silicon SCs, we will also present a reminder of the structural, optical and electronic properties of amorphous silicon, and explain the operation of thin film silicon SCs.
- **Chapter II:** We introduce the basic notions of photonic crystals and their different types, where we will expose the cases of one-dimensional photonic crystal, two-dimensional photonic crystal and three-dimensional photonic crystal, which is a configuration appreciated by the scientific community because of the ease of its implementation: a better light confinement, precise calculation of the forbidden band, and ease of integration. Then, we present the geometrical and physical characteristics of photonic crystals, and more precisely on their guiding principle and the different types of cavities and photonic crystal guides. In the last section of the chapter, we will

present the state of the art on photonic crystals, in addition to the optical properties of different materials and photonic crystals fabrication technologies.

- **Chapter III:** Given the innovative nature of the production of SC structures based on photonic crystals, their design requires a better understanding of modeling tools. We present the different numerical modeling methods used to determine the characteristic parameters of structures and to analyze the propagation of the electromagnetic field (calculation of optical absorption and electronic parameters). In this context, we present the method of Rigorous Coupled Wave Analysis (RCWA). Subsequently, we expose the RSoft software used in this work which is DiffractMOD. With these modeling tools, we can study the optical properties and calculate the electronic parameters of the different photonic crystals structures and represent the distributions of the appropriate electromagnetic field.
- **Chapter VI:** This chapter is devoted to the methodology used to carry out the optoelectronic simulation which is in direct relation with the physical foundations of the materials mentioned above. We will simulate the absorption of the single absorbent layer of Silicon and a-Si:H, as a function of the physical and geometric parameters based on a one-dimensional photonic crystal. Additionally, to study the optical and J-V SC characteristics of different photonic crystals lattices (one-dimensional photonic crystal, half circle, triangle) under the morphological influence using a-Si:H and a-SiGe:H. Moreover, study of the optoelectronic properties under the parametric effect of the SC in addition to the variation of the heights and widths of the gratings with an ultra-precise value, and the effect of mixing these values, using the GaAs semiconductor material properties.

We end this thesis with a general conclusion which summarizes the context of our work as well as the perspectives of future research.

List of references

[1]. A. Perthue, "Vers une amélioration des performances et de la durabilité de cellules photovoltaïques organiques par l'application d'un film composite multifonctionnel," Phd Thesis, Université Blaise Pascal - Clermont-Ferrand II, 2014.

[2]. G. Gomard, "Cristaux photoniques pour le contrôle de l'absorption dans les cellules solaires photovoltaïques silicium ultraminces," Thèse de doctorat, Ecully, Ecole centrale de Lyon, 2012.

[3]. E. Yablonovitch, "Inhibited Spontaneous Emission in Solid-State Physics and Electronics," *Phys. Rev. Lett.*, vol. 58, no. 20, pp. 2059–2062, 1987.

[4]. D. M. Chapin, C. S. Fuller, and G. L. Pearson, "A New Silicon p-n Junction Photocell for Converting Solar Radiation into Electrical Power," *Journal of Applied Physics*, vol. 25, no. 5, pp. 676–677, 1954.

[5]. E. Moulin, "Accroissement de l'absorption lumineuse au sein de cellules solaires à couches minces de silicium par addition de nanoparticules et de nanostructures métalliques," Phd Thesis, Université Paul Verlaine - Metz, 2009.

[6]. A. E. S. John, "Multiple internal reflection structure in a silicon detector which is obtained by sandblasting," US3487223A, 1969.

[7]. Y. Park *et al.*, "Absorption enhancement using photonic crystals for silicon thin film solar cells," *Opt. Express, OE*, vol. 17, no. 16, pp. 14312–14321, 2009.

[8]. A. Bensmain and B. Encadrant : ZEBENTOUT, "Investigation de l'ingénierie de bandes des cellules solaires à hétérojonction a_Si :H/c-Si : Modélisation et simulation numérique" Thèse, Université Sidi Bel Abbes, Algérie. 2018.

Chapter I

Concepts on photovoltaic

Chapter I: Concepts on photovoltaic

I.1. Introduction

Although PV represent a very small share of global energy production, it has been increasing by more than 40% per year for the last ten years [1]. The main definition of the PV effect is the direct conversion of light into electricity. The term PV cell refers to a device that converts light energy into electrical energy. Nowadays, commercially available solar cells are produced using mono crystalline or poly crystalline silicon. These SCs can achieve PV efficiencies of around 24.7% with concentrated light. However, the major disadvantages are the high cost of the material and the high energy consumption during production.

Silicon thin film SCs incorporating hydrogenated amorphous silicon (a-Si:H) or hydrogenated microcrystalline silicon (μc-Si:H) are attracting increasing interest from manufacturers [1]. The very thin films that make up the cells (~1μm thick silicon compared to hundreds of microns for SCs based on monocrystalline or polycrystalline silicon) allow low material consumption. Silicon thin film technology offers a lot of possibilities for production (modules of 1 m² or more). In addition, the moderate temperatures (150-300°C) required for the production of thin films of silicon induce low energy consumption during industrial processes and offer the possibility of using a wide variety of inexpensive substrates, such as glass, stainless steel or plastics. Since SCs are very thin, they can be deposited on flexible substrates, such as metal films or plastic sheets [1].

The fact that connections are an inherent part of the design of thin film solar modules, as opposed to external connections in the case of mono or poly-crystalline cells, greatly simplifies the industrial process. A disadvantage related to a-Si:H technology is the relatively low PV efficiency and the light-induced degradation phenomenon that leads to a decrease in the initial efficiency. Stabilized efficiencies of the order of 4-6% are generally obtained for modules with a single junction of a-Si:H [2]. The concept of multilayer cells (also called the concept of multi-junction cells) is an interesting concept that helps to enhance the stability of thin-film cells. It also improves PV efficiency. The multi-junction cells consist of several single cells deposited on each other elaborated on the basis of alloys of a-Si:H and/or μc-Si:H. The highest stabilized PV efficiency (12%) for tandem SCs was obtained for an a-Si:H/μc-Si:H configuration at the University of Neuchâtel [3]. Stabilized efficiencies of more than 13% were achieved by Yang *et al* [4], for triple stacks (a-Si:H/a-Si:Ge:H/a-Si:Ge:H). However, the main aim of silicon thin film SC manufacturers is to obtain modules with stabilized efficiencies of more than 10%. The company Sharp already markets tandem modules (a-Si:H/μc-Si:H) with a stabilized efficiency of 8.5% [5].

I.2. Photovoltaic cells

It is a device that converts solar energy directly into electrical energy, taking advantage of the PV effect, and consists of a layer of silicon that has some impurities to give it electrical properties, the upper layer corresponding to the photon beams is added to the element phosphorus, to give it the property of pumping female voters when light collides with it and this layer is called the N layer while the boron element is added to the lower layer and

gives it the property of absorbing electrons, this layer is called P. When the luminaries of the solar beam hit the top layer, the electrons give an energy that depends on the intensity of the solar radiation. When there is an electrical conductor between the two layers in the lower layer, this is how an electric current and voltage are formed: SCs are an important source to provide spacecraft and satellites with the electrical energy they need. Solar energy is transformed directly into electricity and is characterized by the production of electricity without causing environmental pollution. Its lifespan can be up to 30 years. The high cost of its production is the main obstacle to its use [6].

Figure. I.1: Represents the PV cell.

Actually, silicon is the most used material for the manufacture of SCs, it represents 90% of the world's production. Despite the development of the thin film industry, using other materials (CdTe, CIGS...etc), silicon should remain the mainly used material for several more years [1]. The silicon sector benefits from a greater maturity than that of thin films. The price of manufacturing silicon plates, however, constitutes an important part of the costs of developing SCs. In order to reduce the consumption of silicon per cell and per watt, several ways exist:

- Reduce the cost of the material, by developing new techniques for producing and forming silicon that are less expensive;
- Increase the conversion efficiency of the SC;
- Decrease the thickness of the cell.

I.2.1. Energy and wavelength of photons

Light waves that propagate in a vacuum at the speed of light can be represented either by an electromagnetic vibration (wave) or by a particle (photon). The energy E of a photon of wavelength λ is given by the Planck relation (equation (I.1)).

$$E_\lambda = hC/\lambda \qquad \text{(I.1)}$$

I.2.2. The conversion principle

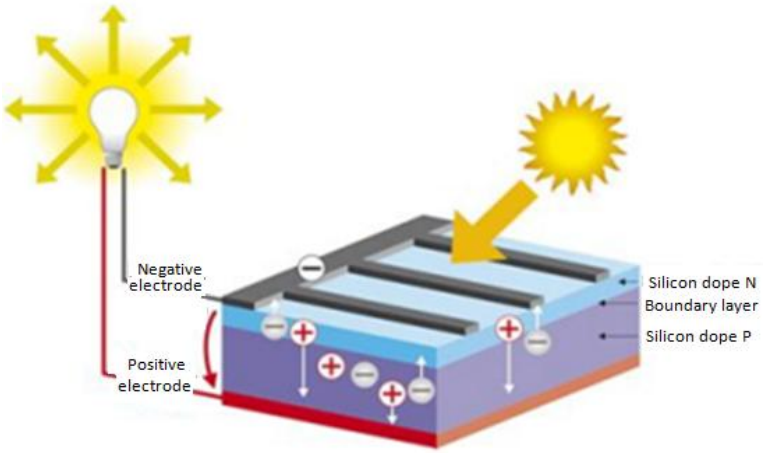

Figure. I.2: The principle of PV conversion [7].

The PV effect is specific to semiconductors and appears when light is absorbed by a semiconductor. When a photon falls on a PV device, there will be three phenomena. The photon can be absorbed by the material, reflected or transmitted into the device. In the first two cases, no current is generated, on the other hand in the case of photon absorption; it has a high chance of meeting an electron and passing it from the valence band to the conduction band thus creating an electron-hole pair (Figure I.3). Only photons whose energy are greater than or equal to the semiconductor gap are capable of creating such pairs. If the gap is too small, a large part of photons will be able to create electron-hole pairs giving rise to a large electric current but a small potential difference in the SC. On the other hand in the case where the gap is high, the current will be low but the potential difference will be important.

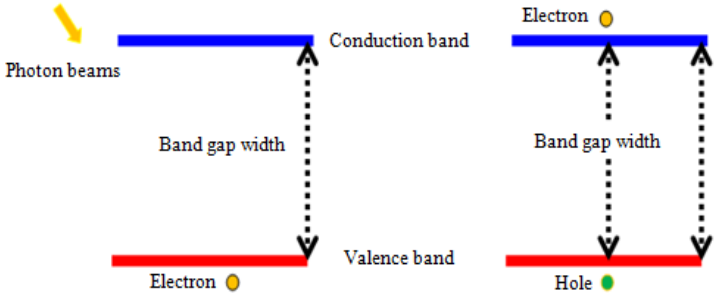

Figure. I.3 absorption of a photon by a semiconductor; (a): before absorption, the electron is in the fundamental state in the valence band, (b): after absorption, the electron is transferred into the conduction band.

The lifetime of the electron-hole pairs created is very short. The free electrons and holes recombine quickly to dissipate it over more energy in the form of photons or phonons. It is necessary to minimize the recombination as much as possible for the load carriers to participate in the creation of an electric current. This is done practically by creating a P-N junction. If we put in contact two doped semiconductors respectively p and n, under the effect of light, the carriers of charges created will diffuse on both sides until the establishment of the equilibrium creating an area called Space Charge Zone (SCZ). The

electric field induced in this area will separate the electrons from the holes, thus prohibiting recombination. In this way, an electrical force is created and can power an external circuit (Figure I.4).

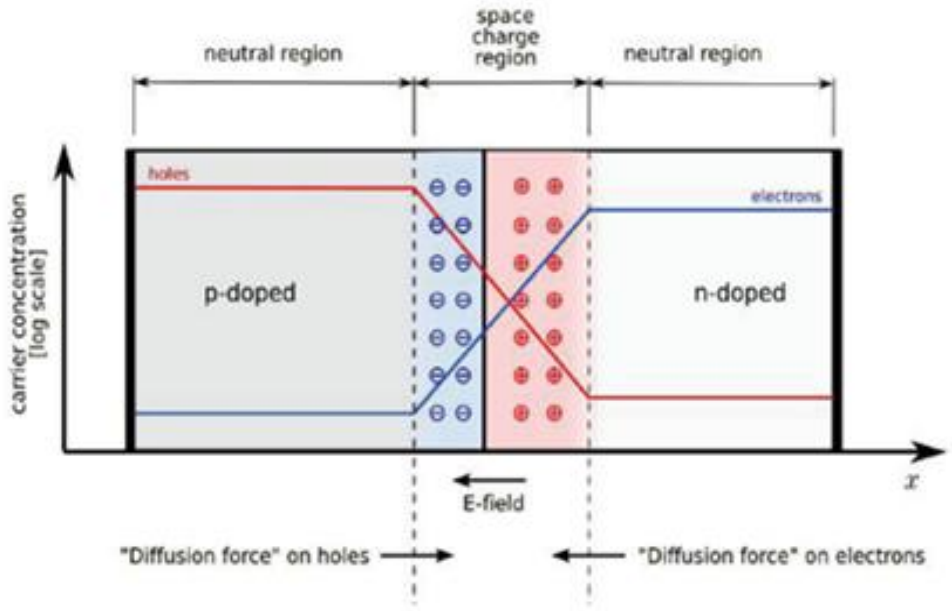

Figure. I.4: P-N junction, creation of a space load zone.

I.2.3. Photovoltaic energy

Among a lot of radiant energy that the sun continuously produces, our planet reaps a tiny part of it on its surface. This solar energy can be described by its spectrum and power. Each photon of solar radiation (Each quantum of electromagnetic energy), has an energy given by equation (I.1).

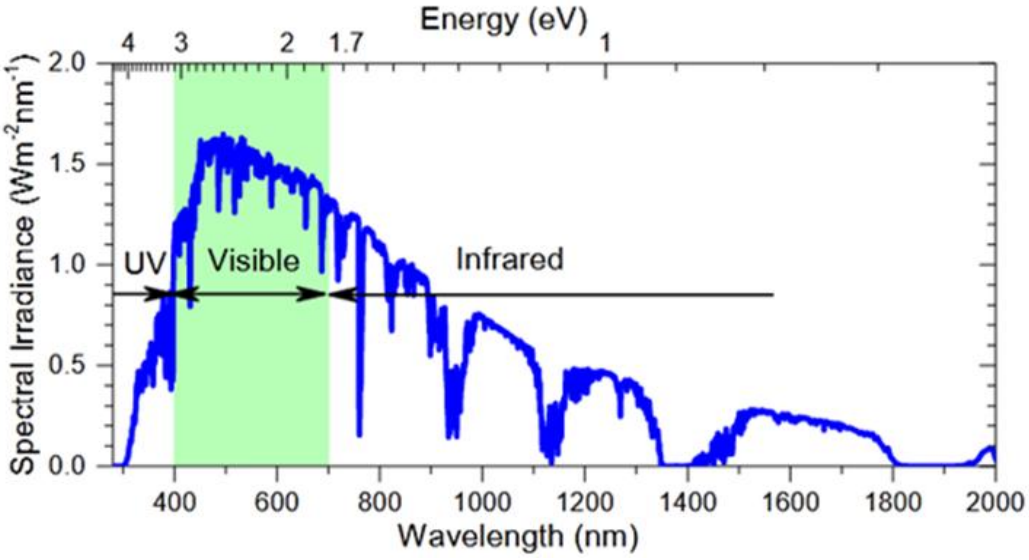

Figure. I. 5: Spectral distribution of solar shining under AM1.5G conditions.

Since the first silicon solar panel manufactured by *Bell Labs* in 1954, that achieved an efficiency of 5%, many advances have been made in the PV field. Silicon-based technologies have always been and remain the most important player in the PV industry.

In 2015, 93% of total PV production came from Si-wafer-based PV technology [8]. The record efficiency of c-Si SCs has not changed significantly since the 90s, but drastic cost reductions due to production technological improvements have led to a strong and cheap industry, and to an energy that is starting to be competitive with conventional energies. Nowadays, efforts are still being made to improve cell efficiency by minimizing shadow losses due to front contacts and reducing the area recombination losses, the technology has almost reached its maximum theoretical efficiency.

The most recent record reported is 26.7% [9], under AM1.5G, approaching the theoretical maximum of 29% efficiency declared in 1961 by Shockley and Queisser [10]. AM1.5G is a reference used as an irradiating standard to compare terrestrial solar cells and modules. It corresponds to the irradiate of the terrestrial sun at an angle elevation of 48.2°, as shown in Figure I.6.a.The atmosphere at this altitude absorbs and disperses solar radiation and attenuates the solar spectrum to an irradiation of 1000W.m^{-2}. The AM1.5G spectrum is designed for flat plates. The AM1.5D spectrum is defined for the work of the solar concentrator. It includes the direct beam of the sun and the circumpolar component in a 2,5 degree disk around the sun. The AM1.5D spectrum has a built-in power density of 900W.m^{-2}. AM_0 is the convention for space applications. The density of solar energy in space is about 1350W.m^{-2}.

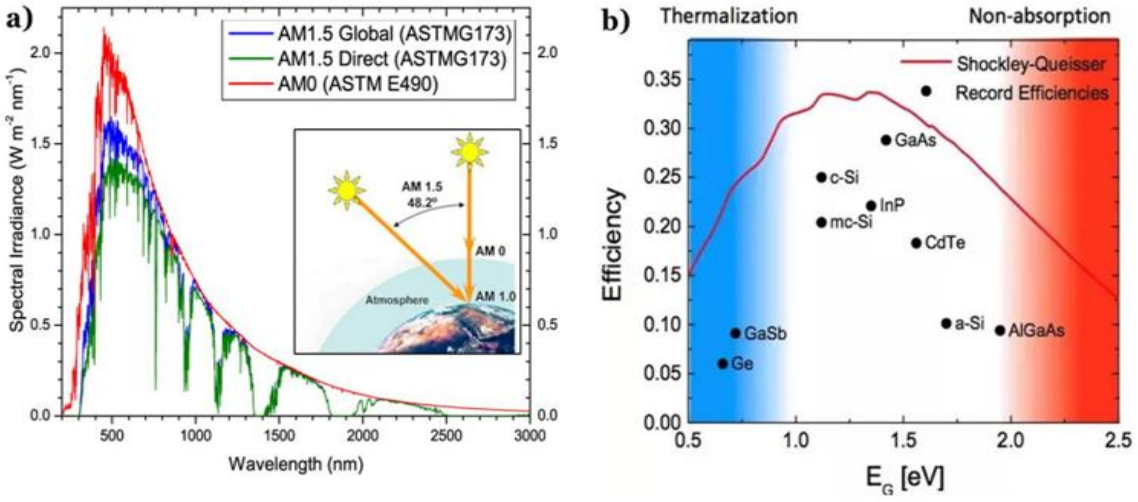

Figure. I.6: (a) Incident spectral radiation from the sun for terrestrial applications (AM1.5G and AM1.5D) and space applications (AM0); (b) Schockley-Queisser limit: maximum theoretical efficiency of a SC according to its band gap, with the best experimental efficiencies.

Indeed, we have been witnessing record efficiencies in all PV sectors. The traditional map published by NREL(National Renewable Energy Laboratory, USA) on the annual records, in the laboratory, of the yields of PV cells shows that PV will still keep a good growth trend over the coming years (Figure I.7).

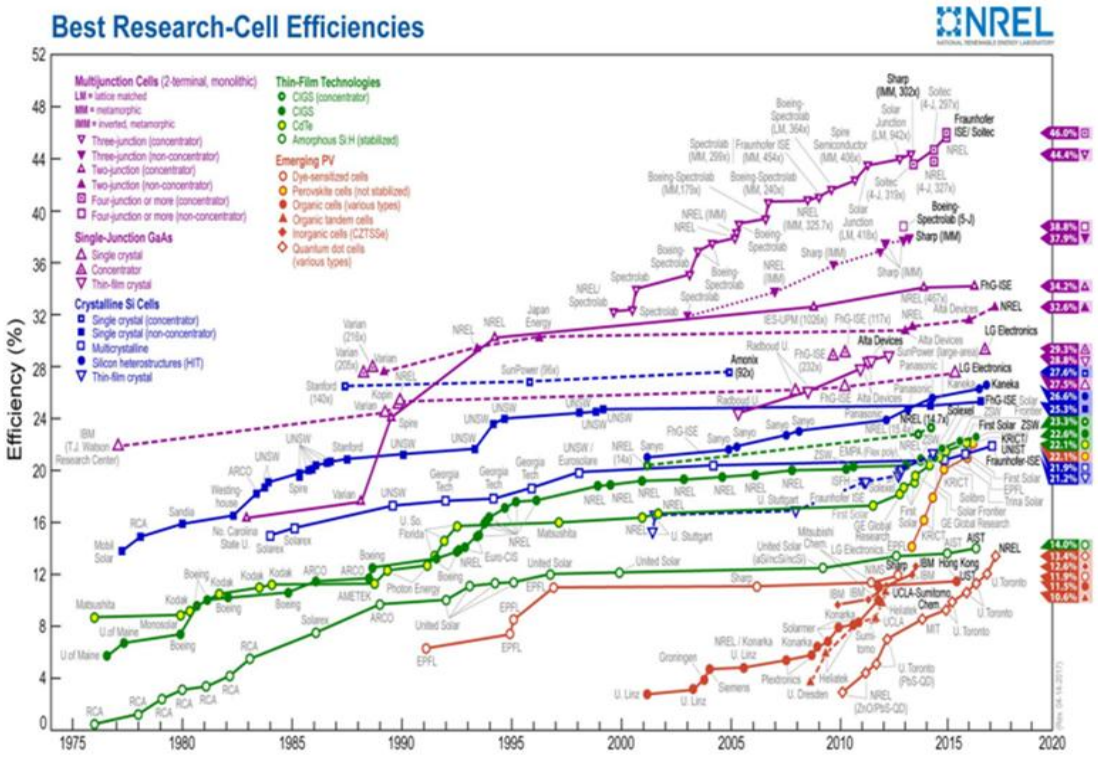

Figure. I.7: NREL graphic with temporal evolution of the best conversion efficiency of research cells for different technologies [11].

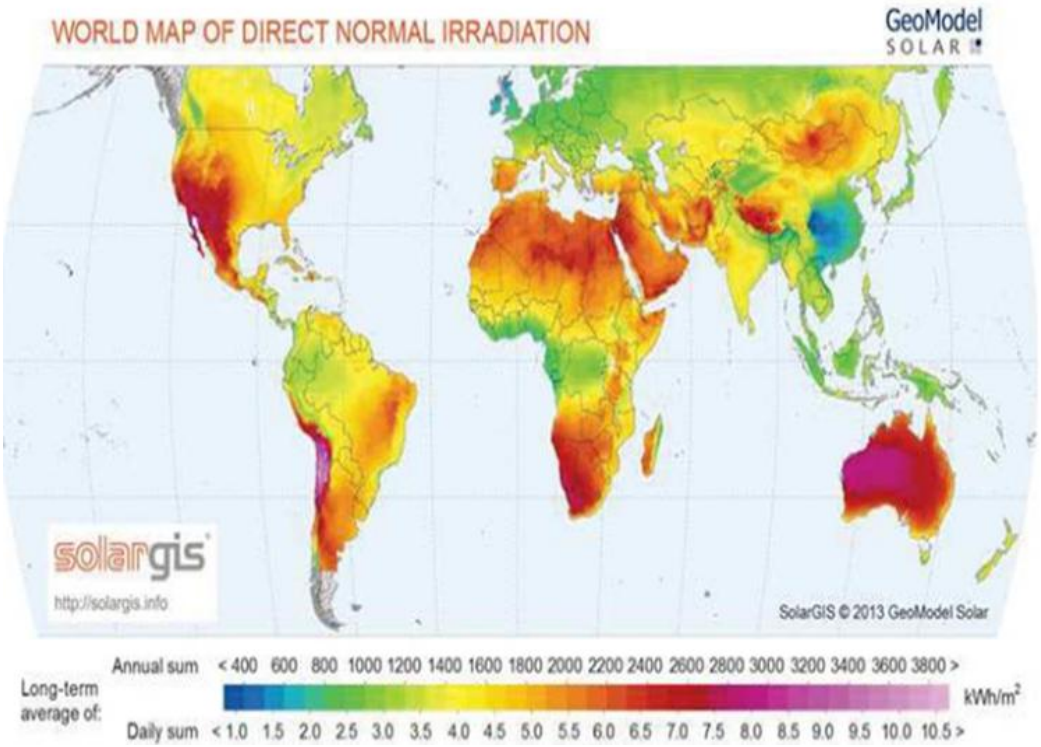

Figure. I.8: World map representing Direct Normal Irradiation energy (IND) [12].

I.2.4. Absorption in the optical state

The absorption of photons is the first step necessary for the PV conversion process. When a material is exposed to sunlight, the atoms exposed to the radiation are "bombarded" by the photons constituting the light, under the action of this bombardment, the electrons of

the upper electronic layers (called electrons of the valence layers) tend to be torn from their orbits. Returning to their initial states, their agitations result in heating of the material. The kinetic energy of photons is transformed into thermal energy.

However, in PV cells, some of the electrons do not return to their initial states but create a low dc electrical voltage. Part of the kinetic energy of photons is thus directly transformed into electrical energy: this is the photovoltaic effect.

On the other hand, and in order to understand the challenges of light management within SCs, let's take the example of an isolated absorbent layer of finite thickness. When a light beam is directed at such a layer, three mechanisms can intervene: the light can be reflected, transmitted or absorbed.

For a given light source, the relative importance of these three phenomena depends on the optical properties of the absorbent layer, the position of the source, the polarization state of the incident light and the wavelength considered if the material is dispersive (Figure I.9).

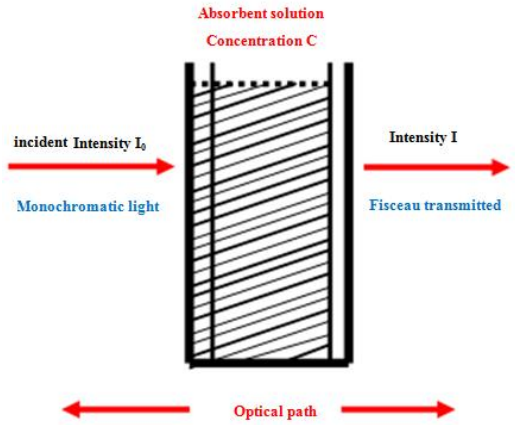

Figure. I.9: A monochromatic light passing through an absorbent solution of concentration C contained in a tank of thickness L.

In all cases, the principle of energy conservation must be respected. Thus, absorption A (or the fraction of absorbed photons) is limited to 1 and its value depends on both optical losses by reflection and transmission:

$$A(\lambda) = 1 - R(\lambda) - T(\lambda) \quad \text{(I.2)}$$

Where, R(λ) et T(λ) represent the fraction of photons reflected and transmitted at wavelength λ. It is a monochromatic light passing through an absorbent solution of concentration C contained in a tank of thickness L.

Some of this ray will be absorbed by the sample and some will be transmitted. Bouguer, Lambert and Beer studied the relationships between I_0 (incident intensity) and I (transmitted intensity). The intensity of a monochromatic light passing through a medium where it is absorbed decreases exponentially, and this intensity has the form:

$$I = I_0 e^{-KLC} \quad \text{(I.3)}$$

- I_0: is the intensity of the incident light;
- I: is the intensity after passing through the tank containing the solution (transmitted intensity);

- *L:* is the distance crossed by the light (thickness of the tank in cm);
- *C:* is the concentration of absorbent species;
- *K:* is a characteristic constant of the sample.

By posing: $I/I_0 = T$, the previous equation can be rewritten:

$$log(I_0/I) = KLC/2.3 = \varepsilon LC \quad (I.4)$$

- *Log* (I_0/I): is called absorbance (A);
- $I/I_0 = T$: is the transmission;
- *T*: is transmission;
- ε: is the molar extinction coefficient ($L.mol^{-1}.cm^{-1}$).

This is a characteristic of the substance being studied at a given wavelength. We then obtain the relation known as the Beer-Lambert law [13].

$$A = log(T) = \varepsilon LC \quad (I.5)$$

I.3. The operation of a solar Cell

The operation of a SC is based on the PV effect, *i.e.* the conversion of light energy into electrical energy. Light absorption allows the conversion of light into electrical charges, which are then collected by an external circuit.

The collection of charges (electrons and holes) requires their separation. In the case of a solar cell based on semiconductors (more particularly silicon), the structure used is the P-N junction: the potential difference created at the junction of two semiconductors of type N and P allows the separation of the carriers. Once the carriers are dissociated, they diffuse towards the end of the cell, causing the appearance of a voltage at the terminals of the latter. For more information on the physics of semiconductors, and more particularly photo piles, a lot of materials exist [14, 15].

The basic structure of a SC is shown in Figure I.10.a. It consists of a substrate of type P, base (whose majority charge carriers are the holes), an area in front face strongly doped N+, called (majority: electrons) [16].

The junction of these two zones shown by the bar graph (Figure I.10.b). It is in this zone that the carriers are separated: the minority positive charges (holes) in the transmitter. The opposite phenomenon occurs for electrons, which are a minority in the base.The scales used in the figure are not respected, the thickness of the emitter is a few hundred nanometres while the substrate, in other words the base, measures from 50 to 300µm. The anti-reflective layer allows, as its name suggests, to avoid the reflection of photons on the surface, and gives the front side its typical color, usually blue.

Then, are represented Figure I.10.a, in the form of a grid on the front side, and generally full plate on the back side, the metal contacts allowing the collection of loads to the external circuit.

I.3.1. Characteristic under illumination and parameters of the solar Cell

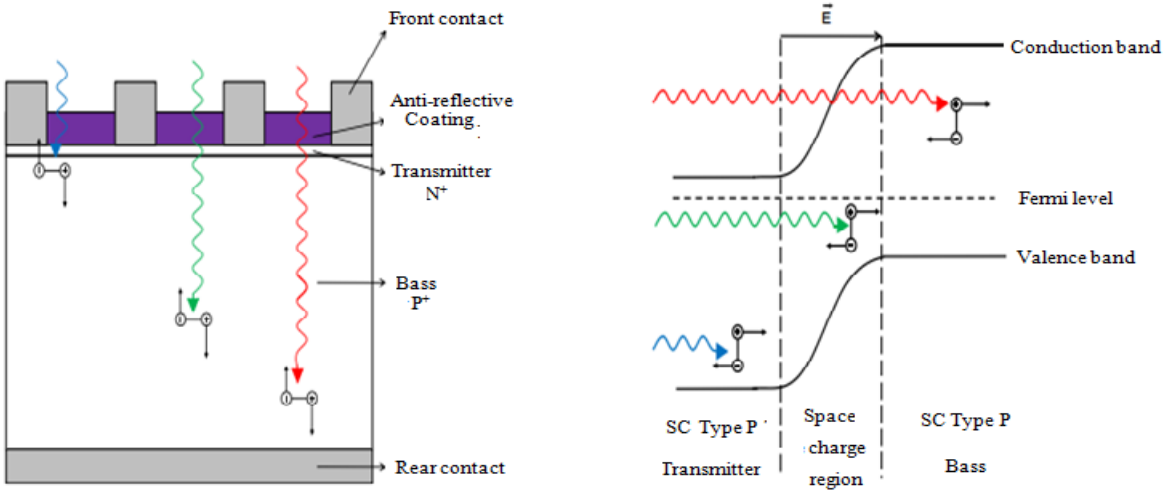

a) Cell structure b) Energy band diagram

Fig. I.10: Schematic diagrams of the operation of a SC with P-N junction.

The ideal I(V) characteristic of the solar cell contains two components [17]. The first highlights the behaviour of the P-N junction under polarization. The cell being under illumination, the second term shifts the characteristic of I_L, or the current resulting from the illumination:

$$I(V) = I_0 \left[exp\left(\frac{qV}{kT}\right) - 1 \right] - I_L \qquad (I.6)$$

- I_0: is the saturation current [A];
- q: the charge of the electron [C];
- k: the Boltzmann constant [eV.K^{-1}];
- T: the temperature [K];
- I_L: is the current resulting from the illumination [A].

This equation reflects a little better the actual characteristic I (V) of a SC, it is often called a two-diode model:

$$I(V) = I_{01} \left[exp\left(\frac{qV}{n1kT}\right) - 1 \right] + I_{02} \left[exp\left(\frac{qV}{n2kT}\right) - 1 \right] - I_L \qquad (I.7)$$

The first formula corresponds to the current produced by the quasi-neutral zones (transmitter and base) of the P-N diode, I_{01} is therefore the saturation current due to the diffusion of the carriers in these zones. n1 (without unit) is the ideal factor translating this diffusion, it is generally equal to 1.

The second formula corresponds to the generation/recombination current taking place in the SCZ. I_{02} is the saturation current in the SCZ. I_L is often called leakage current, since the current resulting from this diode is a tunnel current, or a recombination current via a defect in the SCZ. As for n2, it is the ideal factor translating generations/recombination, it is usually equal to 2.

Finally, as in equation (I.6), the third formula corresponds to the photo-generated current. Equation (I.7) is shown in Figure I.11. From this characteristic, the parameters specific to the PV cell (Vco, P_m, Icc, *ff*, η), extracted from the characteristic I(V), allow to compare different illuminated cells under identical conditions:

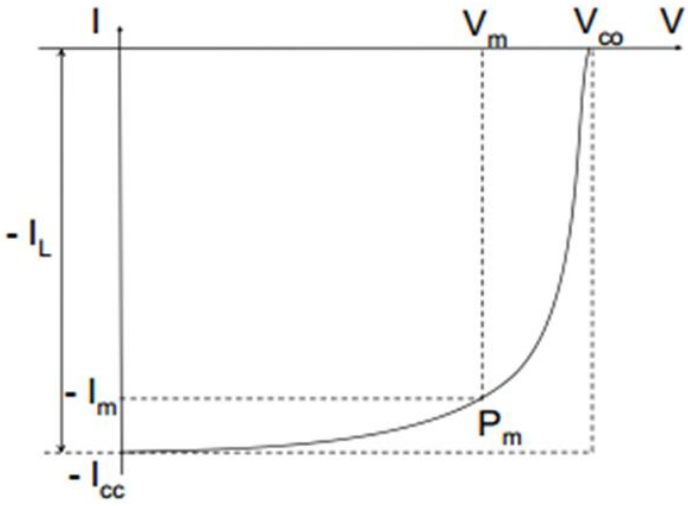

Figure. I.11: I(V) characteristic of a PV cell.

- **The short-circuit current (I_{cc}):** This is the current obtained by short-circuiting the terminals of the cell (taking V=0 in the equivalent scheme. It grows linearly with the illumination intensity of the cell and depends on the illuminated surface, the wavelength of the illumination, the mobility of the carriers and the temperature.
- **Open circuit voltage (V_{co}):** Open circuit voltage is obtained when the current flowing through the cell is zero. It depends on the energy barrier and shunt resistance. It decreases with temperature and varies little with light intensity. The voltage V_{co} is given by the relation:

$$Vco = \frac{kT}{q} ln(\frac{I_L}{I_0} + 1) \quad \text{(I.8)}$$

According to this, let us note here that the Vco depends greatly on the current of saturation I_0.

- **Maximum power (P_m):** The operating point is imposed by the load resistance and not by the cell itself. A judicious choice of load resistance will therefore make it possible to obtain the maximum power, *i.e.*:

$$Pm = Vm.Im \quad \text{(I.9)}$$

  Vm: the voltage corresponding to the maximum power supplied;
  Im: the current corresponding to the maximum power supplied.

- **The filling factor (*ff*):** The power supplied to the external circuit by a photovoltaic cell under illumination depends on the load resistance (external resistance placed at the terminals of the cell). This power is maximum for an operating point Pm (Im and Vm) of the current-voltage curve. It is defined by the following relation:

$$ff = \frac{Vm.Im}{Vco.Icc} \quad \text{(I.10)}$$

– **Efficiency (η):** The efficiency η of PV cells refers to the efficiency of conversion into power. It is defined as the ratio between the maximum ratio delivered by the cell and the incident light power [18].

$$\eta = \frac{Pm}{Pin} = \frac{Icc.Vco.ff}{Pin} \tag{I.11}$$

This efficiency can be improved by increasing the form factor, short-circuit current and open circuit voltage.

I.4. History

The PV effect achieves the direct transformation of electromagnetic energy (solar illumination) into directly usable continuous electrical energy. It was Antoine Becquerel who highlighted the appearance of a voltage at the terminals of two electrodes immersed in an electrolytic solution in 1839, when it was exposed to natural light [19]. Willoughby Smith discovered the photoconductivity of selenium in 1873. It was Werner Von Siemens who presented an article on the PV effect in semiconductors in 1875 at Berlin Academy of Sciences. In 1877 W. G. Adams and R. E. Day developed a solid junction based on selenium whose conversion efficiency was of the order of 1%. However, the first real vision of PV energy goes to Charles Fritts. In 1886, he wrote that PV cells use an energy source that is limitless, costless, and will continue to flood the earth after we finish consuming our fossil fuel reserves.

The scientific and technical world of the time, not having the knowledge in physics to understand the PV effect, concluded that Fritts' work violated the principle of energy conservation and therefore considered it fraudulent. It was not until the explanation of the photoelectric effect by Einstein in 1904 and quantum mechanics that the PV effect became a phenomenon recognized by the scientific community. In 1958, a cell with an efficiency of 9% was developed and, subsequently, the first satellites powered by SCs were sent into space. The efficiency of monocrystalline silicon reached 10% at the end of the 60s, then 14% in 1973. Since the 1990s, and for the reasons mentioned above, PV energy has aroused growing interest and many technological advances have been made so far through several technological sectors. PV electricity production has even increased exponentially since 2006 and projections are quite optimistic for the coming years (until 2030) as shown in Figure I.12.

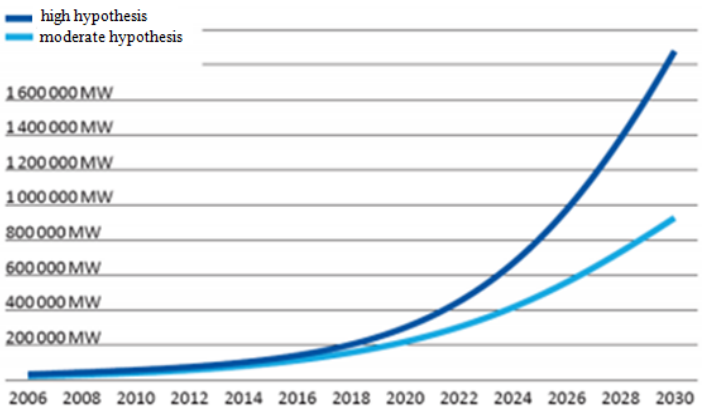

Figure. I.12: Cumulative overall PV capacity by 2030.

I.5. Generations of photovoltaic cells

The objective for PV cells is to access grid parity, i.e. the point from which the electricity delivered by a PV module has a price per kWh comparable to that provided by the grid.

This is a necessary condition so that their installation is no longer dependent on government subsidies and that they can impose themselves definitively on the energy market. If we consider here the PV module, two levers make it possible to lower the price/Watt-peak ratio and thus converge towards grid parity: on the one hand the decrease in the cost of manufacturing the cells and on the other hand the increase in their conversion efficiency. The figure. I.13 below presents the generations of the SC.

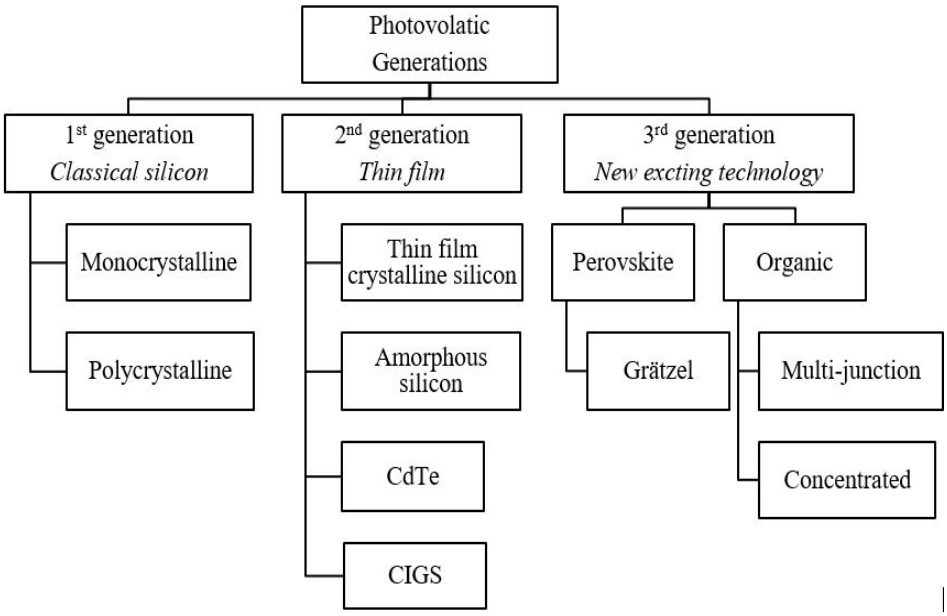

Figure.1.13: The PV cell generation.

I.5.1. First generation

They are large-area, high-quality and made up of first-generation single-junction solar cells. The reduction in production costs of this technology is cancelled due to high labor costs, and material costs especially for silicon. This generation of cells is based on the use of wafers made of monocrystalline silicon or multicrystalline silicon [20], (in the form of plates). It is based on very pure silicon, that is, cells requiring a lot of energy and which are very expensive. Its thickness varies between 180 and 200μm [21]. The lifespan of this generation is 35 years and have only one P-N junction. They enjoy relatively high conversion efficiencies thanks to the almost total absorption of light entering the cell and the bette electronic quality of the active materials. The material cost is their main limitation because it accounts for about 30% of the final price of the PV module [22]. It is made by putting molten silicon in cubic crucibles.

	Multi crystalline	**Monocrystalline**
Manufacture	Cooling of molten silicon in flat-bottomed crucibles, i.e. irregularly oriented crystals are formed, which gives the characteristic bluish appearance with patterns due to crystals.	Strict and progressive control of silicon cooling, requires strong monitoring, that is, obtaining very pure crystals.
Efficiency	10 to 15%	12 to 19%

	110 to 150 Wc/m²	120 to 190 Wc/m²
Benefits	Performance/price ratio.	Very good efficiency.
Disadvantages	– High cost. – Lower efficiency under reduced illumination. – Charge-carrying electrons, generated by sunlight, are partially lost in the volume of silicon due to the presence of residual impurities.	

Table I.1: The difference between the two types of silicon in the first generation.

I.5.2. Second generation

We present the second generation to solve these issues of energy needs and the production costs of SCs. Thin film battery technology has been imminent. A significant reduction in material costs is possible in this technology. They also have the advantage of increasing the size of the unit.

I.5.2.1. Thin film crystalline silicon

The new PV cells that make up the second generation of cells are composed of very little or no silicon. This is explained by the increase in the price of this material, which is abundant on earth. In addition, these cells are famous because they have been significantly reduced in thickness, which explains the ease of manufacturers to create PV panels that are very flexible, lightweight and easy to install.

This is why these cells are called thin film cells, because their absorbance zone is of the order of a few micrometers (0.2-0.35µm). Thus, second-generation cells are more practical, but they still work on the same principle as crystalline cells. We can therefore count several different materials in this new generation such as amorphous silicon (non-crystallized mineral substance, that is to say not having an ordered atomic structure), copper, gallium, selenium, zinc etc.

For example: CIGS (copper, indium, gallium and selenium), a cell devoid of environmental toxicity. A significant reduction in cell cost is allowed by reducing the amount of material required and depositing layers over larger areas [23] from low-cost glass, stainless steel or plastic substrates. Some materials can be deposited at low temperatures, which makes it possible to use flexible substrates. Depending on the electrical performance, thinning of the active layer leads to an increase in V_{co} by reducing the I0 saturation current of the diode that is the basis of the structure of the SCs and reducing the recombination of the charge carriers [21].

Hydrogenated amorphous silicon, which has long been at the forefront due to its hypersensitivity, is CIGS (for Copper Indium Gallium Selenium), which has a record for the production of thin-film cells. With an efficiency of about 20.3% and finally CdTe (cadmium tellurium). It is possible that a thin layer dependent on CdTe (cadmium tellurium) absorbs all the light over its entire useful spectrum with a thickness of about 2 µm [20]. This thickness will be greater than 10µm of a-Si:H due to the low absorption coefficient.

If we limit the thickness of the ultra-thin films to a few hundred nanometres to improve the productivity of the resulting image-carrying group, the active materials can be almost transparent over a wide spectral area.

I.5.2.2. Amorphous silicon cells

Amorphous silicon cells have a low efficiency but react very well even during low sunlight like the inside of a house. These cells appeared in 1976. They form the first cells of the second generation with a thickness of 0.1μm.

Advantages

- Thinner, between 200 nm and 350nm;
- Less expensive than the first generation since they consume less semiconductor material;
- Less polluting during manufacture;
- Operate with low illumination;
- Less sensitive to shading and temperature rises;
- Possibility of creating flexible panels that are easier to install.

The disadvantages

- Growing decrease in cell performance;
- Low efficiency due to the difficulty of moving energy due to the organization of atoms;
- Silicon atoms do not always form covalent bonds, so this disturbs the electronic properties of the material;
- The hydrogen atoms establish bonds with the electrons which have remained free, and thus reduce the number of dangling bonds.

I.5.3. Third generation

Research to improve the efficiency has led to the development of the third generation of solar cells [24]. The poor electrical performance of thin film technology by maintaining low production costs of this technology, non-semiconductor technologies (including polymer-based cells).

The concepts involved include tandem cells or cells containing hot vectors [23]. Switching from the first generation to the second generation has made it possible to reduce the cost of the cell returned to its surface as mentioned previously [21]. However, thin film cells have limited conversion efficiencies, mainly due to their low absorption. This fully confirms current studies which aim to increase absorption in cells from SC layers by introducing concepts from nanoparticles [25]. The objective is to reduce the efficiency gap between the first and the second generation but also to develop strategies likely to improve the management of light in the third generation cells.

I.5.3.1 Organic photovoltaic cells

The semiconductor studied is a polymer such as, for example, poly acetylene. The first organic PV cell appeared in 1985 and had an efficiency percentage of around 1%. It characterized by their development constitutes an attempt to reduce the cost of PV electricity, thinner, flexible, easy and less expensive to produce, while being, resistant, efficiency approximately between 8% and 10%. And for the advantages, we have a strong optical absorption, various substrates, and fairly simple deposition techniques.

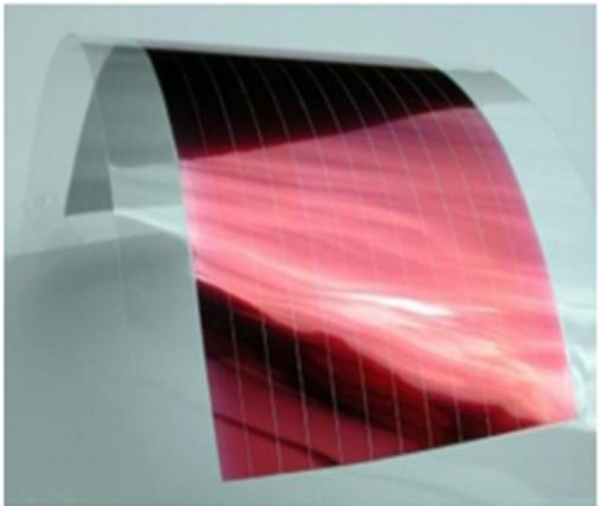

Figure. I.14: Organic PV cell of the 3rd generation.

I.5.3.2 Multi-junction photovoltaic cells

Multi-junction cells are made up of a large number of semiconductors each with a limited spectrum. Choosing materials that have wavelengths very close to each other will allow cells to absorb a larger and fuller spectrum that can achieve efficiency of up to 50%.

Multi-junction cells will make it possible to invent new techniques for producing electricity through solar panels. A semiconductor like silicon can only produce electricity from a certain wavelength of the sun's ray. Thanks to new scientific methods, it is anticipated that the solar rays can be exploited by nearly 80% thanks to these multi-junction cells. This would constitute a great improvement in the efficiency of PV panels today.

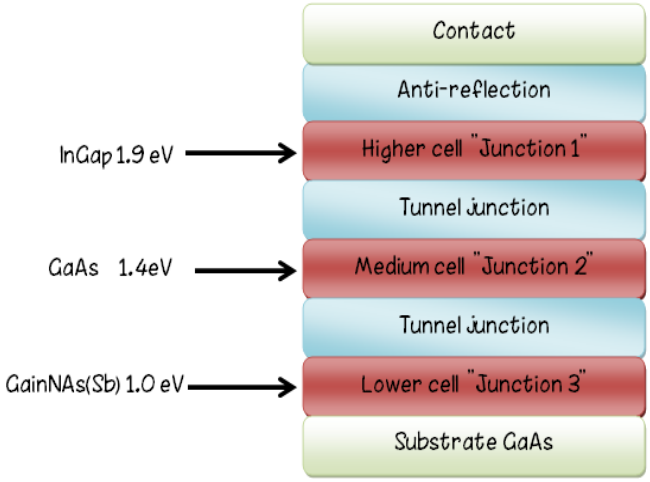

Figure. I.15: Third generation multi-junction PV cell.

Record efficiency: around 40% and maximum 50%. But also there are disadvantages which are: developed for space applications, this type of cell is not yet marketable, requires the use of rare metals, their manufacturing cost is high.

I.5.3.3. Concentrating photovoltaic cells

Figure. I.16: Third generation concentration PV cell.

Concentrated PV plants use optical lenses that focus light on small, high efficiency PV cells. To function, it is necessary to follow the sun throughout the day with a mechanical swivel system. Concentration is obtained by a system of parabolic mirrors or Fresnel lenses, as on automobile headlights.

This technology was first reserved for satellites and space exploration. Then, it was tested in a few prototypes and pilot operations. The efficiency is approximately greater than 50%. This technology is only economically viable today in areas where the sun is very strong. The concentrated light must be well focused on the cell. They are more complex, more fragile, and more delicate to transport and to assemble; require the use of precious metals.

I.5.3.4. Perovskite cells

A perovskite PV cell is a type of PV cell that includes a chemical element with a perovskite structure, most often an organic-inorganic hybrid of lead or a tin halide, in its active layer [26]. Efficiency increased from 3.8% in 2009 [27], 24.2% in 2019 [28] and 28% for the tandem of perovskite and Silicon [28]. Perovskite is one of the promising materials at the moment and could replace silicon in solar panels. Perovskite can be deposited in solution. This allows the realization of PV cells of large surfaces. The commercialization of perovskite cells is based on improving the cost of the installation compared to silicon and organic technologies.

A perovskite SC consists of a glass/FTO substrate with fluorine-doped tin oxide FTO deposited on it, and titanium dioxide TiO_2 on FTO. TiO_2 is used to improve electron transport. The active layer is made of a perovskite material. To improve hole transport, a layer of Spiro-OMeTAD is deposited between the electrode and the active layer.

Figure. I.17: Structure of PV or perovskite cell.

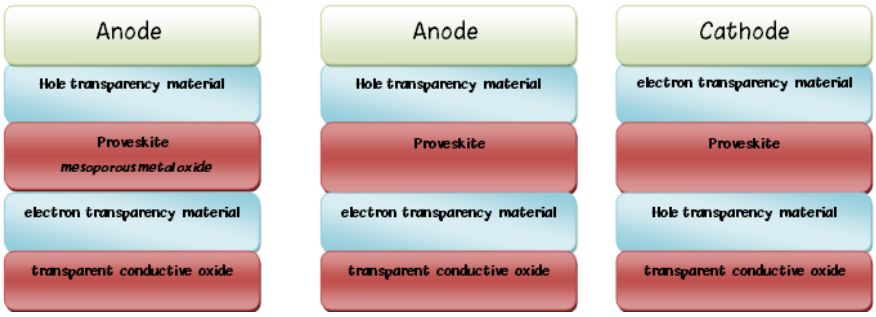

Figure. I.18: Different structures of a perovskites cell.

I.5.3.5. Grätzel PV cells

The Grätzel cell or *dye-sensitized solar cell* (DSSC), is named after its creator, the Swiss chemist Michael GRÄTZEL. They are not currently the most efficient on the market, but they can be produced with low-cost materials and could benefit from technical and design advances. They also have the advantage of being able to produce energy even without direct sunlight or even under low lighting [29]. Unlike conventional PV, light absorption and charge transport are two separate tasks in Grätzel cells, whose operation is inspired by photosynthesis. The light is absorbed by a photosensitive pigment, called dye, deposited on the surface of titanium oxide nanoparticles TiO_2.

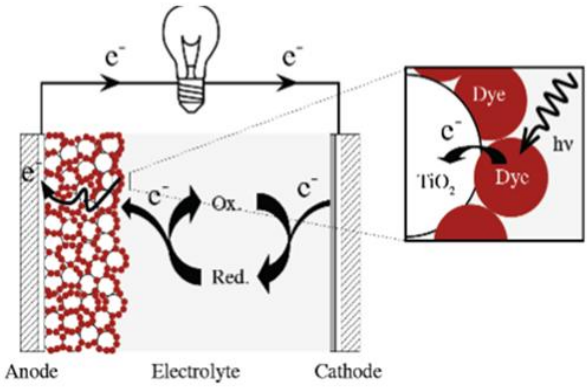

Figure. I.19: The principle of operation of a Grätzel cell.

The coloring dye, adsorbed to the surface of TiO_2, absorbs energy photons that cause it to move from an electronic state to an excited state. Relaxation is done by transferring the excited electron to the conduction band of titanium dioxide. The electrons thus injected pass through the thin layer of TiO_2 to an electrode, the anode, and circulate in an external electrical circuit.

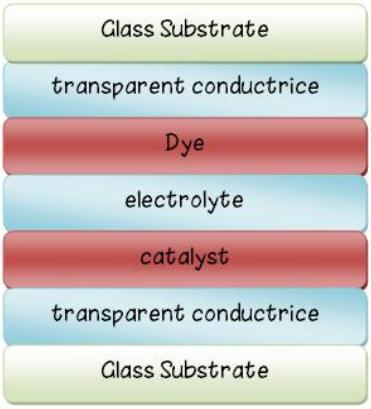

Figure. I. 20: Grätzel Cell.

Highlights:

- Low cost;
- Energy-efficient manufacturing process (energy debt between two and four months);
- Performance stability at high temperatures and over time (estimated service life of 20 years);
- Possible operation in diffuse light or with low illumination;
- Flexible and lightweight;
- Aesthetics: transparency and colors to choose from.

Weaknesses:

- Limited maximum efficiency (11% in the laboratory, compared to 25% for a conventional Monocrystalline silicon cell);
- No feedback on an industrial scale.

Type	Cell efficiency (in the laboratory)	Module (in the laboratory)	Module (commercial)	Level of development
First generation				
Monocrystalline Silicon	24.70 %	22.70%	12-20%	Industrial production
Poly crystalline silicon	20.30%	16.20%	%11-15	Industrial production
Second generation				
Amorphous Silicon	13.40%	10.40%	5-9%	Industrial production
Thin-film crystalline silicon		9.40%	7%	Industrial production
CdTe	19.30%	13.50%	9-11%	Ready for the production
CIGS	16.70%		6-9%	Industrial production
Third generation				
Organic Cell	5.70%	8-10%		Under research
Pérovskite Cell	24.20%	14.24%		Under research
Grätzel cell	11%	8.40%		Under research
Concentration cell	46%	43.6%		Under research
Multi jonctions cells	39%	25-30%		Under research

Table I. 2: Data of three generations of SCs [30].

I.6. Solar cell design and architecture

There are several types of cells that differ in the materials used to build them. Apart from the price, the choice of a type of cell has few consequences for the user, the main difference will be the surface which, at equal power, can vary from single to double.

I.6.1. Silicon solar cells

Silicon is now the most widely used material in PV cells. It is obtained by reducing silica, which is the most abundant compound in the earth's crust, especially in sand or quartz. The first step is the production of what is called metallic silicon, which is only 98% pure, and is obtained from pieces of quartz from gravel or intravenous deposits.

I.6.1.1. Monocrystalline cells

Monocrystalline silicon cells offer the best efficiency among commercially available solar panels: between 13 and 15%. It would therefore take fewer cells to achieve the required energy, but as monocrystalline silicon is also more expensive, its only advantage is that in the end we use a reduced surface area: it takes about 7 square meters to obtain 1 (kW) [31].

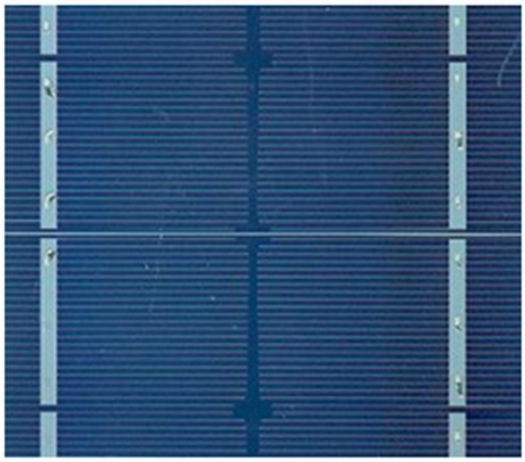

Figure. I.21: Monocrystalline PV cell.

I.6.1.2. Polycrystalline cells

Modules using polycrystalline silicon cells generally have an efficiency of between 12 and 14%. About 8m² of cells are needed to obtain 1kWp. These cells are simpler to manufacture and less expensive than monocrystalline silicon cells [32]. Polycrystalline cells can be recognized by the irregular shapes of the crystals that are clearly visible.

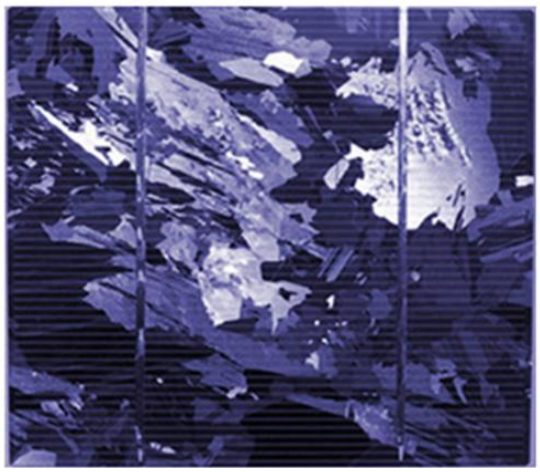

Figure. I.22: Poly-crystalline PV cell.

I.6.1.3. Amorphous cells

Amorphous silicon cells are thin film cells, that is they are made by depositing a thin layer of silicon on a substrate. The thickness of this type of silicon used is much smaller than for monocrystalline or polycrystalline cells which are made from silicon wafers. This type of cell is therefore cheaper and easier to manufacture. Their low thickness makes it possible, for example, to use them to create flexible solar panels. It has a limited efficiency (of the order of 5 to 7%, or about 15m² to obtain 1kWp) and is therefore reserved for applications requiring little power [33].

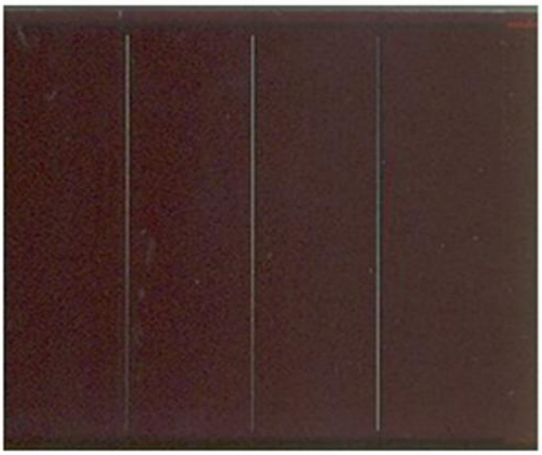

Figure. I.23: Amorphous PV cell.

I.6.2. Thin film solar cells

I.6.2.1. Copper-indium-di-selenium (CIS) or copper-indium-gallium-selenium (CIGS)

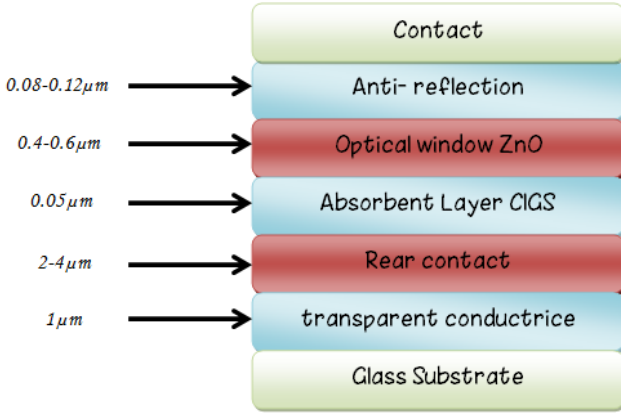

Figure. I.24: Simple structure of a CIGS-based cell.

This type of PV cell uses a semiconductor material made of an alloy of copper, indium, selenium and gallium. This mixture is placed in a very thin layer on the support. It represents the new generation of PV cells. First, it offers a very attractive return, between 10 and 20%. One of the main advantages is that it is made with materials other than silicon and is less toxic. In addition, the support used can be flexible, in order to capture as much sunlight as possible. However, to obtain a better efficiency, it is necessary to provide a larger surface area than other types of cells [33].

I.6.2.2. Cadmium-tellurium (CdTe)

This model is characterized by PV cells having an efficiency of 10.5% (15.8% in vitro) as well as a high absorption. It uses advanced technology to develop the performance of solar panels. The stake is doubly interesting, because it also makes it possible to reduce costs. With a low thermal modulus, this type of cell is made up of toxic products, which is a major disadvantage [33].

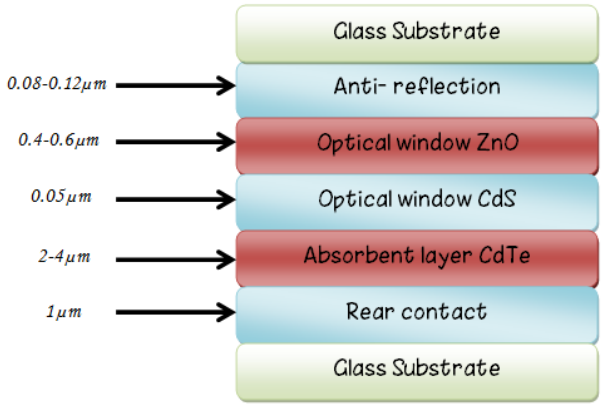

Figure. I.25: Structure of a CdTe PV cell, The P-doped absorbent layer lies under another N-doped semiconductor (CdS), the two layers form a heterojunction.

I.6.2.3. Gallium Arsenic (GaAs)

This type of PV cell uses a semiconductor material such as other efficiencies that it achieves in terms of conversion efficiency 28.8% in single junction GaAs (and now 31.6% in double junction GaAs), it is distinguished by its flexibility [34]. GaAs SCs display better temperature behaviour, these cells, which are very expensive and very popular in the aerospace industry.

I.6.3. The classical substrate structure

The structure of the classic SC is also called "*the standard structure*". As shown in the figure. I.26, the substrate structure is composed of:

- A rear metal molybdenum electrode 0.2 to 1µm thick deposited on a glass substrate.
- An absorbent layer whose thickness can vary from 1 to 3µm.
- A buffer layer with a thickness of 0.01 to 0.1µm each, ensuring respectively the junction and the absence of short circuits.
- An optical window with a thickness of 0.3 to 0.6µm that must combine two essential properties, namely electrical conductivity and optical transparency.
- A front metal grid needed for current collection.

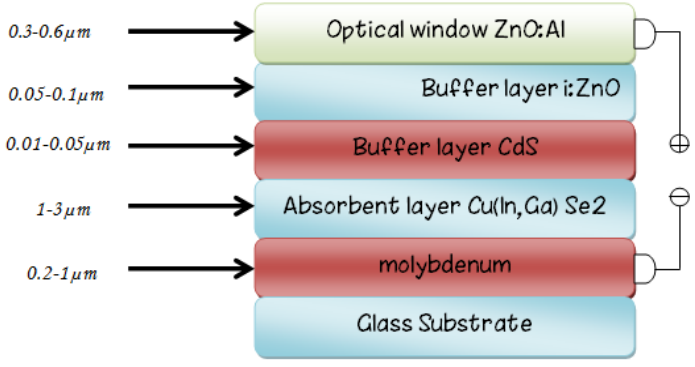

Figure. I.26: Structure of the classical cell [34].

I.6.3.1. Optical window

The optical window must be simultaneously transparent and conductive in the field of the solar spectrum, the transmission of the layers must be greater than 80% and the conductivity greater than 10^4 ($\Omega.cm^{-1}$). In a thin layer, such properties are obtained by

using compounds belonging to the family of transparent conductive oxides (TOC), the most common of which are: SnO2, SnO2:F, In2O3:Sn (ITO) and ZnO:Al (ZAO).

Their transparency is linked to the value of their forbidden band while their electrical properties depend on the composition of the layers and any doping. Generally, a first undoped layer of ZnO is deposited followed by a second layer of either ZnO or ITO (indium tin oxide). The ZnO (non-conductive) layer can be avoided by depositing a thicker buffer layer [34].

I.6.3.2. Buffer layer

The buffer layer is located between the absorbent layer and the optical window. If an absorbent layer/optical window contact is made directly, a PV junction may exist. Its performance will be limited by the mismatch of the forbidden bands and the leakage currents due to the presence of disordered areas at the grain boundaries. Therefore, it is preferable to introduce a thin layer, called a buffer layer, between these two compounds in order to optimize the performance of the cell. This layer must have the following properties:

- An intermediate band gap allowing a "flexible" transition between that of the absorber and the optical window, the value of which is between 2.4 and 3.2 eV.
- N-type conductivity to form the junction with the absorbent layer. In addition, to avoid the effects of current leakage, its conductivity must be lower than that of the absorbent layer by around 10^{-3} ($\Omega.cm^{-1}$).
- It must be morphologically very homogeneous and compact to avoid any short-circuiting effect at the grain boundaries of the absorbent layer.

I.6.3.3. Absorbent layer

The P or N type of absorbent layer has a high absorption coefficient of around 10^{-5} cm^{-1} in the visible range. The band gap is therefore direct but with an optimal value of 1.5 eV. Its conductivity should be in the range of 1 to 10^{-2} ($\Omega.cm^{-1}$).

I.6.3.4. Molybdenum

Molybdenum (Mo) is a preferred back contact material for SCs because it does not react strongly, it forms an ohmic contact with low resistivity, and the conductivity of molybdenum does not degrade upon deposition at high temperature of the SC substrate [35].

I.6.4. Superstrate structure

The term superstrate refers to a solar cell configuration where the glass substrate is not only used as a supporting structure but also as a window for lighting and as part of the encapsulation. During operation, the glass is on top of the actual SC.

The first CIGS superstrate solar cells were grown by spray pyrolysis, the ITO buffer layer, CdS buffer bilayer and absorbent layer were all spray deposited. The absorbent layer was produced in a bilayer rich in Cu and poor in Cu, in order to create a homo-junction inside the absorbent layer. SCs have been prepared by applying back contact and have achieved efficiencies of up to 3% [36].

The insertion of a sprayed ZnO layer between ITO and CdS has been investigated and further improvements in deposition processes have resulted in yields of 5% [37]. It has also been attempted to replace ITO with a layer of ZnO:Al or In [38]. The so-called bilayer process should give a large particle size and low density of defects in the region near the interface. Superstrate SCs grown by vacuum evaporation directly on the front ZnO contact have achieved open circuit voltages of over 800mV and efficiencies of around 3% [39].

The temperature of the substrate during the growth of the CIGS absorber has a great influence on the performance of the cells, a low density of carriers as well as a high concentration of deep defect states have been found by defect spectroscopy [40]. Superstrate cells with a transparent front contact window layer and CdS buffer layer showed yields of 6.7% for evaporated CdS and 8.1% with chemically deposited 8.1% CdS [41]. Electroplating has been used successfully for the fabrication of CIS superstrate SCs on ITO with In_2Se_3 buffer layers (also produced by electroplating), achieving efficiencies of up to 3.4% [42, 43].

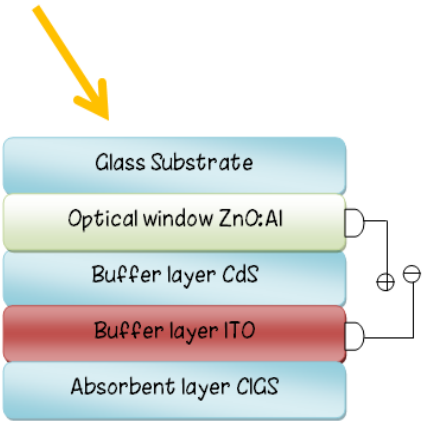

Figure. I.27: Superstrate structure of the SC in Glass, ZnO: Al, i-ZnO, CIGS in thin layers [34].

I.6.5. Tandem cells

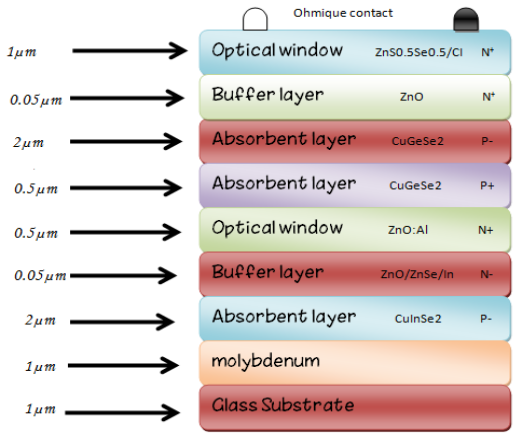

Figure. I.28: Tandem cell based on CuInSe2 and CuGaSe2 [34].

The tandem PV cell is designed from two simple semiconductor layers. This can be a layer of amorphous Si and another of crystalline silicon (mono or poly) for example. It shows all its interest for industrial use [34]. The efficiency of this type of cell is interesting, but its complex manufacture makes it an expensive PV cell to produce. As with all other models,

the cleaning of the solar panel must be optimal in order to enjoy consistent performance and better longevity.

I.6.6. Organic photovoltaic cells

These photovoltaic cells are made of synthetic semiconductor materials. They are known as dye cells, polymer cells or perovskite cells. The performance of organic solar cells depends on many parameters, such as absorption, charge transport, exaction diffusion length, interface states, etc [44]. These PV cells are made from thin organic layers which are deposited in a liquid solution placed between two electrodes. The low cost of manufacture and the non-toxicity of the renewable materials used make it a very attractive solution for the future. A polymer-based solar cell consists of a glass substrate, an anode generally made of ITO (Indium-doped Tin Oxide), an active layer consisting of a conjugated polymer and a metal cathode [45].

The active layer can be made up of:

– A *single type of semiconductor (N or P type*): the structure thus formed is said to be of the Schottky type. The dissociation of the photo-generated carriers occurs at the interface of the semiconductor with the metal electrode. The drawbacks of this type of structure are the small thicknesses of the photoactive region and the migration of charges in the same material, which implies significant recombination of charges [46].

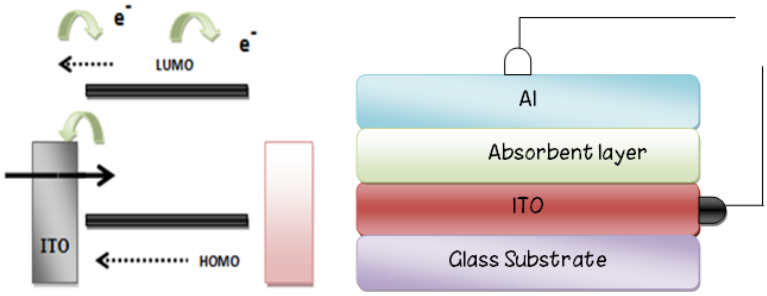

Figure. I.29: Structure of a Schottky-type cell (right) and representation of ITO/organic material /Al energy levels (left).

– Two semiconductors of different types: the structure thus formed is said to be of the heterojunction type. The dissociation of the photo-generated carriers then takes place at the interface of the two semiconductors. This same structure can be achieved by:
A bilayer system (two superimposed layers) in which the donor material (or type P) is in contact with the ITO, and the acceptor material (type N) with the metal electrode (Al). The exaction dissociation zone is located at the interface between these two layers.

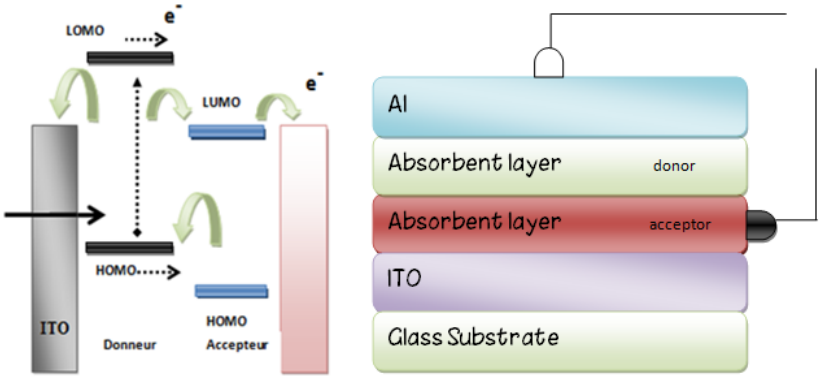

Figure. I.30: Structure of a heterojunction cell (right) and representation of the energy levels of an ITO / donor / acceptor / Al contact (left).

Cells of this type have a larger D and A interface (Donor /Acceptor). Exactions also reach dissociation sites faster [47]. The disadvantage of this type of structure lies in the mastery of the morphology of the structure.

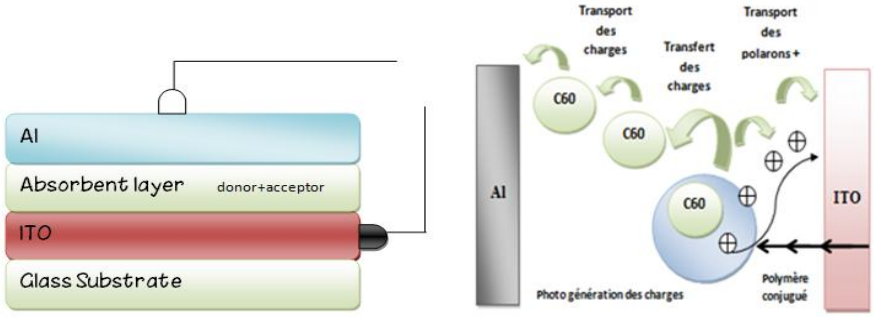

Figure. I.31: Structure of an interpenetrating grating cell (a) and (b) load transfer mechanism [48].

I.6.7. Bifacial cells

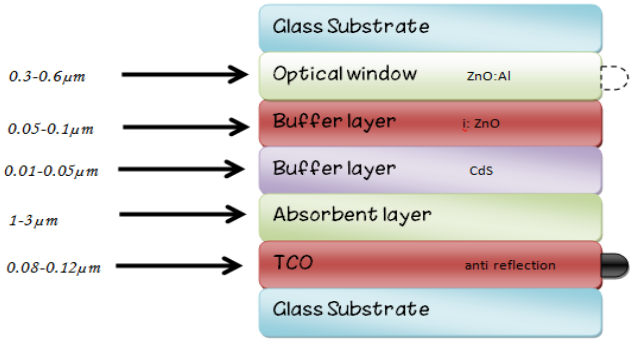

Figure. I.32: Schematic representation of the structure of a BSF bifacial SC [49].

I.6.8. Cell with CdTe band structure

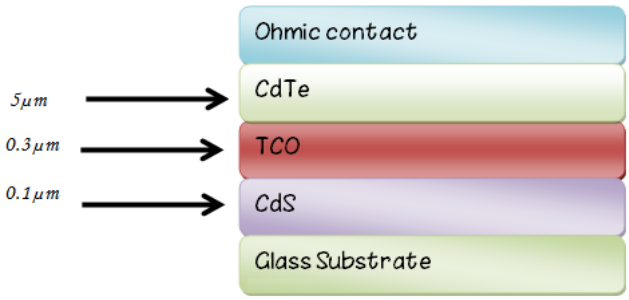

Figure. I.33: Typical structure of a SC based on CdTe active layer [50].

The conversion efficiency is of the order of 16% in the laboratory. On the other hand industrial modules have efficiencies of the order of 10%. The junction is ensured by a layer of CdS. For environmental reasons, this process is always taken with great caution because the use of cadmium for the production of the SC is still the target of several criticisms. Indeed, Cd is an environmentally polluting material [50].

I.7. The art state

Solar energy is an abundant form of potential energy sources, as the Earth collects all of the world's annual energy production, and for this reason PV technology aims to convert these latter abundant resources into electricity. However, recent and ongoing efforts by the PV community have spawned new solar cell concepts such as multiple connections and hot SCs.

I.7.1. Material properties and silicon deposition

I.7.1.1. Structural properties of a-Si:H

Crystalline silicon has the same crystal lattice as diamond. Each tetrahedral silicon atom has four neighbours. This tetrahedral structure stretches a great distance, thus forming an ordered crystal lattice (crystal). It is created by the strict repetition of a periodic elementary cell. In a-Si, variations in the lengths and angles of the bonds have the effect of making the structure of the material random. The fact that the structure is not ordered over long distances implies that the periodicity criteria are no longer met. In a-Si, we observe dangling bonds, i.e. bonds of atoms not linked to their neighbouring atoms. These dangling bonds represent defects in the material, when they are not passivated by hydrogen atoms. Passivation of pendant bonds with hydrogen decreases the density of defects by orders of magnitude, from 1025-1026 to 1021-1022 m^{-3} [51]. SCs based on a-Si:H have a low level of defects (~1022 m^{-3}). However, the presence of hydrogen is associated with degradation of the material by prolonged exposure to light.
This effect is known as the Staebler-Wronski effect [52]. One of the main advantages of a-Si:H over c-Si is the production technique.

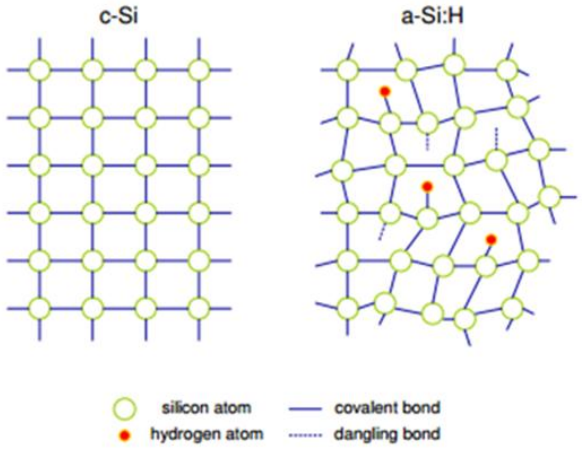

Figure. I.34: Schematic representation of the atomic structure of crystalline silicon (in the left) and amorphous silicon (in the right).

I.7.1.2. Structural properties of µc-Si:H

Hydrogenated microcrystalline silicon (µc-Si:H) is a composite material consisting of crystalline regions, columnar grain boundaries, disordered regions (areas amorphous) and interstices [53, 54]. It must be differentiated from polycrystalline silicon which is composed only of grains of crystalline silicon. µc-Si:H is also known as nanocrystalline silicon (n-Si). A schematic representation of µc-Si:H is given in figure I.35. Under the conditions of high crystallinity, obtained with a low concentration of silane, columns made up of grains of homogeneous crystalline silicon are observed. Depending on the deposition conditions and the substrate, the columns are separated from each other by a-Si:H regions or interstices [55]. As the silane concentration increases, the crystal volume fraction decreases and smaller crystalline silicon grains are observed within an amorphous silicon matrix. For SCs based on µc-Si:H, the composition of the material chosen is that corresponding to the transition zone between the amorphous and crystalline phases [56]. The presence of grain boundaries, amorphous regions and interstices between the grains of crystalline silicon leads to lower mobility than in the case of poly-Si.

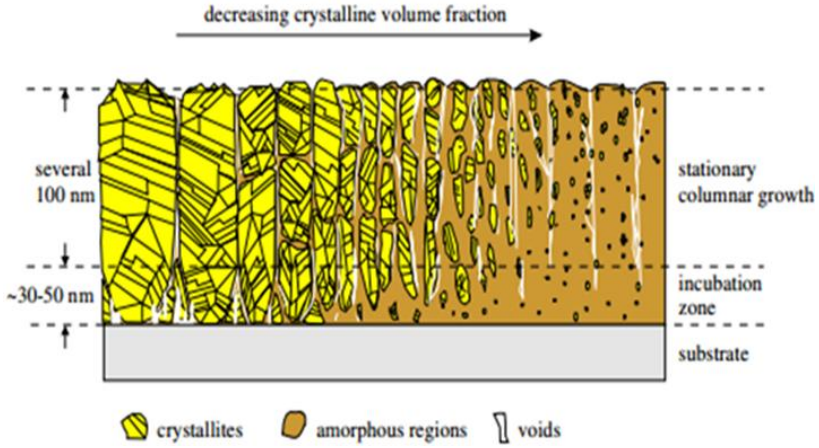

Figure. I.35: Schematic diagram showing the particular microstructure of µc-Si:H, obtained at high frequency by PECVD. From left to right, the composition of the film varies from highly crystalline silicon with a largely amorphous phase [57].

I.7.1.3. Optical properties of c-Si

c-Si has a gap of 1.12eV at ambient temperature and atmospheric pressure. It is an indirect gap semiconductor.

The minimum energy of the conduction band is not at the same time k as the maximum of the valence band.

For direct transitions of electrons from the valence band to the conduction band, the energies of the photons must be much greater than those of the band gap.

Optical transitions can also occur at lower energies by a two-step process involving not only photons and electrons but also phonons.

I.7.1.4. Optical properties of a-Si:H

Since in a-Si:H the conservation of the momentum k is no longer conferred during electronic transitions [58], the material behaves like a quasi-direct semiconductor.

It has a much higher probability of light absorption in the visible (photon energy greater than 1.8eV) than c-Si.

Thus, for a-Si:H films, thicknesses of around 500nm are sufficient to efficiently absorb light waves of wavelength $\lambda \leq 600$ nm.
For energies below 1.8eV, absorption in a-Si:H is determined by the density of localized states (surface states) and dangling bonds (deep defects) of the material.

I.7.1.5. Optical properties of µc-Si:H

The optical absorption spectrum shown in Figure I.36 shows an absorption coefficient higher for µc-Si:H than for c-Si, in the visible range (*i.e.*, for energies greater than 1.8eV). This effect can be explained by the light absorption of amorphous regions of the material and by the phenomenon of light scattering within the µc-Si:H [59, 60]. Between 1.1eV and 1.6eV, µc-Si:H has an absorption coefficient close to that of c-Si. Thus, its absorption is greater in the red and infrared compared to the case of a-Si:H. In the band gap absorption zone (*i.e.*, for energies less than 1.1eV), the absorption coefficient of µc-Si:H greatly exceeds that of c-Si and is slightly more higher than that of a-Si:H. This results from the presence of localized bands (at grain boundaries) and deep defects, similar to those found in a-Si:H [61].

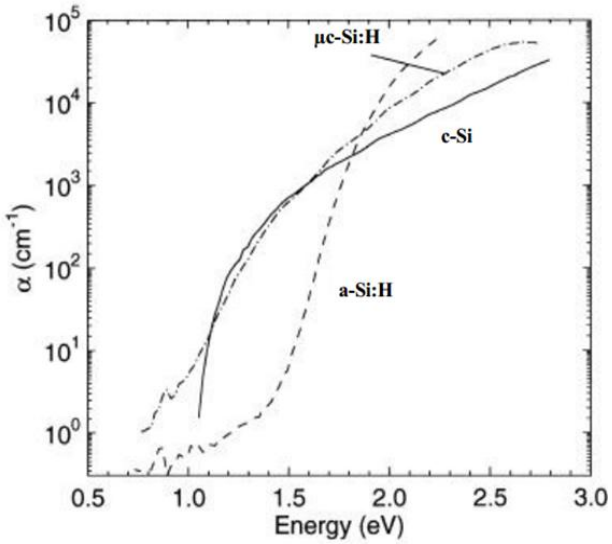

Figure. I.36: Absorption coefficient α of c-Si, a-Si:H and µc-Si:H, measured by photo thermal deviation spectroscopy (PDS). The data comes from the work carried out by [62].

I.7.2. Principle of operation of solar cells

I.7.2.1. Crystalline Silicon

Thin film SCs, *i.e.*, a-Si:H or µc-Si:H, are here compared to conventional SCs based on crystalline silicon (c-Si). These cells are generally based on a P-N junction, obtained by varying the type of doping in the semiconductor.

During light absorption, electrons are excited from the valence band to the conduction band, creating a hole in the valence band. The two types of carrier, electrons and holes, move through the crystal and participate in the photon.

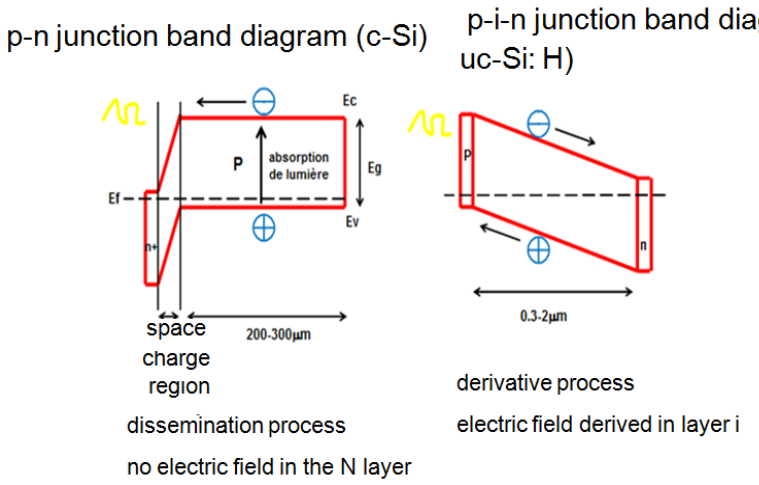

Figure. I.37: (Left) Band diagram of a P-N junction representing the case of a SC based on c-Si, (Right) band diagram of a P-I-N diode corresponding to the case of SCs based on a-Si:H and µc-Si:H.

Electrons and holes resulting from light absorption in solid material can diffusing into the space charge zone and the tail contact, respectively. The difference in potentials between the p and n layers is at the origin of the formation of the space charge zone, exhibiting a high electrostatic field. This is associated with the P-N junction and depends on the doping level. It generally has a thickness of less than 1µm for a SCs based on c-Si.
Due to the mode of movement of charge carriers (by diffusion), crystalline silicon SCs are still called “diffusion PV cells”.

I.7.2.2. Thin films of Silicon

Unlike the case of c-Si, a-Si:H is a material that shows high density defects and therefore short diffusion lengths. In addition, it exhibits a distribution of defects which depends on the position of the Fermi level.

Therefore, a P-N type configuration is not possible for this material [63]. SCs based on a-Si:H consist of a stack of P-I-N or N-I-P layers. An intrinsic (unintentionally doped) absorbent layer with low defect density is inserted between the P and N thin layers. For µc-Si:H based PV cells, exhibiting longer scattering lengths than a-Si:H, a P-I-N or N-I-P configuration is also more suitable.

I.7.3. Equivalent circuit for a P-I-N diode

Figure I. 38, shows a simple equivalent circuit of a pin diode that can be used as a model for thin film silicon SCs. Under illumination, an additional photonic current and of opposite direction I_{ph} is delivered by the cell. The losses in the diode can be represented by a resistor in parallel R_p and a resistor in series R_S. The parallel resistance accounts for local short circuits (shunts) and depends on the light power. The capacitance C_p is associated with the geometric capacitance of the SC. It is related to the surface of the cell and the thickness of the intrinsic layer by equation I.14:

$$C_p = \varepsilon_r \varepsilon_0 \frac{A}{d_i} \qquad \text{(I.14)}$$

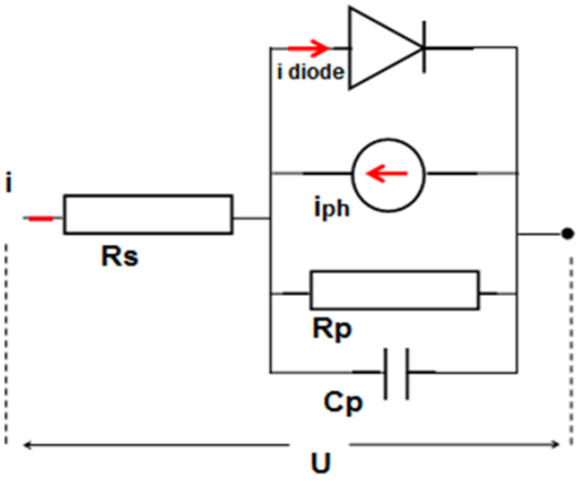

Figure. I.38: Equivalent circuit for a P-I-N diode.

I.7.4. SCs in P-I-N and N-I-P configuration

In this work, thin-film silicon solar cells were engineered in two different configurations, namely a P-I-N configuration and a P-I-N configuration. N-I-P. Figure I.39 shows the basic schematic structure used for the cells of reference (*i.e.* no nanoparticles or no nanostructures) in both configurations. A detailed description of SCs is given in the text when their structure base is changed. The names P-I-N and N-I-P only refer to the order of deposition of the N-I-P layers. As a result, it is mainly the response in the blue that is altered [64].

Since the mobility of the holes in the a-Si:H and µc-Si:H is smaller than that of the electrons, the holes must have the smallest possible distance to travel towards the P junction to achieve an optimal collection. However, there is no fundamental difference in the operation of the two configurations since the response in the red is practically independent of the side where the illumination is on. The differences found for the two configurations result from the difference in growth of the deposited layers.

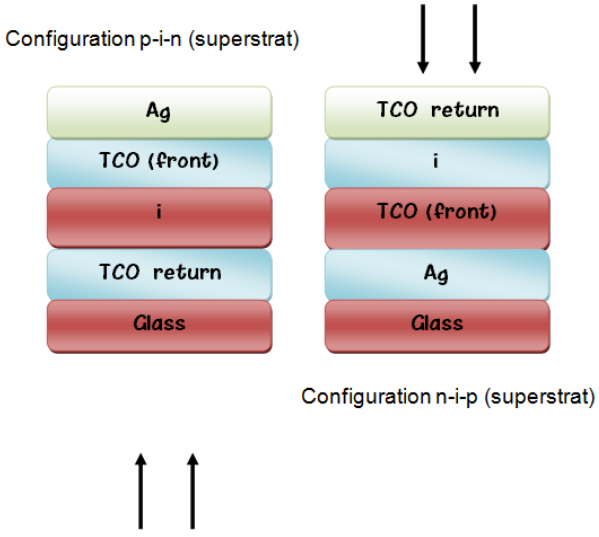

Figure. I.39: Schematic representation of SCs in P-I-N configuration (left) and N-I-P (right). The silver grid of the N-I-P cell, normally placed on the contact before TCO, is not shown.

I.7.5. Doping of silicon nanoparticles

The doping of semiconductors is a key step in the manufacture of components. An important field of research is therefore opening up on the doping of nanostructures silicon for its fundamental and application interest [65, 66]. In fact, the doping of silicon nanoparticles is an essential parameter making it possible to govern their optical and transport properties. While in grains of a hundred nanometres in diameter, the impurities used for doping behave as in solid material, quantum and dielectric confinements have a strong influence on their electronic structure for dimensions of the order of ten nanometres or below [67, 68].

I.7.6. Fundamental and technological losses limiting performance

Obviously, the performance of the SC is limited by various factors, which they be theoretical or technological. We will review them here. In each case, we will see which electrical parameters they influence.

I.7.6.1. Fundamental losses

First, there are fundamental losses that are inevitable. These losses limit the theoretical efficiency of the Silicon SCs at 29.8% [69, 70].

I.7.6.1.1. Incomplete absorption of photons

Photons whose energy is lower than the energy of the band gap (*i.e.* 1.12 eV) do not cannot be absorbed by silicon. They do not then contribute to the creation of pairs electron-hole. This results in a loss of about 27% in efficiency.

I.7.6.1.2. Excess energy of photons

This loss represents about 28% loss on performance under AM1.5. These first two limitations, influencing the short-circuit current I_{cc} and the open circuit voltage Vco, reduce the theoretical efficiency to 45% [71].

I.7.6.1.3. Voltage factor

The short circuit voltage V_{co} cannot exceed the energy of the gap, *i.e.* Eg /q. Added to this is auger recombination, which limit the V_{co} to 0.65V for a thick solar cell, and 0.72 V for a 20 µm thick cell [72].

I.7.6.1.4. Filling factor

Ideally, the form factor would be 1, if the I(V) curve were square. However, the exponential form of the I(V) characteristic, due to the Boltzmann statistic, limits the form factor to 0.89.

I.7.6.2. Technological losses

The losses mentioned above cannot be avoided, even in the case of a SC ideal. Other phenomena further reduce efficiency. These limitations are mostly technological, which means that it is possible to work on improving them. They come in three forms: optical, by recombination and resistive.

I.7.6.2.1. Optical losses

Optical losses are technological losses due to the non-absorption of a photon in the material:

- The front face of the SC is covered by a metal grid (it covers approximately 10% of the front surface in the case of a standard industrial cell), which prevents photons from entering the material.
- Silicon has a very high refractive index, which causes reflection in large area. This can be improved by the anti-reflective layer, whose reflectivity is about 10%.
- If the cell is not thick enough, low energy (or long wavelength), photons may not be absorbed into the thickness of the material.

I.7.6.2.2. Losses by recombination

Once the electron-hole pair is created, the charges must diffuse to the contacts of the cell. However, if they recombine before reaching contacts, they will no longer participate to the generation of current. Different mechanisms exist leading to the recombination of the pair, by volume or by surface [73].

I.7.6.2.3. Resistive losses

The efficiency of the cell is also affected by resistive losses. They are due to parallel resistors, such as leakage from the edges of the PV cell or when the metal on the front panel bypasses the emitter. The second type of loss is due to power losses due to the resistivity of the various elements of the SC: series resistors.

$$I(V) = I_{01}\left[exp\left(\frac{qV-IRs}{n1kT}\right)-1\right] + I_{02}\left[exp\left(\frac{qV-IRs}{n2kT}\right)-1\right] + \frac{V-IRs}{Rp} - I_L \qquad (16)$$

I.8. Conclusion

In this chapter, we have recalled some notions on SCs, its energy power and the properties of its illumination (cell, efficiency, operation, characteristic, absorption, intensity of photons, type of SCs … etc.). The background of photovoltaic energy, the basic operating principle of a PV cell, the use of the current-voltage characteristic of the cell to calculate its various physical parameters as well as the various thin-film photovoltaic pathways. We have presented the different structures of a thin film SC. This theoretical study allowed us to specify the most promising semiconductor for the study of thin film and crystalline Si SCs. We thus present new structures based on one-dimensional PCs in order to improve the efficiency of PV cells.

List of references

[1] X. Deng and E. Schiff, "Amorphous Silicon Based Solar Cells," *Physics*, 2003.

[2] A. Shah, P. Torres, R. Tscharner, N. Wyrsch, and H. Keppner, "Photovoltaic Technology: The Case for Thin-Film Solar Cells," *Science*, vol. 285, no. 5428, pp. 692–698, 1999.

[3] A. Belfar, T. Kadi, and H. Ait-Kaci, "The Improvement of Tandem a-Si:H/µc-Si:H Solar Cells Perfomance by Optimized the Front Contact Barrier Height," in *Proceedings of the Third International Symposium on Materials and Sustainable Development*, Cham, 2018, pp. 15–24.

[4] J. Yang, A. Banerjee, and S. Guha, "Triple-junction amorphous silicon alloy solar cell with 14.6% initial and 13.0% stable conversion efficiencies," *Appl. Phys. Lett.*, vol. 70, no. 22, pp. 2975–2977, 1997.

[5] A. Banerjee, J. Yang, and S. Guha, "Optimization of High Efficiency Amorphous Silicon Alloy based Triple-Junction Modules," *MRS Online Proceedings Library*, vol. 557, no. 1, pp. 743–748, 1999.

[6] H. Derbal, "Cellules solaires photovoltaïques plastiques nanostructurées," Thèse de doctorat, Angers, 2009.

[7] G. Gomard, "Cristaux photoniques pour le contrôle de l'absorption dans les cellules solaires photovoltaïques silicium ultraminces," thèse de doctorat, Ecully, Ecole centrale de Lyon, 2012.

[8] G. Hamon, "III-V/Si tandem solar cells: an inverted metamorphic approach using low temperature PECVD of c-Si(Ge)," these de doctorat. Université Paris-Saclay (ComUE), p. 196, 2018.

[9] K. Yoshikawa *et al.*, "Silicon heterojunction solar cell with interdigitated back contacts for a photoconversion efficiency over 26%," *Nature Energy*, vol. 2, no. 5, Art. no. 5, 2017.

[10] W. Shockley and H. J. Queisser, "Detailed Balance Limit of Efficiency of p- n Junction Solar Cells," *Journal of Applied Physics*, vol. 32, no. 3, pp. 510–519, 1961.

[11] M. A. Green *et al.*, "Solar cell efficiency tables (version 49)," *Progress in Photovoltaics: Research and Applications*, vol. 25, no. 1, pp. 3–13, 2017.

[12] S. Mthwecu, "Modelling and macroeconomic analysis of a Solar PV/diesel hybrid power plant," (Master's thesis, University of Cape Town), 2015.

[13] J. Roussille, "Comparaison de trois méthodes analytiques (sonde fluorimétrique, spectroscopie UV-visible et HPLC) pour le dosage de la chlorophylle a dans les eaux de trois lacs". thèse de Master I, Université de Bordeaux I, 2009.

[14] M. A. Green, "Solar cells: Operating principles, technology, and system applications," *Englewood Cliffs, NJ, Prentice-Hall, Inc., 1982. 288 p.*, 1982.

[15] A. Ricaud, *Photopiles solaires: de la physique de la conversion photovoltaïque aux filières, matériaux et procédés*. Lausanne: Presses polytechniques et universitaires romandes, 1997.

[16] A. Luque and A. Martí, "Theoretical Limits of Photovoltaic Conversion and New-Generation Solar Cells," in *Handbook of Photovoltaic Science and Engineering*, John Wiley & Sons, Ltd, 2010, pp. 130–168.

[17] S. Cells, "Materials, Manufacture and Operation.", 2005.

[18] M. Lasladj, "Simulation numérique des cellules solaires de troisième génération pour des applications spatiales," Thèse de doctorat, 2015

[19] D. M. Chapin *et al.* "A New Silicon p-n Junction Photocell for Converting Solar Radiation into Electrical Power. "Journal of Applied Physics, vol 25, no 5, p. 676-677, 1954.

[20] C. A. Wolden *et al.*, "Photovoltaic manufacturing: Present status, future prospects, and research needs," *Journal of Vacuum Science & Technology A*, vol. 29, no. 3, p. 030801, 2011.

[21] P. A. Basore, "Defining terms for crystalline silicon solar cells," *Progress in Photovoltaics: Research and Applications*, vol. 2, no. 2, pp. 177–179, 1994.
[22] P. Spinelli *et al.*, "Plasmonic light trapping in thin-film Si solar cells," *J. Opt.*, vol. 14, no. 2, p. 024002, 2012.
[23] M. A. Green, Ed., "Energy, Entropy and Efficiency," in *Third Generation Photovoltaics: Advanced Solar Energy Conversion*, Berlin, Heidelberg: Springer, pp. 21–34, 2003.
[24] H. M. Yates, P. Evans, D. W. Sheel, Z. Remes, and M. Vanecek, "Control of tin oxide film morphology by addition of hydrocarbons to the chemical vapour deposition process," *Thin Solid Films*, vol. 519, no. 4, pp. 1334–1340, 2010.
[25] A. V. Shah *et al.*, "Thin-film silicon solar cell technology," *Progress in Photovoltaics: Research and Applications*, vol. 12, no. 2–3, pp. 113–142, 2004.
[26] S. Collavini, S. F. Völker, and J. L. Delgado, "Understanding the Outstanding Power Conversion Efficiency of Perovskite-Based Solar Cells," *Angewandte Chemie International Edition*, vol. 54, no. 34, pp. 9757–9759, 2015.
[27] A. Kojima, K. Teshima, Y. Shirai, and T. Miyasaka, "Organometal Halide Perovskites as Visible-Light Sensitizers for Photovoltaic Cells," *J. Am. Chem. Soc.*, vol. 131, no. 17, pp. 6050–6051, 2009.
[28] M. A Green, *et al.* "Solar cell efficiency tables (version 56)." *Progress in Photovoltaics: Research and Applications* 28.NREL/JA-5900-77544, 2020.
[29] S. Petibon, "*Nouvelles architectures distribuées de gestion et conversion de l'énergie pour les applications photovoltaïques*. " these de doctorat. Université Paul Sabatier-Toulouse III, 2009.
[30] B. Boukezata, A. Chaoui, J.-P. Gaubert, and M. Hachemi, "Système solaire photovoltaïque connecté au réseau électrique et associé à un filtre actif parallèle," Cachan, France, 2014.
[31] A. Zerga, "Optimisation du rendement d'une cellule solaire NP au silicium monocristallin." *Revue des Energies Renouvelables*, p. 95-100, 1998.
[32] S. Bensalem, "Effets de la température sur les paramètres caractéristiques des cellules solaires," Thèse de doctorat, 2018.
[33] E. T. Yu and J. van de Lagemaat, "Photon management for photovoltaics," *MRS Bulletin*, vol. 36, no. 6, pp. 424–428, 2011.
[34] I. Bouchama, "Contribution à l'amélioration des performances des cellules solaires CuIn1-xGaxSe2," Thèse de doctorat, 2018.
[35] P. Pradhan *et al.*, "Effect of molybdenum deposition temperature on the performance of CuIn1−xGaxSe2 Solar Cells," in *2015 IEEE 42nd Photovoltaic Specialist Conference (PVSC)*, 2015, pp. 1–4.
[36] E. Moons, T. Engelhard, and D. Cahen, "Ohmic contacts to p-CuInSe2 crystals," *JEM*, vol. 22, no. 3, pp. 275–280, 1993.
[37] W. H. Bloss, F. Pfisterer, M. Schubert, and T. Walter, "Thin-film solar cells," *Progress in Photovoltaics: Research and Applications*, vol. 3, no. 1, pp. 3–24, 1995.
[38] O. Tosoni, "Conception, élaboration et intégration d'électrodes transparentes optimisées pour l'extraction des charges dans des dispositifs photovoltaïques." thèse de doctorat, Université de Grenoble, 2013.
[39] K. Zweibel, "Thin Films: Past, Present, Future," *Progress in Photovoltaics: Research and Applications*, vol. 3, no. 5, pp. 279–293, 1995.
[40] F. Barbaliscia, P. Masullo, and G. Ravaioli, "Spacial Statistical Correlation of Solar Energy and Eliophany over Italy," in *INTELEC '86 - International Telecommunications Energy Conference*, Oct. 1986, pp. 311–315.

[41] F. Barbaliscia , P. Masullo, et G. Ravaioli, "Spacial statistical correlation of solar energy and eliophany over Italy". In: *INTELEC'86-International Telecommunications Energy Conference*. IEEE, 1986. p. 311-315.

[42] A. El Hdiy and S. Mouetsi, "Identification of traps in an epitaxied AlGaAs/GaAs/AlGaAs quantum well structure," *Journal of Applied Physics*, vol. 108, no. 3, p. 034513, Aug. 2010.

[43] A .Luaue, G. Sala, W. Palz, *et al.* Tenth EC photovoltaic solar energy conference. In: *Proceedings of the International Conference, held at Lisbon, Portugal*. 1991. p. 8-12.

[44] T. Nakada, N. Okano, Y.Tanaka, *et al.* Superstrate-type CuInSe/sub 2/solar cells with chemically deposited CdS window layers. In: *Proceedings of 1994 IEEE 1st World Conference on Photovoltaic Energy Conversion-WCPEC (A Joint Conference of PVSC, PVSEC and PSEC)*. IEEE, 1994. p. 95-98.

[45] M. R. Balboul, A. Jasenek, O. Chernykh, U. Rau, and H. W. Schock, "CuGaSe2-based superstrate solar cells," *Thin Solid Films*, vol. 387, no. 1, pp. 74–76, 2001.

[46] T. Nakada, N. Okano, Y. Tanaka, H. Fukuda, and A. Kunioka, "Superstrate-type CuInSe/sub 2/ solar cells with chemically deposited CdS window layers," in *Proceedings of 1994 IEEE 1st World Conference on Photovoltaic Energy Conversion - WCPEC (A Joint Conference of PVSC, PVSEC and PSEC)*, 1994, vol. 1, pp. 95–98 vol.1.

[47] D. Hatem, "Cellules solaires organiques : choix des matériaux, structures des dispositifs et amélioration du rendement et de la stabilité," vol. 12. n 1, p. 77-86, 2009.

[48] J.-M. Nunzi, "Organic photovoltaic materials and devices," *Comptes Rendus Physique*, vol. 3, no. 4, pp. 523–542, 2002.

[49] T. Uematsu *et al.*, "Development of bifacial PV cells for new applications of flat-plate modules," *Solar Energy Materials and Solar Cells*, vol. 75, no. 3, pp. 557–566, 2003.

[50] A. Ouanoughi, "Amélioration d'absorption des cellules solaires par l'utilisation des cristaux photoniques en couches minces," thèse de doctorat, Université de M'sila, 2018

[51] Kleefstra, M. and Willemen, J.A., "Modelling of amorphous silicon single- and multi-junction solar cells," 1998.

[52] D. L. Staebler and C. R. Wronski, "Reversible conductivity changes in discharge- produced amorphous Si," *Appl. Phys. Lett.*, vol. 31, no. 4, pp. 292–294, Aug. 1977.

[53] M. Luysberg, P. Hapke, R. Carius, and F. Finger, "Structure and growth of hydrogenated microcrystalline silicon: Investigation by transmission electron microscopy and Raman spectroscopy of films grown at different plasma excitation frequencies," *Philosophical Magazine A*, vol. 75, no. 1, pp. 31–47, Jan. 1997.

[54] L. Houben, M. Luysberg, P. Hapke, R. Carius, F. Finger, and H. Wagner, "Structural properties of microcrystalline silicon in the transition from highly crystalline to amorphous growth," *Philosophical Magazine A*, vol. 77, no. 6, pp. 1447–1460, Jun. 1998.

[55] M. Tzolov, F. Finger, R. Carius, and P. Hapke, "Optical and transport studies on thin microcrystalline silicon films prepared by very high frequency glow discharge for solar cell applications," *Journal of Applied Physics*, vol. 81, no. 11, pp. 7376–7385, 1997.

[56] O. Vetterl *et al.*, "Intrinsic microcrystalline silicon: A new material for photovoltaics," *Solar Energy Materials and Solar Cells*, vol. 62, no. 1, pp. 97–108, 2000.

[57] E. Moulin, *"Accroissement de l'absorption lumineuse au sein de cellules solaires à couches minces de silicium par addition de nanoparticules et de nanostructures métalliques*". thèse de doctorat. Université Paul Verlaine-Metz, 2009.

[58] S. M. Kelso, C. C. Tsai, J. W. Allen, S.-J. Oh, and W. B. Jackson, "Energy dependence of the optical matrix element in hydrogenated amorphous and crystalline silicon," *Phys. Rev. B*, vol. 31, no. 8, pp. 5187–5198, 1985.

[59] F. Diehl, B. Schröder, and H. Oechsner, "Light scattering and enhanced optical absorption in hot wire microcrystalline silicon," *Journal of Applied Physics*, vol. 84, no. 6, pp. 3416–3418, 1998.

[60] N. Beck *et al.*, "Enhanced optical absorption in microcrystalline silicon," *Journal of Non-Crystalline Solids*, vol. 198–200, pp. 903–906, 1996.

[61] W. B. Jackson, N. M. Johnson, and D. K. Biegelsen, "Density of gap states of silicon grain boundaries determined by optical absorption," *Appl. Phys. Lett.*, vol. 43, no. 2, pp. 195–197, 1983.

[62] R. Carius *et al.*, "Electronic Properties of Microcrystalline Silicon," *MRS Online Proceedings Library*, vol. 467, no. 1, pp. 283–294, 1997.

[63] E. Sauvain, A. Shah, and J. Hubin, "Measurement of ambipolar mobility-lifetime product and itssignificance for amorphous silicon cells," 1990, vol. 2, pp. 1560–1563.

[64] T. Brammer and H. Stiebig, "Defect density and recombination lifetime in microcrystalline silicon absorbers of highly efficient thin-film solar cells determined by numerical device simulations," *Journal of Applied Physics*, vol. 94, no. 2, pp. 1035–1042, 2003.

[65] Y. Kanzawa, M. Fujii, S. Hayashi, and K. Yamamoto, "Doping of B atoms into Si nanocrystals prepared by rf cosputtering," *Solid State Communications*, vol. 100, no. 4, pp. 227–230, 1996.

[66] M. Fujii, A. Mimura, S. Hayashi, K. Yamamoto, C. Urakawa, and H. Ohta, Improvement in photoluminescence efficiency of SiO2 films containing Si nanocrystals by P doping: An electron spin resonance study,‖ Journal of Applied Physics, vol. 87, no. 4, pp. 1855–1857, 2000.

[67] S. Ossicini *et al.*, "Understanding Doping In Silicon Nanostructures," *IEEE Journal of Selected Topics in Quantum Electronics*, vol. 12, no. 6, pp. 1585–1591, 2006.

[68] M. L. Steigerwald, R. A. Friesner, L. Brus, M. S. Hybertsen, and Z. Zhou, "Structural and chemical trends in doped silicon nanocrystals: First-principles calculations," *Phys. Rev. B*, vol. 71, no. 24, p. 245308, 2005.

[69] E. Degoli *et al.*, "Engineering silicon nanocrystals: Theoretical study of the effect of codoping with boron and phosphorus," *Phys. Rev. B*, vol. 76, no. 8, p. 085302, 2007.

[70] A. Moehlecke, I. Zanesco, and A. Luque, "Practical high efficiency bifacial solar cells," in *Proceedings of 1994 IEEE 1st World Conference on Photovoltaic Energy Conversion - WCPEC (A Joint Conference of PVSC, PVSEC and PSEC)*, 1994, vol. 2, pp. 1663–1666 vol.2.

[71] T. Tiedje, E. Yablonovitch, G. D. Cody, and B. G. Brooks, "Limiting efficiency of silicon solar cells," *IEEE Transactions on Electron Devices*, vol. 31, no. 5, pp. 711–716, 1984.

[72] J. Szlufcik, S. Sivoththaman, J. F. Nlis, R. P. Mertens, and R. Van Overstraeten, "Low-cost industrial technologies of crystalline silicon solar cells," *Proceedings of the IEEE*, vol. 85, no. 5, 1997, pp. 711–730.

[73] M. A. Green, "Limits on the open-circuit voltage and efficiency of silicon solar cells imposed by intrinsic Auger processes," *IEEE Transactions on Electron Devices*, vol. 31, no. 5, pp. 671–678, 1984.

Chapter II

Concepts and generalities on photonic crystals

Chapter II: Concepts and generalities on photonic crystals

II.1. Introduction

A crystal is formed by a periodic arrangement of atoms that consists of a repetition in space of an elementary pattern. In the context of the physics, it is formed by a periodic arrangement of atoms that consists of condensed matter. This creates a periodic potential profile for electrons that determines the bands of energies allowed in the material. In the case of semiconductors, this periodic potential induces a band gap between the conduction and the valence ones. In the context of research concerning the inhibition of spontaneous emission in semiconductors, E. Yablonovitch showed in the late 80s that it was possible to open a band gap for photons by performing a periodic alternation of different dielectric materials [1]. While S. John was interested in Anderson's localization [2], which led to the concept of PCs. First demonstrated in microwaves, the realization of two-dimensional photonic crystal (2DPC) in the near infrared in the mid-90s led to the emergence of a field of research. However, even if the principle of band gap was known at one dimension with Bragg mirrors, the realization of PCs in two dimensional and three dimensional led to the control of light to a more advanced degree, and the field of study of PCs extended ramifications beyond classical optics, as for instance in cavity quantum electrodynamics [3], or cavity opt mechanics [4].

II.2 Definition

PCs or Photonic Band Gap materials (light in cage), are periodic structures of dielectric or metallo dielectric materials whose permittivity is periodically modulated in one or more dimensions of space [5]. In the same way that the periodicity of the potential in a semiconductor crystal affects the propagation of electrons by creating allowed or forbidden energy bands, PCs can prevent the propagation of light in certain directions and frequencies. This latter allowed to propagate in the PC are called modes, all modes form bands. They are separated by frequency ranges for which light cannot propagate, they are called band gaps. There are three categories of PCs according to the number of periodic directions, and are called one-dimensional, two-dimensional and three-dimensional. Figure II.1 illustrates the 3 cases.

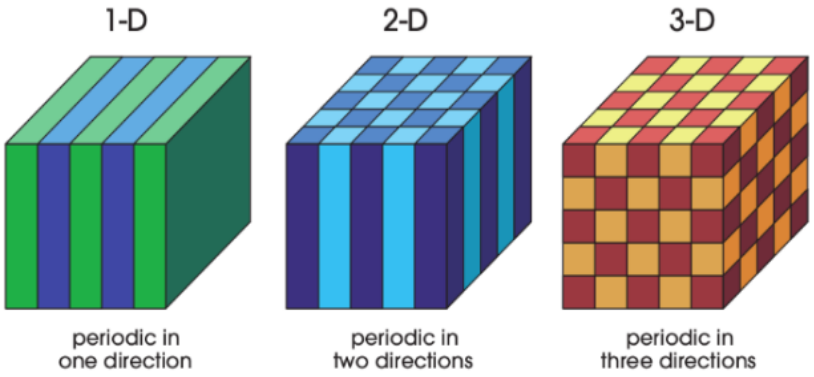

Figure. II.1: Schematic representations of PCs where the refractive index varies periodically according to one, two or three dimensions.

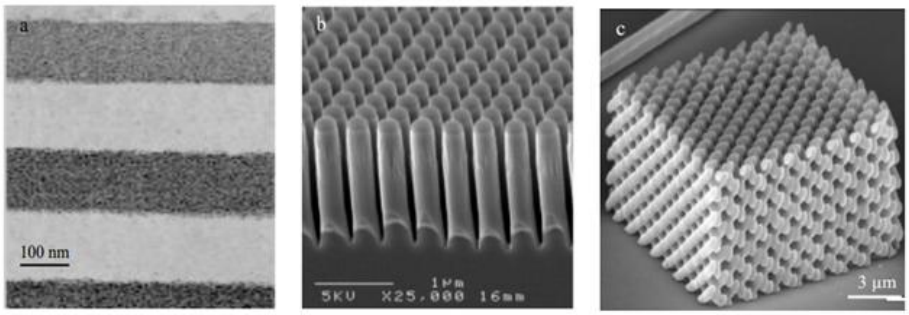

Figure. II.2: Shows scanning electron microscopy (SEM) images of different artificial PCs.

Figure II.2 represent films of SEM of PCs:(a) 1D consisting of an assembly of layers of polyelectrolyte's (the dark parts contain silver nanoparticles and have a refractive index higher than the light parts, devoid of nanoparticles) [6]; (b) two dimensional consisting of an arrangement of InP cylinders [7], and (c) three dimensional consisting of an arrangement of inclined and nested polymer rods [8].

A PC is a dielectric material where the refractive index is periodically modulated [9]. It concerns a crystal because the material consists of a periodic arrangement of dielectric elementary bricks of refractive index N_1 in a matrix of refractive index N_2. The term photonics is added because, the periodicity of the wavelength of light, a PC makes it possible to modulate the propagation of photons. PCs also exist in their natural state inside mineral complexes such as opals and inside biological systems such as the eyes of some cephalopods in the form of periodic gratings of rods, peacock feathers made of keratin crystals or the wings of some butterflies.

Research on PCs has mainly focused on near infrared (1.3µm -1.6µm) due to applications in the field of telecommunications [10]. Silicon is the essential material for industry and for energy production. PCs are transparent media in which the optical index varies periodically. It is transparent in the telecom window and has a very high refractive index (n_{Si}=3.48) as well as a very good mechanical resistance.

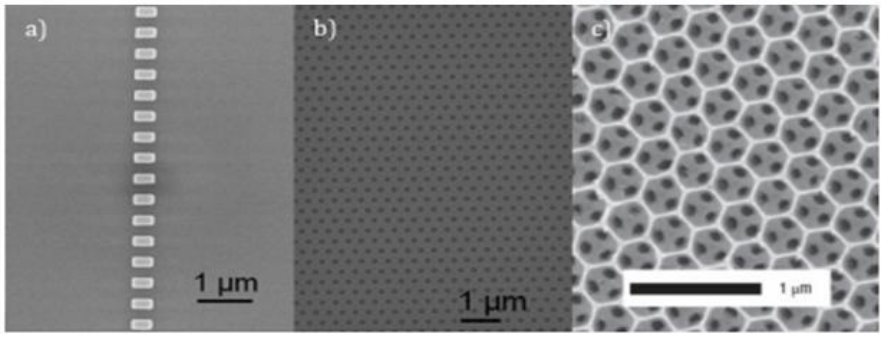

Figure. II.3: Scanning electron microscope (SEM) images of different types of photonic crystals: (a) Bragg's grating; (b) planar photonic crystal and (c) three dimensional photonic crystal [11].

The general principle of PCs had already been used for several decades for the realization of interferential mirrors [12] but it is to E. Yablonovitch and S. Johnson [13] that is due to the generalization to several dimensions in 1987. It is then seen as a way to inhibit spontaneous emission to overcome certain limitations of semiconductor lasers (noise reduction, threshold). However, there are a lot of difficulties. Several dimensions, this index modulation is usually achieved by digging holes in the dielectric material [14, 15],

by stacking balls [16, 17] or dielectric rods in a form called "pile of wood". In the field of optics, it is most often necessary to use semiconductor materials to have a sufficiently high dielectric constant and it was not until the progress of lithography and etching techniques that PCs with characteristic submicron lengths appeared in 1996 [15]. Moreover, from the theoretical point of view, calculations on two dimensional PC and three dimensional PC structures are particularly heavy.

II.3. History

Nowadays, they have attracted significant interest in the scientific community. This interest in these materials, in which the refractive index varies periodically, is due to the fact that they have specific optical properties. It was in 1987 that Eli Yablonovitch and Sajeev John, looking for to reduce the spontaneous emission of light in lasers and semiconductors, proposed a new way to build a Bragg mirror, proposed by W. L. Bragg since the late nineteenth century, in several dimensions. The point is to achieve a three-dimensional periodic structure by a regular assembly of spheres, cylinders and/or beams [18].

A first realization operating at centimetre wavelengths was presented by Yablonovitch in 1991. The proposed structure, the Yablonovite. It is a block of plexiglass machined in three different directions separated from allowing to reproduce the crystalline structure of the diamond. In reality, the PBG material is a three dimensional extension to the microwave frequencies of Bragg mirrors. Being constructed from a periodic stack of dielectric layers of different refractive indices in a single direction of space, the latter allow light to be controlled only in that same direction. On the contrary, three dimensional PC can achieve a complete band gap in all directions of propagation and for all possible polarizations of the wave [19]. That’s why Yablonovitch is considered the father of PCs [1].

II.4. Natural photonic crystals

PCs also exist in their natural state inside mineral complexes such as opals, and inside biological systems such as the eyes of some cephalopods in the form of periodic lattices of rods, peacock feathers made of keratin crystals or the wings of some butterflies and insects. Indeed, nature presents self-organized periodic structures that do not possess a sufficient contrast of clues: this is the case of natural mineral opal. This latter is a rock made up of silica micro beads distributed according to a more or less regular arrangement. In fact, it is a natural PC, even if it does not have a complete band gap [20].

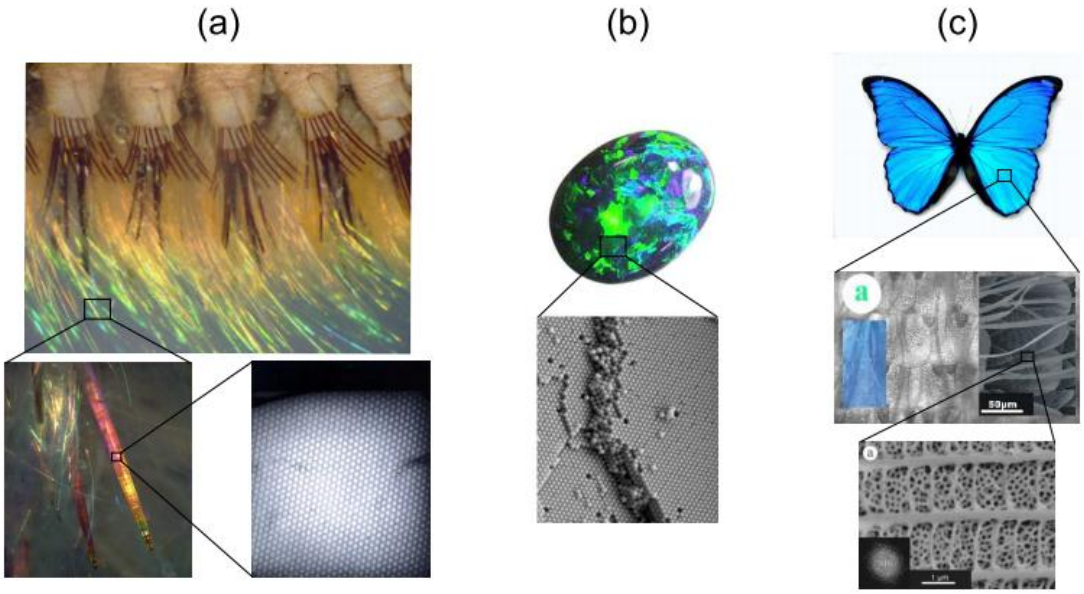

Figure. II.4:Natural PCs: (a) peacock feather, the box on the right is a scanning electron microscope (SEM) image of the cut of a green barb, the two dimensional PC structure is composed of melanin pillars bound by keratin as well as air holes; (b) bracelet mounted with an almost periodic natural opal of silica (c) morphic butterfly [21].

II.5. Planar photonic crystals

The ambition to achieve passive and active optoelectronic functions in integrated optics necessary for telecom applications, such as emission, amplification, modulation or tenability, requires confining light in two dimensions. This can be achieved by components or vertical confinement, of refractive origin, is ensured by a large contrast of indices and lateral confinement by a two dimensional PC. Planar PCs waveguide are artificial structures consisting of a dielectric guiding layer surrounded by two containment layers of refractive indices weaker than that of the core layer, all deposited on a substrate. The propagation is done in the plane where the photons are confined by the contrast of indices. In the same way, one can imagine a PC having a serious dimension in a waveguide.

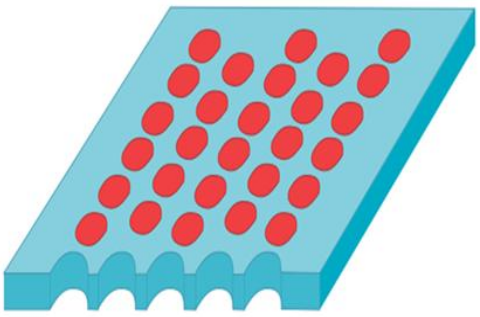

Figure. II.5: Schematic representation of an absorbent layer of a two dimensional PC in a dielectric plane guide.

In addition, we use the following definitions to write the modes of a PCs [22]:

1) **Illumining modes:** These are the ones that propagate in the PCs as well as in the external environment. These delocalized modes are modes of the radiative continuum weakly disturbed by the presence of the membrane.
2) **Localized modes:** We distinguish inside the membrane.
3) **Guide modes:** They are located below the line of light, so they have an evanescent character outside the membrane and propagate there with a theoretically infinite lifespan.
4) **Resonant modes :** Or quasi-guides: these are guide modes that appear above the line of light as a result of the folding of the bands inside the first Brillouin zone, and that constitute resonances in the continuum of illumining modes. The coupling of these modes with the continuum makes them acquire a non-zero radiative component responsible for the existence of losses in the direction perpendicular to the membrane.

II.6. Geometric and physical characteristics of photonic crystals

A PC is characterized by the different materials that compose it, the crystalline system according to which these materials are organized and the relative volumes they occupy in the elementary cell of the crystal [23]. The quantities of these different characteristics are:

II.6.1. Index contrast (Δ_n)

Ratio between the indices of the two materials, which can be compared to the height of the potential barrier of solid state physics [24]:

$$\Delta n = n_h - n_1 \qquad \text{(II.1)}$$

With: n_h is the refractive index of the high index material.
n_1 : The refractive index of the low index material.

II.6.2. Periods (a)

These geometric parameters, chosen according to the frequency range studied, influence the characteristics of the photonic band gap. For example for a 1DPC, the period a = (a_1+a_2) with a_1 the thickness of the permittivity layer ε_1 and a_2 the thickness of the permittivity layer ε_2.

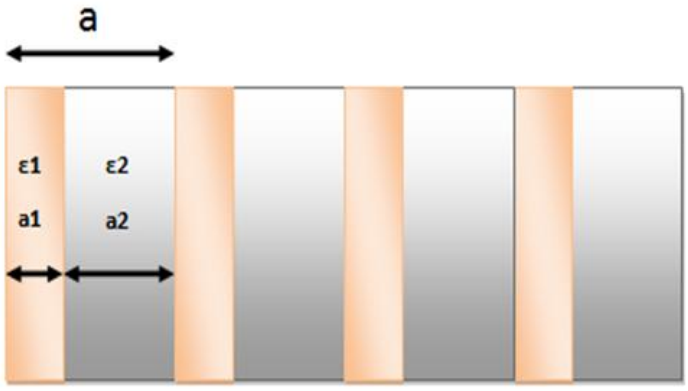

Figure. II.6: The periods of a one-dimensional PC.

II.6.3 The filling factor (*ff*)

It can be compared to the periodic potential drop. If it is taken for the high index material for example, it is defined as the ratio between the volume occupied by this material in the elementary cell of the crystal and the cell volume of the latter. The influence of these different parameters on the behaviour of a photonic structure can be understood by analogy with an induced periodic potential of the arrangement of atoms in a semiconductor [24].

II.7. Defects

By analogy with semiconductor crystals, the functionalities of PCs can be exalted by voluntarily and in a controlled inserting defects within their structure. Defects in PCs can locate modes. In one dimensional PC, the light can be confined to a default plane. In two dimensional PC one can locate the light in a linear defect. Finally in three dimensional PC, we can confine the light to a localized defect, so at a point in the grating.

The two easiest ways to disrupt the periodicity of the grating are:

- Add additional dielectric material: a dielectric defect;
- Remove dielectric material: an air defect.

Creating a defect locates destroys discrete translation symmetry. So theoretically, we can no longer speak in terms of k-wave vectors. In addition, we will focus on the density of states. The defect causes the appearance of a peak of a new state allowed in the density curve at a frequency located in the prohibited band. The width of the peak will decrease if the size of the crystal tends to infinity. States in the band gap cannot extend into the crystal itself. As a result, the modes in the band gap decline exponentially from the defect. So the mode is enclosed around the defect.

Another type of defects are linear defects that are extended in one direction. Linear defects can be considered as an alignment of localized defects. The states in this band are extended in the direction of the line and decline exponentially towards the crystal. If we choose the direction of the line parallel to one of the translation vectors of the crystal, the translation symmetry will be preserved in this direction. As with semiconductors, where energy levels appear in the gap when inserting impurities (atoms other than those of the crystal), extrinsic defects within PCs create permissible energy levels, called defect modes, for particular frequencies in the band gap [25].

In the event that a brick of a PC is replaced by a larger or higher index entity, the mode behaves like a donor mode in a semiconductor. When symmetry is broken by removing part of the material or replacing part of it with a material with a lower refractive index material, this is an acceptor mode. In other words, an extrinsic defect creates a micro cavity in the crystal structure that can trap the energy of an electromagnetic wave.

II.7.1. Defect strategies in photonic crystals

As with semiconductors, the existence of a defect in the periodicity of the crystal will lead to the appearance of permissible levels, called defect modes, in the band gap. The creation of a defect consists in locally breaking the periodicity of the grating by adding or locally removing a little dielectric material. In the case of a grating of holes, the defect consists in

the omission of one or more holes. Defects can also be created by modifying the radius of the holes. There are two types of defects:

II.7.1.1. Spot defects

There are multiple ways to create point defects in PCs. One or more patterns of the crystal may also be removed, added or modified (Figure II.7).

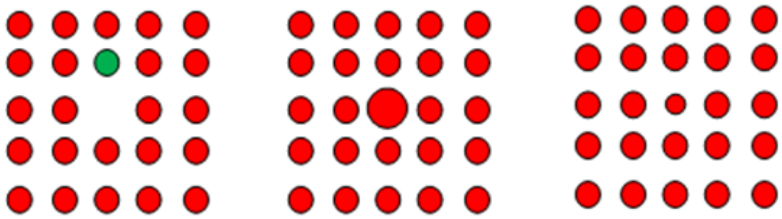

Figure. II.7: (a) defect; (b) and (c) substitution defects [26].

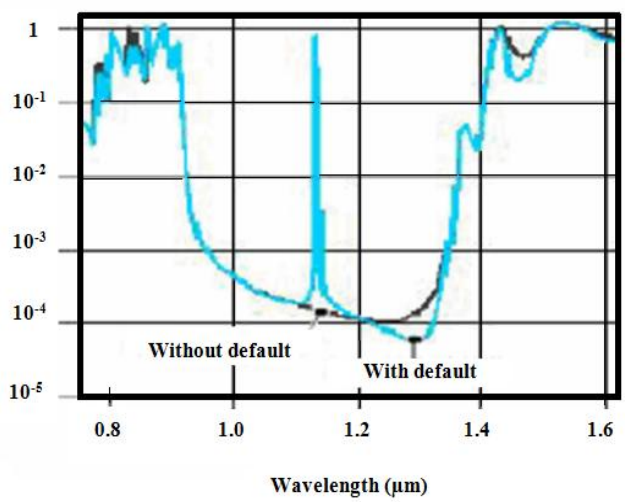

Figure. II.8: Transmission spectrum of a hexagonal crystal of dielectric rods with or without defect [27].

II.7.1.2. Extended defects

Extended defects, of size 1, 2 or 3, can only be obtained in crystals of at least equivalent size. Among these defects, the one dimensional defects ($W_{1)}$ (Figure II.9), are certainly those that have given rise to the greatest number of studies because they are intended to be used as light guides within a given crystal. We can also imagine two dimensional ($W_{2)}$ or three dimensional ($W_{3)}$ defects consisting of a series of W_1 guides, put end to end and oriented in different directions, so as to convey light on all possible paths inside the crystal. One way to achieve such a guide is to place punctual defects, coupled and spaced, in a direction of the two dimensional PC.

The coupling between an infinity of resonators leads to a permissible propagation band in the direction of alignment. This sort of coupled resonator guide was proposed in 1999 [28].

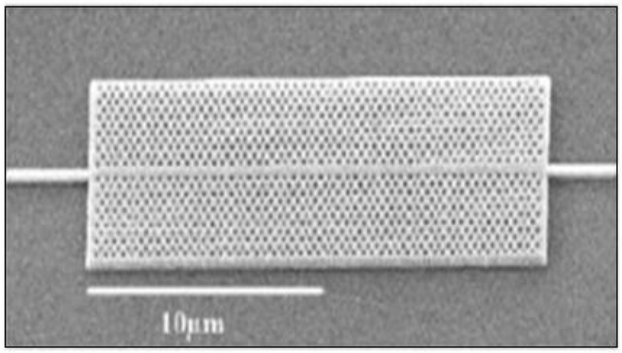

Figure. II.9: Example of a W1 guide to hexagonal PC of air holes on a silicon substrate on insulator [29].

II.8. Properties of photonic crystals

II.8.1. The "electron-photon" analogy

The notions of "Photon Gap" or "Photonic Bands Gap" are derived from the analogy between electrons and photons or, more precisely, from that between electronic wave function and electromagnetic field. These modes of an optical structure are obtained by solving Maxwell's equations, fundamental relations of electrodynamics. Silicon being a linear dielectric medium (we place ourselves here in a linear regime), non magnetic, without charges or current, we can then write Maxwell's equations in the following form:

$$\nabla.\left(\varepsilon(r)E(r,t)\right) = 0 \quad \text{(II.2)}$$

$$\nabla.H(r,t) = 0 \quad \text{(II.3)}$$

$$\nabla.E(r,t) = -\mu_0 \frac{\partial H(r,t)}{\partial t} \quad \text{(II.4)}$$

$$\nabla.H(r,t) = \varepsilon_0 \varepsilon_r(r) \frac{\partial E(r,t)}{\partial t} \quad \text{(II.5)}$$

Where E(r, t) and H(r, t) are the electric and magnetic fields, ε(r) the dielectric constant, ε_0 the electrical permittivity and μ_0 the magnetic permeability of the vacuum. If we are only interested in the harmonic solutions of Maxwell's equations, the fields can be written:

$$H(r,t) = H(r)e^{i\omega t} \quad \text{(II.6)}$$

$$E(r,t) = H(r)e^{i\omega t} \quad \text{(II.7)}$$

Maxwell's equations relating E(r) and H(r) are then rewritten as:

$$\nabla.E(r) = i\omega\mu_0 H(r) \quad \text{(II.8)}$$

$$\nabla.H(r) = i\omega\varepsilon(r)\varepsilon_0 E(r) \quad \text{(II.9)}$$

By putting $c = \frac{1}{\sqrt{\varepsilon_0\mu_0}}$ and by combining (II.7) and (II.8), we obtain the propagation equation in H(r):

$$\nabla.\left(\frac{1}{\varepsilon(r)}\nabla \times H(r)\right) = \left(\frac{\omega}{c}\right)^2 H(r) \quad \text{(II.10)}$$

If we introduce the operator $\vartheta = \nabla \times (\frac{1}{\varepsilon(r)}\nabla)$ the equation (II.9) is in the form:

$$\vartheta H(r) = \left(\frac{\omega}{c}\right)^2 H(r) \quad \text{(II.11)}$$

We recognize the form of an equation with proper values to obtain the proper modes H(r) of the dielectric structure as well as the proper values. Proper modes E(r) are given by the relation:

$$H(r) = \frac{1}{\omega\varepsilon(r)\varepsilon_0}.\nabla.H(r) \quad \text{(II.12)}$$

In the case of an isotropic homogeneous medium (ε(r)=ε), the propagation equation is simply solved by a monochromatic progressive plane wave:

$$E(r,t) = E_0.e^{ik.r}e^{i\omega t} \quad \text{(II.13)}$$

We deduce the dispersion relationship of the medium:

$$|k| = \frac{n\omega}{c} \quad \text{(II.14)}$$

In the case of a periodic medium, the dielectric constant is written ε(r) = ε(r + R), where R is a vector of the real lattice. This allows us to apply Bloch's theorem, analogous to the case encountered in solid state physics:

$$E(r,t) = u_k(r)e^{ik.r}e^{i\omega t} \quad \text{(II.15)}$$

There is then no longer an analytical relationship between the pulsation ω and the wave vector k, with the exception of very special cases. A numerical resolution is then necessary in order to obtain the own modes (r) and proper values ω(k). One of the interesting properties for solving the equation to proper values (10) lies in the law of scale inherent in Maxwell's equations. Indeed, by posing r'= r_a and $\nabla' = \nabla_a$, where a is the mesh parameter of the periodic lattice, we obtain:
$\nabla' = \nabla_a$, where a is the mesh parameter of the periodic grating, we obtains:

$$a\nabla'.\left(\frac{1}{\varepsilon\left(\frac{r'}{a}\right)}\nabla'.H\left(\frac{r'}{a}\right)\right) = \left(\frac{\omega'}{c}\right)^2 H\left(\frac{r'}{a}\right) \quad \text{(II.16)}$$

As ε(r'/a)=ε(r), we find the first equation dividing by a_2 and putting H'(r')=H(r/a) and ω_0=ω/a:

$$\nabla'.\left(\frac{1}{\varepsilon(r')}\nabla'.H'(r')\right) = \left(\frac{\omega'}{c}\right)^2 H'(r') \quad \text{(II.17)}$$

This law of scale therefore allows us to normalize all the quantities of the PC by the grating parameter *a*:

$$\omega = \frac{\omega' a}{2\pi c} = \frac{a}{\lambda} et\ k = \frac{k'a}{2\pi} \quad \text{(II.18)}$$

This simple law of scale is of great importance because it makes it possible to manufacture photonic crystals with similar properties but whose wavelength ranges vary only according to the crystal's mesh parameter. That is, with the same standardized parameters, it is possible to make PCs with the same proper modes operating in the visible, near infrared, microwave domain only by changing the mesh parameter of the crystal (assuming of course that the properties of the material are invariant in wavelength).

II.9. Types of photonic crystals

II.9.1 One dimensional photonic crystal (Bragg mirror)

These structures are commonly known as the Bragg lattice [30]. They are usually achieved by a stack of layers of different refractive index and optical thickness l/4. The being the guided wavelength around which the material must prohibit the propagation of electromagnetic waves under normal incidence. Bragg's gratings have proven their usefulness in many applications: old-fashioned converters for optical fibers, selective wavelength filters, multiplexers [31].

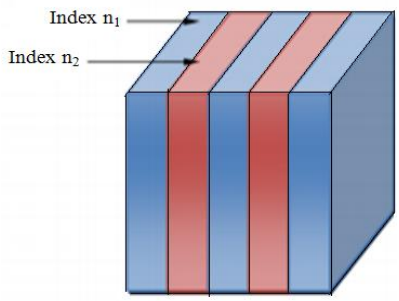

Figure. II.10: One dimensional PC structure [30].

II.9.1.1. Wave propagation on Bragg gratings

Bragg's gratings are successions of different refractive index layers, stacked periodically. The behaviour of the Bragg reflector is explained from the process of multiple interferences.

As shown in Figure II.11, a wave that propagates in the succession of layers, undergoes reflection at each interface. This reflection is accompanied by a change of phase Π if the wave goes from a medium of low index to a medium of high index.

It is carried out without a change of phase otherwise, when the total optical thickness of the alternations is λ/2, the wave reflected by the interface (1) is in phase with those reflected by the interfaces (3), (5), (7). As a result of these constructive interferences, we end up with a total reflection, which means that the wave cannot propagate and that we are in the presence of a photonic band gap.

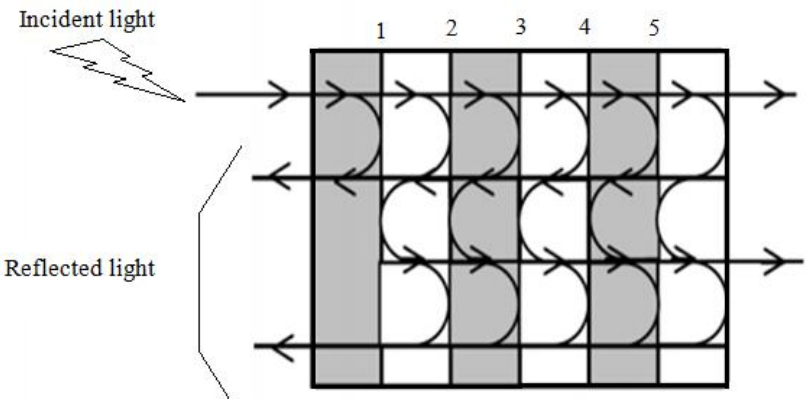

Figure. II.11: Schematic representation of the interference of the waves reflected by each Dioptre [32].

Bragg's gratings have proven their usefulness in many applications: mode converters for optical fibers, selective wavelength filters, multiplexers, laser cavity mirrors.

II.9.1.2. The width and central frequency of the gap

The width of the gap depends on the index contrast of the two media. When this contrast is low, the width of the gap is small (Figure II.12.a) and when it is high, it increases considerably (Figure II.12.b).

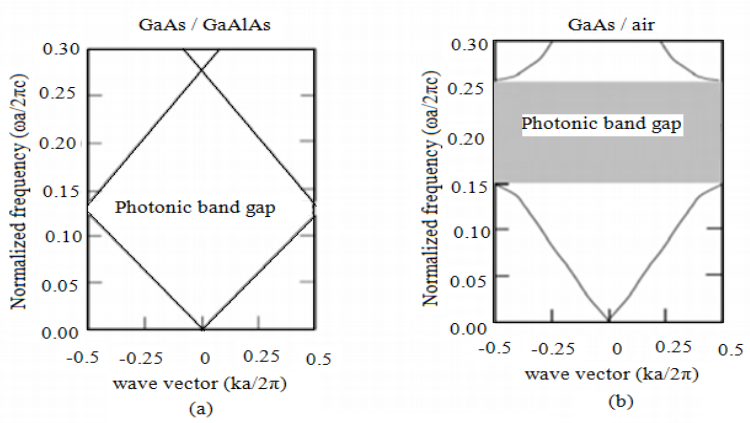

Figure. II.12: Photonic band structures for Bragg gratings of step a with: (a) permittivity layers ε=13 and 12 and (b) permittivity ε=13 and 1 [31].

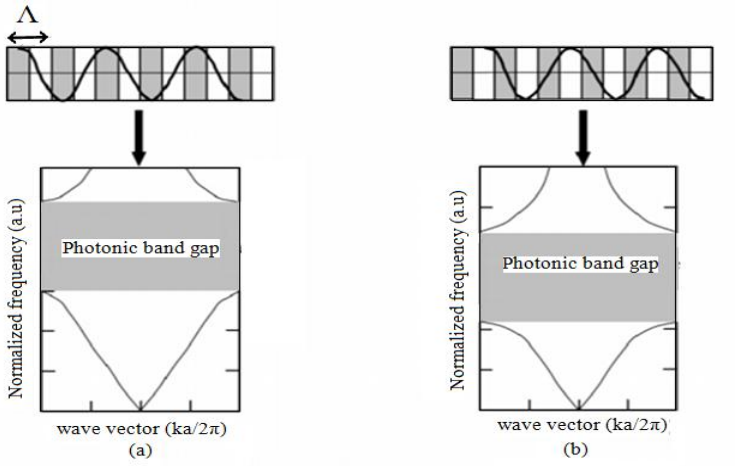

Figure. II.13: Schematic representation of the shift of the central frequency as a function of the location of the electric field in the grating; (a) the electric field at its maximum amplitude in areas of high permittivity; (b) the electric field has its maximum amplitude in areas of low permittivity [32].

II.9.1.3. One dimensional photonic crystals band gap

In this section, we will present the origin of the band gap, a fundamental property of photonic crystals. For this, we will first look at the simple case of the one dimensional PC, or Bragg mirror. This structure is formed by a periodic stack of materials of different refractive indices. The layered structure of a Bragg mirror is shown in Figure II.14.When the spatial period is of the same order of magnitude as the wavelength, the light propagating at normal incidence in the medium is strongly disturbed. In particular, for the Bragg length λ_B, where $\lambda_B=2(n_1a_1+n_2a_2)$, the waves reflected at each interface are in phase, and therefore constructively interfere [33]. A phase shift is therefore induced, and when $k=\pi/a$, the transmitted and reflected waves interfere to form a standing wave.

For this wave vector, the associated wavelength is 2a, which is twice the mesh parameter. Only two node positions are allowed by the symmetry properties of the Bragg mirror: either in the centre of the layer of the low-index material, or in the centre of the layer of the

high-index material. The variation theorem requires low-frequency modes to be placed in the high-index material. By orthogonality of the modes, the higher order mode is then located in the low index material. As the low frequency modes are confined to the high index material, we will speak of dielectric band, while we will speak of air band for high frequency modes. Analogous to the delimitation of the band gap in semiconductors by placing electrons either in the valence band or in the conduction band, the photonic band gap is delimited by the location of the energy of the modes in one or the other of the layers. The width of the gap depends on the index contrast between the two layers of materials.

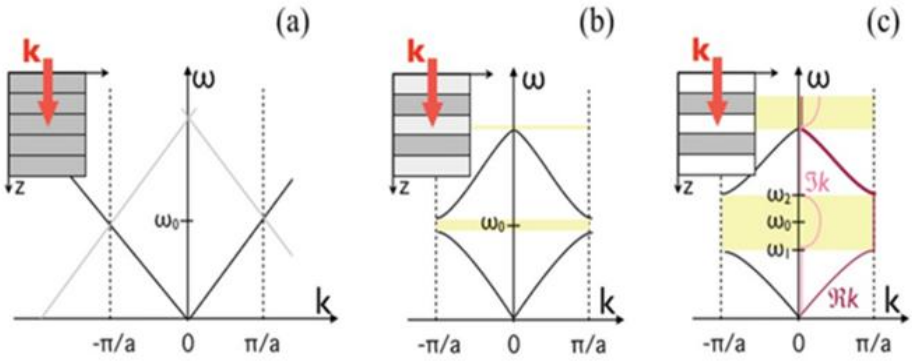

Figure. II.14: (a) Dispersion relationship of a homogeneous medium, folding is due to artificial periodization, (b) opening of a band gap when ε_1, ε_2; (c) the band gap is all the wider the greater the index contrast [33].

II.9.2. Two dimensional photonic crystal

Three dimensional PC still pose many manufacturing problems. For this reason, we were interested in two dimensional PC that can be manufactured easily. Two dimensional PC are composed of a periodic grating of dielectric pillars in the air (disconnected structure) or air holes drilled in a dielectric matrix (connected structure, Figure II.15) [31].

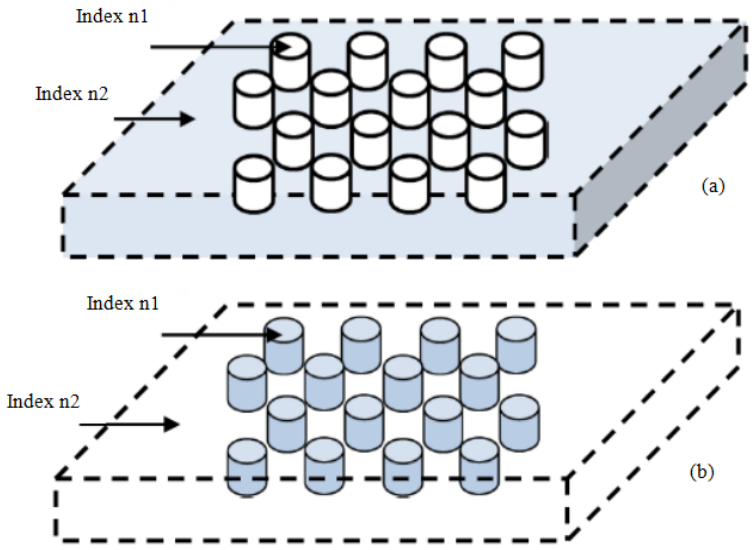

Figure. II.15: Two dimensional PC structures: (a) connected, (b) disconnected [21].

II.9.2.1. Reciprocal grating

In all crystal structures there are two gratings: the direct grating and the grating reciprocal. The direct grating is determined by the unit cell. The most unitary is called primitive. it is underpinned by the three fundamental vectors a_1, a_2, a_3, so that each transition vector of the grating can be put in the form of a linear combination basic vectors [34]:

$$\vec{R} = p_1\overrightarrow{a_1} + p_2\overrightarrow{a_2} + p_3\overrightarrow{a_3} \quad \text{(II.19)}$$

With: $p_1, p_2, p_3 \epsilon \mathbb{Z}$

In geometric crystallography, we introduce the notion of reciprocal lattice which turns out to be very practical for describing the properties of gratings. The reciprocal grating is a grating of Fourier space related to the crystal in which the vector G called the vector of the reciprocal grating, is a translation vector by which the whole of the reciprocal grating is constructed G and defined by [34]:

$$\vec{G} = m_1\overrightarrow{b_1} + m_2\overrightarrow{b_2} + m_3\overrightarrow{b_3} \quad \text{(II.20)}$$

With:

$$\begin{cases} \overrightarrow{b_1} = 2\pi \frac{\overrightarrow{a_2}\times\overrightarrow{a_3}}{\overrightarrow{a_1}.(\overrightarrow{a_2}\times\overrightarrow{a_3})} \\ \overrightarrow{b_2} = 2\pi \frac{\overrightarrow{a_1}\times\overrightarrow{a_3}}{\overrightarrow{a_1}.(\overrightarrow{a_2}\times\overrightarrow{a_3})} \\ \overrightarrow{b_3} = 2\pi \frac{\overrightarrow{a_1}\times\overrightarrow{a_2}}{\overrightarrow{a_1}.(\overrightarrow{a_2}\times\overrightarrow{a_3})} \end{cases} \quad \text{(II.21)}$$

The definition of the latter relation implies that any vector ~ π of the reciprocal grating is normal to the plane formed by the vectors and; $i \neq j$ and $j \neq k$ of the direct grating and that the product scalar=2π. We can therefore write, using the Kronecker delta [34]:

$$a_1\overrightarrow{b_1} = 2\pi\delta_{ij} \quad \text{(II.22)}$$

This relation is in the form of a scalar product, highlights the interest of using the reciprocal grating as the basis of wave vectors in the study of crystalline areas.

II.9.2.2. Brillouin zone

The most important statement of the diffraction condition for solid state physics was given by Brillouin. It is the only construction used in the theory of energy bands for the electrons of a crystal and in the expression of the elementary excitations of crystals. For reason of symmetry. The Brillouin zone and by definition the Wigner Seitz mesh of the reciprocal grating, we represent the vectors joining a site of the reciprocal grating to all neighbouring sites, then we draw the bisector planes perpendicular to these vectors. The smallest volume around the chosen site limited by its planes is called the Brillouin zone, irreducible which contains all the wave vectors of the photon that make it possible to describe the bar graph in a complete way. The upper Brillouin zones can be constructed in the same way that the I^{eme} Brillouin zone is the space limited on the one hand by the bisector planes perpendicular to the vectors joining the site originally to the neighbouring

sites and on the other hand the bisector plans of the lower Brillouin zones. Figure II.16 shows the Brillouin zones of the reciprocal grating of a square structure.

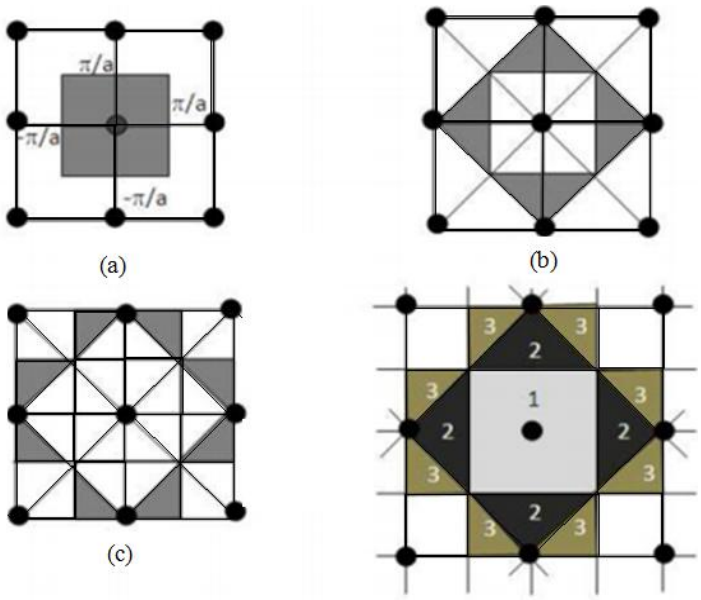

Figure. II.16: The Brillouin zones of the reciprocal grating of a square structure.

II.9.2.3. Different kinds of two dimensional photonic crystal

Depending on the symmetry (square, rectangular, oblique and hexagonal), there are four main types of two dimensional PC:

1) The square lattice

The nodes of the grating are located on a square of Figure II.17.a.This structure made from supposedly infinite air holes has four axes of symmetry that are deduced from each other by rotations of 45°, It has been shown that this type of grating is very sensitive to the angle of incidence and polarization of the electromagnetic wave [35]. It is thus difficult to form a complete band gap, *i.e.* a band gap that prohibits propagation in all directions and for all polarizations [36]. Its Brillouin area is a rectangular isosceles triangle ΓXM [32]. The square grating: the nodes of the grating are located on a square of Figure II.17.a.
In the case of a disconnected structure the TM band gaps are significantly wider than the TE polarization band which has become very narrow and conversely just in the case of a connected structure.

2) The triangular lattice

Each node in the lattice is spaced from its close neighbour by the same distance (Figure II.17.b). This structure has six axes of symmetry that are deduced from each other by rotations of 30° [36], which makes it less sensitive to the angle of incidence, but the complete band gap remains difficult to obtain, on the other hand the "connected" structure of holes in the dielectric offers a better compromise when the diameter of the holes is close to the period of the lattice (high filling factor).
In this case, the walls become so thin that the areas of high dielectric permittivity become disconnected [32]. In the case of the triangular grating, the vectors of the real grating are no longer collinear to those of the reciprocal grating. The first Brillouin zone is a hexagon

and its irreducible Brillouin zone is a triangle (ΓPQ) whose surface is 1/12 of that of the first Brillouin zone [24].

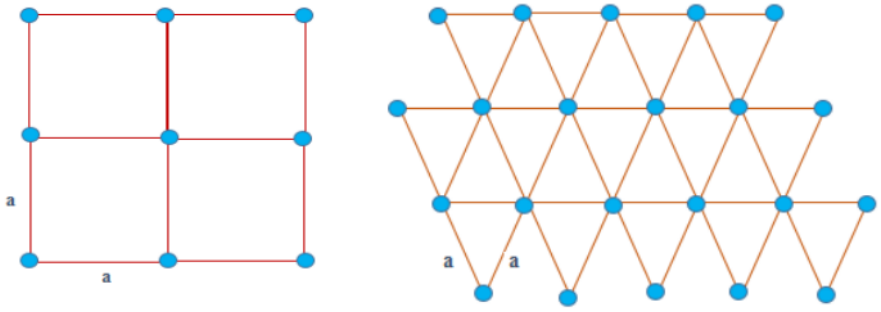

Figure. II.17: Representation of a 2D structure; (a) a square lattice; (b) a triangular lattice [32].

3) The hexagonal lattice

In a hexagonal lattice, there are two structures, the graphite structure and the Boron nitride one.

4) Graphite structure

On a hexagonal lattice, if all the nodes are identical and spaced "a", then this structure is called "graphite" because it is similar to the crystal structure of graphite. Unlike the triangular lattice, it is a lattice with two "atoms" per mesh. The reciprocal one is also a hexagonal lattice and the irreducible Brillouin zone is the same as for the triangular lattice with the main directions denoted ΓK and ΓM. The possibility of a complete band gap had been predicted for the first time in the case of a lattice of cylindrical dielectric rods.

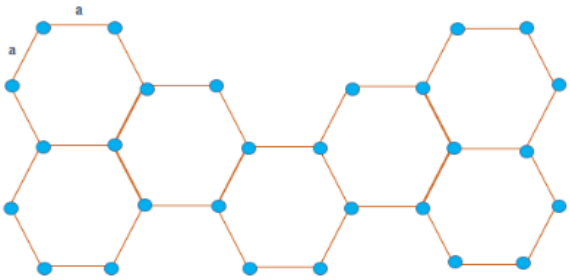

Figure. II. 18: Graphite structure.

5) Boron nitride structure

If one node differs from its next by its nature or dimension, we thus obtain the crystal structure of Boron nitride (figure.II.19). These ones allow to get prohibited big bands.

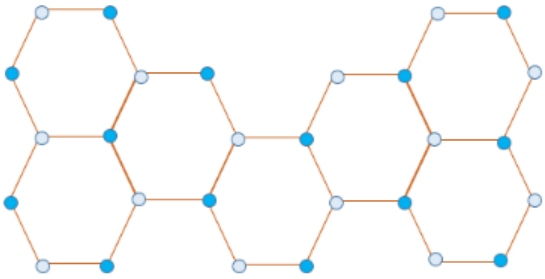

Figure. II.19: Boron nitride.

II.9.2.4. Two-dimensional photonic crystal band gap diagram

Two dimensional PC are usually formed by a periodic grating of air holes in a dielectric medium of high index, or by a grating of micro pillars. The cylindrical shape is imposed by manufacturing constraints related to the size of the patterns (~100nm) [37].

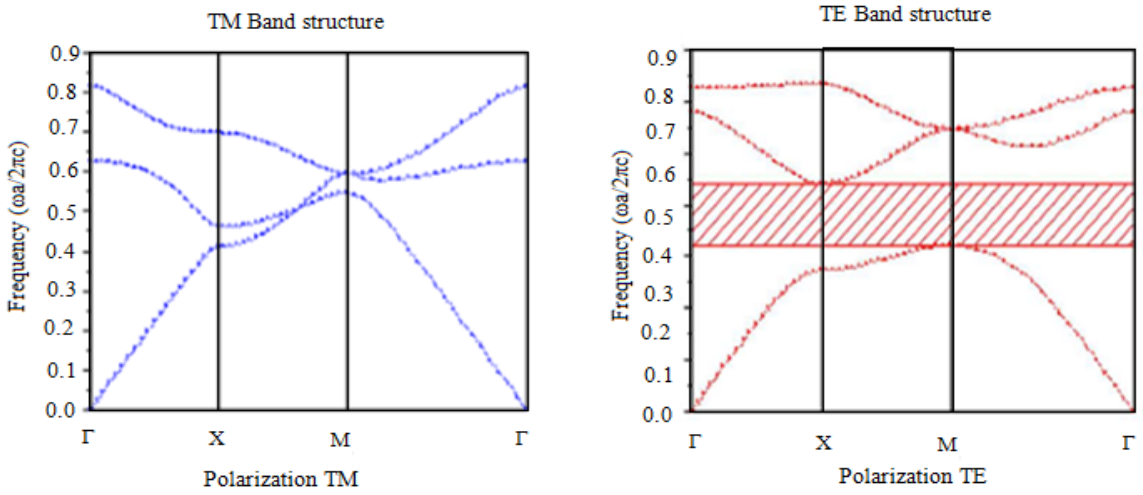

Figure. II.20: Diagram band of a square mesh structure of cylindrical studs in the air.

The triangular lattice is formed by two elementary vectors of the same norm and angular aperture of 60° in real space, or 120° in reciprocal space. The first Brillouin zone is defined according to a hexagon whose centre is the point Γ. Due to the high degree of symmetry of the first Brillouin zone; one can restrict oneself to an irreducible Brillouin zone, which consists of a region bounded by a triangle.

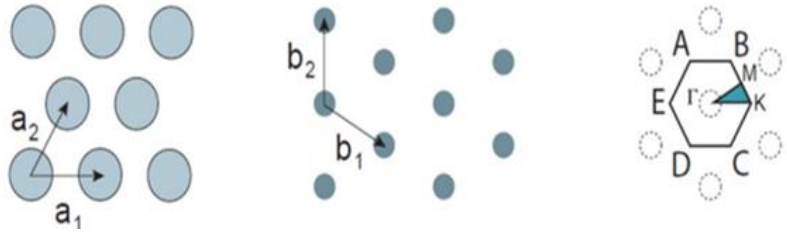

Figure. II.21: Representation of the triangular grating in real space, in reciprocal space, and representation of the first Brillouin zone with the irreducible Brillouin zone formed by the triangle ΓMK.

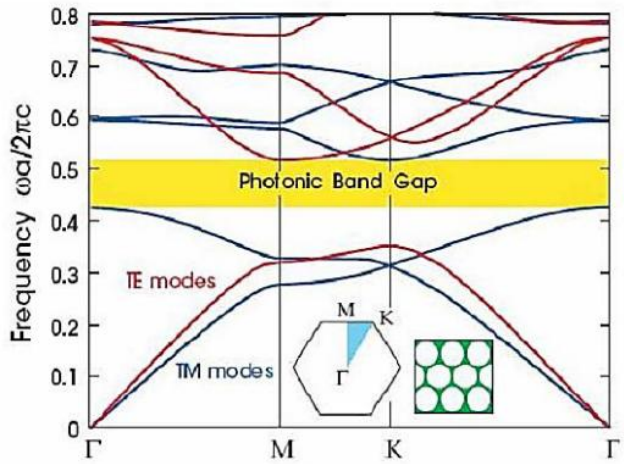

Figure. II.22: (a) Two dimensional bar graph of the triangular grating for a fill factor of 0.3; (b): map of prohibited bands according to the standard radius r/a.

The whole Brillouin zone can be reconstructed by symmetry of rotation. The calculation of the two dimensional bar graph for TE and TM modes for a fill factor of 0.3 shows the existence of a band gap for TE polarization only (Figure II.21).

The no-band map shows that the triangular grating has a band gap for TE polarization as soon as the fill factor is greater than 0.15. The band gap results experimentally in a very strong reflection at the interface between the PC and the refractive access guide.

II.9.3. Three dimensional photonic crystal

Three dimensional PC have attracted and still attract many research efforts. They are the only structure that makes it possible to obtain a band of gap energy in all the directions of space. We have seen that three dimensional photonic crystals have existed in nature for a very long time, but the first three dimensional PC was made in 1990 by K.M Ho *et al.* [38]. It was formed of silicon spheres arranged according to a diamond structure. But history generally retains the famous Yablonovite, a three dimensional structure for microwaves manufactured in 1993 by E. Yablonovitch [39], by drilling holes in Plexiglas at three azimuth angles separated by ~120°. Many methods of manufacturing three dimensional structures have been proposed.

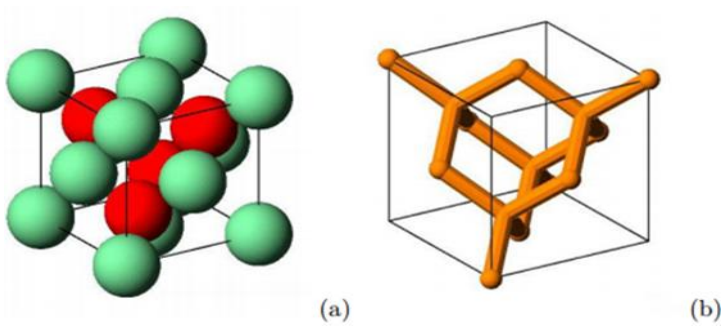

Figure. II.23: 2 types of 3DPC: (a) with spheres; (b) with stems.

The following two have attracted the most research effort:

II.9.3.1 Structures '' Wood piles ''

These three dimensional structures such as that shown in Figure II.24 are obtained by depositing in successive layers of polycrystalline silicon ribbons in silica trenches.

After having built the structure, the silica is removed to obtain a three dimensional Si/air PC whose index contrast is sufficient to open an unidirectional band of forbidden energies (Figure II.24.a) [40]. Similar PCs were made on GaAs by Noda *et al.* [41], by a fusion process of substrate removal. This technique uses standard semiconductor micro fabrication technologies and allows the deterministic introduction of defects into manufactured crystals.

II.9.3.2 Diamond Structures (opal)

The materials of such structures are agencies according to the crystalline system of the diamond for obtaining a complete band gap. Two main technological solutions are noteworthy. One is to build the structure layer by layer by successive stages of deposition and engraving of the two materials that make up the crystal. A lattice of holes is then drilled into the stack to define a third direction of periodicity (Figure II.24.b) [42]. The

second consists in alternately depositing two materials on a substrate having previously a grating of lines on the surface. The modulation of the substrate is preserved during the deposition of materials. These are in fact successive stages of deposit and attack carried out in the same building. A lattice of holes is then engraved in the stack in order to define a third direction of periodicity and reproduce the diamond structure [43, 44].

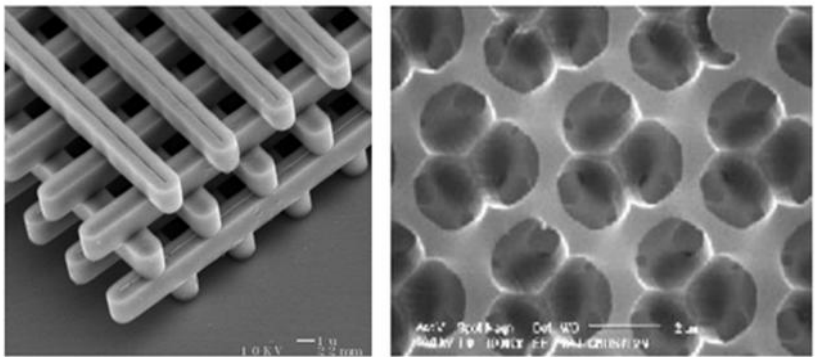

Figure. II.24: Examples of Three dimensional PC; (a) MEB image of a wood pile structure made by UV lithography in silicon; (b) three dimensional diamond periodic structure made of PMMA by X-lithography at the IEF [45].

III.9.3.3 Band gap of three dimensional photonic crystal

One dimensional PC make it possible to reflect photons with energy in a photonic gap and propagating in a direction close to normal at stacking. This accepting cone around normal is all the greater the higher the index difference between materials [12].

In order to master photons in a larger solid angle, it is possible to generalize the concept seen in the previous paragraph to several dimensions. For this, a periodic material with two or three dimensions is made. A band gap is then obtained by covering the one-dimensional band gaps of all directions of the plane or space. It is then easily understandable that the opening of a band gap of reasonable width with two or three dimensions is conditioned by the periodic grating, the pattern and by the index modulation.

The crystal must be relatively isotropic *(i.e.* the first Brillouin zone as circular or spherical as possible so that the different one-dimensional bands gap are not too shifted in energy) and the index modulation must be sufficient (so that the accepting cones of the one-dimensional gaps are wide enough and overlap), unlike the one dimensional case where the gap in the normal direction exists regardless of these characteristics.

In reality, it is not necessary to perform the calculation in all directions of the plane or space because the extremism of the bands are located along the directions of symmetry of the first Brillouin zone. When the band gap is extended to all directions considered and for both polarizations, it will be called a "full" band gap. The search for the structure (latish and pattern) that maximizes the opening of a photonic gap is very complex because of the large number of variables and because of the vectorial character of light (in practice, it is necessary to distinguish the two polarizations in two dimensional PC and three dimensional PC), but it is possible for a given structure [46]. It has been shown that not all crystal lattices can give a complete band: it is impossible for example with a CFC (Cubic Face Cantered) lattice [47], but possible with a diamond type lattice [38]. The first

experimental three dimensional PC with a complete gap was made by Yablonovitch, (Figure II.25) in the microwave field in 1991 [48].

This structure is made by drilling three families of holes along three axes of the diamond-type grating.

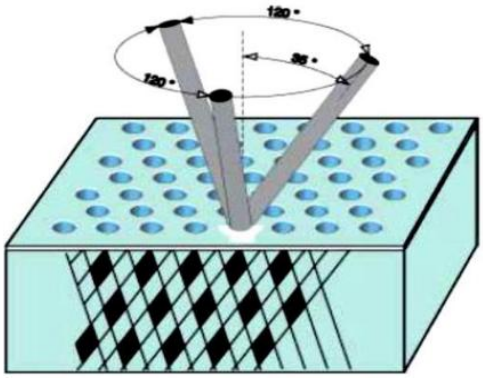

Figure. II.25: Example of three dimensional PC [49].

Many attempts were first made from cubic lattices (simple cubic, cantered and cubic with cantered faces), most of them getting up unsuccessful [50]. These structures most often behave like semi metals if recent results that a narrow omnidirectional band is possible for particular values of the design parameters [51], it is only with CFC gratings with two atoms per mesh, similar to those of diamond and the most common semiconductors (silicon, germanium, gallium arsenide) that large-width omnidirectional band gap bands have been obtained [52, 53].

II.10. Photonic crystals cavity

The first cavities with two dimensional PC were made in 1996. These cavities were developed by including mono defects on the PC lattice.

It is shown that these devices have a high quality factor for resonant modes thanks to the excellent reflection property of the crystal, all this on large cavities with several modes. The photonic band gap can be used to confine light to a reduced volume. If we include a defect in a PC, by removing a few holes in the lattice for example, and if this defect is of the appropriate size to support a mode in the photonic gap, then the light is trapped in this defect. Therefore, an optical cavity is obtained. These cavities can have very small volumes and large quality factors (Q), where Q represents the lifetime of the photon in the cavity. This factor is given by:

$$Q = \frac{\tau\omega}{2} = \frac{\omega}{\Delta\omega} \qquad \text{(II.23)}$$

With:

- τ the lifetime of the photon in the cavity,
- ω the resonance frequency of the cavity and $\Delta\omega$ the width at mid-height of the resonance.

PC nano cavities can be formed by removing and/or modifying one or more holes (more precisely by changing the size or position of the holes) in the perfectly periodic structure.

Such a break in the periodicity of the lattice introduces new energy levels within the photonic band gap.

In two dimensional PC, point defects are usually called *"Hi cavities"*. *H* for hexagon and *i* for the width expressed as the number of missing rows on one side of the hexagon of holes.

The following figure shows some examples of *Hi* cavities on two dimensional PC. However, it should be noted that other types of cavities than hexagonal ones exist. We can also mention among others the cavities types *Li*, with *L* for line, case in which *i* holes are omitted on the same row [54].

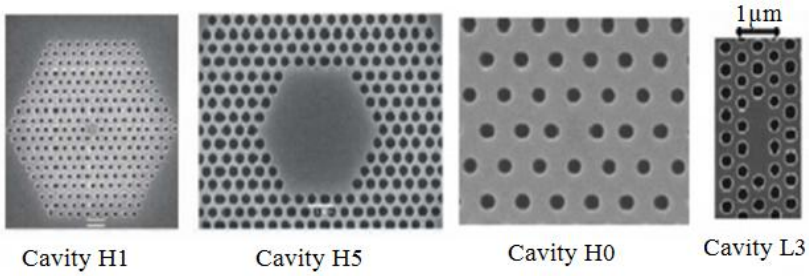

Figure. II.26: Different types of PC cavities [54].

II.10.1. Hexagonal cavity

In a triangular crystal, the hexagonal cavities, the sides of which are the dense rows, constitute a series of canonical cavities. It is convenient to name them by the number of periods along each side. Thus, a single missing hole will correspond to H_1,seven missing holes to H_2, etc. (Figure II.27).

Cavities of type H_n, hexagonal shape, n being the number of missing rows per side of the hexagon are the most studied [55].

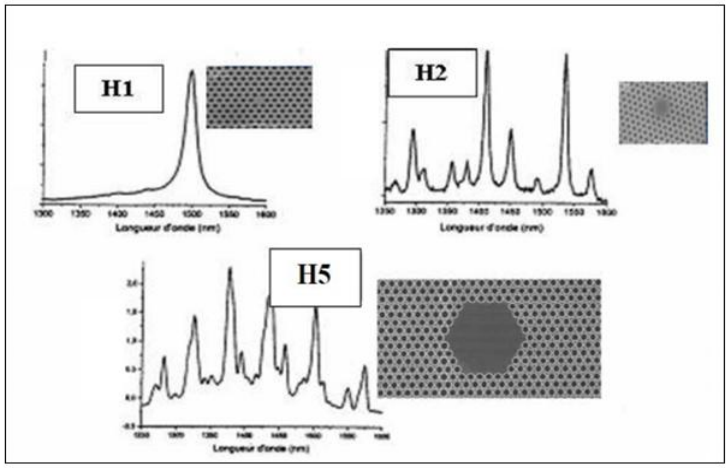

Figure. II.27: Spectral signatures of hexagonal cavities obtained by photoluminescence [56].

II.10.2. Square cavity

In a square two-dimensional lattice, the cavities are of type S_n, of square shape, being the number of missing lines and rows of the square. For example, the cavity S_1 is formed by omitting a line and a row.

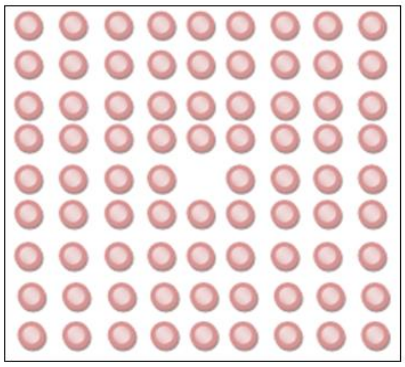

Figure. II.28: Example of a square cavity in a square PC with a mesh parameter 600mm [57].

II.10.3. Triangular cavity

Figure II.29 represents the triangular cavity, which is obtained by omitting several holes in a triangular lattice of air holes of circular section (r=200nm).

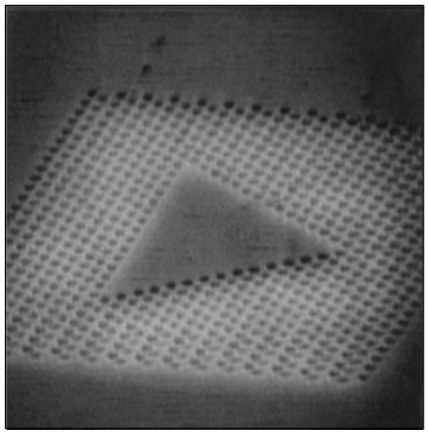

Figure. II.29: Example of a triangular cavity in a triangular PC with lattice parameters 600nm [58].

II.10.4. Rectangular cavity

The triangular two dimensional PC lattice is defined by the following parameters: mesh parameter a=560nm, figure II. 30: represents a rectangular cavity corresponding to the omission of 3 finished rows of holes in the PCs.

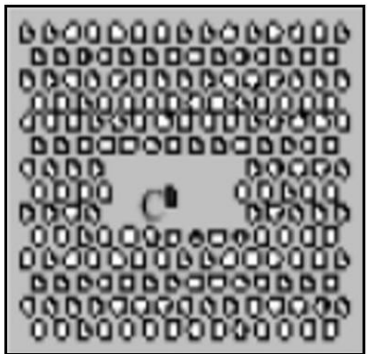

Figure II.30: Example of a rectangular cavity in a triangular PC with a 560nm mesh parameter [59].

II.11. The art state

The accelerated development of means of numerical simulation and nanostructure fabrication has been a favourable melting pot for such studies, resulting in prolific

literature [60]. As a result, it is not possible to describe all of these studies exhaustively. Anti-reflective effects are not involved in light trapping but may be a consequence of nano-structuring [61]. A more recent approach to light manipulation is based on the spatial dispersion of PCs. Here, the dispersion curves of an extended PC, *i.e.* flawless, are used to control the direction of light propagation.

The extremely strong anisotropy of the bands can provide a multitude of very exotic effects, such as super collimation [64], ultra refraction [65], or negative refraction [66], and thus, bring new functionalities to PCs. These effects have been extensively studied in recent years and are now well understood.

II.11.1. Beam propagation in graduated photonic crystals

Extended PCs exhibit spatially homogeneous optical properties. Changing the direction of light propagation therefore requires inserting defects into the structure. There is, however, an alternative to such an approach. In continuous media, light rays passing between two points in space follow the well-known principle of closing the least time, which states that light takes the path that requires the shortest time to get from one point to another. The length of the optical path, defined in terms of the average refractive index, is minimized, or assuming that the refractive index of the medium varies in space implies that the shortest optical path is curved.

This fact is well illustrated by some natural phenomena, such as atmospheric mirages and ionospheric refraction, where the refractive index gradient results from temperature and electron density gradients with height, respectively [67]. In homogeneity can provide an additional handle for manipulating light, allowing the path of light to be begged, and possibly combining different abnormal refractive effects.

II.11.2 Random texturing substrates

As we have seen previously, random texturing on the surface of an absorbent layer increases its absorption by decreasing the reflection and multiplying the number of propagation angles within it, which increases the average optical path of light.

A way to introduce these surfaces is to deposit the different layers of the cell almost in a quasi-compliant way on a randomly textured substrate, which generates the structuring of the front face (Figure II.31).

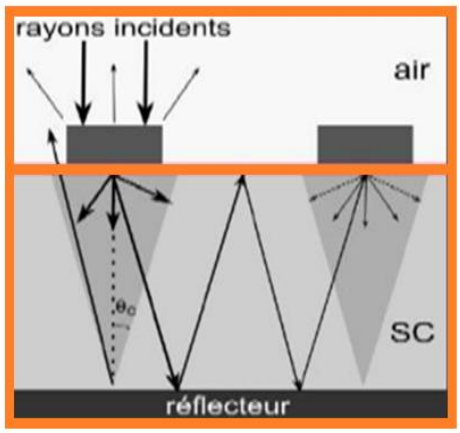

Figure. II.31: Representative diagram of the phenomenon of light scattering by microstructures in front of a solar cell. A total internal reflection is carried out for $\theta > \theta c$ [62].

Thus, the commercial version of these randomly textured substrates is regularly used as a reference to experimentally evaluate the effectiveness of light trapping methods. By depositing the different layers on glass substrates, it is then possible to obtain a significant optical gain without changing the electrical properties of the cell too much [62]. The use of this kind of substrates results in the scattering of light that leads to an increase in absorption in the active layer of the cell, this results in an increase in PV current [63], and it has been established that the increase in absorption for such structures can be described taking into account the fraction of light.

II.11.3 Diffraction lattices

Many authors have also studied the influence of grating profiles. For instance, Naqavi *et al.* simulated three types of one-dimensional lattice on the back side. In the following, we will consider only configurations that specifically exploit diffraction lattices.

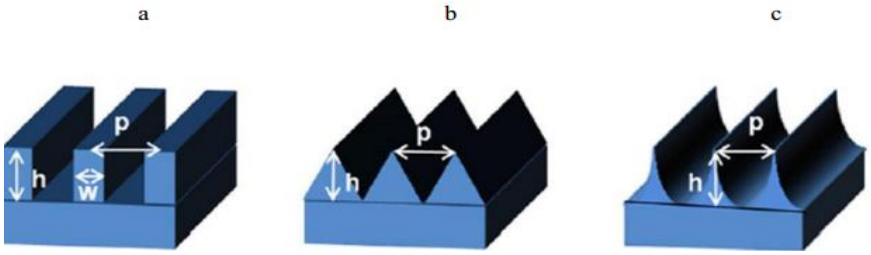

Figure. II.32: Design of one dimensional PC with different profile: (a) rectangular; (b) triangular; and (c) circular [63].

This theme took on increased importance with the decrease in the thicknesses of the active layers and became generalized to different materials and configurations (single lattices on the front or back of the cell, compliant deposition of the cell layers on a structured substrate, double lattice, etc.). Thus, it can consist of diffracting the light with the largest possible propagation angle so that the optical path is maximized (in particular via a total internal reflection on the front side), or coupling the incident light with the guided modes propagating in the absorbent layer. At low wavelengths, diffraction lattices can also contribute to increased absorption by decreasing front-facing reflection losses, as mentioned above [62]. However, a lot of factors can limit the efficiency of diffraction gratings. This is for example the significant parasitic absorption that takes place in the metal when a lattice is formed directly in the reflector on the back side of the cell.

This effect can be mitigated by depositing an oxide layer between the active layer and the metal lattice. Thus, the optimization of diffraction lattices (strictly periodic) must be carried out by reasoning over the entire spectrum to establish valid conclusions.

Unlike randomly textured substrates, these structures allow precise control of the optical properties of the cell through the adjustment of their geometric parameters (period, engraving depth, filling factor, etc). As a result, it is possible to design an optimized diffraction array around a given wavelength in such a way as to improve the integrated absorption of the cell or directly its efficiency. This last point summarizes the challenge of many studies that have set out to define the ideal geometry for these lattices by taking into account three main effects: anti-reflective effects, diffraction efficiency and parasitic absorption at the reflector [62].

II.11.4. Waveguide improvement based on dispersion in photonic crystals

Generally, PCs owe their original optical properties to their high dispersion, leading to a local change in the group speed of light or even to the prohibition of its propagation. In the early years of PCs, researchers mainly focused on the photonic band gap (BIP) properties of PCs and, therefore, their ability to confine light to structural defects such as waveguides and cavities. A more recent approach to light manipulation is based on the spatial dispersion of PCs. Here, the dispersion curves of an extended PC, *i.e.* flawless, are used to control the direction of light propagation. The extremely strong anisotropy of the bands can provide a multitude of very exotic effects, such as super collimation [62], ultra refraction [65], or negative refraction [66], and thus, bring new functionalities to PCs. These effects have been extensively studied in recent years and are now well understood.

II.11.5. Coupling light to super-collimating photonic crystals

Super collimation gives the ability to propagate light in straight lines over large distances without using structural waveguides [67]. Recent studies report the possibility of making devices such as optical routers, multiplexers or polarization separators, by incorporating linear defects into periodic structures [68].

Super-collimating PCs appear in themselves as a possible building block for many interesting applications and it seems very likely that they will play a key role in photonics in the coming years [69, 70].

The integration of PCs implies that they must be effectively coupled to integrated single-mode waveguides. The integrated appearance of the external waveguides is important if all photonic components are to be manufactured on a single chip, while the single-mode condition is required to ensure proper transmission of the light signal between each component. However, the coupling of light to super-collimating photonic crystals remains a real technological challenge. As we will see below, the incident beam must excite very specific Bloch modes in the PCs [71, 72] imposing certain requirements on the design of the excitation waveguide, while the impedance mismatch that occurs at the interfaces between the different components is responsible for the return. In this sense, the different structures and their interfaces must be appropriately designed to overcome the mismatch of mode profile and the impedance mismatch between mode propagation.

The coupling techniques [73, 74] that have been used so far do not meet all the conditions (single-mode propagation, efficient coupling and practical feasibility) simultaneously. More generally, we are not aware of extensive work on the coupling of light from waveguides embedded in super-collimator PCs, and although it has been shown that the limits of PCs are of crucial importance in improving the coupling of light to extended PCs [75, 76] such an approach has not been applied to the super collimation of PCs in particular.

II.11.6. Absorbent photonic crystals

We have seen previously that PCs can be used to assist absorption as an external element to the active layer. This includes, for example, PCs on the back side of cells (coupled or not to diffraction gratings) for the elongation of the optical path or the exploitation of their adjustable optical properties for the creation of intermediate reflectors within tandem cells

[77]. Another configuration is to directly structure the absorbent layer into a PC in order to strengthen the light-matter interaction. In fact, it is necessary to distinguish between superficial corrugation of the active layer and the creation of an absorbent membrane PC.

This can be done in a precise spectral range through the control of PC parameters, which differs from other approaches such as those using randomly textured substrates. In addition, this structuring is particularly effective for the collection of light as mentioned above for biomimetic structures. These effects were first used by Seassal *et al.* to increase absorption by 58% real in a 100 nm thick a-Si:H layer through one dimensional structuring and this, with a view to its integration into a complete SC [78]. In parallel, other research groups have extended this concept for different configurations and materials. Thus, Chutinan *et al.* Have shown by simulation that structuring an active layer of crystalline silicon (c-Si) 2μm thick into an optimized two dimensional PC increases the efficiency of the cell by 11% [79]. Although these results are theoretically instructive, the structure proposed in this study is nevertheless impracticable. It is interesting to note that in this structure, the modes are distributed in "saw teeth" which participates in the elongation of the optical path of light. The effect of the engraving depth was also put forward by Zanotto *et al.* for 1DPC formed in a cell based on a-Si:H (thickness=100nm or 300nm) or c-Si (thickness=500nm or 1000nm) [80].

For a total engraving, the gains can then be up to 12.4% for a-Si:H and 36.5% for c-Si. However, it appears that a partial etching of the active layer is preferable, since it allows a significant gain of the short-circuit current while facilitating the realization of the cells thus designed. In this case, the increase in absorption is explained, among other things, by the coupling of the incident light with the quasi-guided modes of the structure.

The presence of an unstructured layer under the corrugation breaks the symmetry of the system and increases the number of modes accessible for coupling with incident waves [81]. More recently, this study has been generalized by also considering two dimensional gratings (square and triangular) and different thicknesses of the active layer [82].

Optical simulations show that optimized triangular two dimensional gratings can lead to the same absorptions as for square two dimensional gratings, although their Jsc is slightly lower. In addition, the authors sought to compare the Jsc values obtained for the optimized configurations with those calculated within the framework of the Yablonovitch limit. It appears that these values remain below the theoretical limit (Yablonovitch) when considering the entire useful spectrum, but that the introduction of a "controlled disorder" into the structure makes it possible to increase its absorption a little more. This approach, based on Anderson's localization, contributes to increasing the lifetime of photons in the absorbing layer and therefore their probability of absorption [83].

Another research group [81] also studied the partial etching of the active layer ('hybrid system" formed from a membrane PC on a thin unstructured layer) for these same materials (c-Si, a-Si:H) but also for III-V semiconductors (InP and GaAs). The structures analyzed, one dimensional PC and square two dimensional grating of nano-holes or nano-pillars engraved on half of the active layer, have a period and a fixed filling factor and only the influence of the thicknesses of the layers is studied.

For a total thickness of 300nm, the different "hybrid" configurations have an optical gain compared to an unstructured reference and with an optimized anti-reflective layer. In this study, it appears that the absorption in the configuration using nano-pillars is greater than that using nano-holes for direct gap materials. For a-Si:H and c-Si, the gains obtained in these two configurations are almost equivalent.

By increasing the total thickness up to 100nm for the different materials except amorphous silicon (limitation on the diffusion length of the charge carriers), two trends appear according to the nature of the gap. For direct gap materials, the partial nano-structuring of the layer does not increase absorption compared to a flat layer with an optimized AR layer (observed from 600nm in thickness). This is not the case for c-Si (indirect gap), as highlighted in [84].

The transition from these theoretical studies to the manufacture of absorbent PCs took place in several stages. Initially, the concept was validated on the basis of optical demonstrators consisting of a simple ultrathin layer of a-Si:H deposited on a glass substrate and engraved in 1DPC via holographic lithography and plasma engraving [84]. Optical measurements showed an increase in absorption of about 50% over the entire spectrum compared to a flat layer, according to the simulation results.

In a second step, a square grating of holes was transferred into a complete stack comprising transparent conductive layers (TCO), the active layer of a-Si:H and a silver reflector on the back side [85]. The absorption spectra measured by integral sphere showed an increase in absorption over the entire spectrum with, in particular, for long wavelengths (>550nm), the presence of several peaks corresponding to quasi-guided modes.

The technological pathway leading to "photonized" cells was finally presented and the samples obtained were characterized by micro-reflectivity measurements in order to emphasize the homogeneity of the parameters of the PC on the surface of the samples [81]. At the same time, Mallick *et al.* Demonstrated an increase in external quantum efficiency (EQE) in the near infrared thanks to the structuring in two dimensional PC of an ultrathin layer (335nm) of c-Si [86]. It should nevertheless be noted that this last experimental demonstration was carried out on a lateral junction in the absence of a reflector and therefore it provides more of a proof of concept than an operational cell for PV. A problem specific to the manufacture of these cells, namely the effect of surface recombination on the flanks of the PC structured by plasma figure [87] before being studied more specifically by optoelectronic simulations in [88].

II.12. Conclusion

PCs are periodic structures of dielectric materials with a periodic variation in optical index. This latter variation behaves like a periodic potential barrier for photons. Thus, as in the case of an electron moving in the periodic potential created by atoms, a band structure appears, with spectral bands where propagation is allowed and others where it is prohibited. This chapter was devoted entirely to the study of the notion of PCs.

In this chapter, we have given the basic definitions relating to PC structures, such as: the periodicity of the change of their dialectical constants, the shape of the grating and the elements constituting it (form of holes for connected gratings and rods for disconnected

ones). Then, we gave a very important characteristic of PC structures which is their ability to provide a photonic band gap that excludes the propagation of light in wavelengths which are located between its limits.

To be able to benefit from their advantages (*i.e.* their photonic gap), these structures must contain defects introduced by breaking the periodicity of their original gratings (creation of cavities of different shapes, waveguides, etc.), this was also discussed in this chapter. At the end, we have given different forms of cavities and waveguides that can be made on PCs and that can be subsequently exploited for the realization of different applications as we will see in the chapters that follow.

List of references

[1] E. Yablonovitch, "Inhibited Spontaneous Emission in Solid-State Physics and Electronics," *Phys. Rev. Lett.*, vol. 58, no. 20, pp. 2059–2062, 1987.

[2] S. John, "Strong localization of photons in certain disordered dielectric superlattices," *Phys. Rev. Lett.*, vol. 58, no. 23, pp. 2486–2489, 1987.

[3] T. Yoshie *et al.*, "Vacuum Rabi splitting with a single quantum dot in a photonic crystal nanocavity," *Nature*, vol. 432, no. 7014, Art. no. 7014, 2004.

[4] M. Eichenfield, J. Chan, R. M. Camacho, K. J. Vahala, and O. Painter, "Optomechanical crystals," *Nature*, vol. 462, no. 7269, Art. no. 7269, 2009.

[5] J. D. Joannopoulos, S. G. Johnson, J. N. Winn, and R. D. Meade, *Photonic Crystals*. Princeton University Press, 2011.

[6] T. C. Wang, R. E. Cohen, and M. F. Rubner, "Metallodielectric Photonic Structures Based on Polyelectrolyte Multilayers," *Advanced Materials*, vol. 14, no. 21, pp. 1534–1537, 2002.

[7] B.-S. Song, S. Yamada, T. Asano, and S. Noda, "Demonstration of two-dimensional photonic crystals based on silicon carbide," *Opt. Express, OE*, vol. 19, no. 12, pp. 11084–11089, 2011.

[8] M. Deubel, M. Wegener, A. Kaso, and S. John, "Direct laser writing and characterization of 'Slanted Pore' Photonic Crystals," *Appl. Phys. Lett.*, vol. 85, no. 11, pp. 1895–1897, 2004.

[9] P. N. Prasad, *Nanophotonics*. John Wiley & Sons, 2004.

[10] P. Lodahl *et al.*, "Controlling the dynamics of spontaneous emission from quantum dots by photonic crystals," *Nature*, vol. 430, no. 7000, Art. no. 7000, 2004.

[11] T. Baba, "Remember the light," *Nature Photon*, vol. 1, no. 1, Art. no. 1, 2007.

[12] P. Yeh and M. Hendry, "Optical Waves in Layered Media," 1988.

[13] S. G. Johnson and J. D. Joannopoulos, "Block-iterative frequency-domain methods for Maxwell's equations in a planewave basis," *Opt. Express, OE*, vol. 8, no. 3, pp. 173–190, 2001.

[14] E. Yablonovitch and K. M. Leung, "Photonic band structure: Non-spherical atoms in the face-centered-cubic case," *Physica B: Condensed Matter*, vol. 175, no. 1, pp. 81–86, 1991.

[15] T. F. Krauss, R. M. D. L. Rue, and S. Brand, "Two-dimensional photonic-bandgap structures operating at near-infrared wavelengths," *Nature*, vol. 383, no. 6602, Art. no. 6602, 1996.

[16] H. Míguez *et al.*, "Photonic crystal properties of packed submicrometric SiO2 spheres," *Appl. Phys. Lett.*, vol. 71, no. 9, pp. 1148–1150, Sep. 1997, doi: 10.1063/1.119849.

[17] P. Ferrand *et al.*, "Self-assembly of three-dimensional photonic crystals on structured silicon wafers," *Appl. Phys. Lett.*, vol. 81, no. 15, pp. 2689–2691, 2002.

[18] B. Ali, "Etude du couplage dans les guides d'onde à cristaux Photoniques bidimensionnels," Thesis, université de msila, 2015.

[19] P. Pottier *et al.*, "Triangular and hexagonal high Q-factor 2-D photonic bandgap cavities on III-V suspended membranes," *Journal of Lightwave Technology*, vol. 17, no. 11, pp. 2058–2062, 1999.

[20] C. Grillet, "Microcomposants optiques à base de cristaux photoniques bidimensionnels pour l'optique intégrée," These de doctorat, Ecully, Ecole centrale de Lyon, 2003.

[21] B. Wild, "Étude expérimentale des propriétés optiques des cristaux photoniques bidimensionnels et de leur accordabillité," *Infoscience*, 2006.

[22] M. L. V. d'Yerville, "Modélisation de cristaux photoniques bidimensionnels de hauteur finie," These de doctorat, Montpellier 2, 2002.

[23] F. Amal, A. B. Hadjira, and A. Mehadji, "Ultra-Highly Efficient 1×3 and 1×6 Splitters for Terahertz Communication Applications," *IEEE Photonics Technology Letters*, vol. 28, no. 13, pp. 1434–1437, 2016.

[24] I. Bouderradji, "Conception d'un démultiplexeur à cristaux photoniques bidimensionnels," Thesis, Université Mohamed Boudiaf - M'Sila, 2012.

[25] E. Yablonovitch, T. J. Gmitter, R. D. Meade, A. M. Rappe, K. D. Brommer, and J. D. Joannopoulos, "Donor and acceptor modes in photonic band structure," *Phys. Rev. Lett.*, vol. 67, no. 24, pp. 3380–3383, 1991.

[26] Y. Yang and Z. H. Hang, "Topological whispering gallery modes in two-dimensional photonic crystal cavities," *Opt. Express, OE*, vol. 26, no. 16, pp. 21235–21241, 2018.

[27] D. E. Tranca, R. Tomescu, and P. Schiopu, "Design and simulation of infrared optical logic gates based on Si photonic crystal waveguides for high density photonic integrated circuits," in *Advanced Topics in Optoelectronics, Microelectronics, and Nanotechnologies VI*, Nov. 2012, vol. 8411, p. 84110Q.

[28] T. Jaffré, "Caractérisation des matériaux à bande interdite électromagnétique multiperiodiques et leurs applications aux antennes," These de doctorat, Limoges, 2005.

[29] D. Gérard, "Etude en champ proche et en champ lointain de composants périodiquement nanostructurés : cristaux photoniques et tamis à photons," phdthesis, Université de Bourgogne, 2004.

[30] A. D. Bristow *et al.*, "Ultrafast nonlinear response of AlGaAs two-dimensional photonic crystal waveguides," *Appl. Phys. Lett.*, vol. 83, no. 5, pp. 851–853, 2003.

[31] K. Ahmed, "Étude des potentialités de couches minces sol-gel dopées par des nanoparticules magnétiques pour la conception des cristaux magnéto-photonique," Université de M'sila , Département Electronique, 2015.

[32] K. Lenglé, "Traitement tout optique du signal à base de composants à cristaux photoniques en matériaux semiconducteurs III-V," These de doctorat, Rennes 1, 2013.

[33] M. Ortsiefer *et al.*, "2.5-mW single-mode operation of 1.55-μm buried tunnel junction VCSELs," *IEEE Photonics Technology Letters*, vol. 17, no. 8, pp. 1596–1598, 2005.

[34] Q. Rolland, "Couplages acousto-optiques dans les cristaux photoniques et phononiques," phdthesis, Université de Valenciennes et du Hainaut-Cambresis, 2013.

[35] S. Massaoudi, "Etude théorique et expérimentale des matériaux à bandes interdites photoniques bidimensionnels (BIP 2D) en micro-ondes : application à l'ultraréfraction," These de doctorat, Paris 11, 2005.

[36] R. Farha, "Etude d'une structure à cristal photonique 'LOM' gravée dans un guide Ti liNbO3 dopé erbium pour l'émission de la lumière à 1.55 μm," These de doctorat, Evry, Institut national des télécommunications, 2010.

[37] C. Caër, "Cristaux photoniques à fente: vers une photonique silicium hybride à exaltation localisée du champ électromagnétique," phdthesis, Université Paris Sud - Paris XI, 2013.

[38] K. M. Ho, C. T. Chan, and C. M. Soukoulis, "Existence of a photonic gap in periodic dielectric structures," *Phys. Rev. Lett.*, vol. 65, no. 25, pp. 3152–3155, 1990.

[39] E. Yablonovitch, "Photonic band-gap structures," *J. Opt. Soc. Am. B, JOSAB*, vol. 10, no. 2, pp. 283–295, 1993.

[40] S. Y. Lin *et al.*, "A three-dimensional photonic crystal operating at infrared wavelengths," *Nature*, vol. 394, no. 6690, Art. no. 6690, 1998.

[41] S. Noda, K. Tomoda, N. Yamamoto, and A. Chutinan, "Full Three-Dimensional Photonic Bandgap Crystals at Near-Infrared Wavelengths," *Science*, vol. 289, no. 5479, pp. 604–606, 2000.

[42] S. Fan, P. R. Villeneuve, R. D. Meade, and J. D. Joannopoulos, "Design of three- dimensional photonic crystals at submicron lengthscales," *Appl. Phys. Lett.*, vol. 65, no. 11, pp. 1466–1468, 1994.

[43] E. Kuramochi *et al.*, "Drilled alternating-layer structure for three-dimensional photonic crystals with a full band gap," *Journal of Vacuum Science & Technology B: Microelectronics and Nanometer Structures Processing, Measurement, and Phenomena*, vol. 18, no. 6, pp. 3510–3513, 2000.

[44] M. Notomi, T. Tamamura, T. Kawashima, and S. Kawakami, "Drilled alternating-layer three-dimensional photonic crystals having a full photonic band gap," *Appl. Phys. Lett.*, vol. 77, no. 26, pp. 4256–4258, 2000.

[45] A. Chelnokov, S. David, K. Wang, F. Marty, and J.-M. Lourtioz, "Fabrication of 2-D and 3-D silicon photonic crystals by deep etching," *IEEE Journal of Selected Topics in Quantum Electronics*, vol. 8, no. 4, pp. 919–927, 2002.

[46] J. D. Joannopoulos, P. R. Villeneuve, and S. Fan, "Photonic crystals: putting a new twist on light," *Nature*, vol. 386, no. 6621, Art. no. 6621, 1997.

[47] Z. Zhang and S. Satpathy, "Electromagnetic wave propagation in periodic structures: Bloch wave solution of Maxwell's equations," *Phys. Rev. Lett.*, vol. 65, no. 21, pp. 2650–2653, 1990.

[48] E. Yablonovitch, "Photonic band-gap crystals," *J. Phys.: Condens. Matter*, vol. 5, no. 16, pp. 2443–2460, 1993.

[49] E. Yablonovitch, T. J. Gmitter, and K. M. Leung, "Photonic band structure: The face-centered-cubic case employing nonspherical atoms," *Phys. Rev. Lett.*, vol. 67, no. 17, pp. 2295–2298, 1991.

[50] S.-Y. Lin, J. G. Fleming, R. Lin, M. M. Sigalas, R. Biswas, and K. M. Ho, "Complete three-dimensional photonic bandgap in a simple cubic structure," *J. Opt. Soc. Am. B, JOSAB*, vol. 18, no. 1, pp. 32–35, 2001.

[51] E. Yablonovitch, "Photonic Crystals," *Journal of Modern Optics*, vol. 41, no. 2, pp. 173–194, 1994.

[52] S. Satpathy, Z. Zhang, and M. R. Salehpour, "Theory of photon bands in three-dimensional periodic dielectric structures," *Phys. Rev. Lett.*, vol. 64, no. 11, pp. 1239–1242, 1990.

[53] E. Yablonovitch *et al.*, "3-dimensional photonic band structure," *Opt Quant Electron*, vol. 24, no. 2, pp. S273–S283, 1992.

[54] F. Raineri, "Optique non linéaire dans les cristaux photoniques en semiconducteurs III-V," phdthesis, Université Paris Sud - Paris XI, 2004.

[55] H. Rigneault, J.-M. Lourtioz, C. Delalande, and A. Levenson, *La nanophotonique*. Hermes Lavoisier, 2005, p. 339.

[56] R. Sawada, E. Higurashi, T. Ito, M. Tsubamoto, and O. Ohguchi, "Integrated micro-laser displacement sensor," in *Proceedings IEEE The Tenth Annual International Workshop on Micro Electro Mechanical Systems. An Investigation of Micro Structures, Sensors, Actuators, Machines and Robots*, Jan. 1997, pp. 19–24.

[57] O. Levy, B. Z. Steinberg, A. Boag, S. Krylov, and I. Goldfarb, "Mechanical tuning of two-dimensional photonic crystal cavity by micro Electro mechanical flexures," *Sensors and Actuators A: Physical*, vol. 139, no. 1, pp. 47–52, 2007.

[58] J. Goh, I. Fushman, D. Englund, and J. Vučković, "Genetic optimization of photonic bandgap structures," *Opt. Express, OE*, vol. 15, no. 13, pp. 8218–8230, 2007.

[59] Y. Desières, "Conception et études optiques de composants micro-photoniques sur matériaux III-V à base de structures à bande interdite de photon," Thèse de doctorat, Lyon, INSA, 2001.

[60] T. Kondo, S. Matsuo, S. Juodkazis, V. Mizeikis, and H. Misawa, "Multiphoton fabrication of periodic structures by multibeam interference of femtosecond pulses," *Appl. Phys. Lett.*, vol. 82, no. 17, pp. 2758–2760, 2003.

[61] E. T. Yu and J. van de Lagemaat, "Photon management for photovoltaics," *MRS Bulletin*, vol. 36, no. 6, pp. 424–428, 2011.

[62] P. Arguel, "Approches de l'intégration photonique dans les microsystèmes," thesis, Université Paul Sabatier - Toulouse III, 2005.

[63] S. Domínguez *et al.*, "Optimization of 1D photonic crystals to minimize the reflectance of silicon solar cells," *Photonics and Nanostructures - Fundamentals and Applications*, vol. 10, no. 1, pp. 46–53, 2012.

[64] H. Kosaka *et al.*, "Self-collimating phenomena in photonic crystals," *Appl. Phys. Lett.*, vol. 74, no. 9, pp. 1212–1214, 1999.

[65] I. V. Shadrivov, A. A. Sukhorukov, and Y. S. Kivshar, "Guided modes in negative-refractive-index waveguides," *Phys. Rev. E*, vol. 67, no. 5, p. 057602, 2003.

[66] E. Cubukcu, K. Aydin, E. Ozbay, S. Foteinopoulou, and C. M. Soukoulis, "Negative refraction by photonic crystals," *Nature*, vol. 423, no. 6940, Art. no. 6940, 2003.

[67] R. P. Feynman, R. B. Leighton, and M. Sands, "The Feynman Lectures on Physics; Vol. I," *American Journal of Physics*, vol. 33, no. 9, pp. 750–752, 1965.

[68] P. T. Rakich *et al.*, "Achieving centimetre-scale supercollimation in a large-area two-dimensional photonic crystal," *Nature Mater*, vol. 5, no. 2, Art. no. 2, 2006.

[69] D. W. Prather *et al.*, "Self-collimation in photonic crystal structures: a new paradigm for applications and device development," *J. Phys. D: Appl. Phys.*, vol. 40, no. 9, pp. 2635–2651, 2007.

[70] V. Zabelin *et al.*, "Self-collimating photonic crystal polarization beam splitter," *Opt. Lett., OL*, vol. 32, no. 5, pp. 530–532, 2007.

[71] B. Lombardet, L. A. Dunbar, R. Ferrini, and R. Houdré, "Fourier analysis of Bloch wave propagation in photonic crystals," *J. Opt. Soc. Am. B, JOSAB*, vol. 22, no. 6, pp. 1179–1190, 2005.

[72] E. Cassan, D. Bernier, G. Maire, D. Marris-Morini, and L. Vivien, "Bloch wave decomposition for prediction of strong light coupling efficiency into extended planar photonic crystals," *J. Opt. Soc. Am. B, JOSAB*, vol. 24, no. 5, pp. 1211–1215, 2007.

[73] J. Witzens and A. Scherer, "Efficient excitation of self-collimated beams and single Bloch modes in planar photonic crystals," *J. Opt. Soc. Am. A, JOSAA*, vol. 20, no. 5, pp. 935–940, 2003.

[74] M. Augustin *et al.*, "Self-guiding of infrared and visible light in photonic crystal slabs," *Appl. Phys. B*, vol. 81, no. 2, pp. 313–319, 2005.

[75] T. Baba and D. Ohsaki, "Interfaces of Photonic Crystals for High Efficiency Light Transmission," *Jpn. J. Appl. Phys.*, vol. 40, no. 10R, p. 5920, 2001.

[76] B. Momeni and A. Adibi, "Adiabatic matching stage for coupling of light to extended Bloch modes of photonic crystals," *Appl. Phys. Lett.*, vol. 87, no. 17, p. 171104, 2005.

[77] A. Čampa, J. Krč, and M. Topič, "Analysis and optimisation of microcrystalline silicon solar cells with periodic sinusoidal textured interfaces by two-dimensional optical simulations," *Journal of Applied Physics*, vol. 105, no. 8, p. 083107, 2009.

[78] A. Bielawny, C. Rockstuhl, F. Lederer, and R. B. Wehrspohn, "Intermediate reflectors for enhanced top cell performance in photovoltaic thin-film tandem cells," *Opt. Express, OE*, vol. 17, no. 10, pp. 8439–8446, 2009.

[79] Y. Park *et al.*, "Absorption enhancement using photonic crystals for silicon thin film solar cells," *Opt. Express, OE*, vol. 17, no. 16, pp. 14312–14321, 2009.

[80] Y.-C. Lee, C.-F. Huang, J.-Y. Chang, and M.-L. Wu, "Enhanced light trapping based on guided mode resonance effect for thin-film silicon solar cells with two filling-factor gratings," *Opt. Express, OE*, vol. 16, no. 11, pp. 7969–7975, 2008.

[81] S. Zanotto, M. Liscidini, and L. C. Andreani, "Light trapping regimes in thin-film silicon solar cells with a photonic pattern," *Opt. Express, OE*, vol. 18, no. 5, pp. 4260–4272, 2010.

[82] J. Buencuerpo, L. E. Munioz-Camuniez, M. L. Dotor, and P. A. Postigo, "Optical absorption enhancement in a hybrid system photonic crystal – thin substrate for photovoltaic applications," *Opt. Express, OE*, vol. 20, no. 104, pp. A452–A464, 2012.

[83] D. S. Wiersma, "Disordered Photonic Structures for Highly Efficient Thin Film Solar Cells," in *Advanced Photonics & Renewable Energy (2010), paper PWA1*, 2010, p. PWA1.

[84] A. Bozzola, M. Liscidini, and L. C. Andreani, "Photonic light-trapping versus Lambertian limits in thin film silicon solar cells with 1D and 2D periodic patterns," *Opt. Express, OE*, vol. 20, no. 102, pp. A224–A244, 2012.

[85] O. E. Daif *et al.*, "Absorbing one-dimensional planar photonic crystal for amorphous silicon solar cell," *Opt. Express, OE*, vol. 18, no. 103, pp. A293–A299, 2010.

[86] G. Gomard *et al.*, "Light harvesting by planar photonic crystals in solar cells: the case of amorphous silicon," *J. Opt.*, vol. 14, no. 2, p. 024011, 2012.

[87] S. Basu Mallick *et al.*, "Ultrathin crystalline-silicon solar cells with embedded photonic crystals," *Appl. Phys. Lett.*, vol. 100, no. 5, p. 053113, 2012.

[88] X. Meng *et al.*, "Absorbing photonic crystals for silicon thin-film solar cells: Design, fabrication and experimental investigation," *Solar Energy Materials and Solar Cells*, vol. 95, pp. S32–S38, 2011.

Chapter III

Simulation tools and numerical modelling

Chapter III: Simulation tools and numerical modelling

III.1. Introduction

Actually, knowing the propagation of electromagnetic waves well is considered a main point in the prediction of the efficiency of electromagnetic systems, where it is necessary to improve their design, but also to help decision-making in an operational context. A better modeling of the propagation of waves is required because a lot of systems depend on it [1].

A large number of tools for modeling the propagation and diffraction of electromagnetic waves have been developed since the end of the 1960s thanks to the increasing efficiency of computing means. The different methods used to describe the propagation of electromagnetic waves in PCs derive from standard ones commonly used in electromagnetism or in the physics of materials.

This chapter deals with applying of a powerful mathematical tool capable of predicting and analyzing the behaviour of resonant structures which are under study, in this chapter. A lot of researchers have worked to implement this numerical resolution of Maxwell's equations so as to account for the behaviour of various kinds of diffraction lattices.

The objective of this paper is to present the various numerical calculation tools that will be used for the study of the coupling of light with the absorbent layer of a SC. In this regard, we focus on the most commonly used methods: *the Rigorous Coupled Wave Analysis Method* (RCWA). The results of the simulations which are presented in this manual are operated thanks to *«DiffractMod»* of RSoft applied by RCWA methods. The different methods presented are complementary and allow a good description of the trapping of light by PCs.

III.2. Modelling of the propagation of light in periodic areas

Theoretical analysis of diffraction gratings is classically derived in textbooks from the theory of scalar optics, where is composed of a series of parallel and periodic slits milled in an opaque material. The diffracted orders are analyzed by Kirchhoff's diffraction theory by considering each slit as a secondary source of radiation.

By applying the Fraunhofer approximation, the discrete diffractive orders are given by the position of constructive interference between the waves emitted by each source [1]. However, this scalar theory failed to explain the famous spectral anomalies of light diffracted by a reflective metallic lattice which were first reported by Robert W. Wood in 1902 [2].

Interesting is the development of the differential method because it encountered a lot of issues which were not solved until the end of the 20th century. This method is based on the development of pseudo periodic electromagnetic fields in Fourier series, because Maxwell's linear equations contain partial temporal and spatial derivatives [3]. In the case of a one-dimensional lattice, the temporal harmonic Maxwell equations can be separated into two different sets of equations associated with one of the two fundamental polarizations *transverse electric* (TE) and *transverse magnetic* (TM). The spatial derivative

with respect to the coordinate axis along which the midpoint is periodic is calculated by extending the pseudo periodic fields in series by Fourier.

Convergence is generally faster for dielectric gratings because the dielectric permittivity contrast is lower in this case. In addition to this, the problems related to the poor convergence of the method in TM polarization were particularly difficult to identify. In fact, two different problems caused the poor convergence; the first when increasing the number of Fourier components with metallic lattices in TM polarization, and the second problem arises due to the digital instabilities related to the integration process. Therefore, the two problems are distinct, but the second becomes more important when the convergence of the method with respect to the truncation order is weak. This difficulty has given rise to alternative methods of integration. In particular, a method called Rigorous Coupled Wave Analysis (RCWA) dedicated to the integration of rectangular grooves was proposed in the 1980s [4].

III.3. The most used simulation methods and means

Experiments have often been supported by theoretical analyzes, whether to predict or confirm the obtained results. The complexity of the problem does not often result in closed form solutions, and in this case it requires the help of modeling techniques. Maxwell's macroscopic equations describe exactly the behaviour of electromagnetic fields in continuous media. Moreover, assuming that the structure and the materials involved are correctly defined, the issue can be solved quantitatively.

Among the theoretical models dealing with PCs, we must first distinguish two categories that depend on the finite or infinite size of structures and then on their dimensionality (1D, 2D or 3D). In the first of them dealing with crystals of finite thickness, the methods based on transfer matrices [5], and diffraction theories (RCWA) [6] are most often used. They allow calculating the properties reflection and transmission of diffraction by the PC grating [7]. The main techniques used in the second category dealing with crystals of infinite size are based on plane wave decomposition [8, 9].

III.3.1. The plane wave expansion method (PWE)

The Plane Wave Expansion (PWE) method [10] consists of solving the linear wave equation in frequency space by expanding the electromagnetic field on a plane wave basis. The plane wave decomposition method is very efficient in calculating perfectly periodic PC band diagrams. It allows determining the frequency, polarization, symmetry and fielding distribution for the modes of a photonic structure [11].

It can be adapted to study certain non-periodic structures such as waveguides or cavities thanks to the super cell technique [12], but to ensure convergence of calculations. This method requires a large number of plane waves, which induce a high computation time and limit it.

III.3.2. The finite difference time domain method (FDTD)

The Finite Difference Time Domain (FDTD) time domain method is a general method that allows most systems to be simulated [13]. It was first proposed by K. S. Yee [14]. This technique, widely used in electromagnetism, consists in discretizing Maxwell's equations

in space and in the time domain and not in the frequency domain, which leads to the resolution of a finite difference equation by Fourier transform in time [15].

This method allows not only to calculate the band diagrams but also to simulate the temporal evolution of the electromagnetic field propagating in photonic crystal structures, which allows having information on many other quantities. On the other hand, it requires excellent resolution which requires significant computing resources and computer memories, the efficiency of diffraction gratings, it consists in determining the shape of the states in each of the media constituting the multilayer structure. In each of these media, we solve Maxwell's equations [16].

III.3.3. The Rigorous Coupled Wave Analysis method (RCWA)

Fourier methods are considered among the methods currently used for rigorous diffraction calculations of periodic and periodized refractive index distributions [17, 18].

One of the reasons for this is their applicability to a lot of types of periodic or periodized structures in particular dielectric gratings [17].

Their simplicity is another reason, they reduce the system of partial differential equations to a system of ordinary differential equations by projection on a Fourier basis. This simplifies their implementation compared to many other methods such as for instance the integral or finite element method [18].

Among the rigorous Fourier methods, there are different procedures regarding the direction of integration, in which the light propagates between the substrate and the cladding.

The most popular Fourier method is the *Rigorous Coupled Waves Analysis* (RCWA), moreover known as the Fourier modal method and it is based on the solution of an issue of given values at each sampling integration point.

This is particularly effective in the case of binary and stair profiles. It is also a useful alternative, in the case of arbitrarily inclined and curved profiles, the differential method, which integrates numerically and avoids solving a problem of given values at each integration sampling point [17, 19].

RCWA is a semi-analytical Fourier space method that can be used to find exact solutions for electromagnetic waves that diffract through complex lattice structures [6], and it is based on the decomposition of the electromagnetic field and the dielectric permittivity in Fourier series [20, 21] (This method will be detailed in this chapter).

III.3.3.1. Discovery and fabrication of diffraction lattices

The first observation of the unusual propagation of light through a periodic medium was made by F. Hopkinson in 1786 when he observed a lamppost through a silk handkerchief held out between his hands on a summer evening. He was surprised to find that "the silk threads grew to the size of very coarse threads"; but was very surprised to find that "although I moved the handkerchief to the right and left in front of my eyes, the dark bars did not seem to move at all, but remained permanent in front of me" [22].

The latter, a famous astronomer, quickly understood that this observation came from an interesting phenomenon in optics and opens his letter with this comment: "The experiment

with a silk handkerchief and the distant flame of a lamp, is much more curious than one might imagine at first glance".

D. Rittenhouse realized that the phenomenon was due to a diffraction effect and he decided to reproduce the experiment by making what could be considered the first human-made diffraction grating.

To do this, he placed about 55 parallel hairs of about 1/2 inch each on the threads of a pair of fine pitch screws. Then, he observed the sky through a slit. With parallel hairs to the slit, he observed parallel lines. Amazingly, he noticed that "*the red rays are more curved out of their first direction, and the blue rays less";* unlike what happens by refraction" [22]. Fraunhofer's interest in the fabrication and optical characterization of diffraction lattices led to a major breakthrough [23]. Independently of the previous observations of F. Bloch [24], he noticed the cosine dependence of the diffracted rays.

This very dynamic field of research aims to structure matter to adapt electromagnetic waves to a sub-wavelength scale. The development of diffraction gratings has been closely linked to the development of micro and nanotechnologies. The first fabricated gratings were mechanically tuned [25, 26] and most gratings used for spectroscopic applications were tuned gratings.

Cotton's first experiments [27] in 1901 which produced a lattice by recording an interference pattern on a photographic plate followed by the advent of lasers in the 1960s paved the way for the fabrication of holographic lattices. This technique is to cover a photosensitive layer on a substrate (quartz or glass in general) and to create an interference pattern by superimposing two coherent beams. The period of the grating is defined by the angle of incidence of the laser beams θ and their wavelength λ according to the classical interference formula $d=\lambda/2\sin\theta$. This manufacturing step requires collimated beams because slight curvatures of the wave front result in non periodic curved grooves (see Figure III.1, showing an example of holographic placement).

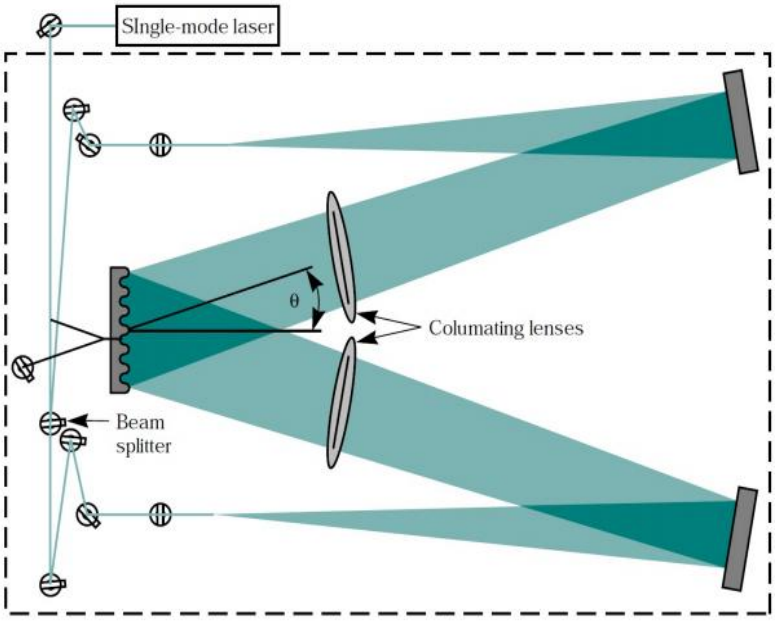

Figure III.1: Schematic presentation of a holographic installation.

III.3.3.2. The starting point: Maxwell's equations

The power counting of super calculators and even PCs is now sufficient to model PCs (Figure III.2).

There is not only one method for modeling PCs, each method has its advantages and disadvantages and is suitable for certain PCs [28].

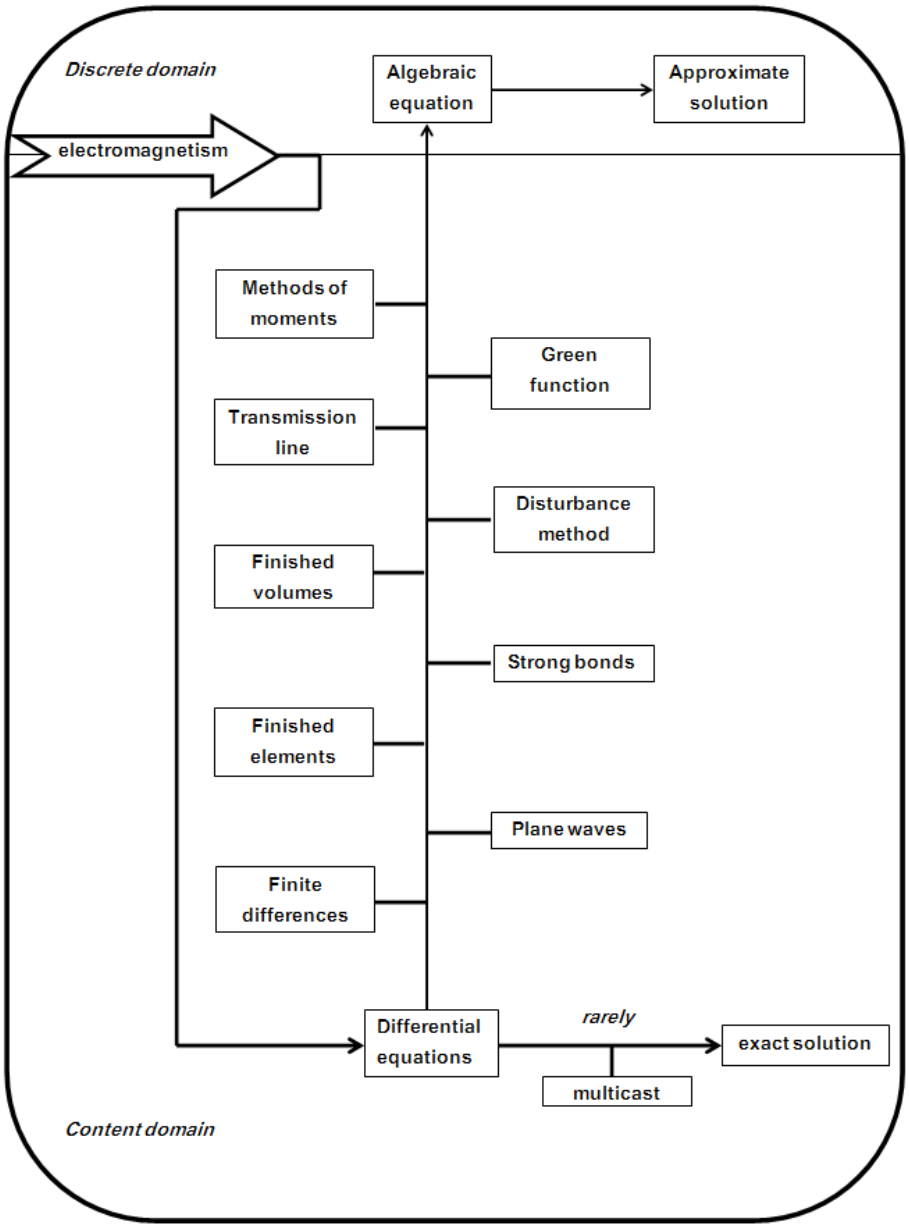

Figure.III.2: Resolution of Maxwell's equations [28].

The non-dispersive, non-conductive, non-magnetic materials and homogeneous Maxwell's equations projected onto a Cartesian coordinate system are written [29]:

$$\begin{cases} \frac{\partial H_x}{\partial t} = \frac{1}{\mu}\left(\frac{\partial E_y}{\partial z} - \frac{\partial E_z}{\partial y}\right) \\ \frac{\partial H_y}{\partial t} = \frac{1}{\mu}\left(\frac{\partial E_z}{\partial x} - \frac{\partial E_x}{\partial z}\right) \\ \frac{\partial H_z}{\partial t} = \frac{1}{\mu}\left(\frac{\partial E_x}{\partial y} - \frac{\partial E_y}{\partial x}\right) \\ \frac{\partial E_x}{\partial t} = \frac{1}{\varepsilon}\left(\frac{\partial H_y}{\partial z} - \frac{\partial H_z}{\partial y}\right) \\ \frac{\partial E_y}{\partial t} = \frac{1}{\varepsilon}\left(\frac{\partial H_z}{\partial x} - \frac{\partial H_x}{\partial z}\right) \\ \frac{\partial E_z}{\partial t} = \frac{1}{\varepsilon}\left(\frac{\partial H_x}{\partial y} - \frac{\partial H_y}{\partial x}\right) \end{cases} \quad \text{(III.7)}$$

In case where the photonic crystals are periodic in two directions (x and y for instance) and infinite in the third direction (z), the previous system of equations is simplified according to the kind of propagation. Here, the propagation takes place in the plane and the variation of the fields is cancelled out in the third direction.

The system of equations (III.7) is simplified and subdivided into two subsystems giving rise to the two transverse electric polarizations TE and transverse magnetic TM. To illustrate that, let us suppose that the crystal is periodic along the x and y directions and is infinite along z. The derivatives with respect to z cancel each other out:

$$\begin{cases} \frac{\partial H_x}{\partial t} = -\frac{1}{\mu}\left(\frac{\partial E_z}{\partial y}\right) \\ \frac{\partial H_y}{\partial t} = \frac{1}{\mu}\left(\frac{\partial E_z}{\partial x}\right) \\ \frac{\partial H_z}{\partial t} = -\frac{1}{\mu}\left(\frac{\partial E_y}{\partial x} - \frac{\partial E_x}{\partial y}\right) \\ \frac{\partial E_x}{\partial t} = \frac{1}{\varepsilon}\left(\frac{\partial H_z}{\partial y}\right) \\ \frac{\partial E_y}{\partial t} = \frac{1}{\varepsilon}\left(-\frac{\partial H_z}{\partial y}\right) \\ \frac{\partial E_z}{\partial t} = \frac{1}{\varepsilon}\left(\frac{\partial H_y}{\partial x} - \frac{\partial H_x}{\partial y}\right) \end{cases} \quad \text{(III.8)}$$

We notice that the evolution of Hx, Hy, and Ez is independent of that of Ex, Ey, and Hz. As a result, two independent systems of equations result, one describing the TE polarization and the other the TM polarization. The propagation of the electromagnetic field can therefore be treated independently for the two polarizations.

III.3.3.3 TE Polarization

TE polarization (Transverse Electric): is the polarization where the electric field is perpendicular to the (y) direction [30]. It is defined by the following system:

$$\begin{cases} \frac{\partial E_x}{\partial t} = \frac{1}{\varepsilon}\left(\frac{\partial H_z}{\partial y}\right) \\ \frac{\partial E_y}{\partial t} = \frac{1}{\varepsilon}\left(-\frac{\partial H_z}{\partial y}\right) \\ \frac{\partial E_z}{\partial t} = \frac{1}{\varepsilon}\left(\frac{\partial H_y}{\partial x} - \frac{\partial H_x}{\partial y}\right) \end{cases} \quad \text{(III.9)}$$

For the grating which has just been described, we first consider the transverse electrical polarization (TE). Here, the incident electric field is normal to the plane of incidence which is the (x, z) plane, and is polarized along the *y* direction.

III.3.3.4 TM Polarization

TM (Transverse Magnetic) polarization: is the polarization where the magnetic field is perpendicular to the (y) direction [31]. It is defined by the following system:

$$\left\{\begin{array}{c} \frac{\partial H_x}{\partial t} = -\frac{1}{\mu}\left(\frac{\partial E_z}{\partial y}\right) \\ \frac{\partial H_y}{\partial t} = \frac{1}{\mu}\left(\frac{\partial E_z}{\partial x}\right) \\ \frac{\partial H_z}{\partial t} = -\frac{1}{\mu}\left(\frac{\partial E_y}{\partial x} - \frac{\partial E_x}{\partial y}\right) \end{array}\right\} \quad \text{(III.10)}$$

This method is based on the principle of centred finite differences. It was found that when the approach we have described for TE polarized light is repeated for magnetic transverse polarized (TM) light, the convergence obtained by increasing the number of harmonics is slow. Therefore, corrections were introduced in the algorithm [32, 33]. Before proceeding with the corrections, let's follow the same procedure as before for the polarized incidence TM and explain why these corrections appear.

III.4. The art state

There are two main types of methods for solving Maxwell's equations to model the propagation of an electromagnetic wave: *rigorous methods* and *asymptotic methods*. The rigorous methods are numerical methods which make it possible to model the electromagnetic problem without approximation. We can list the method of moments [34], or the finite element method [35]. However, due to prohibitive memory size and computation time, these are limited to obstacles with dimensions of the order of a few wavelengths. Our objective being to model the propagation over large distances with respect to the wavelength, these methods are not considered during our study. The alternative to using rigorous methods lies in asymptotic methods.

These are based on approximate formulations and tend towards the exact solution when a parameter (the size of the target, the distance, etc.) becomes large in relation to the wavelength. They are therefore particularly suited to our problem of modeling propagation over large distances. Classically, it is the concept of radius that is used within the framework of geometrical optics [36], or of the uniform theory of diffraction [37].

The wave propagation is modelled in these methods by rays according to Fermat's principle: they are referred to as asymptotic ray methods. However, these methods are rarely developed in three dimensions. Indeed, above large three dimensional scenes, the number of interactions between the wave and the relief can be very important. So when the scene becomes more complex, the number of rays required “explodes” which significantly increases the necessary computation time.

Asymptotic current methods are based on the asymptotic expression of surface currents distributed over the obstacles treated. The field radiated by the obstacle is calculated as the radiation of these asymptotic surface currents. These methods are physical optics [38], and the physical theory of diffraction [39]. However, the surface currents are only calculated on condition of knowing the incident field at the considered surface. This last field is not in our context of three-dimensional scenes not only due to the direct field of the antenna but is sensitive to reflections and diffractions that can be introduced by the relief. To calculate

the field resulting from these interactions, one cannot do otherwise than to appeal to the rigorous methods or to the asymptotic ray methods.

III.5. Simulation software

III.5.1. Foreword of RSoft CAD

RSoft CAD is the main program of RSoft Component Design Suite and acts as a control program for the passive device simulation modules of RSoft BeamPROP, FullWAVE, BandSOLVE, GratingMOD, DiffractMOD, FemSIM and ModePROP. It allows defining the most important input required by these simulation modules: the material properties and the structural geometry of a photonic device. A user first designs a structure in the CAO interface and then uses one or more simulation engines to model various aspects of the device.

This modular approach to designing and simulating photonic devices is one of the greatest strengths of RSoft's component design suite. Each program in the suite is designed to "play well" with the other programs, creating an area in which data can be shared between modules. Virtually all input and output files are in a simple ASCII text format, which allows the user even greater control over the operation of the program as well as the third-party programs to be integrated into the suite. While RSoft Component Design Suite is designed to be used through the Graphical User Interface (GUI), command line operation is also possible. This, along with the modularity of the suite, allows for complex scripting capability.

III.5.1.1 Numerical simulation steps with RSoft

– **Opening of the window RSoft CAD**

The RSoft CAD program appears as in figure III. 3. There is a menu bar at the top of the window, two toolbars with icons just below, another toolbar along the left edge of the window, and a status line at the bottom of the window.

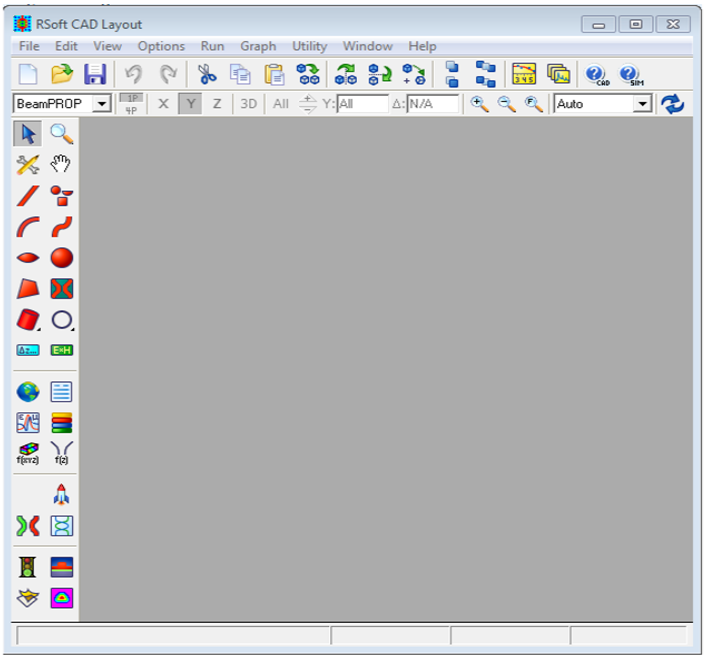

Figure III. 3: The RSoft CAD window, showing the menu bar at the top, the toolbars at the top left, and the status line at the bottom.

– **Creation of a new design file**

RSoft CAD provides the key entry for each of the RSoft simulation engines: the distribution of the refractive index of the problem to be modelled. This is determined by the geometry, arrangement and optical properties of the components the user has placed. RSoft CAD allows users to specify this information in a simple and user-friendly way. To create a new design file, click the *New Circuit* icon (the leftmost icon on the top toolbar) or choose *File/New* from the menu. The start-up dialog box will appear as shown in Figure III. 4 where basic information about the structure and the simulation tool to use.

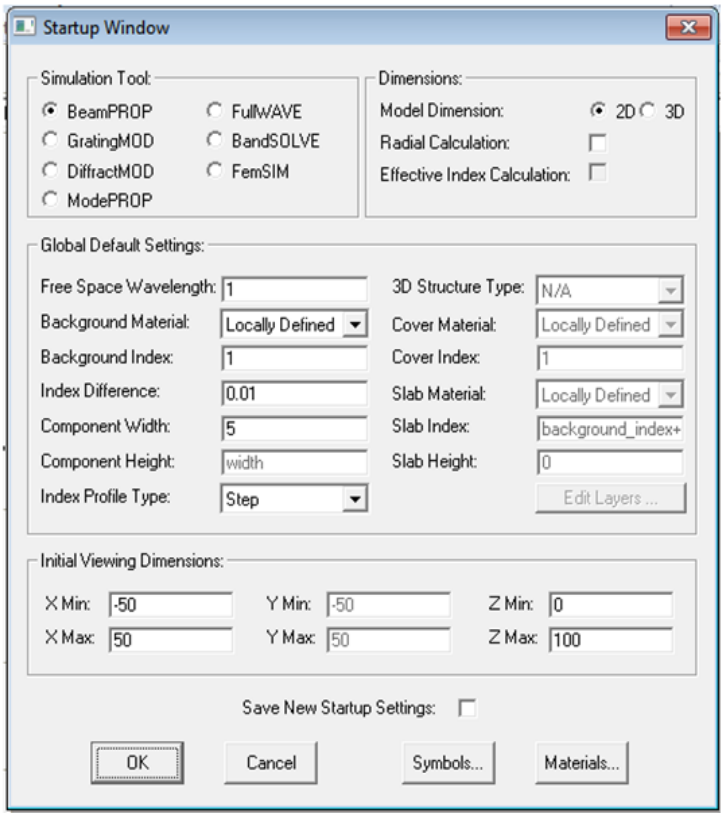

Figure III. 4: Start-up window.

The view shown in figure III.5 shows the XZ: X plane represents the horizontal direction; Z represents the vertical direction. The axes are indicated by light gray lines. If it was a two dimensional structure, there would be no Y axis and this would be the only view possible.

Since this is three dimensional design, the Y axis is outside the window and it is also possible to display the YZ and XY planes: click on the X, Y and Z buttons in the *toolbar display tools* (the second toolbar above) to shift between views.

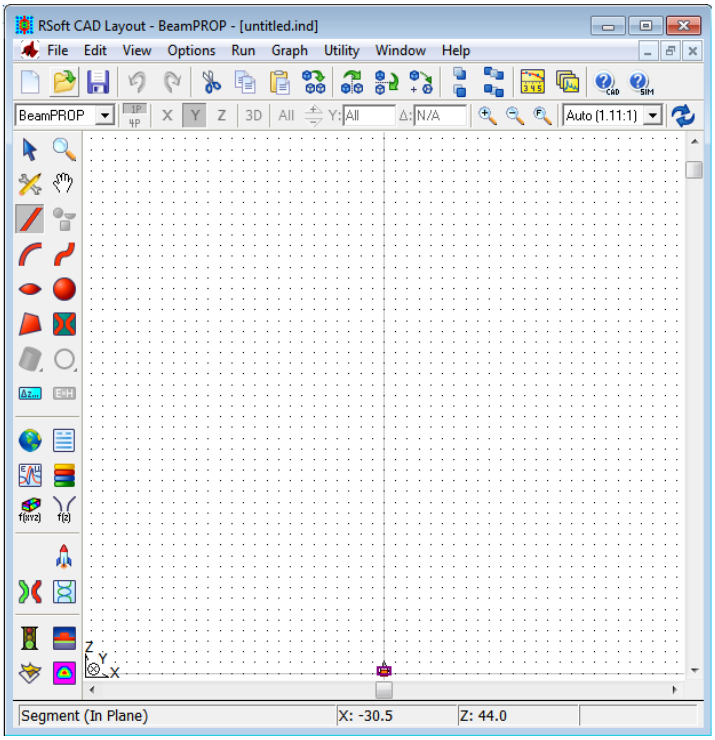

Figure III. 5: Illustration of a layout window where components are added to the circuit. The simulation domain and launch field are also displayed.

The mouse appears as a cross-reference and the display of coordinates in the status line indicates the position of the mouse in real coordinates [µm].

– **Definition of variables**

It is generally advantageous to create variables that will represent various aspects of the structure. As an example, we will create a variable to represent the length of a component. Click the *Edit Symbols* icon on the left *toolbar* to open the *Symbol Table Editor* as shown in Figure III. 6.

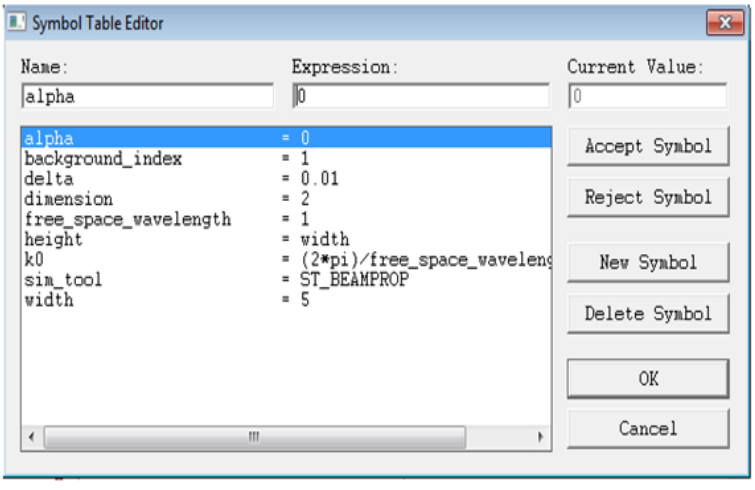

Figure III. 6: Table of symbols Editor

– **Drawing a component**

RSoft CAD components (usually referred to simply as "components") are the basic elements from which a design is created. A wide variety of components can be used, including segments (rectangular, cylindrical, multilayer, diffuse, etc.), conical objects,

lenses, user-defined polygons, spheres, cylinders, and fully user-defined objects. Any number and combination of these components, which have their own local, geometric and material parameters, can be incorporated into a base material of a specific index to create the distribution of the refractive index of the entire structure.

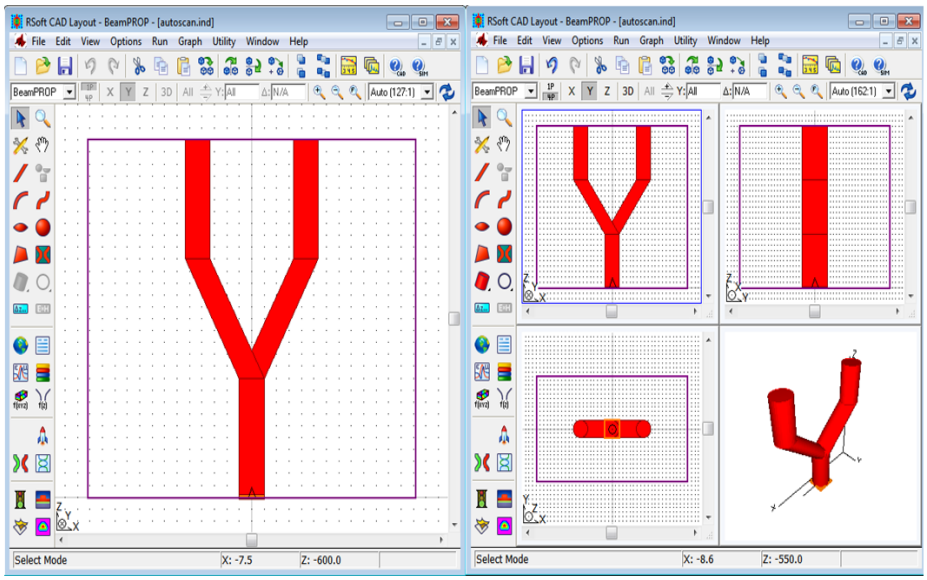

Figure III. 7: a) A fiber component as it appears in the XZ plane after drawing, and b) Multi-pane view clearly showing the fiber component. The multi-pane view is not available for 2D structures.

– **The Component Properties**

To set exactly the properties of the component in order to have precise control over the properties of the component such as refractive index, position and size. This is done through the Component Properties dialog box shown in Figure III. 8.

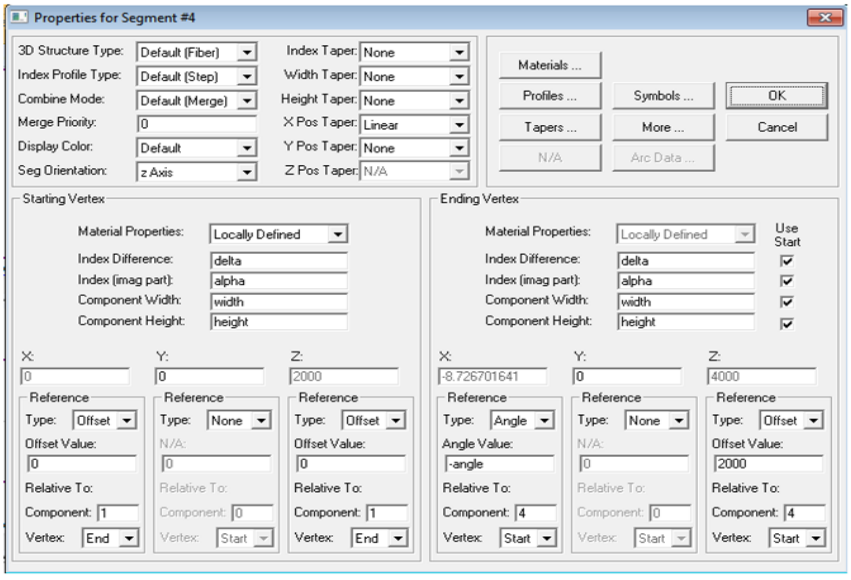

Figure III. 8: The component Properties dialog box for the fiber component.

– **Checking the layout of the structure**

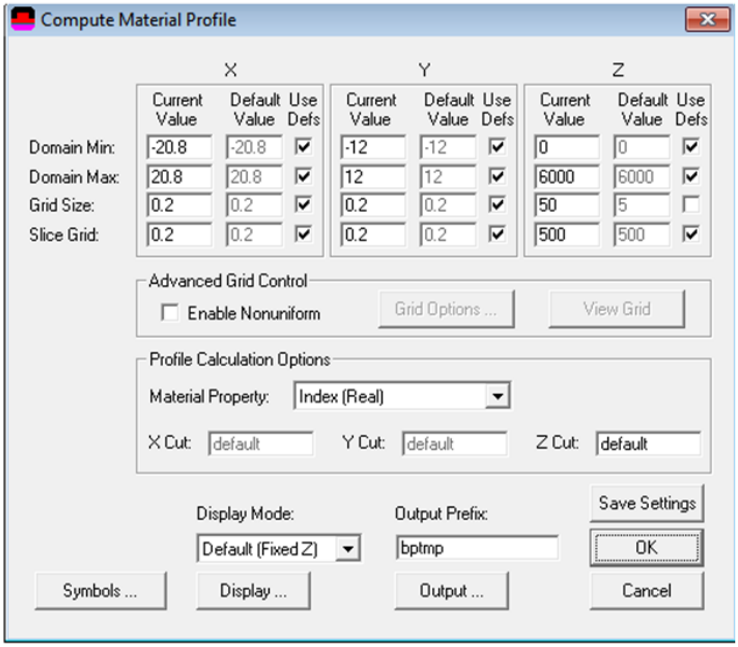

Figure III. 9: The calculate Index Profile dialog box.

III.5.3. Associated simulation modules

RSoft CAD is the main control program for a series of simulation modules licensed separately from RSoft. Among these simulation modules, we mentioned some typical applications:

III.5.3.1. FullWAVE

FullWAVE is ideal for designing complex photonic cameras. The software uses the Finite Difference Time Domain Simulation (FDTD) method, which enables the analysis of devices, such as photonic bandgaps and ring resonators, that cannot be modelled with techniques such as the Effective Beam Propagation (BPM) method.

III.5.3.2. BandSOLVE

BandSOLVE is a simulation module for generating and analyzing photonic band structures. This simulation module is based on an advanced optimized implementation of the plane wave expansion technique for periodic structures. It is ideal for the production of band structures for conventional photonic band gap structures such as 2D and 3D photonic crystal waveguides and fault sites.

III.5.3.3. GratingMOD

This software tool allows you to model and analyze many devices that integrate gratings and various types of filters, and easily integrates with RSoft's award-winning simulation tools. It provides both front and back analysis, enabling the calculation of grating spectra from known geometries and the synthesis of grating structures from grating spectra.

III.5.3.4. DiffractMOD

DiffractMOD is a general design tool for diffractive optical structures such as diffractive optical elements, periodic subwavelength structures, and photonic band gap crystals [40]. It

is based on the Rigorous Coupled Wave Analysis (RCWA) technique and can simulate 2D and 3D structures with arbitrary lattice structure and unit cell index profile [41]. In addition to dielectric materials, dispersive and lossy material structures such as metallic systems can also be used [42]. Typical applications include diffractive optical elements (DOD), photonic band gap structures, wavelength filters, optical metrology, nano-lithography, polarization sensitive devices, artificial dielectric coatings, systems photovoltaics, 3D displays, optical interconnects, optical data storage, spectroscopy, microlens arrays, and beam splitting, combining and shaping [43].

1) Operation of the graphical user interface

Operating the DiffractMOD GUI is a very simple process and can be broken down into basic steps:

– **Establishment of the structure**

We consider that an RSoft CAD window has been launched, and that a layout window has been opened which contains the circuit to be simulated; it can be a newly created circuit or a previously saved circuit loaded via the *File/Open* menu item. The general operation of the RSoft CAD program is described in the RSoft CAD manual.

– **Choosing the DiffractMOD simulation engine**

The first step in launching a DiffractMOD simulation is to verify that the simulation tool has been set to DiffractMOD in the Global Settings dialog box.

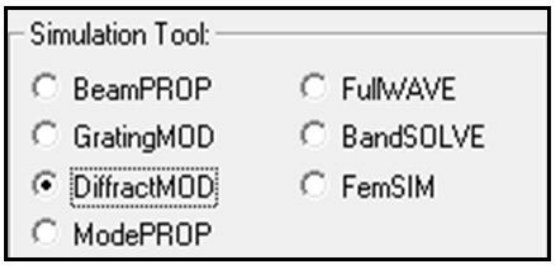

Figure III. 10: The Simulation tool option as indicated in the global Parameters dialog box.

– **Configuration of simulation parameters**

In the simulation settings dialog box shown in Figure III.11 by clicking the perform simulation icon (*green light*), in the RSoft CAD toolbar on the left. This dialog box allows you to enter the required parameters for a digital simulation and also controls other important aspects of the simulation.

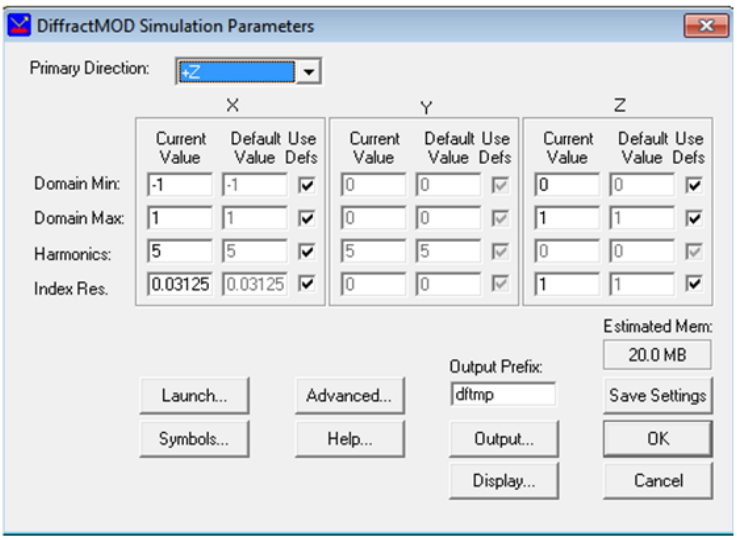

Figure III.11: The diffractMOD simulation parameters window where basic digital simulation parameters are entered.

2) The main direction

DiffractMOD requires a structure to be periodic in one (for a 2D simulation) or two (for a 3D simulation) dimensions [44]. In both cases, the normal coordinate at this periodicity is called the main direction and can be considered the main axis along which the field moves. The main direction can be set to +Z, -Z, +X, -X, +Y, and -Y. The sign indicates in which direction the launch field moves primarily along the main axis. For instance, if the grating is periodic in the X and Y directions, then the main direction should be set to +Z or -Z depending on the direction from which the initial field is incident.

Figure III. 12: The section of the DiffractMOD Simulation Settings dialog box where the main direction is chosen.

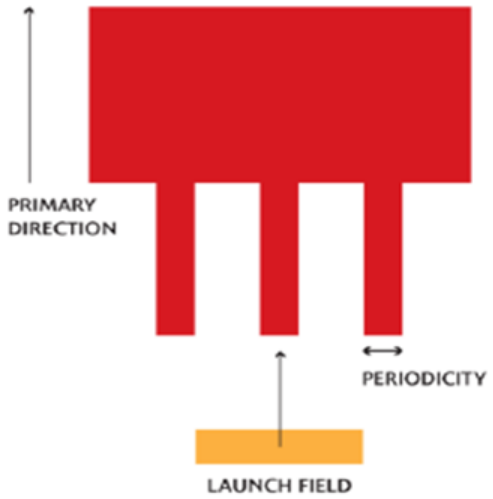

Figure III. 13: The main direction is defined as being transverse to the periodicity and the main direction in which the incident light moves.

– **The launch pad (Launch field)**

A key element of a DiffractMOD simulation is the launch field used to excite the structure: a plane wave with an arbitrary wavelength and an incident angle (defined by k) and a polarization (defined by E).

Launch properties are set in the Plane Wave Launch Options dialog box, which can be opened by clicking the Edit Launch Field button on the left RSoft CAD toolbar or by clicking the Launch button in the DiffractMOD Simulation Settings dialog box. This dialog box has separate commands for the K-vector and the-E-vector that are discussed in the following sections.

– **The vector-k (wavelength and direction)**
  The wave vector k defines the wavelength and direction of the launch field.

Wave Length

The wavelength of the incident light is set using the Free Space Wavelength [μm] option in the Global Settings dialog box.
When a simple scan of parameters on the wavelength is performed, the wavelength is defined by the scan values entered in the Output Options dialog box.

Launch direction

The direction of the wave vector k is defined by one (in 2D) or two (in 3D) angles. These angles are defined at the top of the Plane Wave Launch Options dialog box.

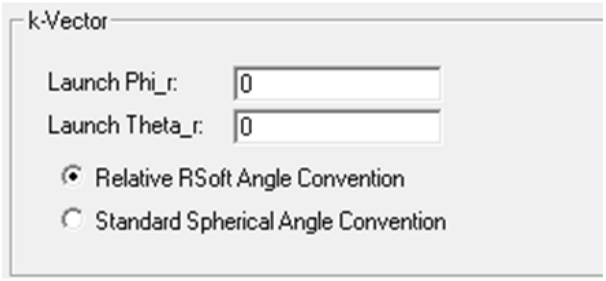

Figure III. 14: The part of the Plane Wave Launch Options dialog box where the k-Vector (input angle) options are set.

DiffractMOD supports two angle conventions: the RSoft relative angle convention (a) and the standard spherical angle convention (b). Depending on the convention chosen in the Plane Wave Launch Options dialog box, the text labels shown in Figure III. 15.

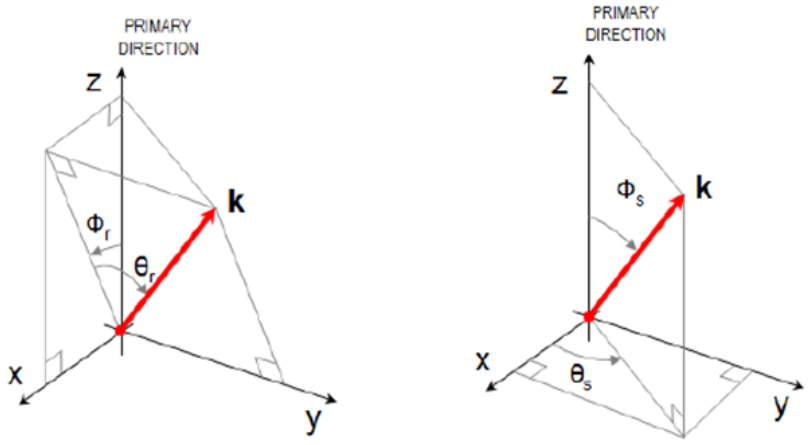

Figure III. 15: The two angle conventions supported by DiffractMOD: a) The RSoft relative angle convention and b) the standard spherical angle convention.

– **Vector E (polarization)**

The polarization of the DiffractMOD launch field is defined by the direction of the vector-E. Polarization options are set at the bottom of the Plane Wave Launch Options dialog box. Separate commands are given for 2D and 3D.

Figure III. 16: The part of the Plane Wave Launch Options dialog box where the vector-E (polarization) options are set.

Polarization in 2D

In 2D, the polarization can be TE (out of plane, Ey) or TM (in the plane, Ex).

Polarization in 3D

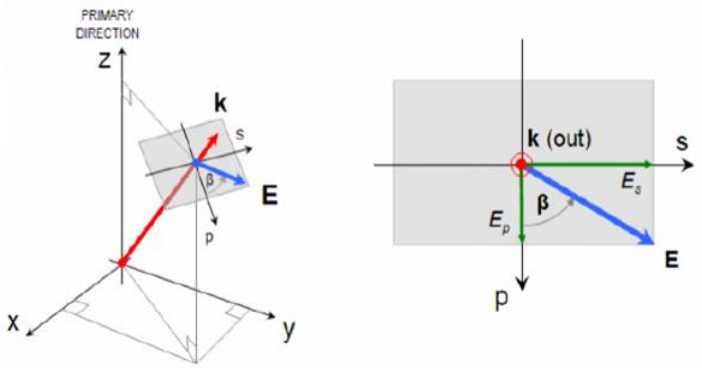

Figure III. 17: The plane wave polarization plane for DiffractMOD 3D simulations: a) the polarization plane (P-S) is normal to the wave vector k, and b) the polarization plane with the s and p components of the E field represented.

In three dimensional, the polarization of vector *E* is defined as being in a plane of polarization (*P*-*S*) normal to the direction defined by the wave vector *k*. In this plane, one angle defines the *P* and *S* components of *E* and another defines the phase difference between the p and s components. The options that control 3D polarization are:

– **Angle of polarization**

It sets the orientation of the vector E in the polarization plane. This angle is called the angle β in Figure III. 17. That angle is defined in such a way that a value of 0, which is the default value, corresponds to the polarisation *"P"*, and a value of 90 corresponds to the polarization *"S"*. The polarization *"P"* is defined in such a way that it is in the plane created by the primary direction and the wave vector *k*, and that it is oriented away from the primary direction. For the singular case where k is oriented along the primary direction, a polarization *"p"* is oriented along the X axis (when the primary direction is along *Z*). The direction of polarizations is defined as being within the plane of polarisation so that the cross product of '*P*' and '*S*' is along *k*.

– **Phase Difference**

This angle defines the phase difference between the components *"s"* and *"p"* of the vector E shown in Figure III. 17.b. A value of 0, which is the default value, corresponds to the linear polarization.

3) Drawing Basic Shapes in RSoft CAD

– **Rectangles, squares, cubes, boxes, etc.**

Rectangles, squares, cubes, boxes, and other "square" objects can be drawn using the segment component type with a channel structure type (required in 3D only). The segment component type has a start and an end vertex. The width (along *X)* and, in 3D, the height (along *Y)* can be adjusted. The length of the segment (distance between vertices) is usually defined along the *Z* axis even if it can be rotated as needed. The easiest way to set the length is to set the Z coordinate of the end vertex to be offset by the desired length from the starting vertex.

– **Circules, cylindres, etc.**

Circles, cylinders and other objects of circular cross-section can be created in two ways:

• Via a segment component type with a channel structure type

This type of segment is similar to the channel segment described in the previous section but has a circular/elliptical cross-section in the XY plane (not turned). The width and height parameters control the diameters along X and Y respectively of the circle/ellipse. This is the most convenient way to create circles or cylinders in the XY plane.

• Via a lens or a circle-like component

These types of components can be used to easily create circles or cylinders in the XZ plane.

– **Pyramids, triangles, cones, etc.**

Pyramids, triangles, cones and other shapes that have a square or circular base and arrive at a point (or a smaller version of the base such as a truncated pyramid) can easily be created using the segment component type and a width and/or cone of height. A conicity modifies a structural property along the Z axis of the segment.
Thus, for example, the use of a fiber segment and the definition of the width and end height on 0 and a linear conicity give a cone shape. The position of a segment can also be tapered, allowing for flexible designs.

– **Trapezoidal shapes**

Trapezoidal shapes can be obtained with cones in the XZ plane or by using the side wall angle function in the XY plane.

– **Substrates**

A lot of grating models contain a substrate. In most cases, this substrate can be created using a large rectangular segment larger than the simulation domain along the periodic coordinates.

4) The SC utility

Solar cells are by nature optical and electronic devices. To model these types of devices with precision, the SC utility uses one of the optical models listed below to calculate either an absorption spectrum of the device or the total energy density within the structure.
This optical information is then transmitted to one of the electrical models.

5) The Use of the SC utility

The SC utility can be opened via the Utility menu item in the RSoft CAD window. It is divided into two main sections, one for optical calculation and the other for electrical calculation and it is illustrated in Figure III. 18.

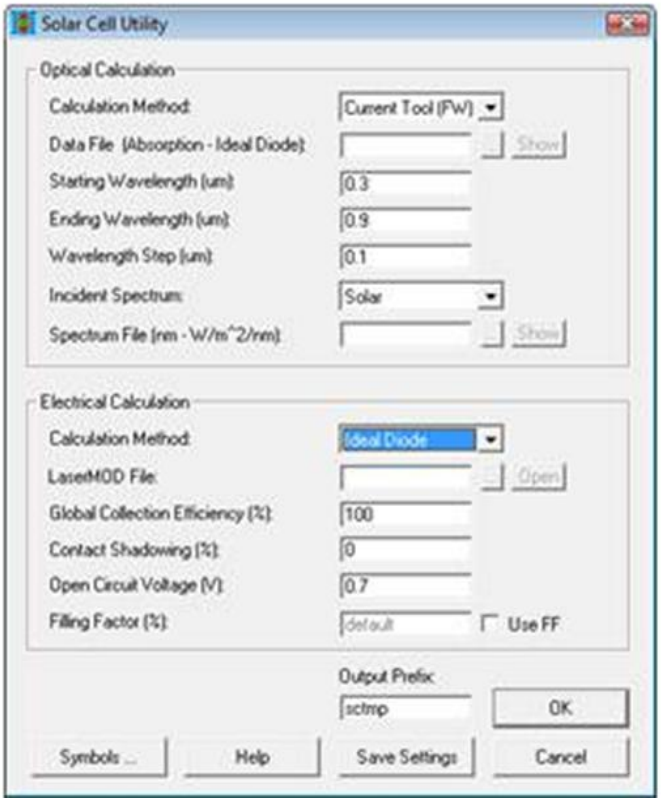

Figure III. 18: The SC Utility dialog box.

Once the calculation is started, the simulation window of the solar cell utility will create the requested simulation engine windows. When an absorption spectrum needs to be generated through simulation, a pause or interrupt in the Utility window will not stop the current simulation point, but will prevent the next one from starting. Once the simulation is complete, the status and results will be reported as shown in Figure III. 19.

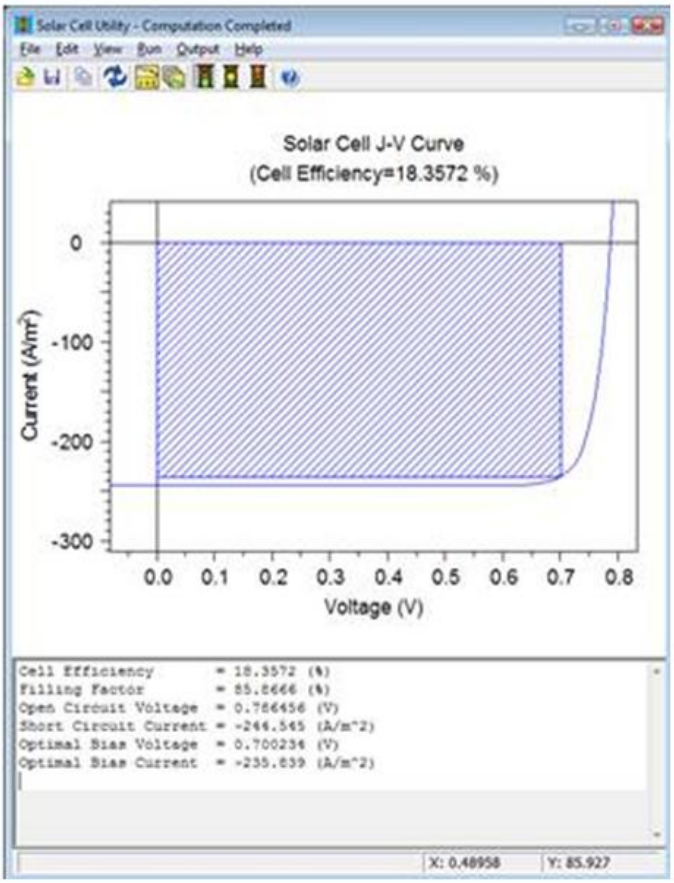

Figure III. 19: The simulation window of the SC utility with the default J-V output.

The shaded rectangle represents the fill factor, the point on the curve where V=0 is the short circuit current Jsc, the point on the curve with a current of 0 is the open circuit voltage Voc and the point on the curve that defines the shaded rectangle is the optimal bias point.

By default, the J-V curve will be displayed in the simulation window. Quantum efficiencies and various spectra (incident, sampled and total absorption) can also be displayed. The sampled spectrum represents the interpolated incident spectrum and can be useful in determining whether the sampling frequency is high enough to obtain accurate results.

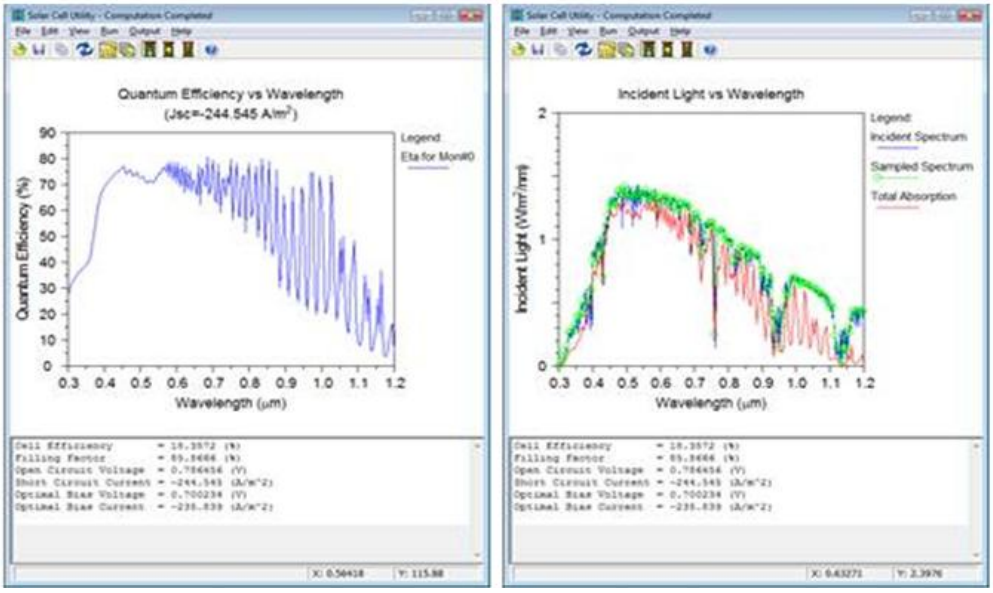

Figure III. 20: The utility simulation window showing a) quantum efficiency results, and b) spectral results showing incident spectra, sampled and absorbed.

When multiple absorption monitors are used, the external quantum efficiency of each monitor as well as the total will be displayed together.

III.6. Conclusion

Periodic structures play an important role in nanotechnology. Using the most important attribute of this type of structure, namely periodicity, manufacturing and simulation methods have been presented in this chapter. An electromagnetic simulation method called Rigorous Coupled Wave Analysis (RCWA) has been developed, integrated into DiffractMOD in the RSoft CAD numerical simulation software. We have shown the accuracy and effectiveness of this tailor-made method for calculating the optical response of periodic structures and electrical properties. In addition, a new algorithm to optimize and comprehensively interpret multi-periodic structures for photon control has been proposed. As an example, we combined this algorithm with the RCWA method to study light trapping in a low-absorption material. In addition, given the efficiency and simplicity of the "unique" model design principle, this method inspires the design and optimization of periodic models in different disciplines.

List of references

[1] M. Born and E. Wolf, *Principles of Optics: Electromagnetic Theory of Propagation, Interference and Diffraction of Light.* Elsevier, 2013.

[2] R. W. Wood, "XLII. On a remarkable case of uneven distribution of light in a diffraction grating spectrum," *The London, Edinburgh, and Dublin Philosophical Magazine and Journal of Science*, vol. 4, no. 21, pp. 396–402, 1902.

[3] M. Neviere and E. Popov, *Light Propagation in Periodic Media: Differential Theory and Design*. CRC Press, 2002.

[4] M. G. Moharam and T. K. Gaylord, "Rigorous coupled-wave analysis of planar-grating diffraction," *J. Opt. Soc. Am., JOSA*, vol. 71, no. 7, pp. 811–818, 1981.

[5] D.M. Whittaker and I. S. Culshaw, "Scattering-matrix treatment of patterned multilayer photonic structures," *Phys. Rev. B*, vol. 60, no. 4, pp. 2610–2618, 1999.

[6] P. Dansas and N. Paraire, "Fast modeling of photonic bandgap structures by use of a diffraction-grating approach," *J. Opt. Soc. Am. A, JOSAA*, vol. 15, no. 6, pp. 1586–1598, 1998.

[7] M. Nevière and F. Montiel, "Deep gratings: a combination of the differential theory and the multiple reflection series," *Optics Communications*, vol. 108, no. 1, pp. 1–7, 1994.

[8] S. G. Johnson and J. D. Joannopoulos, "Block-iterative frequency-domain methods for Maxwell's equations in a planewave basis," *Opt. Express, OE* ,vol. 8, no. 3, pp. 173–190, 2001.

[9] M. Dems, R. Kotynski, and K. Panajotov, "PlaneWave Admittance Method — a novel approach for determining the electromagnetic modes in photonic structures," *Opt. Express, OE*, vol. 13, no. 9, pp. 3196–3207, 2005.

[10] N. Gisin, G. Ribordy, W. Tittel, and H. Zbinden, "Quantum cryptography," *Rev. Mod. Phys.*, vol. 74, no. 1, pp. 145–195, 2002.

[11] S. G. Johnson, S. Fan, P. R. Villeneuve, J. D. Joannopoulos, and L. A. Kolodziejski, "Guided modes in photonic crystal slabs," *Phys. Rev. B*, vol. 60, no. 8, pp. 5751–5758, 1999.

[12] R. D. Meade, K. D. Brommer, A.M. Rappe, and J. D. Joannopoulos, "Photonic bound states in periodic dielectric materials," *Phys. Rev. B*, vol. 44, no. 24, pp. 13772–13774, 1991.

[13] A. Reineix and B. Jecko, "A new photonic band gap equivalent model using finite difference time domain method," *Ann. Télécommun.*, vol. 51, no. 11, pp. 656–662, 1996.

[14] K. Yee, "Numerical solution of initial boundary value problems involving maxwell's equations in isotropic media," IEEE Transactions on *Antennas and Propagation*, vol. 14, no. 3, pp. 302–307, 1966.

[15] S. G. Johnson, A. Mekis, S. Fan, and J. D. Joannopoulos, "Molding the flow of light," *Computing in Science Engineering*, vol. 3, no. 6, pp. 38–47, 2001.

[16] M. G. Moharam and T. K. Gaylord, "Diffraction analysis of dielectric surface-relief gratings," *J. Opt. Soc. Am., JOSA*, vol. 72, no. 10, pp. 1385–1392, 1982.

[17] W. E. Kock, "Metal-Lens Antennas," *Proceedings of the IRE*, vol. 34, no. 11, pp. 828–836, 1946.

[18] H.C. Hulst and H.C. van de Hulst, *Light Scattering by Small Particles*. Courier Corporation, 1981.

[19] Y. A. Vlasov, X.-Z. Bo, J.C. Sturm, and D. J. Norris, "On-chip natural assembly of silicon photonic bandgap crystals," *Nature*, vol. 414, no. 6861, Art. no. 6861, 2001.

[20] C.M. Soukoulis, S. Linden, and M. Wegener, "Negative Refractive Index at Optical Wavelengths," *Science*, vol. 315, no. 5808, pp. 47–49, 2007.

[21] K. Knop, "Rigorous diffraction theory for transmission phase gratings with deep rectangular grooves," *J. Opt. Soc. Am., JOSA*, vol. 68, no. 9, pp. 1206–1210, 1978.

[22] M. G. Moharam and T. K. Gaylord, "Rigorous coupled-wave analysis of metallic surface-relief gratings," *J. Opt. Soc. Am. A, JOSAA*, vol. 3, no. 11, pp. 1780–1787, 1986.

[23] N. Chateau and J.-P. Hugonin, "Algorithm for the rigorous coupled-wave analysis of grating diffraction," *J. Opt. Soc. Am. A, JOSAA*, vol. 11, no. 4, pp. 1321–1331, 1994.

[24] F. Hopkinson and D. Rittenhouse, "An Optical Problem, Proposed by Mr. Hopkinson, and Solved by Mr. Rittenhouse," *Transactions of the American Philosophical Society*, vol. 2, pp. 201–206, 1786.

[25] S. L. Ziegler, "A New Double-disc Ophthalmoscope, with Independent Driving Gears, and Improved Electric Light Attachment," *Trans Am Ophthalmol Soc*, vol. 13, no. Pt 3, pp. 687–691, 1914.

[26] F. Bloch, "Über die Quantenmechanik der Elektronen in Kristallgittern," *Z. Physik*, vol. 52, no. 7, pp. 555–600, 1929.

[27] J. von Fraunhofer, *Kurzer Bericht von den Resultaten neuerer Versuche über die Gesetze des Lichtes, und die Theorie derselben*. 1823.

[28] A. A. Michelson, "The Ruling and Performance of a Ten-Inch Diffraction Grating," *Proc Natl Acad Sci U S A*, vol. 1, no. 7, pp. 396–400, 1915.

[29] M.C. Hutley, "Back to the future in optics," *J. Opt. A: Pure Appl. Opt.*, vol. 1, no. S, pp. 790–793, 1999.

[30] J. D. Joannopoulos, "Self-assembly lights up," *Nature*, vol. 414, no. 6861, Art. no. 6861, 2001.

[31] K. Vynck, "Optical properties of nanostructured dielectric materials: from photonic crystals to metamaterials," These de doctorat, Montpellier 2, 2008.

[32] M. G. Moharam and T. K. Gaylord, "Rigorous coupled-wave analysis of grating diffraction— E-mode polarization and losses," *J. Opt. Soc. Am., JOSA*, vol. 73, no. 4, pp. 451–455, 1983.

[33] P. Lalanne and G.M. Morris, "Highly improved convergence of the coupled-wave method for TM polarization," *J. Opt. Soc. Am. A, JOSAA*, vol. 13, no. 4, pp. 779–784, 1996.

[34] M. Niggemann, M. Glatthaar, A. Gombert, A. Hinsch, and V. Wittwer, "Diffraction gratings and buried nano-electrodes—architectures for organic solar cells," *Thin Solid Films*, vol. 451–452, pp. 619–623, 2004.

[35] L. Li, "Use of Fourier series in the analysis of discontinuous periodic structures," *J. Opt. Soc. Am. A, JOSAA*, vol. 13, no. 9, pp. 1870–1876, 1996.

[36] T. Weiland, "Time Domain Electromagnetic Field Computation with Finite Difference Methods," *International Journal of Numerical Modelling: Electronic Networks, Devices and Fields*, vol. 9, no. 4, pp. 295–319, 1996.

[37] A.C. Polycarpou, "Introduction to the Finite Element Method in Electromagnetics," *Synthesis Lectures on Computational Electromagnetics*, vol. 1, no. 1, pp. 1–126, 2006.

[38] Y. A. Kravtsov and Y. I. Orlov, "Geometrical Optics of Inhomogeneous Media," *Geometrical Optics of Inhomogeneous Media by Yu. A. Kravtsov*,1990.

[39] J.B. Keller, "Geometrical Theory of Diffraction*," *J. Opt. Soc. Am., JOSA*, vol. 52, no. 2, pp. 116–130, 1962.

[40] C. A. BALANIS, "Geometrical theory of diffraction," *Advanced Engineering Electromagnetics*,pp. 743–764, 1989.

[41] J.-F. ROUVIERE, "Calculus of diffraction by diedres and dielectric or metallic prisms by the uniform theory of diffraction validation by exact methods," These de doctorat, Toulouse 3, 1997.

[42] R. Petit, *Electromagnetic Theory of Gratings.* Springer Science & Business Media, 2013.

[43] M. G. Moharam, D. A. Pommet, E.B. Grann, and T. K. Gaylord, "Stable implementation of the rigorous coupled-wave analysis for surface-relief gratings: enhanced transmittance matrix approach," *J. Opt. Soc. Am. A, JOSAA*, vol. 12, no. 5, pp. 1077–1086, 1995.

[44] E. Popov and M. Nevière, "Maxwell equations in Fourier space: fast-converging formulation for diffraction by arbitrary shaped, periodic, anisotropic media," *J. Opt. Soc. Am. A, JOSAA*, vol. 18, no. 11, pp. 2886–2894, 2001.

Chapter VI

Results and discussions

Chapter VI: Results and discussions

VI.1. Introduction

In order to meet the needs of engineers to design optical devices of very small sizes, it is necessary to be able to cope with the design and optimization of these devices in an efficient manner. A priori, the design and optimization of these devices prove to be very difficult because analytical solutions cannot be obtained given the complexity of certain geometries. It seems risky for engineers to build complex devices without having to In advance, a very good approximation of the expected performance, given the complexity and difficulty of their manufacture [1].

Hence the need to efficiently and digitally design and optimize these devices before their realization. For this, it is necessary to appeal to numerical analysis.

Micro and nanophotonics modeling, necessary for the fine optimization of advanced optical devices, involves numerically solving Maxwell's Partial Differential Equations (PDEs) in three-dimensional space accurately and quickly [2].

The modeling is very interdisciplinary in particular electromagnetic modeling, involving both physics, applied mathematics and computer science.

Understanding the physics of the nanophotonics problem is essential for the choice of modeling hypotheses, the choice of an efficient method and the definition of an optimized algorithm [3]. It is an important part, if not the most important, in the process of developing an effective digital method. Numerical analysis is necessary for the analysis and control of errors in an algorithm. It is also necessary in the study of convergence and conditioning of iterative solvers in solving the system of linear equations obtained after transformation of Maxwell's equations. We can say, in general, that numerical analysis allows here to verify the efficiency of the choice of the numerical model used to solve Maxwell's equations applied to nanophotonics problems. Finally, the development of an optimal numerical calculation algorithm relies on a good knowledge of programming (coding, debugging).

VI.2. Adopted strategy for the nanophotonic structures development

The various ways of improving absorption in a thin film absorbent system depend essentially on the geometric parameters and optical properties of the photoactive material (n and k indices, thickness of the layer) as well as on the optical indices of the materials which contain it [4].

We regularly took the example of a thin film amorphous silicon SC to review the state of the art of these optical trapping methods. Thus, since these relate to the semiconductor compound and its environment, we can simplify the study of optical trapping to a simple photoactive model limited to a thin layer of amorphous silicon deposited on glass. Optical trapping structures can be easily adapted when moving from a simple system to a complete solar cell by considering the indices of the added layers [5].

VI.3. Process for manufacturing ultra-fine nanostructured silicon solar cells

we wanted to provide technological solutions for the problem of manufacturing ultra-fine nanostructured silicon SCs. We have made a particular effort to thin and polish the silicon layers as much as possible to test the structures simulated. However, the most significant result is the development of a nanostructuring process for rough, non-planar and flawed silicon layers [6]. This last innovative process makes it possible to simply integrate a nano-structuring improving the trapping of light on different ways.

This geometry has the potential to reduce the rear contact area, as well as the dark saturation current, thereby improving the open circuit voltage of the cell [7].

The samples produced with this process are the subject of extensive characterizations and present promising first optical and electronic results which remain to be reinforced.

VI.4. Increase absorption in absorbing layers

We saw in the strategy adopted for the thesis project that the absorption of a thin film of amorphous silicon can be increased in part through the integration of a PC [8].

In this part, special attention is given to understanding the optical properties of this type of system. This theoretical study (carried out according to the RCWA method) makes it possible to identify the characteristics of the optimal PC.

The development of the stack is developed in a second step and then the absorption properties are characterized and compared to the simulation.

VI.5. Association of an optimal photonic crystal in a photovoltaic system

The increase in absorption of a given system depends on the optical properties of the optical trapping structures employed, in other words on their geometric parameters. Numerical simulation optimization makes it possible to determine these optimal parameters, thus limiting the quantity of experiments to be carried out [9].

The first step in optimization involves identifying the parameters that have the greatest influence on the optical properties of the system, as well as setting the constraints and the optimization method. In this chapter, we define these optimization criteria before presenting the optimal results.

Then, by relying on a geometric and adulatory optical approach, we will study the propagation of light in the optimal photoactive system with the aim of understand why it absorbs better than with other parameters or structures.

VI.6. Optoelectronic properties and design of an absorbing photonic crystal

VI.6.1. Optoelectronic properties

In this chapter, we will attempt to present in more detail our approach which will be illustrated with an absorbing membrane PC. Firstly, we will describe the methodology used to calculate the optoelectronic properties of the different structures studied.

Where, we propose an analysis of the coupling properties of the modes exploited for the trapping of the light from the theory of the coupled modes [10].

We will come back to the optical properties of the absorbent membrane based on the PCs at one dimension to study the geometric properties by changing the period values for each of the unpatterned SC and the one dimensional PC in a-Si:H in order to identify the mechanisms responsible for the shape of their absorption spectra.

Then, the different morphological properties of unpatterned materials were studied as well as the properties of one dimensional PC, half circle, and triangular lattice structures for two types of materials namely; a-Si:H and a-SiGe:H, where the study showed that the latter is more efficient. The incidence angle effect on both materials, where the results showed that the significant improvement in optical and electrical characteristics occurs for the triangular grating especially in the a-SiGe:H case, this latter is found to be more efficient in terms of the optical and electrical properties for PV applications. Finally, we proposed and analyzed the optoelectronic properties of absorbent thin layer of SCs made by various grating structures with GaAs semiconductor material, where an examined based on precision parametric effect of heights and widths variation as well as the J-V SC characteristics was made. On other hand, the execution delivered by the cells depends on the simplicity of both the design and the type of material of the absorbent thin film, to involve the quality of absorption in thin film cells. However, as stated previously, all of these shapes have structured nano, ultrafine gratings that are made depending on efficient semiconductor materials in the PV field. The aim is to provide the elements which make it possible to understand why the introduction of a nanostructuring of the PC type in an ultrathin layer leads to an increase in its absorption over the entire spectrum considered [11].

All results are obtained mainly through simulations based on the rigorous coupled wave analysis method (RCWA). Indeed, this modal Fourier method is particularly well suited to treating the propagation of an electromagnetic wave arriving on a periodic medium such as a PC.

VI.6.2. Integration and conception of a photonic crystal in an absorbent thin film photovoltaic system

The PCs that we have prepared theoretically increase the absorption of light in a thin layer of a-Si. However, an increase in light trapping is not sufficient for applications such as PV [12]. Due to the losses by recombination, all the absorbed photons do not systematically contribute to producing efficient charge transfers [13].

In this part, the impact of an integrated absorbent layer on a one dimensional PC, on the efficiency of a solar cell when it is integrated at the back, *i.e.* between the substrate and the conductive layer. The aim is to show that the optical trapping allowed by the one dimensional PC is sufficient to increase the generation and collection of electrons. The basic structure for this discussion is an absorbent layer. The latter having a fixed thickness of 100 nm.

This layer will then be introduced into a complete cell and will play the role of a layer active. The singularity of the approach developed in this thesis consists in structuring this

absorbent layer into a PC membrane and numerically optimizing its absorption over the entire useful spectrum. We will consider both unpatterned structures, 1DPC, based on the membrane geometric, morphological and parametric effect exhibiting a period, a height and a width of gratings, respectively. These configurations are illustrated in figure VI.1.a and VI.1.b.

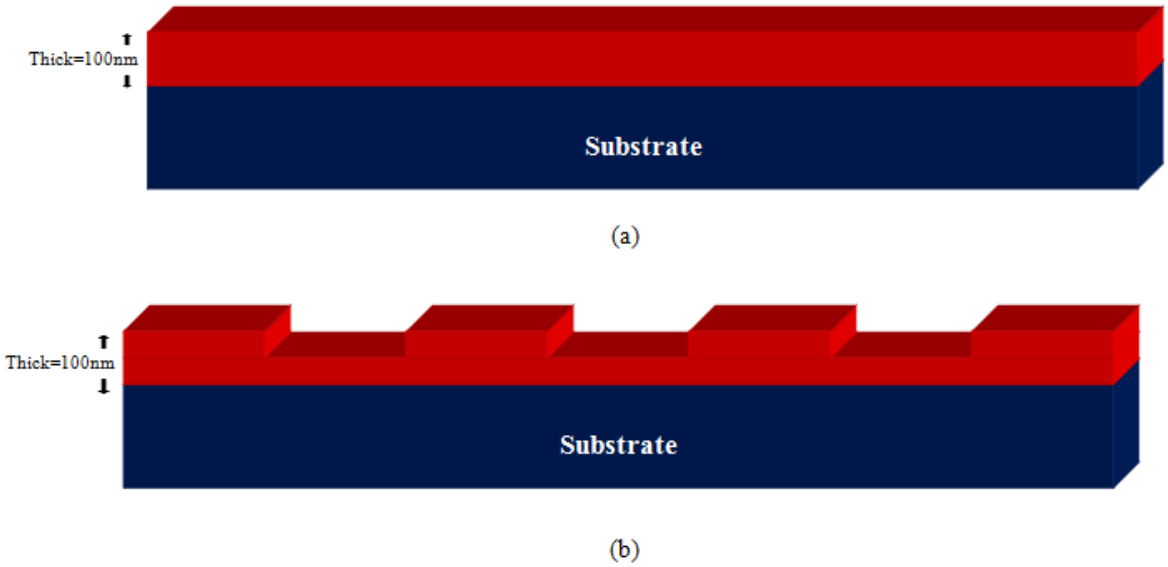

Figure VI.1: (a) Unpatterned layer SC structure on a glass substrate, (b) 1DPC.

Design and simulation become very important before the manufacturing process. The period is the same in both directions of space, which allows independence of the topography of the structure in the two plane directions of space. The incident light can then be trapped in resonances which correspond to a wavelength associated with the physical and geometric parameters of the two structures [14].

The numerical tools used for the simulations are based on the method of rigorous coupled waves analysis (RCWA), it was used to study the influence of the geometrical parameters of the structure on the absorption in the range of the spectrum lengths wave.

VI.6.3. Results and discussions

In this chapter, we study the impact of the geometric parameters of the PC on absorption properties. The systems consist of an absorbent layer, a PC with variable geometric parameters and an amorphous silicon layer. First, the study takes in consideration the influence of the parameters of one dimensional PC on a constant silicon thickness. Second, we analyze the effect of increasing silicon thickness on light trapping properties, depending on the geometric parameters. This study makes it possible to evaluate the work of numerical and experimental optimization. The absorption of PCs is optimized by varying the period and fill factor under normal incidence of light and for a fixed thickness of the one dimensional PC layer.

VI.6.4. The importance of optimizing geometric parameters for optical trapping

In this section, we will take into account both unpatterned structures, PCs, with a membrane dimension having a period, and a hole width denoted L and D. These configurations are illustrated in figures VI.2.a and VI.2.b.

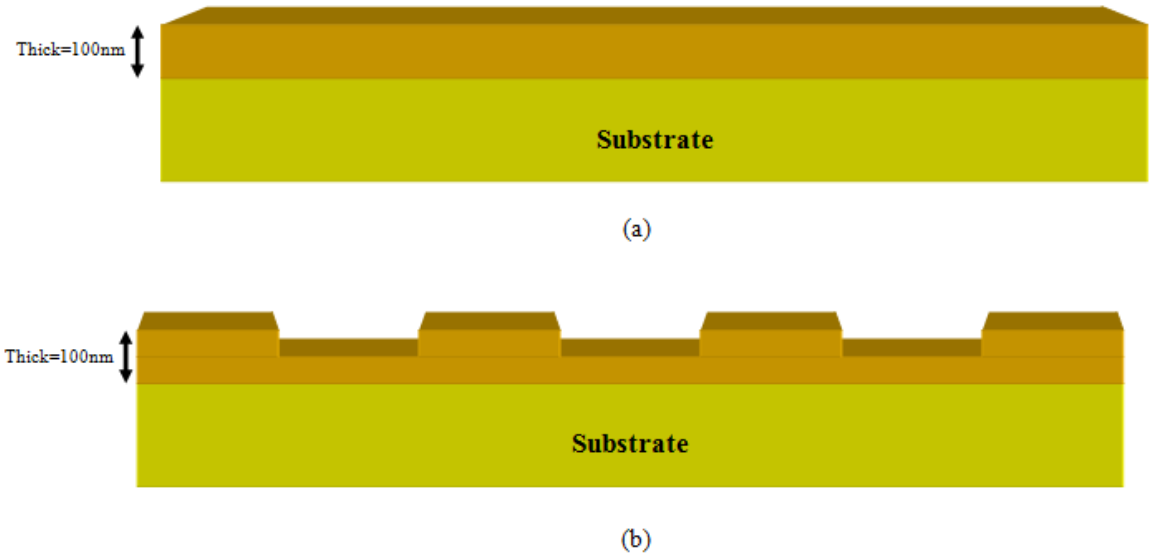

Figure VI.2: (a) Thin film SC structure made by unpatterned layer on a glass substrate, and (b) The patterned layer with one dimensional PC.

For comparison, the first layer consists of an unpatterned absorbent thin layer on a substrate of glass, while the second absorbent layer consists of a patterned absorbent thin layer on the one dimensional PC. The incident light can then be trapped in resonances which correspond to a wavelength associated with the physical and geometric parameters of the three structures. The period is the same in both directions of space, which allows independence of the topography of the structure in the two plane directions of space.

The main parameters of the PC are the lattice cte L and the filling factor *ff*. The structure serving as the basis for this discussion is an absorbent layer of silicon and a-Si:H, where the latter having a fixed thickness of 100nm, then it will be introduced into a complete cell and will play the role of active layer, when light emitted at this resonance can then be locked at the wavelength, associated with the parameters of the two structures [15]. This study aims to demonstrate the concept of this interest in the special case of solar cells, based on the a-Si:H and silicon layers with a thickness of up to 100nm. It is not only for economic reasons that the thickness of the absorption thin layer is limited, but also because of the low propagation length of the PV contained in this material [16].

Our study focuses on the use of silicon because it is cheaper in the market and most industries are based on it, because of its technological importance in the manufacture of solar chips and photovoltaic production [17]. We have also used a-Si:H because it is more sensitive than silicon [18], which is a hydrogen atom, and it is not present in the chemical bond gave, which makes it more sensitive and more reactive to the sunlight compared with silicon [19]. Table VI.1 presents the most important physical parameters of silicon and a-Si:H.

Parameters	Silicon	a-Si:H
Band gab [eV]	1.1	1.7-1.8
Photo-conductivity [s/cm]	$10^{-2} – 10^{-4}$	$10^{-4} – 10^{-5}$
Boiling point [°C]	3265	2900
Density [g/cm^3]	2.33	2.285

Table VI.1. Physical properties of the silicon and a-Si:H.

VI.6.5. Analysis of the results

The absorption of the PCs is optimized by varying the period and the filling factor under a normal incidence of the light and for a fixed thickness of the 1DPC layer. For a thickness equal to 100nm of the a-Si:H absorbent layer.

VI.6.5.1. The absorption with the patterned and the unpatterned thin layers

Spectral properties of a new set of parameters used are shown in figure VI.3.

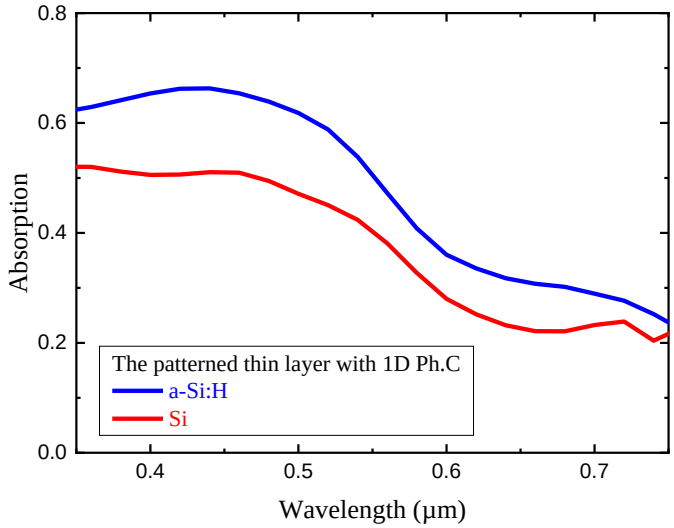

(a)

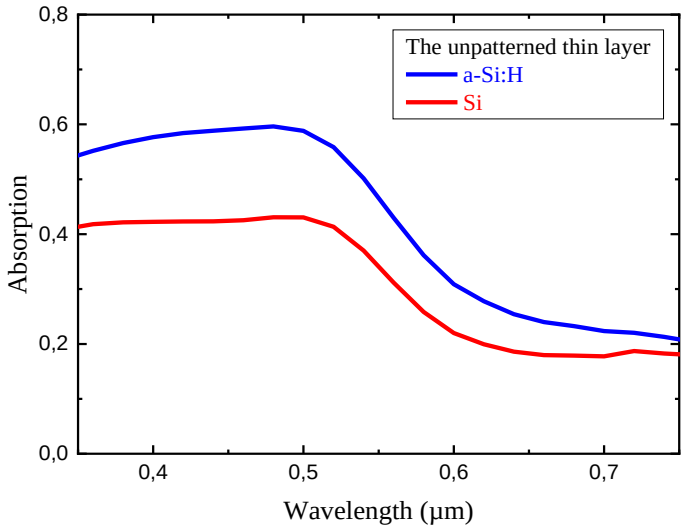

(b)

Figure VI.3: The variation of the absorption power of a:Si-H and Si, on (a) Thin layer patterned Spectral structure of the 1DPC, (b) thin layer unpatterned spectral structure.

We have used the RSoft simulation software to simulate the two patterned and unpatterned thin layer structures. The absorption was monitored as the wavelength varies. All of our studies are in the visible spectrum, that's in between ~(350nm-750nm) [20]. With the help of RSoft CAD software, we put the lattice on L=500nm for 1DPC to calculate the ideal parameters.

The structure of the integrated absorption of one dimensional PC thin layer is first optimized by varying the L for the thickness of 100nm. After that, the absorption is compared with the unpatterned thin layer. We have noticed that the spectra corresponding to the layer of one dimensional PC differ from the spectrum of the unpatterned thin layer. For the one dimensional PC layer in a-Si:H, the highest absorption ratio of 62% reaches between ~(350nm-500nm), and the absorption up to ~(500nm-600nm) begins to decrease due to the extinction coefficient (*k*) [21], until the ratio reaches 32% between the ends of the wave of 610 nm and 750 nm.

This concerns a-Si:H, but for silicon, the amount of absorption up to 52% between the ends of the wave 350nm and 450nm, which is less knowledgeable than a-Si:H. They also begin decreasing between (450nm-610nm) until they reach 20% ~(610nm-750nm).

In the second curve, an unpatterned thin film SC, we can observe; as for a-Si:H, the absorption ratio reaches 54% ~(350 nm-520 nm) and is also declining due to the effect of extinction coefficient and the efficiency of the SC until it reaches 20% ~(620 nm-750 nm). As for the Si, up to about 41% ~(350nm- 520nm) and then decreasing to reach the ratio of 15% ~(630nm-750nm).

For the first result, the absorption in the SCs and the increase in the efficiency ratio is better by using PCs that have the ability to do so [22], and the quantity of the Si absorption is little compared with a-Si:H) [23].

VI.6.5. 2. The lattices parameters variation

The dimension was chosen in order to maintain as much of the optical band gap as possible [24]. The simulation of certain values of parameter L (lattice parameter) was repeated. Thus, for the used process, we determined the absorption of different values for the lattice parameter L=400nm, L=500nm and L=600nm respectively. In addition, we calculated the absorption in the two structures with the same thickness =100nm.

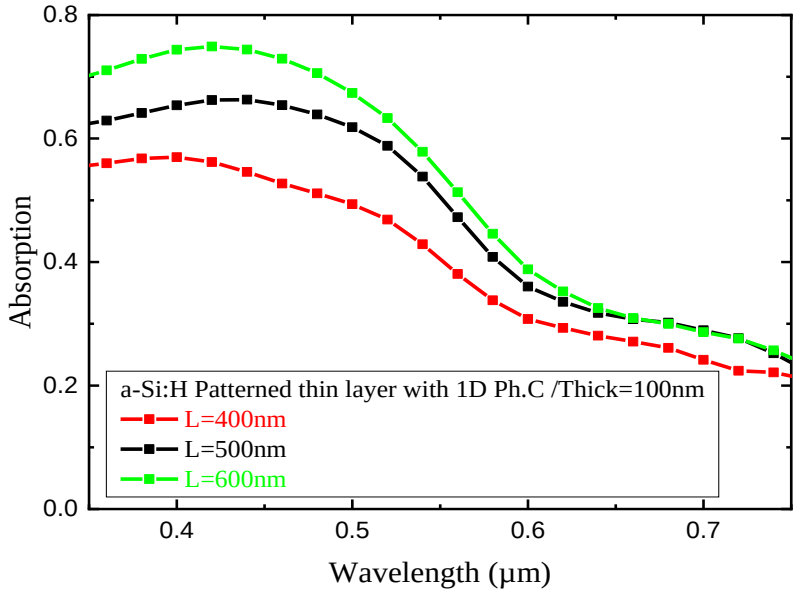

(a)

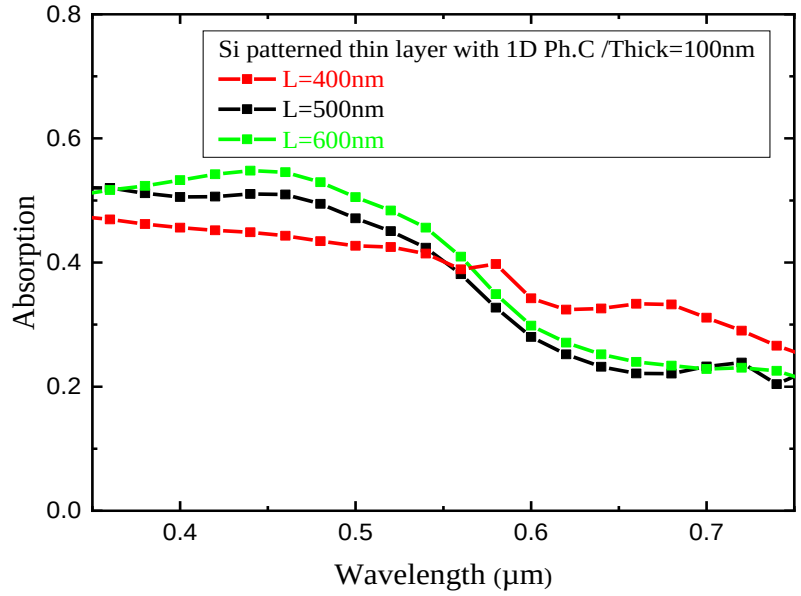

(b)

Figure VI.4: Variation of lattice parameter (L=400 nm, L=500 nm and L=600nm) on the absorption power of a:Si-H (a) and Si (b) with a thickness of layer 100nm.

The two curves cross the one dimensional PC patterned layer for the purpose of studying the role change in a-Si-H and silicon in the absorbent layer of the SC. In a-Si:H patterned layer one dimensional PC, the absorption ratio up to 70% at L=600nm, and reaches the lowest drop between 580nm and 750nm. With the lattices varying, in L=400nm, we noticed that the absorption ratio reached about 55%, which is lower compared to L=600nm.

On the other hand, with the Silicon absorbent layer one dimensional PC, we can observe that the absorption rate in thin layer SC, reached 52% at L=500nm and L=600nm, but starting from 400 nm, increases the ratio of L=600nm to 55% to begin decreasing ~(550 nm-750 nm). As for L=400 nm, it is less than 48% until it reaches 32% between 600nm and 750nm.

When we conducted a study of the variation of lattice parameter constant (L), we have found that the better one is L=600nm in both curves. The thing that can be deduced here, is when the (L) is larger, the absorption rate increased especially between 350nm and 500nm. That is to say, the (L) is a powerful factor for increasing efficiency in thin film SCs and in nanotechnology for nanoparticles and patterning [25].

In fact, the absorption is usually higher regardless of the used wavelength. For instance, the absorption between 350nm and 500nm for a-Si:H patterned thin layer, approximately two times greater than the silicon patterned thin layer.

The absorption can be improved globally by a combination of the effect of slow lighting patterns and the thorough regression of reflection [26], probably because of high average index in the case of one dimensional PC. The absorption of the patterned structure becomes two times greater in the wavelength range between 350nm and 500nm in a-Si:H patterned thin layer.

Furthermore, the slow light pattern is affected by a relatively low refractive index. Therefore, the spatial spacing between places of diffusion of light is limited [27], and the incidence angle is increasing. The manufacture of these PV cells requires the need to verify the uniformity of absorption with respect to the change of topographic parameters [28].

After that, we need to know the processing techniques that are usually used, to develop new patterns of Sub-Wavelength (SbW) on a planar surface [29].

After the comparative study of SCs influencing the optical properties, we have found that the improvement in light absorption was between ~(350 nm-580 nm), which means an increase in efficiency. This means that there is a qualitative improvement through the choice of material quality is a:Si-H compared with silicon [30].

We have explained chemically that the loss of hydrogen (H_2) in a-Si:H compared with Si has caused a high agitation and a high sensitivity to this substance, which in turn causes more agitation of the sun to the lattice parameter in the absorbent layer of the SC [31], which in turn contributes to a high efficiency.

In our study, we tried to develop the idea by studying the vertical position of the incidence angle in the solar cell, which in turn contributed to the enhancement of the absorption of light in the solar cell using PCs. We conclude the difference between silicon and a-Si:H in terms of cost and ease of fabrication is probably that the silicon was condition to rapidly cooled in a vacuum environment [32], and a-Si:H was rapidly cooled in an aerated (in the present of H_2) environment [32]. The coupling of emitted light greatly increases the absorption of the a-Si:H layer, using a simple one dimensional PC layer, which makes it possible to find out how to enhance the absorption of light in absorbent thin layer of the SC.

VI.7. Morphological effect of the PCs structures

Our contribution consists of enhancing the absorption ratio of the photon beams by the active thin film of the SCs and by employing the PCs technology.

Therefore, we investigated the ability of absorbing photon beams in the visible light spectrum by active PV thin film of 100nm thickness, based on the morphological effect of

different structures for one dimensional PC. In this part, we have studied the optical and the electrical properties of two types of semiconductor materials (a-Si:H and a-SiGe:H). a-Si:H is more sensitive and responsive to solar radiation due to the presence of hydrogen atom H_2 **[**18]. On the other hand, the presence of germanium in a-SiGe:H enhances the light absorption by reducing the band gap energy [33].

Most of the SCs are made of silicon because it is both available and cheap. The major drawback of using germanium is the effect of the temperature which affects stability.

a-Si:H is characterized by the presence of a hydrogen atom (H_2) which allows the SC to be more sensitive to photon beams to enable it to have higher absorption [18]. Amorphous films characteristics should be improved to attain the prime performance of a-Si:H thin film which requires sophisticated devices and materials.

a-SiGe:H thin film is famed to be one of the favorable PV devices and it is prepared from a blend gas of GeH_4, H_2 and SiH_4, which is fabricated with several deposition techniques, usually, with Plasma Enhanced Chemical Vapor Deposition (PECVD) or Hotwire Chemical Vapor Deposition (HWCVD) [34]. Table VI. 2. shows the physical parameters of a-SiGe:H and a-Si:H, in which the thin film of the SC was made.

The physical parameters	a-Si:H	a-SiGe:H
Band gab [eV]	1.7 -1.8	1.0 -1.7
DC dielectric [$F.m^{-1}$]	3.9	3.75
Permittivity [$F.m^{-1}$]	20.1306	24.6613
Electron affinity [eV]	1.75	1.39
Photo-conductivity [s/cm]	10^{-4}-10^{-5}	10^{-5}-10^{-7}
Urbach energy [meV]	42-50	>45
Thermal-conductivity [$W.m^{-1}.K^{-1}$]	1.38	1.36
Light-induced decomposition after 1000 hours [%]	15-30	10-20

Table VI. 2: The physical parameters of a-Si:H and a-SiGe:H thin films [35].

VI.7.1 Analysis of the results

A numerical simulation has been placed to enhance the dimensions of the diverse types of PCs. Table VI. 3. shows the values of the optical properties calculated, which we were able to model an integrated SC thin film with unpatterned and 1DPC by using the two semiconductor materials a-Si:H and a-SiGe:H in the linear regime.

Parameters	The value
Free space wavelength [µm]	0.63
Lattice cte (period) [µm]	0.5
k_0 [m^{-1}/s^{-1}]	(2. π)/free space wavelength
Wavelength corresponding to the band gap (λg) [µm]	1.107
Frequency [HZ]	1/free space wavelength
Substrate of glass (refractive index)	1.5
Total hydrogen concentration [cm^{-3}]	5.0×10^{21}
Total electron concentration [cm^{-3}]	2.0×10^{23}
Defect state density freeze in temperature [K]	500

Table VI.3. The used parameters of a-Si:H as well as a-SiGe:H for thin film PV cells with PhCs used in the linear regime.

VI.7.1.1. Optical Properties

The subsequent step in the manufacturing process depends on the immediate conveyance of PCs from the unpatterned absorbent layer to the patterned layer. Figure VI.5.a and figure VI.5.b below present the active layer infrastructure in linear regime.

Figure VI.5.a shows an unpatterned absorbent thin film on a substrate of glass, whereas, the second consists of a one dimensional PC absorbent thin film on a glass substrate. Two types of grating structures are made by a-Si:H and a-SiGe:H semiconductor materials.

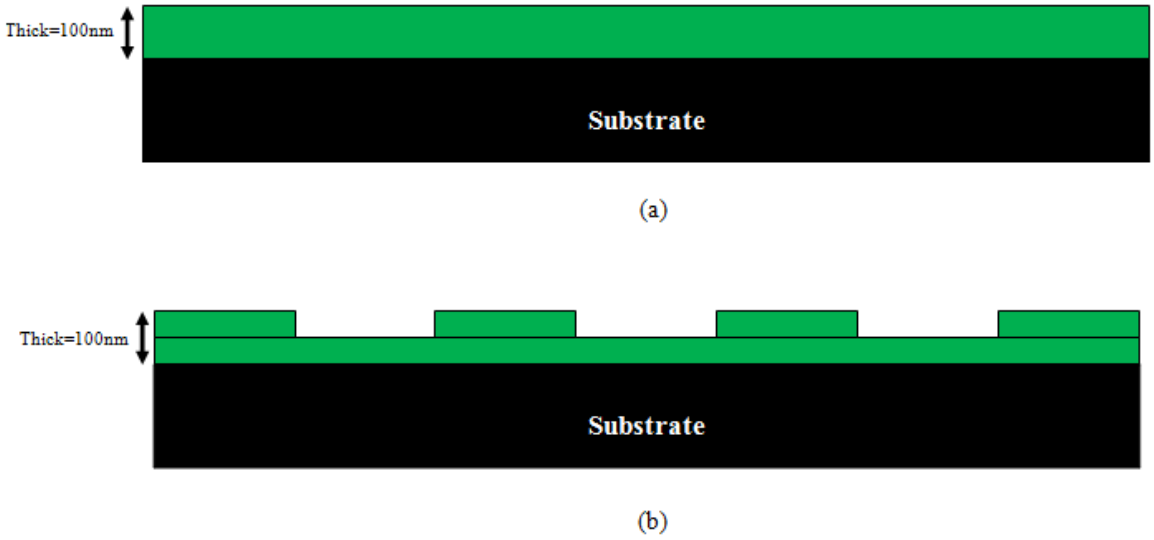

Figure VI.5: (a) Unpatterned and (b) one dimensional PC lattice structures, made by a-Si:H and a-SiGe:H respectively.

The emitted light resonance depends on the associated wavelength with the same parameters of two grating structures. In both unpatterned and one dimensional PC, the specific parameters are wavelength (λ), the lattice parameter constant (L=500nm), the layer's width (D) likewise equal to 500nm. The thicknesses of two arrangement grating structures are considered the same, they are equal to 100nm.

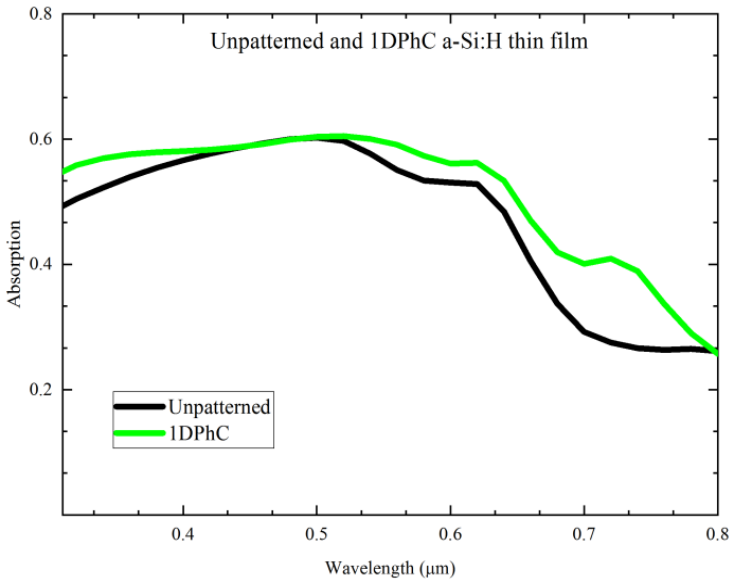

(a)

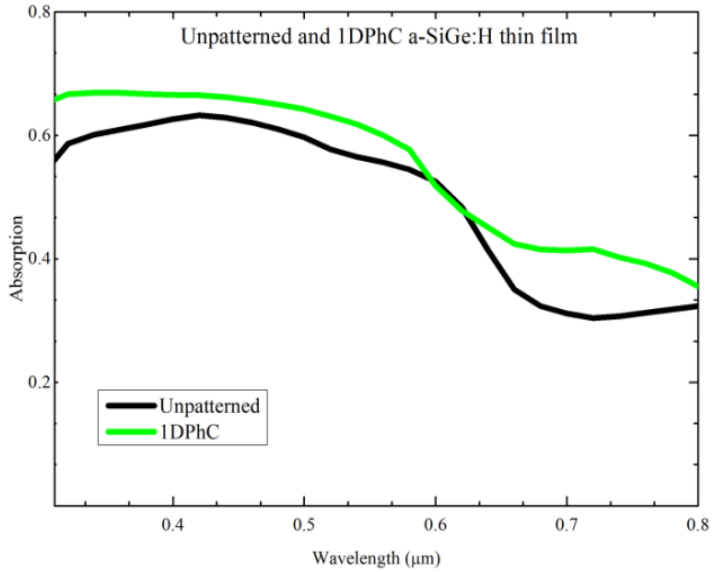

(b)

Figure VI.6: Optical absorption of (a) a-Si:H thin film made by unpatterned and one dimensional PC, (b) a-SiGe:H thin film made by unpatterned and one dimensional PC lattice structures.

In figure VI.6.a and figure VI.6.b we got the absorption energy of the a-Si:H and a-SiGe:H. For a-Si:H semiconductor material, the one dimensional PC is more adequate than unpatterned lattice structure; where the highest absorption ratio is 63.37% when the lattice constant was between (462nm to 546nm) and reached to 58% in unpatterned one. Then, it began to decrease due to the extinction coefficient (k) in both structures until the ratio reaches 25.99% at lattice constant of 800nm. The absorption ration was up to 62.9% for unpatterned and reaches to 68.7% once the pattern period was between 398nm and 455nm with a-SiGe:H semiconductor material in one dimensional PC. This absorption ration was greater than of a-Si:H. Furthermore, the absorption ratio was decreasing to reach 35.5% in 1DPC at grating period of 800nm and up to about 30.4% in the unpatterned lattice.

Correspondingly, the enhancement of the absorption ratio in the lattice constant between 300nm and 500nm in one dimensional PC of two types of materials is around 5.8%. In addition, the absorption in the SCs is affected by the presence of proportion germanium in a-SiGe:H compared to a-Si:H used in the manufacture of the thin film solar cell, as well as PCs which can increase the absorption rate.

Ouanoughi, A *et al*. [33], conducted a numerical simulation to design the geometry of a solar cell made by one dimensional PC in order to improve its absorption.

Their results show an enhanced absorption in one dimensional PC grating structure that is apparent compared to the unpatterned one, which proves the ability of the structure to produce PCs solar cells. In addition, for wavelengths range of lattice constant of 0.38µm and 0.5µm, we found an enhancement in the absorption ratio with 24% in unpatterned and 3.37% in 1DPC grating with a-Si:H thin film, whereas in the case of the a-SiGe:H thin film, the enhancement in the absorption ratio was 28% which higher than in a-Si:H with unpatterned and 8.7% with one dimensional PC lattice. This enhancement due to employing grating period pattern is due to the light trapping effect which is mainly attributed to Fabry–Pérot resonance modes due to the large index contrast between air and semiconductor layer, which is ubiquitous in the thin film layer, which can trap light effectively [36].

VI.7.1.2. Optimal morphological design

In this part, we exploit the effect of the morphology of the structure of the absorbing layers on the absorption rate. For this reason, we studied various grating structures (half circle and triangle) based on previous studies [37].

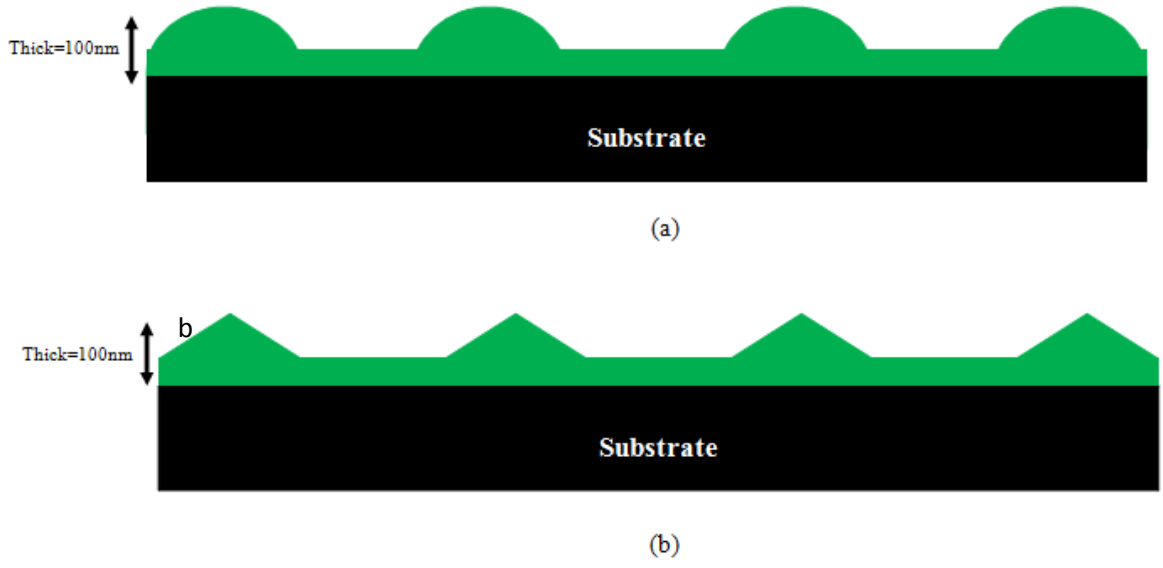

Figure VI.7: Geometrical lattice of (a) half circle, (b) triangle lattices made by a-Si:H and a-SiGe:H.

Figure VI.7 (a and b) represents the studied lattice structures of the half circle and the triangle, based on both a-Si:H and a-SiGe:H semiconductor materials with the same lattice constant (500nm), the same thickness (100nm) and the same visible light in the optical wavelength for TE-polarized of the light deposited on a glass substrate. For the proposed

two structures, a half circle that can be used to construct arithmetic and geometric means of lengths, we have used a radius of 250nm.
On the other hand, we use the isometric triangle where all the three sides are of the same length, all the three angles are equal to 60°, with a height and width equal to 500nm. Figure VI.8 shows the geometrical dimensions of both shapes.

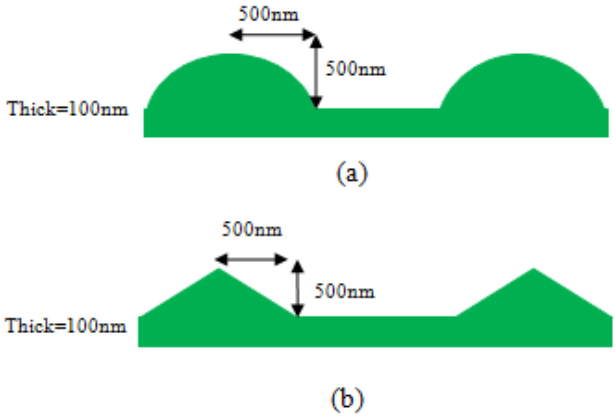

Figure VI.8: Dimensions of the simple proposed gratings of (a) half circle and (b) isometric triangle.

Figure VI.9 represents the simulation results of the absorption energy of both a-Si:H and a-SiGe:H semiconductor material with half circle and triangular gratings.

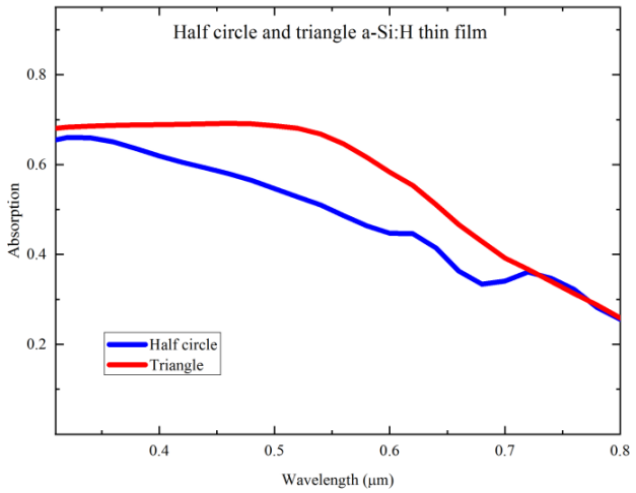

(a)

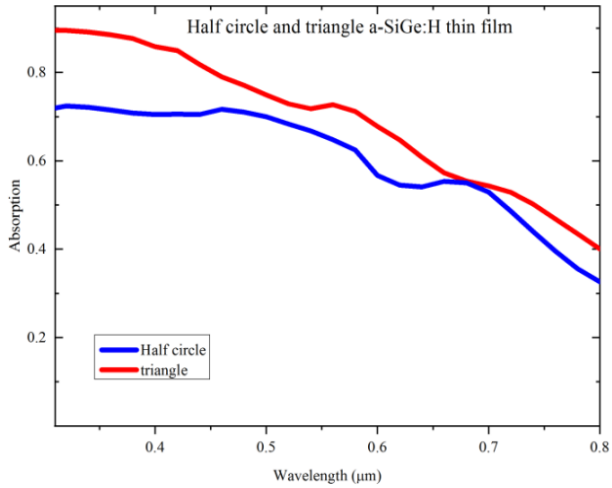

(b)

Figure VI.9: Optical absorption of the half circle and triangle gratings made by (a) a-Si:H and (b) a-SiGe:H.

In Figure VI.9.a, the absorption in triangle grating reaches 69.7%, however it is equal to 65.6% in half circle grating during (~300nm-500nm). After that, the absorption ratio was decreasing under the influence of extinction coefficient (k) until lattice parameter is equal to 800nm, which achieves 26% for triangle and 24.7% in half circle gratings. In Figure VI.9.b in comparison with a-Si:H, a noticeable improvement of peak absorption energy with a-SiGe:H which is estimated at 16% an enhancement of the absorption in the triangular structure which is 5.4% in the half circle grating in the range from 300nm and 500nm (the best visual field absorption). PCs dimensions have been improved by integrated design of numerical simulation and experiment techniques. While we use different grating structures for one dimensional PC based on a-Si:H and a-SiGe:H, we found that the absorption ratio in triangular grating is better compared to the half-circle grating. The obtained results were positive with those previously reported by Dominguez, S *et al.* [38] and Heidarzadeh, H with Tavousi, A [39], who showed that the triangular structure is better grating for the optical absorption enhancement, which allowed more photon beams to come into thin film of PV cell to enhance the absorption efficiency by using the dispersion influence. The geometrical parameters have an important effect on the distribution spectral of the absorbent PCs, which can be done in the full distance of wavelength if the PCs dimensions are adequately altered. However, the obstacles and reasons that are still being studied currently about the efficiency and absorption capacity of SCs silicon PV is still very expensive. While for the triangle lattice, the waveguide mode resonance or leaky mode resonance effects lead to light trapping and increase the absorption in the active layer. In addition, the morphological effect on PCs with different dimensions can excite micro cavity resonance effects, which can trap light effectively [40]. Both the excellent geometrical properties and micro cavity effect make the triangle grating outperform the 1DPC and half circle grating structures.

VI.7.1.3. Electronic properties

The SC is distinguished under the AM1.5G insulation using current density versus voltage J-V with the characteristic device parameters (V_{oc}, J_{sc}, *ff*, η) and external quantum efficiency properties (EQE). In this section, the electrical properties of each grating used

with two types of semiconductor materials (a-Si:H and a-SiGe:H) are investigated based on several electrical output parameters; V_{oc} [V] is the open circuit voltage where there is no current flows through the external circuit [41].

$$V_{oc} = \frac{kT}{q} \ln\left(\frac{J_{sc}}{J_{so}} + 1\right) \quad \text{(VI.1)}$$

Where: k [$J.K^{-1}$] is Boltzmann's constant; T[K] the absolute temperature; q[eV] the electron energy; J_{so}[mA/cm^2] the reverse bias saturation current; J_{sc}[A/cm^2] the short circuit current density [42]. Where η[%] is the ratio of energy output from the SC to the input energy from the sun, given by:

$$\eta = \frac{P_{max}}{P_{in}} = \frac{J_m \times V_m}{P_{in}} = \frac{J_{sc} \times V_{oc} \times ff}{P_{in}} \quad \text{(VI.2)}$$

With: P_{max}[W] is the total maximum power; P_{in}[W/m^2] is the total incident power; *ff* is the filling factor; it can be defined as the ratio of the actual maximum obtainable power to the product of the open circuit voltage and short circuit current, we obtained it from the device J-V curve or using the following equation [43]:

$$ff = \frac{J_m \times V_m}{J_{sc} \times V_{oc}} \quad \text{(VI.3)}$$

Where: J_m[A/cm^2] is the maximum current density; V_m[V] is the maximum voltage. In this section, we studied different shapes of one dimensional PC with a-Si:H as absorber thin film. Figure VI.10 shows the simulation results of a thin film PV cell made by a-Si:H, depending on lattice morphology of structures.

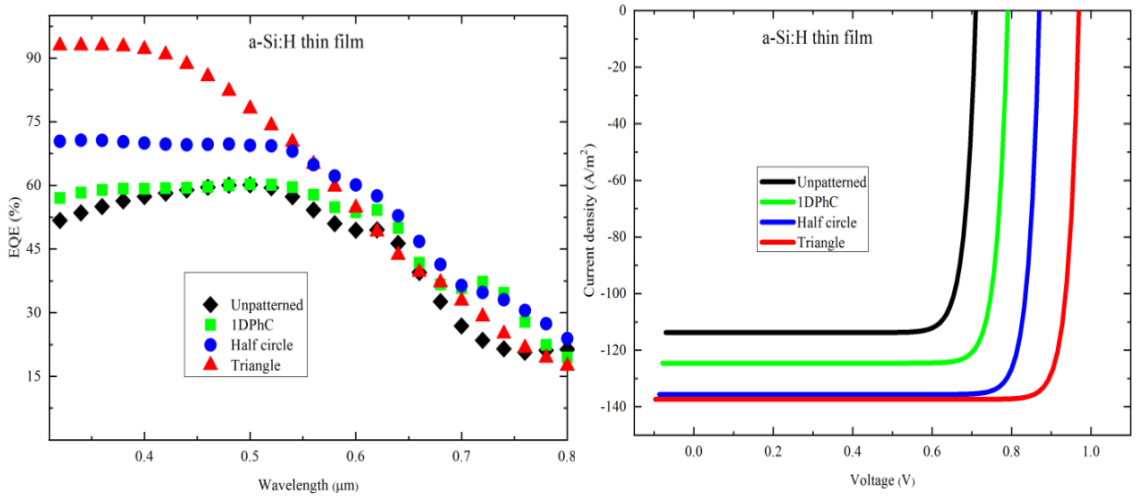

(a) (b)

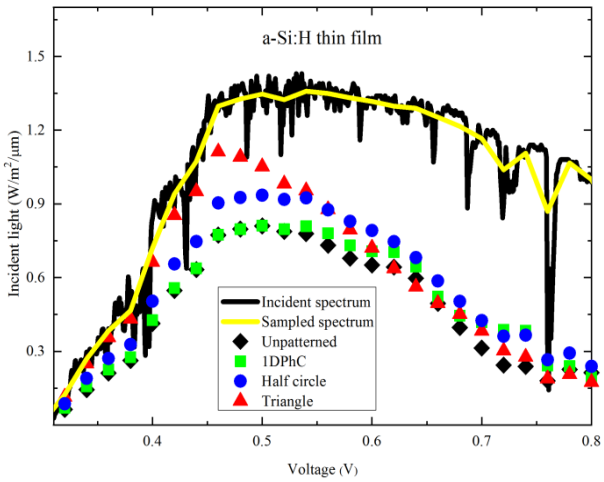

(c)

Figure VI.10: (a) the EQE graphs, (b) the J-V curves and (c) smooth spectral distribution of the studied AM1.5 solar spectrum with different lattice structures studied made by a-Si:H of thin film SCs.

Figure VI.10.a shows the EQE curves of a-Si:H thin film SCs with varying PCs shapes using improved geometrical parameters. Figure VI.10.b shows J-V curves of a a-Si:H thin film SC leading to outstanding values of V_{oc} and J_{sc} and Figure VI.10.c shows the computed spectral distribution graph for the proposed simple gratings for the studied solar spectrum AM1.5. The net current is always flowing from one contact towards the other, where it is always positive relative to one contact and negative relative to the other. Thus, the direction of the current measured depends only on which electrode you reference to ground and the measured current sign does not depend or affect the physical charge within the device [44]. We can summarize the results in the following table:

	Unpatterned	**1DPC**	**Half-circle**	**Triangular**
P_{max}[W]	68.4	84.57	102.59	117.20
ff [%]	84.75	85.92	86.9	87.94
V_{oc}[V]	0.71	0.79	0.87	0.97
J_{sc}[A/cm^2]	113.8	124.6	135.7	137.4
J_{so}[A/cm^2]	109.3	120.2	131.3	133.4
η[%]	7.61	9.4	11.4	13.01

Table VI.4. The simulation results of a-Si:H thin film SC energy conversion efficiency.

The better result in the a-Si:H case, was the triangle grating with the highest values of all electrical parameters of efficiency. This efficiency reached 13.01%, and the total improvement efficiency among the unpatterned and triangle models was 5.4%. However, the maximum power noticed in the triangle model is 117.20W, which makes a difference of 48.8W over the unpatterned grating structure. The results showed that the cell efficiency with a-Si:H presents useful numerical simulation ones. This makes the doping semiconductor materials suitable in terms of absorption efficiency, as well as being more sensitive to the sunlight. As clearly shown in figure.VI.10 and table.VI.4, we can explain the reason for the increase in the J-V characteristics devices parameters, where V_{oc}, *ff* and the efficiency of different grating structures is progressively higher to reduce the recombination loss affecting V_{oc}, the parasitic resistance losses which primarily limit the *ff* as well as V_{oc} and J_{sc}, and eventually optical losses which have a large effect on photo-

generated carriers and J_{sc}. The EQE values shown in figure VI.10.a, where the highest value was at triangle case in the point 300nm of the wavelength, where it makes a difference of 0.41V than unpatterned one. In addition, figure VI.11 presents the numerical simulation of the a-SiGe:H thin film PV cell lattices on linear regime with the same parameters as above.

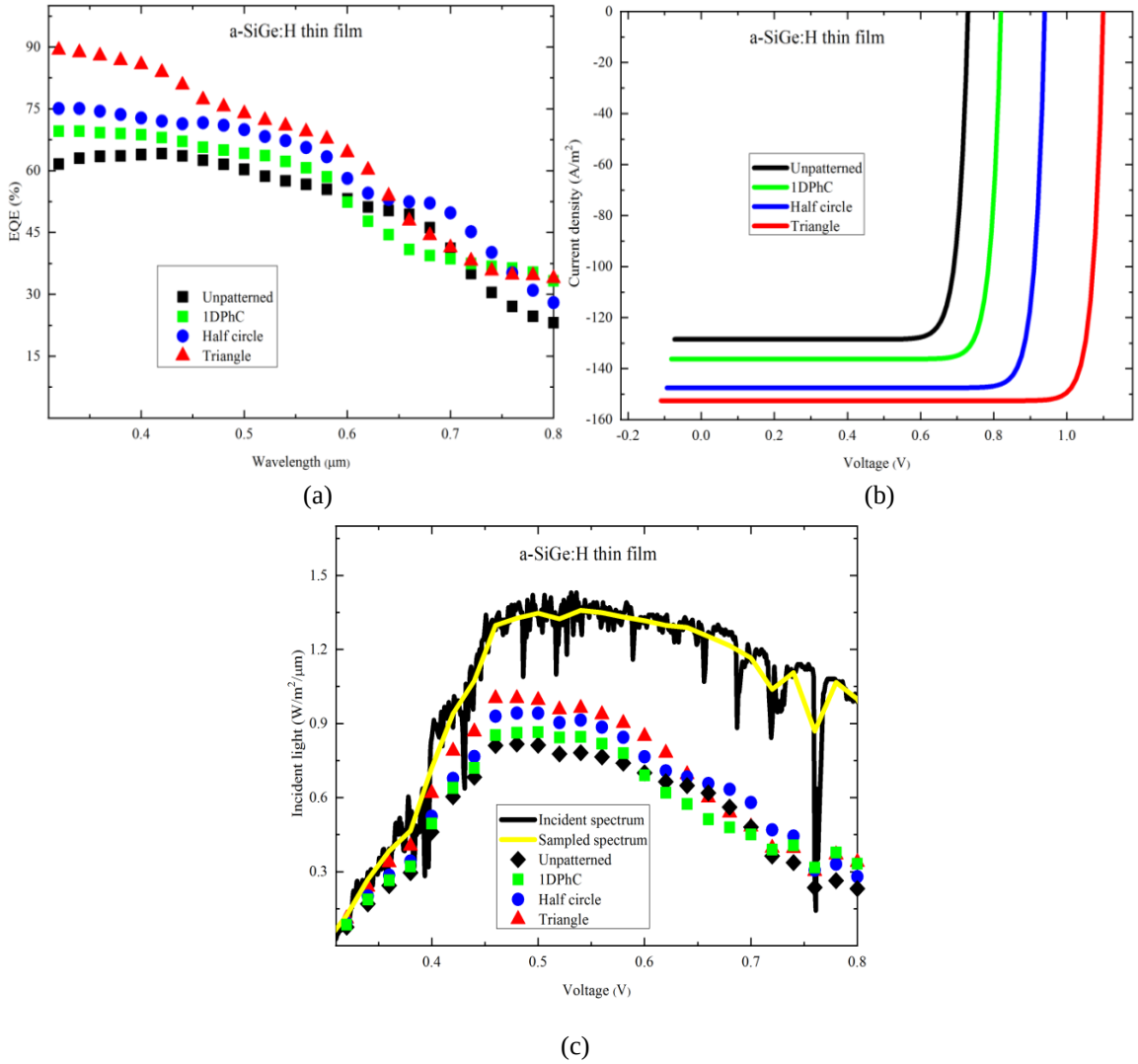

Figure VI.11: (a) The EQE graphs, (b) the J-V curves and (c) the smoothened spectral distribution, studied by different grating structures studied, made by a-SiGe:H thin film.

Figure VI.11.a shows the EQE graphs of a-SiGe:H thin film with diverse models of PCs.Figure VI.11.b shows J-V curves of a-SiGe:H thin film SC with different V_{oc} and J_{sc} results values and figure VI.11.c shows the computed spectral distribution graph for the proposed simple gratings for the studied solar spectrum AM1.5. The a-SiGe:H thin film SC electrical output results are concise in table VI.5.

	Unpatterned	**1DPC**	**Half-circle**	**Triangular**
P_{max}[W]	79.79	96.38	121.52	149.47
ff [%]	85.06	86.3	87.65	89.05
V_{oc}[V]	0.73	0.82	0.94	1.1
J_{sc}[A/cm^2]	128.5	136.2	147.5	152.6
J_{so}[A/cm^2]	123.6	131.6	143.1	148.7
η[%]	8.86	10.71	13.50	16.6

Table VI.5.The energy conversion efficiency simulation results of a-SiGe:H thin film SC.

The a-SiGe:H thin film SC shows higher J_{sc} with a hydrogenated PV cell; and reducing the band gap of the absorbent layer through the growth of Germanium content within the layer is probably accompanied by V_{oc} and *ff* losses. Better results in the a-SiGe:H semiconductor material case was that of triangular grating. The numerical simulation results showed that the efficiency was adequate by using a-SiGe:H with the balance of a-Si:H, owing to the presence of germanium concentration which in turn affects the use of a smaller energy band gap. The efficiency was found to reach 16.6% in the case of triangle which allows an improvement efficiency of 7.74% compared to unpatterned grating. Moreover, the triangle maximum power observed is 14.95W which makes a difference of 7.15W in comparison with the unpatterned model. J_{sc} gradually increasing as the V_{oc} and *ff* values, as V_{oc} and *ff* remained less in the unpatterned grating thin layer than in the other grating structures especially in triangular one, which can be condoled to the loss of the improved recombination of electron hole dual in an unpatterned grating [45].

The smoothened spectral distribution variation for different forgoing grating structures are shown in figure VI.11.c. Furthermore, this figure shows the performance improvement for the triangular structure as compared to the other shape values, as shown in the previous results. In view of decrease carrier lifetime in a-Si materials, the enough carrier collection foremost rely on the inner electronic domain which play an essential function in representing and detaching the carriers to set the electrodes, where the redistribution of Germanium atoms in absorber layer can raise V_{oc} and *ff* while this is somewhat detrimental for J_{sc} [46].

As clearly shown in figure VI.10.a and figure VI.11.a, the EQE of different structures of solar cells was decreasing gradually according to the morphological design of the studied gratings. The improvement in EQE occurs because photon beams are absorbed and then reemitted at longer emission wavelengths, where the highest value was at the beginning point of studies wavelength (300-400nm), where in triangle case reached by 0.9V; 0.72V in half circle, 0.69V in 1DPC and 0.59V was unpatterned. A slighter dropping in the EQE is obvious for the bias during 0.59V and 0.9V while a comparatively considerable fall is clear for a bias over 0.9V. In triangle case, the 0.9V bias shows a very large reduction in the EQE. In this condition, the carrier collection probably suffers from the high density of defects or traps which hinders their movement for the collection, can be used to distinguish the recombination losses in the forgoing thin absorber layers. Depending on the results obtained by Yousif, B *et al*. **[**47], a remarkable improvement especially in a-SiGe:H semiconductor material in the triangle grating was noticed, as well as an enhancement in solar cell efficiency of 4.36%. On the other hand, in the case of a-Si:H, a noticeable improvement of SC efficiency was estimated 0.77%.

The electrical properties of amorphous thin film are sensitively dependent on the density of energy and the distribution of local gap states, where the main advantage of a-SiGe:H is the capacity of the unstable optical band gap to lower energies by increasing the germanium concentration in the layer [48].

VI.7.1.4. The incidence angle (θi) effect

In this section, the incidence angle influence of photon beams on the absorbent layer is investigated. We estimated the extent of the photon beams distribution by variation of the incidence angle from 0° to 90° in the case of a-Si:H and a-SiGe:H. The incidence angle (θi) is in between a ray incident made by photon beams and the perpendicular line to the absorbent layer at the point of incidence according to Snell's law [49]:

$$\frac{\sin\theta_i}{\sin\theta_r} = \frac{n_2}{n_1} \quad \text{(VI.4)}$$

And:

$$\theta_i = \sin^{-1}\left(\frac{(\sin\theta_r \times n_2)}{n_1}\right) \quad \text{(VI.5)}$$

Where: θ_r angle of reflection; n_1 incidence medium refractive index; n_2 transmitted medium refractive index. Figure VI.12 presents the changes of light absorption in absorbent layer using unpatterned, 1DPC, half circle and triangular gratings, depending on the variation of the incidence angle from 0° to 90° with an increment of 5° in the case of both a-Si:H and a-SiGe:H.

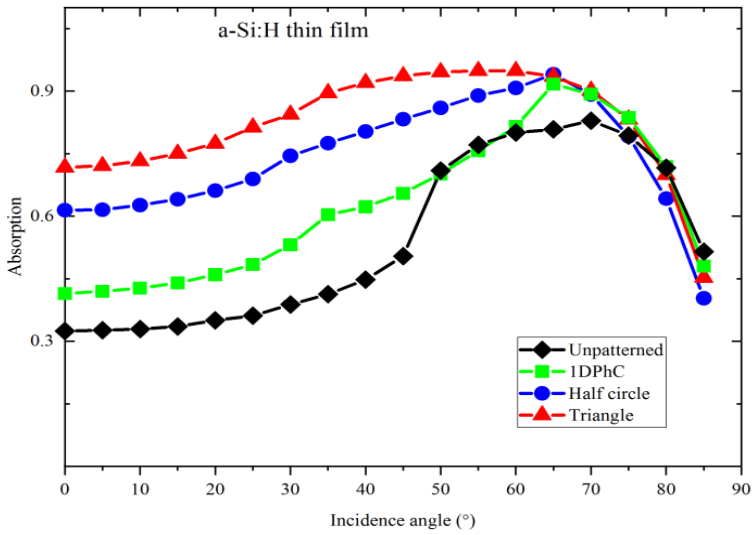

(a)

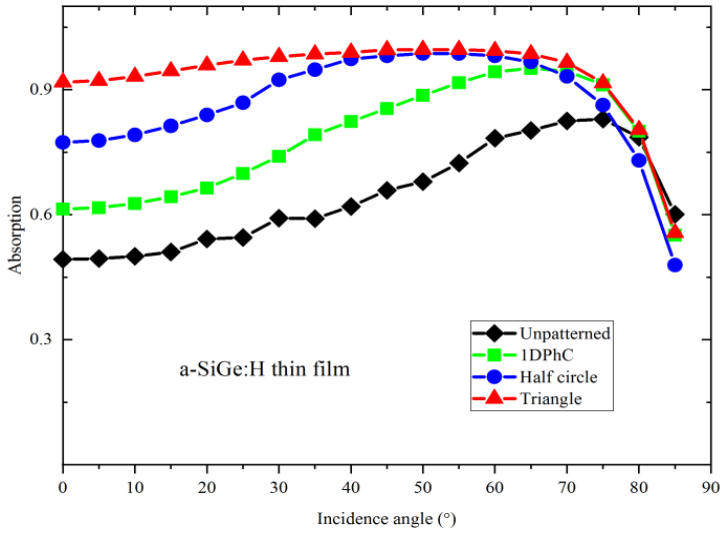

(b)

FigureVI.12: Incidence angle effect on absorbent layer of different gratings made by (a) a-Si:H and (b) a-SiGe:H.

The absorption ratio was increasing with the increase the incidence angle until it reaches the highest absorption ratio at 50°-70°, and then it begins to decrease until it is completely absent at the horizontal position at 90°. At incident angles (50°-70°), the absorption ratio using the triangle grating improved by 14.41% compared to the unpatterned grating (figure VI.12.a and figure VI.12.b). The peak of absorption ratio is 94% in the triangle shape, 92% in the half circle, 90% in 1DPC and it reached 79% approximately with unpatterned grating. On the other hand, in Figure VI.12.b we noted the absorption ratio in a-SiGe:H is better compared with a-Si:H, while we find an enhancement in the peak (appeared in the incident angles at 50°-70°) of 5% in triangular, 4% in half-circle, 2% in 1DPC and 2% in unpatterned lattices.

Thereafter, all absorption ratios with a-Si:H and a-SiGe:H begin to decrease until they are completely absent at 90°, *i.e.*, there is no absorption (the horizontal condition: incident angle is 90°). When comparing with Mudachathi, R and Tanaka, T results [50], we found an enhancement in the absorption ratio, where it begins to expanded above an incident angle between 0° to 70° (maximum in the range 50° to 70°) in both a-Si:H and a-SiGe:H thin films, several studies have shown that the most appropriate angular range in which the absorption is more available is between 50° to 70°, moreover, the material quality and morphology used in addition to the climate condition with the temperature variations should be considered [51]. In addition, owing to the limited thickness of the absorbent thin film, not all photon beams are absorbed into the absorbent layer. Therefore, the absorbent layer must be thick to absorb as much light as conceivable and the thickness must not exceed the length of the carrier spread [51].

VI.8. Effects of the mixture ultra-precision lattices in photonic crystals

In this part, we analyzed the thin film SC with the suggested nano lattice photonic structure's efficiency for purposes of comparison on the bases of the simulated results. We studied the structural effect that depends on the parametric effects of the active layer. For this reason, we investigated and optimized the ability of absorption of photon beams in the visual spectrum of the light wavelength in the linear system, on absorbent thin film [52].

Thus, we have proposed an attractive and highly absorption design SC to studied the optoelectronic properties of GaAs semiconductor material in a simple trapezoidal lattice of PCs by studying the effect of the parametric side of mixed ultra-precision lattice structure to obtain the maximum absorption and path length improvement. The device performance is revealed due to the modification in the structure design because of improved light-matter interaction and we provided theoretical predictions for certain geometries which lead to better performance of SC. This latter within which the optical mean path length of the incident photon beams in the active layer virtually becomes more than the absorption depth required to absorb those photons and so consequently they could be absorbed without practically any noticeable increase in the thickness of the SCs.

Design and simulation become very important before fabrication, due to its low cost, quick analysis, low risk and meaningful insight that it may provide [53].

The semiconductor material plays an essential role in the manufacture of the SC. We have studied Gallium Arsenide (GaAs), because it has several electrical, optical, thermal and physical properties better than those of silicon. Table VI.6 shows the most important physical and optical parameters of GaAs, in which the thin film of the SC was made.

Parameters	The value
Energy band gap [eV]	1.424
Intrinsic carrier concentration [cm^{-3}]	$1.79.10^{6}$
Electron mobility [$cm^2.V^{-1}.s^{-1}$]	≤ 8500
Hole mobility [$cm^2.V^{-1}.s^{-1}$]	≤ 400
Electron diffusion coefficient [$cm^2.s^{-1}$]	≤ 200
Hole diffusion coefficient [$cm^2\ s^{-1}$]	≤ 10
Melting point [°C]	1238
Density [$g.cm^{-3}$]	5.3176
Thermal conductivity [$W.cm^{-1}.°C^{-1}$]	0.55
Thermal diffusivity [$cm^2.s^{-1}$]	0.31
Expansion coefficient [$°C^{-1}$]	$5.73.10^{-6}$
Radiative recombination coefficient [$cm^3.s^{-1}$]	7.10^{-10}
Molecular weight [$kg.mol^{-1}$]	144.645

Table VI.6: The most physical parameters of GaAs [54,55].

Our research focuses on numerical simulations, which in turn are closely related to purely evidence based on solving equations, whereas the energy carried by one photon at a wavelength λ is:

$$E(\lambda) = h\upsilon = \frac{hc}{\lambda}\,[eV] \qquad (VI.6)$$

Where, h= $4.1357e^{-15}$ [eV/s] is the Planck constant, c= $2.99.10^{8}$ [m/s] is the speed of light in vacuum, and (λ) is the wavelength. By using conservation of energy [56], the absorption of the solar cells can be expressed as:

$$A(\lambda) = 1 - (\sum_i R_i + \sum_i T_i) \qquad (VI.7)$$

Where, A(λ) is the calculated optical absorption spectrum; R_i and T_i are the reflected and transmitted efficiencies. The single-pass absorption is assuming perfect antireflection but no light trapping [57]. That is, the normal incident light passes through the semiconductor material only once. The absorption of single-pass can be expressed as:

$$A = 1 - e^{-\alpha d} \qquad (VI.8)$$

Where, α is the absorption coefficient, d is the thin film thickness.
Given a specific incident spectrum S(λ) [$W/m^2.nm$] the total number of photons incident at a wavelength (λ) is therefore [58]:

$$N_s(\lambda) = \frac{S(\lambda)}{E(\lambda)} = \frac{\lambda}{hc} S(\lambda) \qquad (VI.9)$$

The total absorption spectrum of the entire device is the sum of the absorption spectra within each layer A_i (λ) as [58]:

$$A(\lambda) = \sum_i A_i(\lambda) \qquad (VI.10)$$

Given these spectra, the number of absorbed photons at a wavelength λ within each layer is therefore [58]:

$$n_i(\lambda) = \frac{S(\lambda)A_i(\lambda)}{E(\lambda)} = \frac{\lambda}{hc}S(\lambda)A_i(\lambda) \quad \text{(VI.11)}$$

Where, S(λ) is a spectrum specific incident [59], and E(λ) is the energy of the incident photon, equivalent to hc/λ, where h is Planck's constant and c is the velocity of light in free space. Given the parameters defined above, several electrical outputs can be computed [60]:

The External Quantum Efficiency (EQE) is defined as:

$$EQE\ (\lambda) = \frac{n_{e-h}(\lambda)}{n_s(\lambda)} = \sum_i n_i A_i(\lambda) \quad \text{(VI.12)}$$

The Internal Quantum Efficiency (IQE) is defined as:

$$IQE\ (\lambda) = \frac{EQE\ (\lambda)}{A(\lambda)} = \frac{\sum_i n_i A_i(\lambda)}{\sum_i A_i(\lambda)} \quad \text{(VI.13)}$$

In order to quantitatively illustrate the absorption performance of PV cells, the power conversion efficiency of PV cells is calculated and compared by the following expression:

$$\eta = \frac{P_{max}}{P_{in}} = \frac{J_m V_m}{P_{in}} = \frac{J_{sc} V_{oc} ff}{P_{in}} \quad \text{(VI.14)}$$

Where, P_{max} [mW] is the total maximum power; P_{in} [W/m^2] is the incident solar power, given by:

$$P_{in} = \int S(\lambda)d\lambda \ [W/m^2] \quad \text{(VI.15)}$$

J_{sc} [mA/cm^2] is the short-circuit current density, that relates to the photon absorption, can be calculated by:

VI.8.1. Analysis of the results

A numerical simulation has been placed to enhance the optoelectronic properties of the diverse simple grating types based on PCs. Table VI.7 shows the values of the optical properties given, which we could model an integrated thin film PV cell by using GaAs in the linear regime.

Parameters	The values
Background material (substrate)	SiO_2
Duty [µm]	0.5
Free space wavelength [µm]	0.63
Freq [HZ]	1/Free space wavelength
Height [µm]	0.5
k_0 [m^{-1}/s^{-1}]	(2.π)/Free space wavelength
Lambda-g [µm]	1.105
Nar [µm]	1.9859
Nperiod [µm]	0.5466
Ntar [µm]	0.1229
Ntg [µm]	0.382
Period [µm]	0.5
Polarization [µm]	0

RCWA material dispersion [µm]	1
RCWA output absorption [µm]	1

Table VI.7. The used parameters of GaAs thin film PV cell with PCs used in the linear regime.

VI.8.1.2. Optical properties

Figures VI.13.a, b and c below present the active layer infrastructure in linear regime. The figure VI.13.a shows a planar absorbent thin film on, whereas, the second consists of a 1DPC absorbent thin film, and the third presents the trapezoidal absorbent thin film, made by GaAs semiconductor materials. According to the results of Tilli M et *al.* [61], the three types of this grating structure are based on a substrate of SiO_2.

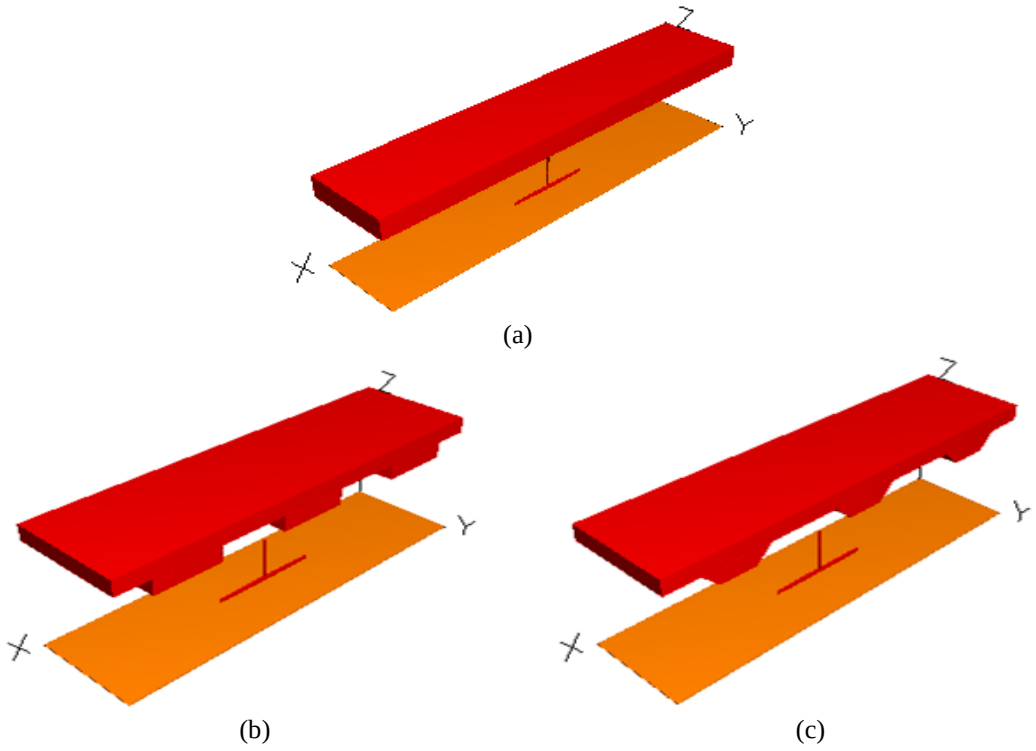

Figure VI.13: (a) planar, (b) 1DPC and (c) trapezoidal grating structures made by GaAs, respectively.

The specific parameters of the foregoing gratings are wavelength (λ), the frequency, the lattice parameter constant (L=500nm), the layer's height (H) and width (D) equal to 500nm. The thicknesses of this arrangement grating structures are considered the same; they are equal to 100nm. Figure VI.14.a, VI.14.b and VI.14.c shows the contour maps of the spectral absorption properties as a function of the wavelength for the forgoing simple grating structures.

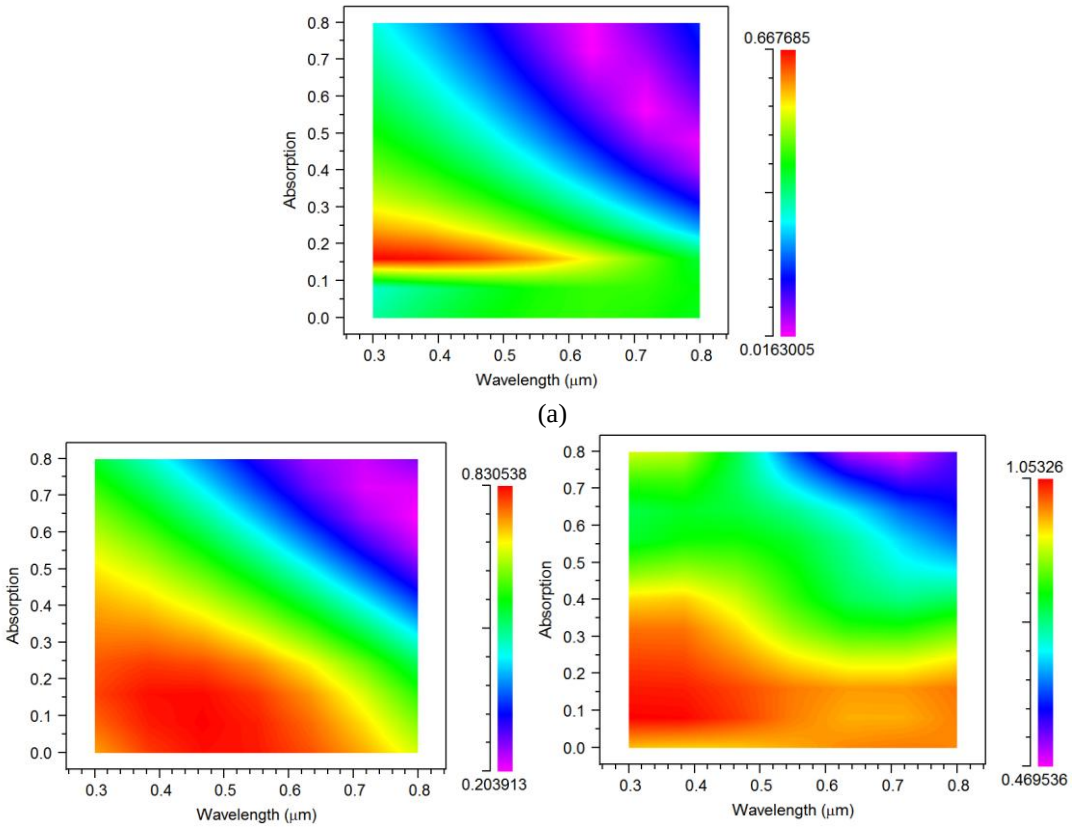

Figure VI.14: Represent the contour map of (a) planar, (b) 1DPC and (c) trapezoidal grating structures made by GaAs.

A large optical absorption often occurs in the visible wavelength range, from 380 to 750nm. In figure VI.14.a and figure VI.14.b, we see that the optical absorption using planar and one dimensional PC gratings gradually decreases beginning from the short visible light spectrum on the wavelength region, demonstrating that a smaller wavelength can prevent reflection in the short wavelength region.

With increasing wavelength, higher absorption can shift into a long wavelength range due to excitation of resonant effects. It is known that the simple trapezoidal lattice structure can excite the waveguide mode resonance, resulting in light trapping and increased absorption in the active layer as shown in figure VI.14.c. These resonance behaviours are highly dependent on the geometric parameters [62].

VI.8.2.2. Optical absorption in simple lattices

The subsequent step in the manufacturing process depends on the immediate conveyance of PCs from the planar absorbent layer to the simple trapezoidal grating layer. The emitted light resonance depends on the associated wavelength with the same parameters of three grating structures.

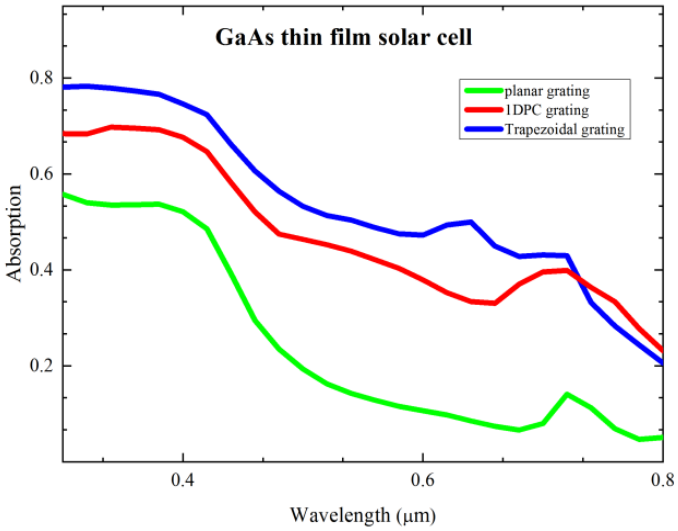

Figure VI.15: Absorption energy of GaAs thin film made by planar, one dimensional PC and trapezoidal grating structures.

In figure VI.15, we gave the absorption energy of the GaAs on different simple grating structures (planar, one dimensional PC and trapezoidal). Absorption control was at different wavelength points of the visible light spectrum. We notice that the spectra corresponding to the layers of simple trapezoids are different from the spectrum of the planar and one dimensional PC thin layers as below. For the simple trapezoidal grating, the absorption is more adequate than planar grating structure; where the ratio of absorption between 300 nm and 480 nm up to about 54.2% in the planar, 67.8% in one dimensional PC and reaches to 79.6% in the simple trapezoidal shape which is greater absorption rate. Eldaif O *et al.* [63] have done simulation work to design the geometry of a solar cell made by 1DPC in order to improve its absorption. Their results show an enhanced absorption in the trapezoidal grating using the GaAs semiconductor material that is apparent compared to the planar one, which proves the ability of the structure to produce PCs SCs.

In addition, for wavelengths range of 380nm and 750nm, and compared with the results obtained, we found enhancement ratio absorption of 29% in a simple trapezoidal grating, 20% with 1DPC and 4% in a planar lattice.

Through the peak absorption of the photon beams in solar spectrum in the visible region, semiconductor materials absorb at these points, where the band gap has a relation. It absorbs at the peaks at about 650nm and 750nm as noted, that is, at the end of the visible region as we want to consider all the points in this area because of its importance for the light beam of the solar spectrum. Then, it begins decreasing gradually during the visible wavelength points, due to the incident waves of short wavelengths are difficult to couple with the fundamental waveguide mode in the trapezoidal and thus are reflected due to poor impedance matching [64].

VI.8.3.3. Parametric effect

In order to enhance the absorption into thin PV layers, firstly, we studied the enhancement of optical absorption used GaAs. In this part, we tried to exploit the effect of the parametric side of the absorbing layer with change the heights and widths with a precision grating structure variations. For this reason, we studied simple trapezoidal grating based on one dimensional PC. We have chosen the changing of the heights and widths variations on ultra-accurate values of 70nm, 140nm, 210nm in addition to the mixture heights and widths between the previous values.

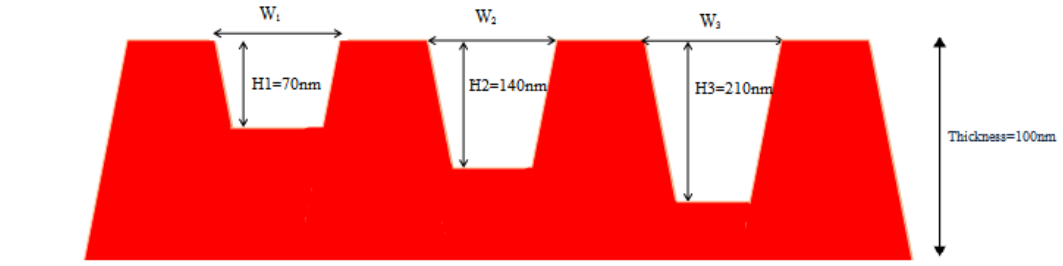

(a)

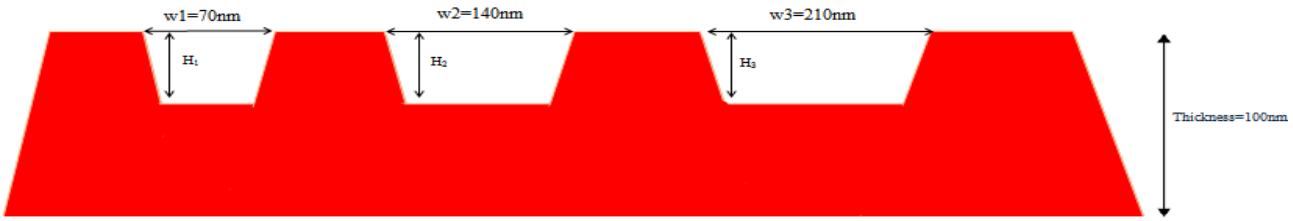

(b)

Figure VI.16: Trapezoidal parametric effect of (a) heights and (b) widths variations made by GaAs.

Figure VI.16, represents the studied mixed trapezoidal grating structure, by changing the effect of (a) the heights, and (b) widths with an ultra-precision values, based on GaAs with the same lattice constant, the same thickness. Moreover, the study was done on the same visible light in the optical wavelength deposited on a SiO_2 substrate. Figure VI.17.a and VI.17.b represent the simulation results of the absorption energy of both height and width with a mixed variation, based on GaAs semiconductor material.

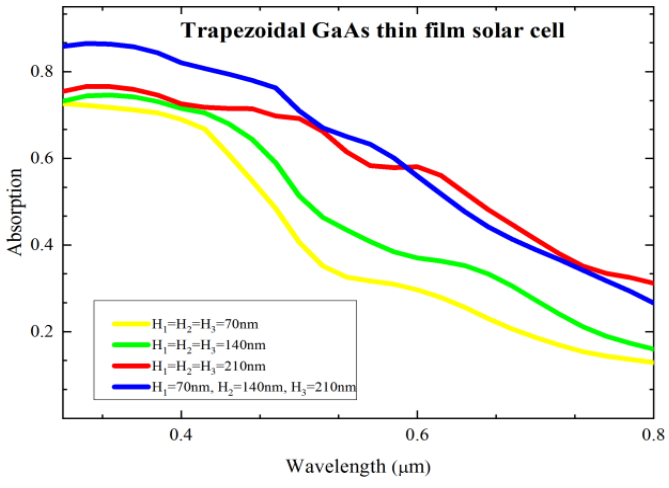

(a)

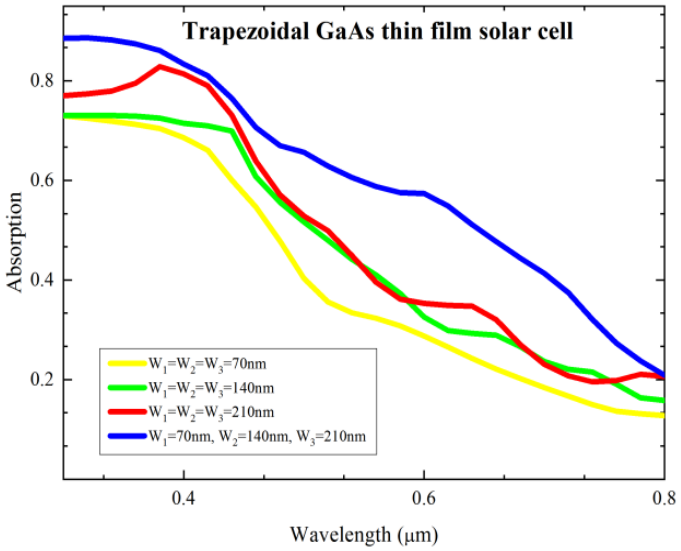

(b)

Figure VI.17: Optical absorption of trapezoidal grating with different and mixed (a) heights and (b) widths, made by GaAs.

The absorption is somewhat better with width than height variation and this is what we noticed from our results, where it increases as the parametric effect is grow, until we notice an enhancement when mixing the ultra-precision values of heights and widths between them. Whereas by using 70nm value the absorption reaches to 72.5% in height and 73% in width, 74.1% in height and 75% in width by using 140nm, 77.5% in height and 78.6% in width by using 210nm, however it is equal to 86.6% in height and 89.9% in width by using the mixed lattices, all this results during (~300-500nm). After that, the absorption ratio begins to decrease under the influence of extinction coefficient (k) until the 800nm wave.

PCs dimensions have been improved by integrated design of numerical simulation and experiment techniques. While we have used different parametric effect of the height and width precision lattices values for a simple trapezoidal based on GaAs, we have found that the absorption ratio in width lattice is better compared to the height lattice, in addition the best absorption is in the combination of the heights and the widths of the lattice. This is confirmed by Fang J *et al.* [65], who showed that the mixing between the ultra-fine values under the lattice is better than the simple lattice for the absorption enhancement, which allowed more light to come into thin film of SC to enhance the absorption efficiency by using the dispersion influence. Whereas the geometrical parameters have an important effect on the distribution spectral of the absorbent PCs, which can be done in the full distance of wavelength if the PCs dimensions are adequately changed. The light trapping effect is mainly attributed to Fabry–Pérot resonance modes due to the large index contrast between air and GaAs layer, which is ubiquitous in the thin film layer [66]. While for simple trapezoidal lattice, the waveguide mode resonance or leaky-mode resonance effects lead to light trapping and increase the absorption in the active layer [66]. In addition, the mixed trapezoidal grating with different dimensions can excite micro cavity resonance effects, which can trap light effectively. Both the excellent geometrical properties and micro cavity effect make the mixed lattice outperform the simple trapezoidal lattice [66].

VI.8.3.4. Solar cell J-V characteristics

The PV cell is distinguished by its means of efficiency conversion measured as incident power percentage and translated to a power. The current density versus voltage J-V, external quantum efficiency (EQE) properties, and the incident light are the most important characteristics. In this section, we will compute the electrical properties of each simple grating used with GaAs semiconductor material; where we studied simple shapes of planar, 1DPC and trapezoidal with GaAs as absorber thin films. Figure VI.18 shows the simulation results of thin GaAs PV cells where, (a) the J-V characteristics, (b) the external quantum efficiency variation and (c) the computed spectral distribution graph for the proposed simple gratings for the studied solar spectrum AM1.5.

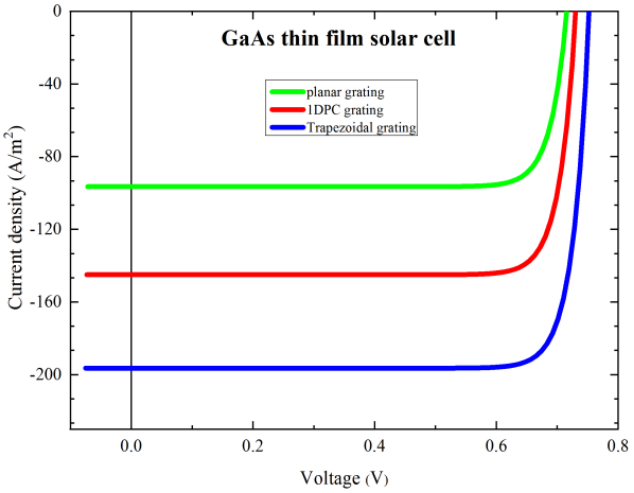

(a)

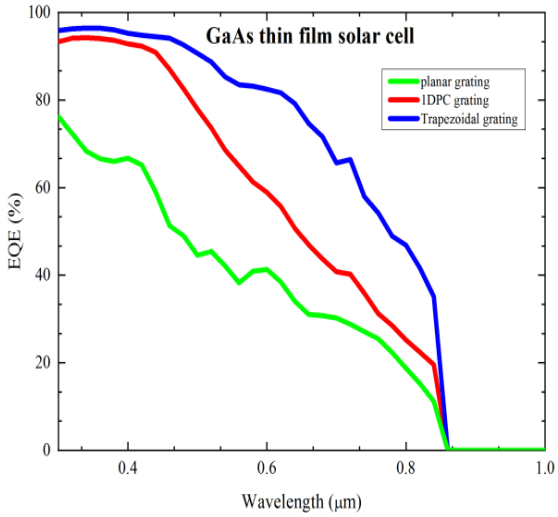

(b)

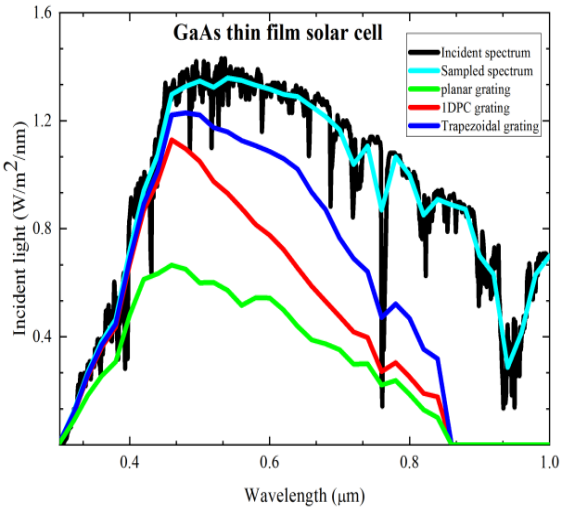

(c)

Figure VI.18: (a) the J-V SC characteristics, (b) the external quantum efficiency and (c) smooth spectral distribution of the studied AM1.5 solar spectrum, with simple grating of planar, 1DPC and trapezoidal structures studied, made by GaAs of thin absorber layer of a SC.

The better result was the simple trapezoidal grating case with a valuable enhancement among the planar and the 1DPC structure, where the thin film SC efficiency presents useful numerical simulation results. This makes the grating structure suitable in terms of absorption efficiency by relying on resonance effects integrated in the leakage pattern to

light trapping and increasing absorption in the thin absorbent film of PV cells, in addition to being more sensitive to sunlight [67]. Figure VI.19 shows the numerical results of thin GaAs SCs studied by mixture and simple heights parametric effect of trapezoidal lattice structure.

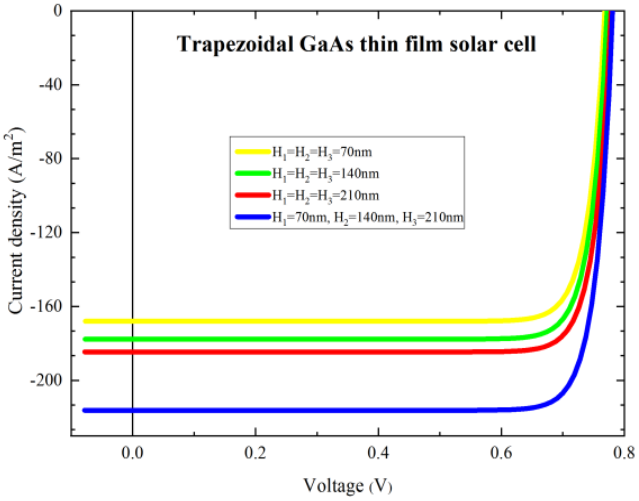

(a)

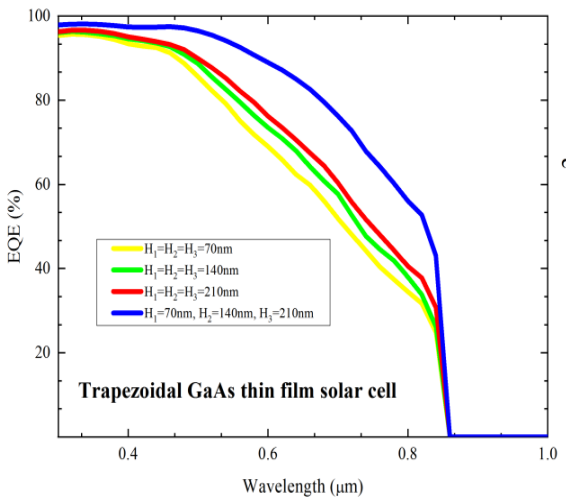

(b)

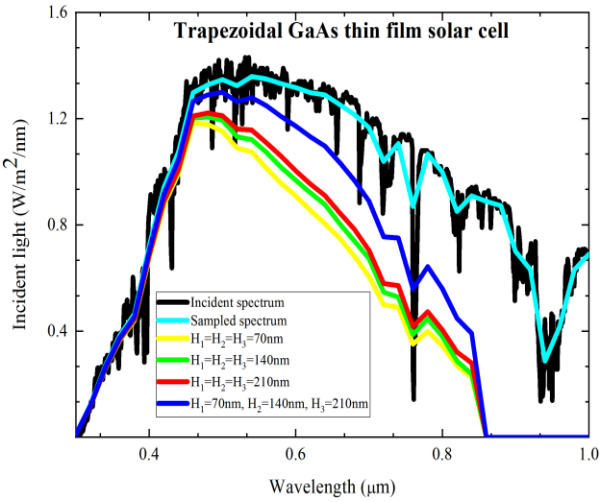

(c)

Figure VI.19: (a) the J-V SC characteristics, (b) the external quantum efficiency and (c) the smoothened spectral distribution for the considered AM1.5 solar spectrum, studied by parametric effect of mixed and simple precision heights of trapezoidal grating structure made by GaAs of thin film SCs.

In this section, we have used the geometrical effects to study the optoelectronic properties of the absorbent layer of a SC through the contrast of the ultra-fine grating heights of a trapezoidal shape. We varied the grating by the same ultra-precision values of 70nm, 140nm and 210nm and we came to mixing these values in one-mixing gratings. We found an enhancement by increasing the values of the grating heights, whereas when we combine the heights values into one mixture of thin film SCs, the results are more improved and more efficient. The better result was in the case of mixture accurate grating values; whereas the results show that it exhibits excellent unidirectional properties. Therefore, such broadband and unidirectional properties of the proposed precision grating structure can be widely used in a thin film PV field [68]. For improvement, a numerical simulation

results of thin GaAs SC are studied by simple and mixed widths of trapezoidal grating structure, and it is shown in figure VI.20, where (a) the J-V solar characteristics, (b) the external quantum efficiency variation and (c) the spectral distribution graph for the considered AM1.5 solar spectrum.

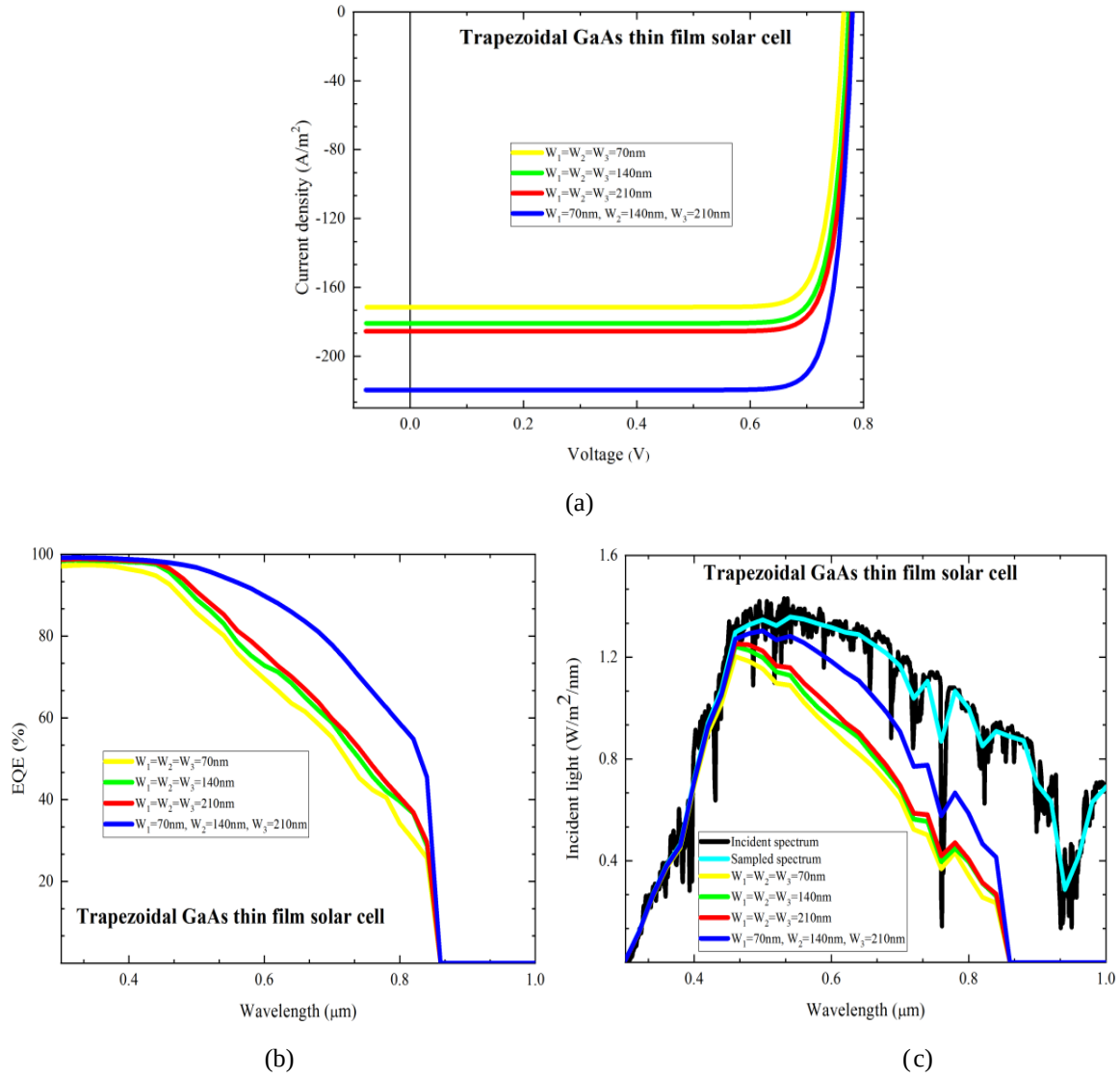

(a)

(b) (c)

Figure VI.20:(a) the J-V SC characteristics, (b) the external quantum efficiency and (c) the smoothened spectral distribution, studied by parametric effect of mixed and simple precision widths of trapezoidal grating structure made by GaAs of thin film SCs.

As shown in the results, the figure VI.20 also shows the performance enhancement for the width variation with more effect than the height one, where we can observe that the enhancement in the absorption is achieved for almost the entire incident wavelength range as a simple trapezoidal in our design and functions, not only to trap the high wavelength photons but also to maximize the coupling of the incident light by reducing reflections from the top. In order to quantitatively compare the optical absorption performance with different lattice structures, Table VI.8 shows the calculated simulation results of the power conversion efficiency with different lattices.

\

Table VI.8. The energy conversion efficiency of GaAs thin film PV cells with different structures.

	***ff*[%]**	**Voc[V]**	**Jsc[mA/m^2]**	**Vob[V]**	**Jso[mA/m^2]**	**Pmax[mW]**	**η[%]**
Planar lattice	84.839	0.716	9.651	0.632	9.271	5.859	6.5092
1DPC lattice	85.065	0.731	14.497	0.646	13.939	9.007	10.006
Simple Trapezoidal lattice	85.391	0.752	19.641	0.667	18.906	12.619	14.018
H_1=H_2=H_3=70nm	85.617	0.768	16.797	0.683	16.185	11.049	12.275
H_1=H_2=H_3=140nm	85.672	0.772	17.766	0.686	17.121	11.753	13.057
H_1=H_2=H_3=210nm	85.76	0.779	18.458	0.693	17.794	12.323	13.691
Height's mixture	85.794	0.781	21.618	0.695	20.843	14.487	16.094
W_1=W_2=W_3=70nm	85.572	0.765	17.144	0.680	16.516	11.224	12.469
W_1=W_2=W_3=140nm	85.699	0.774	18.083	0.688	17.429	11.998	13.328
W_1=W_2=W_3=210nm	85.769	0.779	18.551	0.693	17.883	12.399	13.774
Width's mixture	85.791	0.781	21.961	0.694	21.172	14.709	16.341

The efficiency of the simple trapezoidal lattice with different heights and widths is calculated respectively for comparison. We noticed that the effect of the nano-photonic is much higher than the planar lattice. As shown in table VI.8, it is clear that the mixture ultra-precision grating structure holds the highest short-circuit current density and the total maximum power compared to other structures. In addition, the effect of the width of the grating is more effective than its height, in accordance with the spectral visible absorption.

The efficiency value reached 14.018% in the simple trapezoidal shaper, 10.006% with 1DPC, and up to 16.094% when we mixed the ultra-precision values of heights and amount to about 16.341% in the case of mixture accurate values of width.

Additionally, we have noticed a lesser efficiency when we refer to the ultra-fine values compared to the simple trapezoidal lattice structure. Improved mixture grating structure shows higher efficiency than the simple trapezoidal grating structure, where it is 14.81% in height and 16.57% in width. The efficiency of the different precision values of 70nm, 140nm and 210nm with the same geometrical parameters is lower than the simple trapezoidal lattice structure, which means that the optical absorption of the simple lattice outperforms the simple grating of accurate values.

The numerical simulation results of the absorbent thin GaAs SC and compared to the planar grating shape showed that the 1DPC case indicate an improvement of 53.72%, on the other hand the enhancement rate for the simple trapezoidal lattice reached 115.36%. In addition to this, the mixed lattice showed an improvement of 147.25% in height case and 151.04% in width case. Depending on our results [66], we have noticed a remarkable improvement, as we found an efficiency improvement of the GaAs thin film PV cells with respect to more accurate lattice height variations. We have found 19% in the simple trapezoidal lattice, and 12.41% in the mixture lattices with more accurate values. The aim is to expand with respect to the parametric side by studying the case of width effect, where we have found an improvement of 58.22% compared with the heights one. Our results show that the structured surface microstructures can strongly affect the optoelectronic properties due to multiple reflections and diffractions compared with the planar surfaces. A parametric study has been carried out by investigating the effects of filling ratio, and

mixtures of heights and widths with ultra-precision values on the spectral absorption of a GaAs lattice. We have found that the magnitude and wavelength of the peaks, due to micro cavity resonance, strongly depend on the dimensions of grating, where the significant improvement in optical and electrical characteristics occurs for the ultra-fine parametric effect, where the height's variation of the mixed precision lattices shows an enhancement of 147.25% and 151.04% in the case of the width's variation of the mixed precision gratings. The geometrical effect in thin film shows the effectiveness of the design aspect in producing high efficiency SCs, whereas the mixed widths ultra-precision values of the grating shows an enhancement of 58.22% compared to the mixed accurate heights lattices [66].

VI.9. Conclusion

Our study aims at enhancing the absorption of SCs based on PCs. Thin film absorbers were investigated based on the optical and the J-V characteristics, where the method used was RCWA. To summarize, we have shown some properties related to both the absorption of photons lifetime in PV cells using 1DPC and the absorption of light in the hard cells to enhance the performance of the efficiency. We consider that the proposed design is tolerant in terms of malfunctions during the manufacturing process, which makes it possible to fabricate with low cost for nanotechnology such as the three-dimensional lithography or a nano-particle. The performances delivered by the cells depend critically on the morphology and the material type of the absorbent thin film, in particular, to involve the quality of absorption in thin film cells.

On one hand, the different properties of unpatterned materials were studied as well as the properties of one dimensional PC, half circle, and triangular lattice structures for two types of materials namely; a-Si:H and a-SiGe:H. The study showed that the latter is more efficient, and the incidence angle effect on both materials was also studied. The a-SiGe:H is found to be more efficient in terms of the optical and electrical properties for PV applications.

Furthermore, we proposed and analyzed the optoelectronic properties of SCs made by various grating structures. The geometrical effect in thin film shows the effectiveness of the design aspect in producing high efficiency SCs, whereas the mixed widths ultra-precision values of the lattice shows an enhancement compared to the mixed accurate heights lattices. The execution delivered by the cells depends on the simplicity of both the design and the type of material of the absorbent thin film, to involve the quality of absorption in thin film cells. The significant improvement in optical and electrical characteristics occurs for the ultra-fine parametric effect, where the height's and width's variation shows an enhancement of the mixed precision lattices.

List of references

[1] S. B. Mallick, M. Agrawal, A. Wangperawong, E. S. Barnard, K. K. Singh, R. J. Visser, M. L. Brongersma, and P. Peumans,"Ultrathincrystalline-silicon solar cells with embedded photonic crystals", Applied Physics Letters,100:053113 ,2012.

[2] E. Ozbay.Plasmonics," Merging photonics and electronics at nanoscale dimensions .Science, vol. 311, no. 189, 2006.

[3] Lalanne P. and Morris G. M., Journal of Optical Society of America A 1996, 13, 779

[4] Lincot D., "La conversion photovoltaïque de l'énergie solaire", Recherche et Innovation, DÉCOUVERTE, 344-348, 452007.

[5] Marzolin, C., Smith, S. P., Prentiss, M. and Whitesides, G. M., Advanced Materials 10, 571, 1998.

[6] Pedrotti F. L., Pedrotti L. S., "Introdcution to optics", 2nd Edition, Prentice-Hall Inc, New Jersey, 1993.

[7] Berenger, Jean-Pierre. "A perfectly matched layer for the absorption of electromagnetic waves." *Journal of computational physics* 114.2 185-200, 1994.

[8] Kanamori, Yoshiaki, Emmanuel Roy, and Yong Chen. "Fabrication of soft nanoimprint stamps and polymer subwavelength gratings by spin coating techniques." *Nanophotonics, Nanostructure, and Nanometrology*. Vol. 5635. International Society for Optics and Photonics, 2005.

[9] Lee, Dongwook, and Kijung Yong. "ZnO-based nanostructuring strategy using an optimized solution process in CuInS2 superstrate photovoltaics." *The Journal of Physical Chemistry C* 118.15 7788-7800, 2014.

[10] M. S. Alias *et al.*, "Focused-ion beam patterning of organolead trihalide perovskite for subwavelength grating nanophotonic applications," *J. Vac. Sci. Technol. B, Nanotechnol.Microelectron. Mater. Process. Meas. Phenom.*, vol. 33, no. 5, p. 051207, 2015.

[11] L. Monnami, "Développement et caractérisation de cellules photovoltaïques à base de pérovskites," Lyon, 2016.

[12] Q.G. Du, C.H. Kam, H.V. Demir, H.Y. Yu, and X.W. Sun, Broadband Absorption Enhancement in Randomly Positioned Silicon Nanowire Arrays for Solar Cell Applications, Optics Letters 36, 1884–86, 2011.

[13] J. Schlipf, "The Morphology of Hybrid Perovskite Thin Films for Photovoltaic Application Formation & Disintegration ~," Technische Universität München, 2018.

[14] J. R. Vig, "UV/ozone cleaning of surfaces," *J. Vac. Sci. Technol. A Vacuum, Surfaces, Film.*, vol. 3, no. 3, pp. 1027–1034, May 1985.

[15] Wu M S, Vail E C, Li G S, Yuen W, Chang-Hasnain C J, *J.IEEE Photonics Technology Letters* 8(1), 98–100, 1996.

[16] Ferry V E, Verschuuren M A, Li H B T, Schropp R E I, Atwater H A, Polman A, *J. Applied Physics Letters* 95(18), 183503, 2009.

[17] Alsema E, Wild M J, *Proc. MRS*, 895, 2005.

[18] Amer N M, Jackson W B, Optical Properties of Defect States in a-Si: H. *Hydrogenated Amorphous Silicon (Optical Properties)* Chapter 3 pp 83–112, 1984.

[19] Pearton S J, Stavola, M, Corbett, J. W, *J. Materials Science Forum* 38-41, 25–38, 1991.

[20] LiY, Zou, Y, *J. Advanced Materials*20(15), 2952–2958, 2008.

[21] Lipinski M, Zieba P, Jonas S, Kluska S, Sokolowski M, Czternasetk H, *J. Opto-electronics Review*12(1), 41–44, 2004.

[22] Priolo F, Gregorkiewicz T, Galli M, Krauss, T F, *J. Nature Nanotechnology*, 9(1), 19–32, 2014.

[23] Thevenot, M., et al., *Progress in Electromagnetics Research Symposium*, 1998.
[24] Moulé A J, Meerholz K, *J. Advanced Functional Materials*19(19), 3028–3036, 2009.
[25] Huang Y F, Chattopadhyay S, Jen Y J, Peng C Y, Liu T A, Hsu Y K, Pan C L, Lo H C, Hsu C H, Chang Y H, lee CS, Chen KH, ChenLC, *J. Nature Nanotechnology*, 2(12), 770–774, 2007.
[26] Green M A, Jianhua Zhao Wang A, Wenham S R, *J. IEEETransactions on Electron Devices* 46(10), 1940-1947, 1999.
[27] Tenent R C, Barnes T M, Bergeson J D, Ferguson A J, To B, Gedvilas L M, Heben M J, Blackburn J L, *J. Advanced Materials*, 21(31), 3210-3216, 2009.
[28] Zhao G, Jiao Y C, Zhang F, Yang X, *J. Electromagnetic Waves and Applications*, 24(1), 33–40, 2010.
[29] VaillantF, JousseD, *J. Physical Review B*, 34(6), 4088–4098, *1986.*
[30] Zhao S, Gao Z, Chen C, Wang G, Zhang B, Chen Y, Zhang J, Li X, Qin Y. *J. Carbon* 98, 196–203, 2016.
[31] Ouanoughi A, Hocini A, Khedrouche D *J. Frontiers of Optoelectronics*,9(1), 93–98, 2015.
[32] Sadoun, B., Mouetsi, S., Hocini, A and Hocini, A., *IOP Conf. Ser.: Mater. Sci. Eng.*, 1046(1), 012014, 2021.
[33] Si, F. T., Isabella, O. and Zeman, M., Solar Energy Materials and Solar Cells, 163, 9, 2017.
[34] Veldhuizen, L. W., Vijselaar, W. J., Gatz, H. A., Huskens, J. and Schropp, R. E., Thin solid films, 635 66, 2017.
[35] Idda, A., Ayat, L. and Dahbi, N., Journal of Ovonic Research, 15(5), 2019.
[36] Wang, L., Zheng, Z., Gou, Y., Liang, W. and Yu, W., Optics Communications, 483, 126673, 2021.
[37] Nam, Y. M., Huh, J.and Jo, W. H., Solar Energy Materials and Solar Cells, 94(6), 1118, 2010.
[38] Dominguez, S., Garcia, O., Ezquer, M., Rodriguez, M. J., Lagunas, A. R., Pérez-Conde, J. and Bravo, J.,Photonics and Nanostructures-Fundamentals and Applications, 10(1) 46, 2012.
[39] Heidarzadeh, H. and Tavousi, A., Materials Science and Engineering: B, 240 1, 2019.
[40] Wu, W. and Magnusson, R., Opt. Lett., 37(11), 2103, 2012.
[41] Taguchi, M., Terakawa, A., Maruyama, E.and Tanaka, M., Progress in photovoltaics: research and applications,13(6), 481, 2005.
[42] Schuttauf, J. W., Niesen, B., Lofgren, L., Bonnet-Eymard, M., Stuckelberger, M., Hanni, S., Boccard, M., Bugnon, G., Despeisse, M., Haug, F. J, Meillaud, F and Ballif, C., Solar Energy Materials and Solar Cells, 133, 163, 2015.
[43] Qi, B. and Wang, J., Phys. Chem. Chem. Phys., 15(23), 8972, 2013.
[44] Moon, S. Y., You, D. J., Lee, S. E.and Lee, H., Current Applied Physics, 13(7), 1502, 2013.
[45] Gupta, N. D., & Janyani, V., IEEE J. Quantum Electron., 53(2), 1, 2017.
[46] Chung, J. W., Park, J. W., Lee, Y. J., Ahn, S. W., Lee, H. M. and Park, O. O., Jpn. J. Appl. Phys., 51(10S), 10NB16, 2012.
[47] Yousif, B., Abo-Elsoud, M. E. A. and Marouf, H., Optical and Quantum Electronics, 51(8), 1, 2019.
[48] Gordijn, A., Zambrano, R. J., Rath, J. K.and Schropp, R. E., IEEE Transactions on Electron Devices, 49(5), 949, 2002.
[49] Stigloher, J., Decker, M., Körner, H. S., Tanabe, K., Moriyama, T., Taniguchi, T., Hata, H., Madami, M., Gubbiotti, G., Kobayashi, K., Ono, T and Back, C.H., Phys. Rev. Lett., 117(3), 037204, 2016.
[50] Mudachathi, R and Tanaka, T., Adv. Nat. Sci: Nanosci. Nanotechnol., 9(1), 015010, 2018.

[51] Sadoun, B., Mouetsi, S., Hocini, A and Derdour, R., "Morphological design of the photonic crystals influence on improving the optoelectronic properties of a-SiGe:H thin film solar cell," Jordan Journal of Physics. 16(1), , 2023 (Promise to publish).

[52] Zeng L, Yi Y, Hong C, Liu J, Feng N, Duan X, Kimerling L C and Alamariu B A Efficiency enhancement in Si solar cells by textured photonic crystal back reflector, *Appl. Phys. Lett.* 89 111111, 2006.

[53] Hocini A, Bouchelaghem A, Saigaa D, Bouras M, Boumaza T and Bouchemat M Birefringence properties of magneto-optic rib waveguide as a function of refractive index, *J Comput Electron* 12 50–5, 2013.

[54] Li H, Chen Y, Wei Z and Chen R, Optical property and lasing of GaAs-based nanowires *Sci. China Mater.* 63 1364–81, 2020.

55] Anon Gallium Arsenide (GaAs) Semiconductors *AZoM.com*, 2013.

[56] Hoshiba M, Simulation of multiple-scattered coda wave excitation based on the energy conservation law *Physics of the Earth and Planetary Interiors* 67 123–36, 1991.

[57] Atalay I A, Gunes H A, Alpkilic A M and Kurt H, Multi-objective particle swarm optimization on ultra-thin silicon solar cells *J Opt* 49 446–54, 2020.

[58] Li S S, *Semiconductor Physical Electronics* (Springer Science & Business Media), 2012.

[59] Abass A, Shen H, Bienstman P and Maes B, Angle insensitive enhancement of organic solar cells using metallic gratings *Journal of Applied Physics* 109 023111, 2011.

[60] Polo J, Alonso-Abella M, Martín-Chivelet N, Alonso-Montesinos J, López G, Marzo A, Nofuentes G and Vela-Barrionuevo N, Typical Meteorological Year methodologies applied to solar spectral irradiance for PV applications *Energy* 190 116453, 2020.

[61] Tilli M, Motooka T, Airaksinen V-M, Franssila S, Paulasto-Kröckel M and Lindroos V, Chapter 6 - Thin Films on Silicon *Handbook of Silicon Based MEMS Materials and Technologies (Second Edition)* Micro and Nano Technologies (Boston: William Andrew Publishing) 124–205, 2015.

[62] Wu W and Magnusson R, Total absorption of TM polarized light in a 100nm spectral band in a nanopatterned thin a-Si film *Opt. Lett., OL* 37 2103–5, 2012.

[63] Meng X, Gomard G, El Daif O, Drouard E, Orobtchouk R, Kaminski A, Fave A, Lemiti M, Abramov A, Roca i Cabarrocas P and Seassal C, Absorbing photonic crystals for silicon thin-film solar cells: Design, fabrication and experimental investigation *Solar Energy Materials and Solar Cells* 95 S32–8, 2011.

[64] Zhao B and Zhang Z M, Perfect Absorption With Trapezoidal Gratings Made of Natural Hyperbolic Materials *Nanoscale and Microscale Thermophysical Engineering* 21 123–33, 2017.

[65] Fang J, Gou Y and Deng J, Complex trapezoid grating for light trapping in thin-film solar cells: super-fine structure *Optica Applicata* Vol. 50, 2020.

[66] Sadoun, B., Mouetsi, S and Hocini, A, "Ultra-precision trapezoidal grating mixture of photonic crystal's effect on enhancing the optoelectronic properties of thin film GaAs solar cell," *Physica scripta*. 96(12), 125508, 2021.

[67] Wang L, Zheng Z, Gou Y, Liang W and Yu W, "Fabry–Perot resonance assisted dual-layer coating with enhanced wavelength-selective refection and emission for daytime radiative cooling" *Optics Communications* 483 126673, 2021.

[68] Maystre D, Nevière M and Petit R, Experimental Verifications and Applications of the Theory *Electromagnetic Theory of Gratings* Topics in Current Physics ed R Petit (Berlin, Heidelberg: Springer) pp 159–225, 1980.

General conclusion

General conclusion

In order to converge on enhancing the absorption of SCs based on PCs, thin film absorbers have been developed in our thesis. The studies undertaken throughout this thesis focused on thin film SCs, giving rise to so called 2nd generation cells.

Actually, the performance delivered by cells is critically dependent on the morphology of the absorbent thin film, in particular to affect the quality of absorption in thin film cells, as well as the electronic properties. This issue is at the heart of the study presented in this thesis. Our approach consists of studying solar cells made from efficient types of semiconductor materials (Si, a-Si:H, a-SiGe:H and GaAs) and to propose different geometric configurations; in order to find the best combination resulting in a better absorption. To optimize the 1DPC based on SCs, we simulated the latter using the rigorous coupled waves analysis method (RCWA).

The geometric parameters of the structures studied were varied, in order to obtain better absorption efficiency, this simulation is carried out using RSoft software which provides a theoretical prediction of the absorption as a function of the geometric parameters.

For the one dimensional structure it has been shown that the absorption spectra increase with increasing lattice and thickness. Furthermore, it is noted that 1DPC structures absorb incident light better than the unpatterned layer. Another design of a PC SC was proposed (unpatterned, 1DPC, half circle and triangular) by the morphological effect, based on a-Si:H and a-SiGe:H. The absorption spectra and the electronic proprties of these structures are studied as a function of the morphological design and physical (a-Si:H and a-SiGe:H) parameters. Then, we have studied the optical properties and the J-V characteristics of the absorber layer solar cell integrated with the trapezoidal grating structure by studying the parametric effect (heights and widths) and giving an ultra-precision values then mixing them in one cell. In context, we have studied the absorption of thin films as a function of wavelength for application in SCs. Thus, we have tried to achieve high photon density of the states in the 1DPC layer, by positioning the photonic band gap in the non-absorbing region of the photovoltaic material and the edge of the PBG in the weakly absorbing region. We have studied the performance of the considered structure and determined the geometric parameters which allow better absorption, in addition to improving the electronic characteristics, allowing the high efficiency. In summary, the results obtained show that; The results obtained show that the absorption of the one dimensional patterned structure is considerably improved compared to the unpatterned layer. Then in the 2nd case, we obtain an idol triangular efficiency than the unpatterned, 1DPhC and half circle. We observed that the best incidence angle is between 60° and 70°. Moreover, when we mixing the ultra precision values in one thin film solar cell using GaAs, we obtain a better optoelectronic properties (optical absorption, Voc, Jsc, ff, n and Pmax). The simulation results also showed that the absorption efficiency of sunlight as a function of the parametric effect over a visible spectrum of a trapezoidal structure is better compared to a layer 1DPC.

As perspectives, we propose the study and development of absorbent thin film SCs based on other types of materials compatible with integrated optics 3DPC.

Annex

Annex-A

SCIENTIFIC PRODUCTION

Publications in international journals with reading committee

[1]. Sadoun, B., S. Mouetsi, and A. Hocini. "Optical properties of one-dimensional photonic crystal and light absorption enhancement in planar a-Si: H solar cell." IOP Conference Series: Materials Science and Engineering. Vol. 1046. No. 1. IOP Publishing, 2021.

[2]. Boumediene Sadoun, Souheil Mouetsi, Abdesselam Hocini and Roumaissa Derdour, "Morphological design of the photonic crystals influence on improving the optoelectronic properties of a-SiGe:H thin film solar cell" Jordan Journal of Physics. 16(1), 2023 (Promise to publish).

[3]. Sadoun Boumediene, Souheil Mouetsi, and Abdesslam Hocini. "Ultra-precision trapezoidal grating mixture of photonic crystal's effect on enhancing the optoelectronic properties of thin film GaAs solar cell." Physica Scripta 96.12 (2021): 125508.

[4]. Hocini, A., S. Mouetsi, and B. Sadoun. "Design of high sensitive glucose concentration sensor of photonic crystal cavity." IOP Conference Series: Materials Science and Engineering. Vol. 1046. No. 1. IOP Publishing, 2021.

International communications conferences

[1]. Boumediene Sadoun and Souheil Mouetsi. "Study of the one-dimensional photonic crystals to enhance the absorption into solar cells" The International Conference on functional Materials (ICFM2019), March 24th-28th, 2019, Hammamet, Tunisia.

[2]. Boumediene Sadoun and Souheil Mouetsi. "Effect of photonic crystals to absorb light in photovoltaic cells on Si", the International Conference of Nano Materials and their Applications (NANOMAT2019), April 27th-29th, 2019, Hammamet, Tunisia.

[3]. Boumediene Sadoun and Souheil Mouetsi. "Enhanced light absorption of solar cells on germanium with one-dimensional photonic crystals", the International Conference of Nano Materials and their Applications (NANOMAT2019), April 27th-29th, 2019, Hammamet, Tunisia.

[4]. Boumediene Sadoun, Souheil Mouetsi and Abderraouf Hocini. "Absorbing Photonic Crystals for Thin layer a:Si-H of photovoltaic cells", the International conference on computer sciences and renewable energy (ICCSRE2019), July 22nd-24th, 2019, University of Agadir, Morocco.

[5]. Boumediene Sadoun and Souheil Mouetsi. "Comparative study on the optical properties of the PV cells on silicon to produce high yields using photonic crystals", The 2nd Algerian-German International Conference on New Technologies and their

Applications (AGICNT2019), September 22nd-23rd, 2019, University of Setif 1, Algeria.

[6]. Boumediene Sadoun and Souheil Mouetsi. "Absorption enhancement in thin film amorphous silicon in solar cells", The 3rd International Congress of Quantum Physics and Chemistry (CIPCQ2019), November 4th-6th, 2019, University of Bejaia, Algeria.

[7]. Boumediene Sadoun, Souheil Mouetsi, Abdesselam Hocini and Abderraouf Hocini. "Optical properties of one-dimensional photonic crystal to enhance light absorption in a:Si-H planar solar cell", The 5th International conference on advanced sciences (ICAS2019), (November 9th-12th, 2019), harghada, Egypt.

[8]. Abderraouf Hocini, Souheil Mouetsi, Abdesselam Hocini and Boumediene Sadoun. "Design of high sensitive glucose concentration of photonic crystal cavity", The 5th International conference on advanced sciences (ICAS2019), November 9nd-12rd, 2019, Harghada, Egypt.

[9]. Boumediene Sadoun and Souheil Mouetsi. "Effect of thin film photovoltaic cells based on one-dimensional photonic crystal using RCWA", The 1st International workshop on environmental engineering (IWEE2019), November 16th-17th, 2019, University of Setif 1, Algeria.

National communications conférences

[1]. Boumediene Sadoun and Souheil Mouetsi. "Etude des propriétés optique des cristaux photonique pour l'amélioration de l'absorption dans les cellules solaire", 1re journée nationale en énergies renouvelables et matériaux avancées (JNERMA2018), November 13th, 2018, University of Oum El Bouaghi, Algeria.

[2]. Boumediene Sadoun and Souheil Mouetsi. "Effect of the photonic crystals to improve the absorption of light in solar cells", Journées d'étude sur les sciences appliqués au service du développement durable (JSADD2018), December 8th-9th, 2018, Higher school in applied sciences, University of Tlemcen, Algeria.

[3]. Boumediene Sadoun and Souheil Mouetsi. "Improved light absorption in photovoltaic cells based on photonic crystals", Journée nationale: étude des matériaux elaboration et modélisation (JNEM2018), December 13th, 2018, University of Geulma, Algeria.

[4]. Boumediene Sadoun and Souheil Mouetsi. "Effet de la couche absorbante dans les cellules solaire en SiO_2 sur le péagage de la lumière à l'aide de cristaux photonique 1D", Conférence nationale sur la chimie des matériaux (CNCM2019), July 2nd-3rd, 2019, University of Boumerdes, Algeria.

Abstract

Photovoltaic generations has intensified over the last decade, moving from the most basic applications based on elementary devices to one of the most important applications of energy especially after the exploitation of semiconductor materials which play a central role in photovoltaic systems. Research on the optimal array structure has generated much interest due to its potential application in light trapping in thin film photovoltaic cells. Photonic crystals with their nanoengineering function have made it possible to obtain high efficiency solar cells.

Our thesis work aims to study and design new structures of thin-film solar cells based on photonic crystals in order to improve its optoelectronic properties, especially the absorption of light in solar cells by adjusting the parameters, geometric and morphological. The proposed structures are designed with ultra-precision on a substrate with a thickness of up to 100nm. The first part of the results obtained is based on the study of the absorption of light by influencing the optical properties of thin film solar cells. The second part is devoted to the study of the morphological effect of a one-dimensional photonic structure on the one hand and the study of the effect of the angle of incidence on the other hand. The simulations are performed using the DiffractMod simulation software developed by RSoft, using the Rigorous Coupled Wave Analysis (RCWA) method. The results obtained allow us to conclude that the use of the properties of photonic crystals improves the absorption rate of light in solar cells.

Keywords: Photovoltaic, Photonic crystals, Optoelectronic, Absorption, Simulation.

Résumé

La génération du photovoltaïque s'est intensifiée au cours de la dernière décennie, passant des applications les plus basiques basées sur des dispositifs élémentaires à l'une des applications les plus importantes de l'énergie surtout après l’exploitation des matériaux semi-conducteurs qui jouent un rôle central dans les systèmes photovoltaïques. La recherche sur la structure de réseau optimale a suscité beaucoup d'intérêt en raison de son application potentielle dans le piégeage de la lumière dans les cellules photovoltaïques à couches minces. Les cristaux photoniques avec leur fonction nano-ingénierie ont permis d'obtenir des cellules solaires à haut rendement.

Notre travail de thèse a pour but l'étude et la conception de nouvelles structures de cellules solaires en couches minces à base des cristaux photoniques afin d’améliorer ses propriétés optoélectroniques surtout l’absorption de la lumière dans les cellules solaires on jouant sur les paramètres, géométrique et morphologique. Les structures proposées sont conçues de manière ultra-précise sur un substrat d'une épaisseur allant jusqu'à 100nm. La première partie des résultats obtenus est basée sur l'étude de l'absorption de la lumière en influençant les propriétés optiques des cellules solaires en couches minces. Quant à la deuxième partie, elle est consacrée à l'étude de l'effet morphologique d’une structure photonique unidimensionnelle d’une part et l’étude de l'effet de l'angle d'incidence d’autre part. Les simulations sont réalisées à l'aide du logiciel de simulation DiffractMod développé par RSoft, En utilisant la méthode d'analyse rigoureuse des ondes couplées (RCWA). Les résultats obtenue nous a permet de conclure que l’utilisation des propriétés des cristaux photonique améliorent le taux d’absorption de la lumière dans les cellules photovoltaïques.

Mots clés : Photovoltaïque, Cristaux photoniques, Optoélectroniques, Absorption. Simulation.

الملخص

تزايد الاهتمام بمجال الكهروضوئية خلال العقد الماضي، حيث انتقل من التطبيقات الأساسية القائمة على الأجهزة الأ ساسية إلى أحد أهم التطبيقات في مجال الطاقة وخاصة عند استعمال مواد أشباه الموصلات التي كان لها دور ا مركزيا في الأنظمة الكهروضوئية .لقد ولّد البحث عن الهيكل الشبكي الأمثل اهتمامًا كبيرًا نظرًا لتطبيقه المحتمل في تركيز الضوء في الخلايا الكهروضوئية ذات الأغشية الرقيقة. البلورات الضوئية بخصائصها ذات الهندسة النانوية مكنتها من الحصول على خلايا شمسية عالية الكفاءة.

هدفنا من هذه الرسالة هو دراسة وتصميم هياكل جديدة للخلايا الشمسية ذات الأغشية الرقيقة متكونة من بلورات ضوئية لتحسين عملية امتصاص الكهرباء داخل الخلايا الكهروضوئية من خلال دراسة تأثير العوامل الهندسية والشكلية للخلايا. الهياكل المقترحة تم تصميم ها بدقة فائقة على قاعدة بسمك يصل إلى 100 نانومتر. الجزء الأول من النتائج المحصل عليها يرتكز على دراسة امتصاص الضوء من خلال دراسة التأثير على الخصائص الضوئية للخلايا الشمسية ذات الأغشية الرقيقة . أما الجزء الثاني فيعتمد على دراسة التأثير الشكلي للهياكل الضوئية أحاديّ البعد من جهة ومن جهة أخرى دراسة تأثير زاوية الانعكاس. تم إجراء عمليات المحاكاة باستخدام برنامج محاكاة DiffractMod الذي طورته شركة RSoft باستخدام طريقة تحليل الموجة المزدوجة الصارمة (RCWA). النتائج المحصل عليها تثبت لنا فعالية استخدام البلورات الضوئية في تحسين عملية امتصاص الضوء داخل الخلايا الشمسية.

الكلمات المفتاحية: الخلايا الكهروضوئية، البلورات الضوئية، الكهروضوئية، الامتصاص. المحاكاة.